Development of two multiaxial fatigue analysis methods for ductile metals based on energy considerations

Ph.D. THESIS
presented to obtain the degree of
Doctor of Philosophy in Industrial Engineering

Luis Pallarés Santasmartas

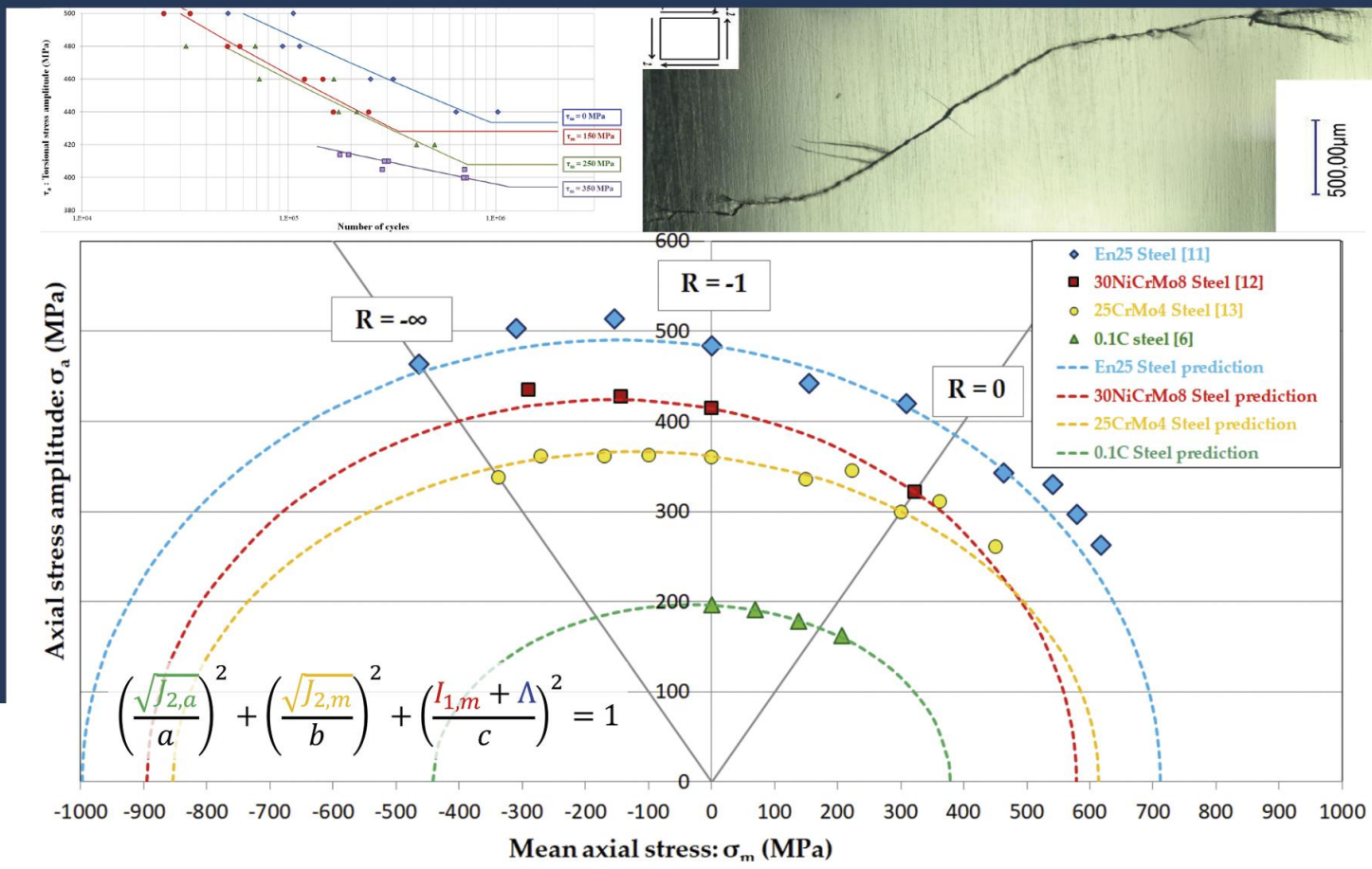

THESIS ADVISOR
Dr. Joseba Albizuri Irigoyen

September 2020, Bilbao

eman ta zabal zazu
Universidad del País Vasco
Euskal Herriko Unibertsitatea

INGENIARITZA MEKANIKOA SAILA
DEPARTAMENTO DE INGENIERÍA MECÁNICA

Universidad del País Vasco Euskal Herriko Unibertsitatea

INGENIARITZA MEKANIKOA SAILA
DEPARTAMENTO DE INGENIERÍA MECÁNICA

Tesis Doctoral

DEVELOPMENT OF TWO MULTIAXIAL FATIGUE ANALYSIS METHODS FOR DUCTILE METALS BASED ON ENERGY CONSIDERATIONS

Presentada por:

Luis Pallarés Santasmartas

en el

Departamento de Ingeniería Mecánica

perteneciente a la

Universidad del País Vasco

Euskal Herriko Unibertsitatea

Para la obtención del título de

Doctor Ingeniero Industrial

Dirigida por

Prof. Dr. Joseba Albizuri Irigoyen

Bilbao, _____ de _____ de _____

A mis padres,

a mi hermano,

y a Ainhoa

AGRADECIMIENTOS

Me gustaría comenzar este trabajo agradeciendo a Rafael Avilés, quien fue codirector de esta tesis durante los 4 primeros años, y de quien partió la idea de escoger un tema tan fascinante como la fatiga multiaxial, cuyo ámbito parecía inalcanzable y solamente reservado a algunos pocos especialistas de talla mundial. Por las discusiones de fatiga que durante años nos hicieron crecer a todos. Y sobre todo por implicarse personalmente y ayudarme en muchos momentos difíciles. Muchísimas gracias por todo.

Quiero transmitir mi agradecimiento a Nicolas Saintier, director de la estancia internacional en Burdeos, por abrirme las puertas de la École Nationale d'Arts et Métiers y darme la oportunidad de realizar una estancia de un año que recordaré muchísimo cariño. Muchísimas gracias a Frank Girot por gestionar todos los aspectos para que esta estancia en Burdeos fuera posible.

A Jonathan Merzeau, quien estaba a cargo del manejo de la máquina LISE de fatiga torsional, por su enorme capacidad de trabajo y para transmitir ilusión en los proyectos todos los días de mi estancia. Gracias a él pudimos realizar ensayos de una enorme dificultad desde el punto de vista técnico.

A Thierry Palin-Luc, a quien agradezco su ayuda con los ensayos de fatiga torsional, y por su asesoramiento en multitud de cuestiones referentes a la fatiga de materiales, que siempre ofreció de manera altruista. A Catherine Froustey, por la alegría que transmite a todo el mundo, y por su inspiración para desarrollar un método basado en consideraciones energéticas.

A Héloïse Rolland, Ilan Raphaël, Mohand Ouarabi, Pietro del Sorbo y Lorenzo Capelli, doctorandos de la ENSAM Bordeaux, por ofrecerme su amistad, y con

quienes he compartido debates filosóficos y buenísimos momentos que hicieron que mi estancia en Burdeos fuera una de las etapas más felices de mi vida.

Quisiera expresar mi agradecimiento a todo el Departamento de Ingeniería Mecánica de la ETSI de Bilbao, por permitirnos realizar los ensayos de fatiga en sus instalaciones. Agradezco a Adrián Rodríguez por ayudarme en el mecanizado y el tratamiento térmico de las probetas de fatiga; y a Alexander Avilés por compartir multitud de datos de ensayos que han sido de gran utilidad.

Y por supuesto, me gustaría expresar un especial agradecimiento a Joseba Albizuri, mi director de tesis, por su paciencia y su implicación personal para ayudarme a que esta Tesis haya sido posible. Joseba no solamente me ha ayudado en los aspectos técnicos de la Tesis, sino también en los aspectos más personales de la dirección: transmitiendo tranquilidad y claridad en los momentos de incertidumbre, y gestionando mi estancia en Burdeos. Muchísimas gracias por todo.

A todos mis compañeros de Gaztelueta, y en especial a Javier Ibarra, Joseba Goirigolzarri, José Manuel Gutiérrez y Jorge Ugalde, por enseñarme a ser un mejor profesor. A Don Curri, Don Fernando y Don Jesús Mari, por su inestimable comprensión para ayudarme a crecer en Cristo.

A mi prometida Ainhoa Liendo, quien ha sido un enorme apoyo durante la fase final de esta tesis, transmitiendo comprensión y alegría, y de quien admiro su altruismo y su eterna ilusión ante los retos.

Por último, quisiera agradecer de todo corazón a mis padres y a mi hermano su ayuda y acompañamiento a lo largo del camino.

ABSTRACT

This thesis presents the development of a multiaxial fatigue method based on a physical model formulated from energetic considerations, its scope of use being high cycle fatigue. To this end, an extensive experimental fatigue campaign has been carried out on 34CrNiMo6 steel.

The document contains a comprehensive review of the fundamental aspects of metal fatigue, taking into account the historical evolution and the different advances and discussions up to the present day. The main conclusion drawn from this historical review is that the effects with the greatest influence on multi-axial fatigue are the effect of mean axial and shear stresses.

Thus, the bibliographic review includes the effect of axial mean stresses, which has been approached from a novel perspective in relation to the shapes of the curves in the Haigh diagram, and showing the experimental correlation for ductile steels similar to the one studied in this Thesis. In addition, a study has been carried out on the effect of mean shear stresses on torsional fatigue, an aspect rarely dealt with in the literature and which has given rise to many debates in the field of multiaxial fatigue research.

Once the fundamental effects on high-cycle multi-axial fatigue had been established, the best known multi-axial fatigue methods were analysed and compared against a large database of multi-axial tests, with the aim of analysing in a general way which aspects should be incorporated in the multi-axial method to be developed.

The test campaign developed includes static tests, rotating bending fatigue tests, axial fatigue tests and torsional fatigue tests. The latter were carried out in

Bordeaux in 2016, during which the author spent an international stay at the École Nationale Superieure d'Arts et Métiers.

Taking into account the experimental results of the torsion tests, it could be observed that they precisely followed an energy balance between static and alternating elastic distortion energy. However, this hypothesis was insufficient to adjust experimentally the tests obtained in axial fatigue, in which there is a rupture of symmetry in the Haigh diagram.

In order to obtain a better experimental correlation, two methods have been developed: the first combines the virtues of two of the most successful stress invariant methods, namely those of Crossland and Marin, and was published in the International Journal of Fatigue in April 2018. As a final objective of the thesis, a fully energetic multi-axial fatigue method has been developed that uses the elastic energy of volume change (hydrostatic) as a mechanism to model the rupture of symmetry in the axial Haigh diagram. This method has an advantage over other methodologies as it can be modified to include other types of energy, such as plastic energy, to extend its scope of use to low cycle fatigue.

TABLE OF CONTENTS

Table of Contents **9**

Index of figures **13**

Index of tables **23**

Nomenclature and acronyms **25**

Chapter 1. Objectives of the Thesis and Methodology **33**
1.1. Context and direct background 33
1.2. Organisation of the Thesis 35
1.3. General objectives of the research and particulars of this Thesis 38
1.4. Historical Evolution of Multiaxial Fatigue 42
1.5. Current state of the art 50
1.6. Towards a new multiaxial fatigue method 53

Chapter 2. General Aspects of Metal Fatigue **61**
2.1. Fatigue curves 61
2.2. The fatigue limit 63
2.3. The estimation of the fatigue limit 66
2.4. The volumetric fatigue limit 68
2.5. S-N Curve Models 70
2.6. The JSME model for S-N curves 73
2.7. Cyclical yield stress 74
2.7.1. The concept of monotonic yield stress 74
2.7.2. Cyclical plasticity yield 75
2.7.3. Ramberg-Osgood's cyclic plasticity model 76
2.7.4. A relevant example chosen from the literature 81

Chapter 3. Effect of mean axial stresses **85**
3.1. Introduction 85
3.2. Uniaxial criteria 89
3.2.1. Classical uniaxial methods 89
3.2.2. Advanced uniaxial methodologies 98
3.2.3. Other methodologies of interest 108
3.3. Theories about the effect of axial mean stresses 119
3.4. Experimental results from literature 122
3.4.1. Introduction 122
3.4.2. Smith's collection of experimental results [Smith, 1942] 123

3.4.3. The Study of O'Connor and Morrison's of mean stresses on steels [O'Connor, 1956]. 127
3.4.4. The collection of experimental results from Sines [Sines, 1959] 132
3.4.5. Klubberg's collection of experimental results 134
3.4.6. Other experimental results of ductile steels 137
3.4.7. Other experimental results of aluminium 140
3.5. Further investigation on the shape of the Haigh diagram 144
3.6. Discussion 147
3.6.1. Haigh diagram shape 147
3.6.2. Theories of the effect of mean stresses 148
3.6.3. Modelling of axial mean stresses: 150

Chapter 4. Effect of mean torsional stresses 153
4.1. Introduction 153
4.2. Historical review of the effect of the mean torsional stresses 154
4.3. Review of relevant results from the literature 167
4.4. Relationship between mean axial and torsional stresses 176
4.5. Effect of mean shear stress in multiaxial fatigue models 179
4.6. Discussion 181

Chapter 5. Multiaxial fatigue methods 187
5.1. Introduction 187
5.2. Classic fatigue methods 191
5.2.1. Worst Principal Full Range-Goodman 195
5.2.2. Von Mises Full Range-Goodman 195
5.2.3. Worst Principal Walker-Goodman 195
5.2.4. Von Mises Walker-Goodman 195
5.2.5. Worst Principal SWT-Goodman 196
5.2.6. Von Mises SWT-Goodman 196
5.3. Methods based on stress invariants 196
5.3.1. Marin 196
5.3.2. Froustey 198
5.3.3. Sines 199
5.3.4. Crossland 200
5.3.5. Kakuno-Kawada 201
5.3.6. Altenbach-Zolochevski 202
5.3.7. Vu-Halm-Nadot 203
5.3.8. Matsubara-Nishio 204
5.4. Critical Plane Methods 205
5.4.1. Stulen-Cummings (MD) 212

5.4.2. Findley (MD) 212
5.4.3. Matake (MSSR) 213
5.4.4. Yokobori 214
5.4.5. Dang Van Method (MSSR and MD) 214
5.4.6. McDiarmid (MD) 215
5.4.7. Robert (MD) 216
5.4.8. Zhang-Yao Method (MSSR) 216
5.4.9. Susmel-Lazzarin Method (MSSR) 217
5.4.10. Papuga (MD) 220
5.5. Discussion 222
5.5.1. Computational cost 222
5.5.2. Influence of mean normal stresses 223
5.5.3. Influence of mean torsional stresses 223
5.5.4. Effect of Phase Shift 224
5.5.5. Ability to use for finite life 225

Chapter 6. Analysis and discussion of multiaxial fatigue methods 231
6.1. Experimental database 231
6.2. Overall results for the entire test sample 237
6.3. Study of multi-axiality without other effects 251
6.4. Study of the effect of the phase shift 265
6.5. Study of the influence of mean axial stresses 279
6.6. Study of the influence of the mean torsional stresses 293
6.7. Discussion 306
6.7.1. Relative importance of the individual effects 306
6.7.2. Influence of mean axial stresses 307
6.7.3. Influence of mean torsional stresses 307
6.7.4. Quantities and parameters used for the formulation of the methods 308

Chapter 7. Experimental Campaign 313
7.1. Material 313
7.1.1. Introduction: selection of the material 313
7.1.2. Sensitivity to mean stresses 315
7.1.3. Elastic behaviour against mean stresses 316
7.1.4. Elasticity for low number of cycles 317
7.1.5. Low number of cycles for the fatigue limit 319
7.1.6. Homogeneity of the microstructure 320
7.1.7. Selection of the material 323
7.2. Selected material: DIN 34CrNiMo6 steel 324
7.2.1. Chemical properties and microstructure 324

7.2.2. Monotonic mechanical properties 325
7.3. Design and calculation of a multiaxial fatigue campaign 326
7.4. Axial fatigue tests 330
7.4.1. Specimens 330
7.4.2. Testing machinery of axial fatigue campaign 331
7.4.3. Experimental results on axial fatigue 332
7.4.4. Fractographic analysis 334
7.5. Torsional fatigue tests 338
7.5.1. Specimens 338
7.5.2. Testing machinery of the torsional fatigue campaign 339
7.5.3. Experimental results 341
7.5.4. Fractographic analysis 344
7.6. Mean axial and torsional stress sensitivities for the experimental campaign on DIN 34CrNiMo6 steel 347
7.7. Experimental agreement of multiaxial fatigue methods 349
7.7.1. Correlation of multiaxial fatigue methods with torsional fatigue tests 349
7.7.2. Correlation of multiaxial fatigue methods with axial fatigue tests 351
7.8. Discussion 353
7.8.1. Selection of the material and design of the experimental campaign 353
7.8.2. Axial and torsional fatigue experimental campaigns 353
7.8.3. Experimental agreement with multiaxial fatigue methods 354

Chapter 8. Development of two Multiaxial Fatigue Methods 357
8.1. Introduction 357
8.2. Modelling of torsional fatigue with mean torsional stresses 359
8.3. *"Global approach"* multiaxial fatigue method 361
8.4. Energetic multiaxial fatigue criterion 369

Chapter 9. Conclusions and Further Works 381
9.1. Conclusions 381
9.2. Further works 388

BIBLIOGRAPHY 391

Annex A: Parameters of Global Approach Method 411

Annex B: Parameters of Energetic Method 415

INDEX OF FIGURES

Figure 1-1. *Conventional Fatigue Limit* *34*
Figure 1-2. *Rotating bending machine used by Wöhler [Moore, 1921]* *43*
Figure 1-3. *Gerber's diagram [Weibull, 1961]* *44*
Figure 1-4. *Experimental results of Gough, Pollard and Clenshaw [Gough, 1951]* *47*
Figure 2-1. *S-N curve with the different fatigue regions [Castillo, 2009]* *61*
Figure 2-2. *S-N curves of JIS SNCM439 steel at different tempering temperatures [Oguma, 2004]* *62*
Figure 2-3. *Typical S-N curve in rotating bending showing abrupt knee [Nishijima, 1993]* .. *63*
Figure 2-4. *Relationship between ultimate tensile strength and Vickers hardness [Nishijima, 1993]* *64*
Figure 2-5. *Relationship between ultimate tensile strength and Vickers hardness for 18 low alloy quenched and tempered steels* *65*
Figure 2-6. *Histogram of* $\sigma'_{-1/}\sigma_{UTS}$ *and adjustment by Log-Weibull for the 18 quenched and tempered steels contained in NIMS.* *67*
Figure 2-7. *Histogram of* $\sigma'_{-1/}$ *HV and adjustment by means of Largest Extreme Value for the 18 quenched and tempered steels contained in NIMS.* *68*
Figure 2-8. *Volumetric Fatigue Limit [Pyttel, 2011]* *69*
Figure 2-9. *S-N curves of Rotating bending and torsion of a steel 4340 [Findley, 1956]* *71*
Figure 2-10. *Difference in percentage with respect to the fatigue limit as a function of the number of cycles for an AISI 4340 steel [Findley, 1956].* *72*
Figure 2-11. *Relationship between axial and torsional fatigue limits as a function of the number of cycles [Findley, 1956].* *72*
Figure 2-12. *JSME modelling for the realization of S-N curves with 14 specimens.* *74*
Figure 2-13. *Cyclic curve for a SNCM 439 steel hardened and tempered at 630ºC.* *78*
Figure 2-14. *Determination of the LCF parameter* $\sigma'_{yc0.2}$ *for steels and aluminium alloys* *80*
Figure 2-15. *Number of cycles for a cyclic plastic deformation of 0.2%.* *80*
Figure 2-16. *Cyclic and monotonic curves for steel S355J2 [Gómez, 2011]* *81*
Figure 3-1. *Representation of constant stress tests with mean stresses [Dowling, 2009B]* *85*
Figure 3-2. *Haigh diagram with the lines of theories not based on fracture or yielding [Lüpfert, 2004].* *87*
Figure 3-3. *Haigh diagram with different criteria according to ductility [Klubberg, 2011]* *88*

Figure 3-4. *Goodman diagram showing fatigue strength values for R=0 and R=-1 [Weibull, 1961].* 91
Figure 3-5. *Haigh diagram with lines corresponding to some uniaxial theories about the effect of axial mean stresses [Susmel, 2005].* 95
Figure 3-6. *Haigh diagram with experimental results of a 25CrMo4 steel [Grün, 1991] together with Dietmann, Gerber and Peterson lines.* 97
Figure 3-7. *Haigh diagram normalized with different Lüpfert lines depending on the value of parameter p [Lüpfert, 2001].* 99
Figure 3-8. *Diagram of Haigh presenting Stüssi's method [Weibull, 1961]* 102
Figure 3-9. *Haigh diagram of a 25CrMo4 steel [Grün, 1991] together with the modified Bahuaud, Dietmann and Gerber lines.* 105
Figure 3-10. *Haigh diagram with representation of the FKM standard, adapted from [Lee, 2012]* 106
Figure 3-11. *Haigh diagram with representation of the FKM regulation, and experimental data of a 30CrNiMo8 steel [Rausch, 2011].* 108
Figure 3-12. *Deformation stress diagrams with energy per cycle (a) completely reversed stresses (b) mean non-zero stress [Moore, 1924].* 109
Figure 3-13. *Comparison between Moore-Jasper's empirical method and Jasper's method for experimental results at the University of Illinois [Moore, 1924].* 112
Figure 3-14. *Haigh diagram comparing Moore and Jasper's lines with Grün's experimental results [Grün, 1991].* 113
Figure 3-15. *Haigh diagram for Ti 6Al 4V with Jasper's modified equation [Nicholas, 2002].* 115
Figure 3-16. *Walker parameter values for different types of aluminiums [Dowling, 2009A]* 117
Figure 3-17. *Adjustment of Grün experimental data [Grün, 1991] with the Smith-Watson-Topper and Walker methods* 118
Figure 3-18. *Compilation of Smith results [Smith, 1942] for unnotched ductile materials* .. 124
Figure 3-19. *Compilation of Smith results [Smith, 1942] for notched ductile materials* 125
Figure 3-20. *Compilation of Smith results [Smith, 1942] for cast irons (fragile) with and without notch* 127
Figure 3-21. *Haigh diagram normalized with compilation of experimental results of O'Connor and Morrison steels [O'Connor, 1956]* 129
Figure 3-22. *Haigh diagram normalized the experimental results of O'Connor and Morrison [O'Connor, 1956].* 130

Figure 3-23. *Haigh diagram normalized the experimental results of O'Connor and Morrison and some of the most used uniaxial criteria [O'Connor, 1956].* *131*
Figure 3-24. *Normalized Haigh diagram showing results compiled by Sines [Sines, 1959] for steels and aluminiums.* *133*
Figure 3-25. *Haigh diagram showing the effect of mean stresses for ductile materials [Klubberg, 2011].* *135*
Figure 3-26. *Haigh diagram showing the effect of mean stresses for semi ductile materials [Klubberg, 2011].* *136*
Figure 3-27. *Haigh diagram showing the effect of mean stresses on brittle materials [Klubberg, 2011]* *137*
Figure 3-28. *Haigh diagram with experimental results of Ukrainetz 0.1C ductile steel [Ukrainetz, 1960]* *139*
Figure 3-29. *Haigh diagram with experimental results of two Woodward aluminiums [Woodward, 1956].* *141*
Figure 3-30. *S-N curves for Woodward aluminiums in compression showing initiation and rupture [Woodward, 1956].* *142*
Figure 3-31. *Haigh diagram with experimental results of a D16T aluminium [Sochava, 1977].* *143*
Figure 3-32. *Axial Haigh diagram with experimental results for ferritic materials with the extreme lines of behaviour [Pallarés, 2018A].* *145*
Figure 3-33. *Axial Haigh diagram with experimental results in compression for ductile materials [Pallarés, 2018A].* *147*
Figure 4-1. *Torsional fatigue tests with mean shear stresses on SAE 3140 steels [Smith, 1939]* *156*
Figure 4-2. *Collection of torsional fatigue tests with mean shear stresses on several ductile materials [Smith, 1942]* *157*
Figure 4-3. *Aluminium 76S-T61 torsional Haigh diagrams* *158*
Figure 4-4. *Experimental results of torsional fatigue on S65A steel presented in final form by Gough and Clenshaw [Gough, 1951]* *159*
Figure 4-5. *Torsional fatigue campaign on En25 steel [Chodorowski, 1956]. Mean stresses normalized with the torsional yield strength* *160*

Figure 4-6. *Linear influence of the mean shear stress and its correlation for the fatigue data on En25 steel [Chodorowski, 1956]* *161*
Figure 4-7. *Independence of the mean torsional stress for a 0.1% Carbon steel [Ukrainetz, 1960]* *162*
Figure 4-8. *Microstructure of the 0.1% C steel [Ukrainetz, 1960]* *162*
Figure 4-9. *Wang-Miller modelling of torsional fatigue [Wang, 1991]* *165*
Figure 4-10. *Haigh torsional diagram for a 39NiCrMo3 steel [Davoli, 2003]* *166*
Figure 4-11. *Normalized maximum shear stress-alternating shear stress diagram, 25 steel and aluminium alloys represented [Pallarés, 2018B]* *169*
Figure 4-12. *Mean-shear-stress effect, represented only the tests in which the maximum shear stress is below the torsional yield strength [Pallarés, 2018B]* *170*
Figure 4-13. *Normalized torsional Haigh diagram with the experimental results of a 14S-T aluminium alloy and a VDSiCr spring steel [Pallarés, 2018B]* *172*
Figure 4-14. *Normalized torsional Haigh diagram, 25 different steel and aluminium alloys represented and the 34CrNiMo6 of this work [Pallarés, 2018B]* *173*
Figure 4-15. *Normalized Haigh torsional diagram showing eight different cast irons [Pallarés, 2018B]* *174*
Figure 4-16. *Sensitivities to mean axial and torsional stresses [Zenner, 2000]* *178*
Figure5-1. *Classic yield theories together with fatigue experimental results by Sawert shown in [Sines, 1959]* *191*
Figure 5-2. *Stress correction methods used in the classic methods presented within this Thesis* *193*
Figure 5-3. *Application scheme of the Vu-Halm-Nadot method [Vu, 2010].* *203*
Figure 5-4. *Critical plane concept in an isotropic polycrystalline material [Papadopoulos, 1997].* *206*
Figure 5-5. *Persistent fatigue-induced slip bands. [Chan, 2010]* *206*
Figure5-6. *Formation of a crack by intrusions and extrusions [Susmel, 2002]* *207*
Figure 5-7. *Actual and calculated initiation orientation of the Susmel method [Susmel, 2007]* *208*
Figure 5-8. *Measurement of load paths by the MCC and MCE. Adapted from [Li, 2009]* ... *209*
Figure 5-9. *Spherical coordinates used to search for the critical plane [Susmel, 2002]* *211*
Figure 5-10. *Influence of normal stresses and the m parameter [Susmel, 2008]* *218*

Figure 5-11. *Improvement of experimental results [Susmel, 2008]* *218*
Figure 5-12. ρ_{lim} *value that determines the maximum damage threshold of normal stresses [Susmel, 2008]* *219*
Figure 6-1. *Ideal error distribution of a multi-axial method*..... *236*
Figure 6-2. *Error distribution of Worst Pr. FR-Goodman for the entire sample*..... *241*
Figure 6-3. *Error distribution of von Mises FR-Goodman for the entire sample* *241*
Figure 6-4. *Error distribution of Worst Principal Walker R.-Goodman for the entire sample* *242*
Figure 6-5. *Error distribution of von Mises Walker R.-Goodman for the entire sample* *242*
Figure 6-6. *Error distribution of Worst Pr.Walker 0.5-Goodman for the entire sample* *243*
Figure 6-7. *Error distribution of von Mises Walker 0.5-Goodman for the entire sample*..... *243*
Figure 6-8. *Error distribution of Sines for the entire sample*..... *244*
Figure 6-9. *Error distribution of Crossland for the entire sample*..... *244*
Figure 6-10. *Error distribution of Marin for the entire sample* *245*
Figure 6-11. *Error distribution of Vu-Halm-Nadot for the entire sample*..... *245*
Figure 6-12. *Error distribution of Dang Van MSSR for the entire sample* *246*
Figure 6-13. *Error distribution of Dang Van MD for the entire sample*..... *246*
Figure 6-14. *Error distribution of Matake for the entire sample* *247*
Figure 6-15. *Error distribution of Findley for the entire sample*..... *247*
Figure 6-16. *Error distribution of McDiarmid MSSR for the entire sample*..... *248*
Figure 6-17. *Error distribution of McDiarmid MD for the entire sample*..... *248*
Figure 6-18. *Error distribution of Robert for the entire sample* *249*
Figure 6-19. *Error distribution of Zhang-Yao for the entire sample*..... *249*
Figure 6-20. *Error distribution of Susmel for the entire sample*..... *250*
Figure 6-21. *Error distribution of Papuga for the entire sample*..... *250*
Figure 6-22. *Error distribution of Worst Principal FR-Goodman in multiaxiality*..... *255*
Figure 6-23. *Error distribution of von Mises FR-Goodman in multiaxiality* *255*
Figure 6-24. *Error distribution of Worst Principal Walker R.-Goodman in multiaxiality*.... *256*
Figure 6-25. *Error distribution of von Mises Walker R.-Goodman in multiaxiality* *256*
Figure 6-26. *Error distribution of Worst Principal Walker 0.5-Goodman in multiaxiality* .. *257*
Figure 6-27. *Error distribution of von Mises Walker 0.5-Goodman in multiaxiality*..... *257*
Figure 6-28. *Error distribution of Sines in multiaxiality*..... *258*

Figure 6-29. *Error distribution of Crossland in multiaxiality* *258*
Figure 6-30. *Error distribution of Marin in multiaxiality* *259*
Figure 6-31. *Error distribution of Vu-Halm-Nadot in multiaxiality* *259*
Figure 6-32. *Error distribution of Dang Van MSSR in multiaxiality* *260*
Figure 6-33. *Error distribution of Dang Van MD in multiaxiality* *260*
Figure 6-34. *Error distribution of Matake in multiaxiality* *261*
Figure 6-35. *Error distribution of Findley in multiaxiality* *261*
Figure 6-36. *Error distribution of McDiarmid MSSR in multiaxiality* *262*
Figure 6-37. *Error distribution of McDiarmid MD in multiaxiality* *262*
Figure 6-38. *Error distribution of Robert in multiaxiality* *263*
Figure 6-39. *Error distribution of Zhang-Yao in multiaxiality* *263*
Figure 6-40. *Error distribution of Susmel in multiaxiality* *264*
Figure 6-41. *Error distribution of Papuga in multiaxiality* *264*
Figure 6-42. *Error distribution of Worst Principal FR-Goodman for phase shift effect* *269*
Figure 6-43. *Error distribution of von Mises FR-Goodman for phase shift effect* *269*
Figure 6-44. *Error distribution of Worst Pr. Walker R.-Goodman for phase shift effect* *270*
Figure 6-45. *Error distribution of von Mises Walker R.-Goodman for phase shift effect* *270*
Figure 6-46. *Error distribution of Worst Pr. Walker 0.5-Goodman for phase shift effect* *271*
Figure 6-47. *Error distribution of von Mises Walker 0.5-Goodman for phase shift effect* *271*
Figure 6-48. *Error distribution of Sines for phase shift effect* *272*
Figure 6-49. *Error distribution of Crossland for phase shift effect* *272*
Figure 6-50. *Error distribution of Marin for phase shift effect* *273*
Figure 6-51. *Error distribution of Vu-Halm-Nadot for phase shift effect* *273*
Figure 6-52. *Error distribution of Dang Van MSSR for phase shift effect* *274*
Figure 6-53. *Error distribution of Dang Van MD for phase shift effect* *274*
Figure 6-54. *Error distribution of Matake for phase shift effect* *275*
Figure 6-55. *Error distribution of Findley for phase shift effect* *275*
Figure 6-56. *Error distribution of McDiarmid MSSR for phase shift effect* *276*
Figure 6-57. *Error distribution of McDiarmid MD for phase shift effect* *276*
Figure 6-58. *Error distribution of Robert for phase shift effect* *277*
Figure 6-59. *Error distribution of Zhang-Yao for phase shift effect* *277*
Figure 6-60. *Error distribution of Susmel for phase shift effect* *278*

Figure 6-61. *Error distribution of Papuga for phase shift effect..... 278*
Figure 6-62. *Error distribution of Worst Principal FR-Goodman for mean axial stress..... 283*
Figure 6-63. *Error distribution of von Mises FR-Goodman for mean axial stress 283*
Figure 6-64. *Error distribution of Worst Pr.Walker R.-Goodman for mean axial stress..... 284*
Figure 6-65. *Error distribution of von Mises Walker R.-Goodman for mean axial stress 284*
Figure 6-66. *Error distribution of Worst Pr. Walker 0.5-Goodman for mean axial stress ... 285*
Figure 6-67. *Error distribution of von Mises Walker 0.5-Goodman for mean axial stress... 285*
Figure 6-68. *Error distribution of Sines for mean axial stress..... 286*
Figure 6-69. *Error distribution of Crossland for mean axial stress..... 286*
Figure 6-70. *Error distribution of Marin for mean axial stress 287*
Figure 6-71. *Error distribution of Vu-Halm-Nadot for mean axial stress 287*
Figure 6-72. *Error distribution of Dang Van MSSR for mean axial stress 288*
Figure 6-73. *Error distribution of Dang Van MD for mean axial stress..... 288*
Figure 6-74. *Error distribution of Matake for mean axial stress 289*
Figure 6-75. *Error distribution of Findley for mean axial stress 289*
Figure 6-76. *Error distribution of McDiarmid MSSR for mean axial stress..... 290*
Figure 6-77. *Error distribution of McDiarmid MD for mean axial stress 290*
Figure 6-78. *Error distribution of Robert for mean axial stress 291*
Figure 6-79. *Error distribution of Zhang-Yao for mean axial stress 291*
Figure 6-80. *Error distribution of Susmel for mean axial stress..... 292*
Figure 6-81. *Error distribution of Papuga for mean axial stress..... 292*
Figure 6-82. *Error distribution of Worst Principal FR-Goodman for mean shear stress..... 296*
Figure 6-83. *Error distribution of von Mises FR-Goodman for mean shear stress 296*
Figure 6-84. *Error distribution of Worst Pr. Walker R.-Goodman for mean shear stress.... 297*
Figure 6-85. *Error distribution of von Mises Walker R.-Goodman for mean shear stress ... 297*
Figure 6-86. *Error distribution of Worst Pr. Walker 0.5-Goodman for mean shear stress .. 298*
Figure 6-87. *Error distribution of von Mises Walker 0.5-Goodman for mean shear stress.. 298*
Figure 6-88. *Error distribution of Sines for mean shear stress..... 299*
Figure 6-89. *Error distribution of Crossland for mean shear stress..... 299*
Figure 6-90. *Error distribution of Marin for mean shear stress 300*
Figure 6-91. *Error distribution of Vu-Halm-Nadot for mean shear stress..... 300*
Figure 6-92. *Error distribution of Dang Van MSSR for mean shear stress 301*

Figure 6-93. *Error distribution of Dang Van MD for mean shear stress* *301*
Figure 6-94. *Error distribution of Matake for mean shear stress* *302*
Figure 6-95. *Error distribution of Findley for mean shear stress* *302*
Figure 6-96. *Error distribution of McDiarmid MSSR for mean shear stress* *303*
Figure 6-97. *Error distribution of McDiarmid MD for mean shear stress* *303*
Figure 6-98. *Error distribution of Robert for mean shear stress* *304*
Figure 6-99. *Error distribution of Zhang-Yao for mean shear stress* *304*
Figure 6-100. *Error distribution of Susmel for mean shear stress* *305*
Figure 6-101. *Error distribution of Papuga for mean shear stress* *305*
Figure 7-1. *Haigh diagram with the criterion to determine the maximum elastic stress ratio R [Nishijima, 1993]* *316*
Figure 7-2. *Graphical definition of the number of transition cycles Nt* *318*
Figure 7-3. *Typical Vickers hardness after hardening as a function of depth [Nishijima, 1993]* *321*
Figure 7-4. *Schaffler diagram for NIMS stainless steels* *322*
Figure 7-5. *Microstructure of 34CrNiMo6 steel* ***a.*** *Longitudinal section* ***b.*** *Transverse section* *325*
Figure 7-6. *"Hourglass" specimen used in axial fatigue tests. Dimensions in millimetres [Pallarés, 2018A]* *330*
Figure 7-7. *Instron 8805 MTB axial fatigue machine located at the E.T.S. de Ingenieros de Bilbao [Avilés, 2018]* *331*
Figure 7-8. *Experimental S-N fatigue curves of DIN 34CrNiMo6 steel for different stress ratios (R) [Pallarés, 2018A]* *333*
Figure 7-9. *Haigh diagram with the experimental results at* $2x10^6$ *cycles and a 2nd order polynomial interpolation showing a concave downward shape.* *334*
Figure 7-10. *Specimen microscopic cross-section fractures, showing initiation in the surface for the following cases:* ***(a)*** $R=-2;\ \sigma_a= 440$ *MPa;* $\sigma_m= 0$ *MPa; Ncycles=986,700;* ***(b)*** $R=-1;\ \sigma_a= 430$ *MPa;* $\sigma_m= 0$ *MPa; Ncycles=1,722,153;* ***(c)*** $R=-0.5;\ \sigma_a= 430$ *MPa;* $\sigma_m= 0$ *MPa; Ncycles=1,193,924 [Pallarés, 2018A]* *335*
Figure 7-11. *Fatigue fracture cross-section of a test specimen after 1,101,291 cycles with a maximum stress* $\sigma_{max}=1,040$ *MPa in a R=0.05 axial test [Pallarés, 2018A]* *336*

Figure 7-12. *Fatigue Specimen macroscopic fractures at:* ***(a)*** *R=-2; σ_a=440 MPa; σ_m=0 MPa; Ncycles=986,700;* ***(b)*** *R=-1; σ_a=430 MPa; σ_m=0 MPa; Ncycles=1,722,153;* ***(c)*** *R=-0.5; σ_a=430 MPa; σ_m=0 MPa; Ncycles=1,193,924 [Pallarés, 2018A]* *337*

Figure 7-13. *"Hourglass" specimen used in torsional fatigue tests. Dimensions in millimetres [Pallarés, 2018B]* *338*

Figure 7-14. *"LISE" machine used in the torsional fatigue campaign* *340*

Figure 7-15. *Torsional S-N curves with different leves of mean shear stress [Pallarés, 2018B]* *342*

Figure 7-16. *Torsional Haigh diagram with the experimental results at 2×10^6 cycles [Pallarés, 2018B]* *343*

Figure 7-17. *Surface crack patterns in the failed specimens:* ***a)*** *τ_a = 440 MPa; τ_m = 0 MPa; Ncycles = 1,026,120* ***b)*** *τ_a = 430 MPa; τ_m = 150 MPa; Ncycles = 812,704* ***c)*** *τ_a = 440 MPa; τ_m = 250 MPa; Ncycles = 174,792* ***d)*** *τ_a = 405 MPa; τ_m = 350 MPa; Ncycles = 709,944 [Pallarés, 2018B]* *345*

Figure 7-18. *Surface crack patterns in the failed specimen: τ_a = 340 MPa; τ_m = 500 MPa; Ncycles = 944,988 [Pallarés, 2018B* *346*

Figure 7-19. *Axial and mean shear stress sensitivity indices for the range 50,000 < Ncycles < 1,000,000 [Pallarés, 2019]* *348*

Figure 7-20. *Torsional Haigh diagram with predictions from various theories and experimental results at 2 x 10^6 cycles [Pallarés, 2018B]* *349*

Figure 7-21. *Axial Haigh diagram with predictions from various theories and experimental results at 2 x 10^6 cycles [Pallarés, 2018A]* *351*

Figure 8-1. *Proposed method in a torsional Haigh diagram together with the experimental fatigue results [Pallarés, 2018B]* *364*

Figure 8-2. *Proposed method in an axial Haigh diagram together with the experimental fatigue results [Pallarés, 2018B]* *365*

Figure 8-3. *Sketch of the uniaxial and torsional variables in terms of stress invariants [Pallarés, 2019]* *369*

Figure 8-4. *Axial Haigh diagram with the experimental results for 34CrNiMo6 steel and the predictions from the proposed energetic method, Equation (8-6).* *375*

Figure 8-5. *Haigh diagram with the experimental results for several structural steels and their predictions from the proposed method, Equation (8-6).* *377*

Figure 9-1. *Multiaxial fatigue method in the medium fatigue life range [Mamiya, 2011]* 389

INDEX OF TABLES

Table 2-1. *Low alloy quenched and tempered steels and their static and fatigue properties in rotating bending and reverse torsion.* *66*
Table 2-2. *Models of S-N curves most used in the literature [Castillo, 2009].* *70*
Table 2-3. *Incremental passage tests for a steel SNCM 439 hardened and tempered at 630ºC [Nishijima, 1993]* *77*
Table 3-1. *Experimental values of Lüpfert parameter p for structural steels NRIM JIS standards [Nishijima, 1993]* *100*
Table 3-2. *FKM recommended values for parameters a_M and b_M as a function of material type [Lee, 2012]* *107*
Table 3-3. *Fatigue tests used in the characterization of the axial Haigh diagram shapes [Pallarés, 2018A]* *144*
Table 4-1. *Torsional fatigue tests on aluminiums and steels [Pallarés, 2018B]* *167*
Table 4-2. *Torsional fatigue tests on cast irons [Pallarés, 2018B]* *168*
Table 6-1. *Database of tests by Papuga [Papuga, 2011A]* *233*
Table 6-2. *Global results for the entire database (422 tests)* *238*
Table 6-3. *Obtained results for multiaxiality without other effects (134 tests)* *252*
Table 6-4. *Obtained results for phase shift effect without mean stress (52 tests)* *266*
Table 6-5. *Obtained results for the mean axial stress effect (97 tests)* *280*
Table 6-6. *Obtained results for the mean torsional stress effect (42 tests)* *294*
Table 7-1. *Table of equivalences between standards of Japanese NIMS steels* *314*
Table 7-2. *Mechanical characteristics of Japanese steels studied by NIMS* *315*
Table 7-3. *Sensitivity to static mean stresses* *315*
Table 7-4. *Maximum elastic R (Stress ratio)* *317*
Table 7-5. *Ranking according to the number of transition cycles Nt* *319*
Table 7-6. *Ranking according to the number of cycles in the fatigue limit* *320*
Table 7-7. *Values of ideal critical diameters [Nishijima, 1993]* *321*
Table 7-8. *Rankings in each of the five criteria and average index* *323*
Table 7-9. *Chemical composition of 34CrNiMo6 steel (at.%)* *324*
Table 7-10. *Individual monotonic tests* *325*

Table 7-11. *Design of a multiaxial fatigue campaign with various combinations of stress. Legend: Green colour means a fixed value; Blue indicates a test result* *327*

Table 7-12. *Experimental procedure for the S-N curves and fatigue limits of pure torsional fatigue* *328*

Table 7-13. *Experimental procedure for the S-N curves and fatigue limits of mean axial + reversed torsional fatigue tests* *329*

Table 7-14. *Experimental procedure for the S-N curves and fatigue limits of mean torsion + reversed axial fatigue tests* *329*

Table 7-15. *Obtained fatigue strengths at $2x10^6$ cycles for the different stress ratios together with the α and β Basquin parameters of the inclined part of the S-N curves* *333*

Table 7-16. *Obtained torsional fatigue strengths at 2×10^6 cycles* *342*

Table 7-17. *Relative errors of the multiaxial fatigue methods for torsional fatigue at 2×10^6 cycles [Pallarés, 2018B]* *350*

Table 7-18. *Relative errors of the multiaxial fatigue methods for axial fatigue at 2×10^6 cycles [Pallarés, 2018A]* *352*

Table 8-1. *Parameters of the proposed method applied to 34CrNiMo6 steel* *364*

Table 8-2. *Relative errors in τ_a (%) of the proposed physical theory for $N = 2x10^6$ cycles. Positive values mean conservative results predicted by the theory, negative values non-conservative results.* *365*

Table 8-3. *Relative errors in σ_a (%) of the proposed physical theory for $N = 2 \times 10^6$ cycles. Positive values mean conservative results predicted by the theory, negative values non-conservative results.* *366*

Table 8-4. *Parameters of the proposed method applied to 34CrNiMo6 steel* *373*

Table 8-5. *Relative errors (%) of the proposed physical theory for $N=2x10^6$ cycles. Positive values mean conservative results predicted by the theory, negative values non-conservative results.* *375*

Table 8-6. *Parameters of the proposed method applied to several structural steels extracted from the literature. The values of τ_0 were obtained by means of the Zenner formula, Equation (8-11)* *376*

NOMENCLATURE AND ACRONYMS

a	generally designates a multiaxial fatigue parameter
A	elongation at break (%)
A_0	nominal area of the tensile test specimen
A_f	area of the tensile test specimen in the breaking section
AISI	*American Iron and Steel Institute* (USA)
AFNOR	*Association Française de Normalisation* (Francia)
ASM	*The Materials Information Society* (ant. *American Society for Metals*) (internacional)
ASME	*American Society of Mechanical Engineers* (USA)
ASTM	*American Society for Testing and Materials* (USA)
α	Basquin S-N curve parameter; Nicholas parameter for stored energy
b	generally designates a multiaxial fatigue parameter
BS	*British Standards* (UK)
β	Basquin S-N curve parameter
γ	Walker stress correction parameter
Λ	parameter of rupture of the symmetry in the axial Haigh diagram of the multiaxial fatigue energy method developed
c	generally designates a multiaxial fatigue parameter
CPA	*critical plane analysis* methods
d, D	generally designates a diameter
DIN	*German Institute for Standardization* (Alemania)
E	Young's module
ε_{ur}	real fracture deformation, ductility
ε_{ut}	engineering deformation at break
HB	Brinell hardness
HCF	*high-cycle* fatigue
HRC	Rockwell-C hardness
IA	methods based on *integral analysis*
IDSA	multiaxial fatigue analysis methods based on stress or deformation invariants (*Ilyushin deviatoric space analysis*)
ISO	*International Organization for Standardization* (internacional)
I_1	first invariant of the stress tensor
I_{1a}	amplitude of the first invariant of the stress tensor
I_{1m}	mean value of the first invariant of the stress tensor
$I_{1,max}$	maximum value of the first invariant of the stress tensor
$I_{1,max}$	minimum value of the first invariant of the stress tensor

J_2	second invariant of the stress deviator tensor
J_{2a}	amplitude of the second invariant of the stress deviator tensor
J_{2m}	mean value of the second invariant of the stress deviator tensor
$J_{2,max}$	maximum value of the second invariant of the stress deviator tensor
$J_{2,min}$	minimum value of the second invariant of the stress deviator tensor
κ	fatigue ratio: σ_{-1}/τ_{-1}. For a von Mises material, it takes a value of $\sqrt{3}$. For a Rankine material (brittle), it takes a value of 1.
JIS	*Japanese Industrial Standards* (Japan)
JSA	*Japanese Standards Association* (Japan)
JSME	*Japanese Society of Mechanical Engineering* (Japan)
l, L	generally designates a length or a distance
L_0	reference *length* in the tensile test (5 times the diameter of the specimen)
LCF	*low-cycle* fatigue
m	*Normal stress influence parameter in Susmel method*
m_{Walker}	*Walker mean stress correct-ion exponent*
MCC	Minimum Circumscribed Circle (calculation method of shear stress amplitude)
MCE	Minimum Circumscribed Ellipse (calculation method of shear stress amplitude)
MD	multiaxial fatigue method based on the critical plane of greatest damage defined by a function (*maximum damage*)
MEF	finite element method
MSS	multiaxial fatigue method based on the critical plane of *maximum shear* stress
MSSR	multiaxial fatigue method based on the critical plane of *maximum shear stress* range
M_σ	sensitivity to axial mean stresses
M_τ	sensitivity to mean torsional stresses
p	Lüpfert parameter for mean stress
v	Poisson coefficient
N	duration in number of cycles
Nf	number of test specimen fatigue limit cycles
N_a	amplitude of stress normal to the critical plane
N_m	mean value of the stress normal to the critical plane
N_{max}	maximum value of the stress normal to the critical plane
N_{min}	minimum value of the stress normal to the critical plane
N_t	number of transition cycles

NIMS	*National Institute for Material Science* (Japan)
NRIM	*National Research Institute for Metals* (Japón). Renamed NIMS in 2001.
r	usually designates a radius or a distance
R	generally, load ratio or stress ratio; sometimes radius and deviation parameter in Excel
R_a	average roughness
R_σ	axial stress ratio
R_τ	shear stress ratio
Rm	ultimate tensile strength (σ_{uts})
run-out	*number* of cycles at which a test is interrupted if the specimen has not previously ruptured
Rz	average roughness at depth
S_1	Maximum principal stress
SAE	*Society of Automotive Engineers*
SEM	electron microscope (*scanning electron microscope*)
σ	in general designates stress
σ_0	fatigue limit with repeated axial stress, R_σ = 0 (*repeated axial fatigue limit*)
$\sigma_{0.05}$	fatigue limit for a R_σ = 0.05
σ_{-1}	fatigue limit with alternating axial stress, R_σ = -1 (*fully reversed axial fatigue limit*)
σ'_{-1}	fatigue limit of polished specimens in the bending specimen test, R_σ = -1 (*fully reversed bending fatigue limit*)
σ_a	alternating component of a variable axial stress
σ_f	fracture stress
$\sigma_{f,B}$	fracture stress corrected by Bridgman's formula
σ_H	hydrostatic stress
$\sigma_{H,a}$	amplitude of hydrostatic stress
$\sigma_{H,m}$	mean value of the hydrostatic stress
$\sigma_{H,max}$	maximum value of the hydrostatic stress
$\sigma_{H,min}$	minimum value of hydrostatic stress
σ_K	fatigue strength in the S-N knee (conventional fatigue limit)
σ_m	mean value of the axial fatigue stress
σ_{max}	maximum axial stress
σ_{min}	minimum axial stress
σ_{uts}	*ultimate tensile strength* (engineering)
σ_{yp}	monotonic *yield point* stress
$\sigma_{yp\ 0.02}$	monotonic *yield* stress calculated with a 0.02% plastic strain

σ'_{yp}	cyclical yield stress
$\sigma'_{yp\ 0.02}$	cyclical yield stress calculated with a 0.02% plastic strain
τ	generally denotes shear stress
τ_{-1}	torsional fatigue limit, R_τ = -1 (*fully reversed torsional fatigue limit*)
τ_0	repeated fatigue limit in torsion, R_τ = 0 (*repetated torsional fatigue limit*)
τ_a	alternating component of a variable torsional stress
τ_a^*	alternating shear stress in the critical plane
τ_m	mean component of a variable torsional stress
τ_m^*	mean shear stress in the critical plane
τ_{min}	minimum value of the torsional stress in fatigue
τ_{max}	maximum value of the torsional stress in fatigue
τ_{max}^*	maximum shear stress in the critical plane
τ_{yp}	monotonic shear yield strength
τ_{uss}	ultimate shear strength
$W_{compression}$	energy stored in compression (Nicholas method)
$W_{tensile}$	energy stored in tension (Nicholas method)
W_D	distortion elastic energy
W_H	elastic energy of increase of volume (hydrostatic)
Z	reduction of area (%)

SECTION I

Background, general aspects, introduction

Chapter 1:

THESIS OBJECTIVES AND METHODOLOGY

CHAPTER 1. OBJECTIVES OF THE THESIS AND METHODOLOGY

1.1. Context and direct background

The subject and the work carried out in this Thesis are part of the research lines of the ADM group (Mechanical Analysis and Design) of the Department of Mechanical Engineering of the UPV/EHU. This is a consolidated Research Group directed by Professor Avilés, recognised and financed as such by the Basque Government for more than ten years and until 2021 (2015 call) and whose antecedents go back to its previous existence as a Research Group of the UPV/EHU from 1998. The general research topic is very broad and deals with calculation methods for machine design and therefore also includes the development of fatigue analysis methods, especially in two lines: one on multiaxiality and the other on the effect of various surface treatments on the fatigue behaviour of metals, which is specifically where this Thesis is included.

The phenomenon of Fatigue is undoubtedly one of the most deeply researched topics in engineering. Its importance lies in the fact that it affects a large number of parts in engineering, with sometimes catastrophic failures, such as those occurring in Liberty series ships or Comet aircraft.

Material Fatigue could be defined as a process of progressive and localized change in a material subject to conditions that cause fluctuating stresses at one or more points and that may end in cracks or complete fracture after a sufficient number of fluctuations.

However, *"it could be said of research in Fatigue that it belongs to those areas of research in which, as in Economics or Sociology, great efforts have produced a surprisingly low amount of knowledge.* [Freudenthal, 1974].

Since the 19th century, with the development of railways and structures subjected to dynamic stresses (bridges, etc.), an attempt has been made to tackle the phenomenon of fatigue on the part of engineers. Wöhler's [Wöhler, 1870] research made it possible to determine the existence of the so-called "fatigue limit", a theoretical limit of stress amplitude that allows an infinite life to be obtained. With this criterion of "infinite life" most machines are usually designed, greatly simplifying the calculations for the engineer [Sonsino, 2007].

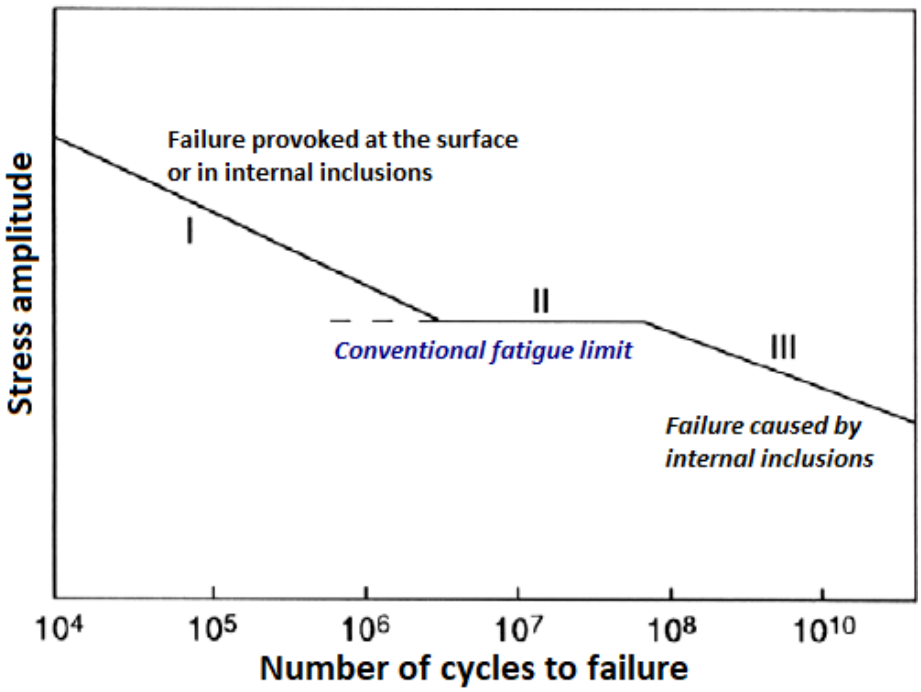

Figure 1-1. *Conventional Fatigue Limit*

The fatigue limit exists in a multitude of metallic materials, especially in ferritic and superalloys, and is usually located around 10^6 cycles (Fig 1.1). Materials that do not have a fatigue limit, such as aluminium, have this value normalized in a certain number of cycles. [Sonsino, 2007].

Currently, due to the demands of some machines, a new concept has emerged, called the "very high cycle" fatigue limit, located around 10^9 cycles. The phenomena that create this second fatigue limit are fundamentally caused by internal imperfections of the material (mainly inclusions); while the causes of the conventional fatigue limit have other causes different from the internal ones: persistent sliding bands (movement of dislocations), pores, surface defects, and alpha particles in the case of double-phase Titanium [Chan, 2010].

In the present work, life will only be analysed taking into account this conventional fatigue limit, mostly used in current engineering codes [Sonsino, 2007]. In other words, only the fatigue limit corresponding to the first change of slope, in the range of 10^6 cycles, will be taken into account.

1.2. Organisation of the Thesis

The present Thesis consists of 9 chapters divided into 2 sections. ***The Section I: Background, general aspects, introduction*** starts with the chapter named ***Objectives and Methodology***, a brief introduction about the high cycle fatigue is presented, together with a historical review of the most important milestones achieved in the fatigue field, and especially in the multiaxial fatigue. The objectives of the Thesis are presented next, taking into account the current state

of the art. Moreover, the way of dealing with the multiaxial fatigue within this Thesis will be described, with a new approach based on non-aprioristic assumptions.

The second chapter, ***General aspects of metal fatigue***, is an introduction regarding the high cycle fatigue, the fatigue strength and the fatigue limit. Some of the most used concepts are explained, and some empirical correlations are presented. A physical explanation of the surface and volumetric fatigue limits are presented, which will be furtherly developed in successive chapters.

The following chapter deals with the ***Effect of mean axial stresses***, which is historically the most studied and important effect in the fatigue field. If a multiaxial fatigue method is to be developed, the mean axial stresses have to be taken into account properly. A great deal of experimental results is presented together with the physical theories, including those related to critical planes and energetic theories. A special emphasis on mean compression stresses and the shape of Haigh diagrams are taken into account.

In the multiaxial fatigue field, the ***Effect of mean torsional stresses*** is a controversial subject. An extensive study of this problem is presented in chapter 4, comparing some of the most used theories with experimental results. The shape of the Haigh diagram reveals some important characteristics to be taken into consideration for the development of multiaxial fatigue methods. A further comparison between the effect of mean axial and mean torsional stresses is presented, leading to conclusions of paramount importance which will be taken into account in the mathematical formulation of the multiaxial fatigue criteria.

The fifth chapter presents the ***Multiaxial fatigue methods***, showing the most popular criteria, including the ones based on stress invariants, the critical plane methods, and the ones based on the integral approach. Moreover, some classic methods are also presented, based on the experience in the aeronautical field of the author of the Thesis. The formulations are presented together with some qualities of the methods for their application to the mean axial and mean torsional stress problems.

The ***Section II: research work performed*** starts with the chapter devoted to the ***Analysis and discussion of multiaxial fatigue calculation methods***, in which the classic and advanced multiaxial fatigue criteria are compared with experimental results taking into account 4 different effects: multiaxility, phase shift, and mean axial and torsional stresses. Moreover, the overall results for the entire test sample are also shown. A subsequent discussion will allow to infer some interesting features of the different multiaxial fatigue methods.

In chapter 7 the ***Experimental campaign*** is described with the previous design and the static and fatigue tests. It must be noted that the design of the campaign, which started with the selection of the material, was performed taking into account the results of other researchers on steels. Finally, the results are shown in graphics and tables in order to enhance the comprehension for the readers.

The chapter 8 describes the ***Development of two multiaxial fatigue methods***, which have been published in Q1 journals. The first one is an extension of the Crossland method, using the balance of elastic distortion energy proposed by Marin. The second criterion takes into account the physics of the fatigue problem and is purely based on energetic considerations. The process of

development of the methods is described in this chapter, together with the agreement with the experimental results.

The final chapter includes the ***Conclusions and Further Works***. The conclusions are summarized after a discussion process which has been performed all along the Thesis. A great deal of further works is described, as the new methodologies can be further developed in order to be applied to limited number of cycles. Moreover, testing for some load cases could not be completed, so that more publications can be published in a future to further develop and validate the methodologies presented within this Thesis.

1.3. General objectives of the research and particulars of this Thesis

The aim of this Thesis is the development of original models that reflect the fatigue behaviour of a quenched and tempered 34CrNiMo6 steel and similar materials such as structural and mild steels and aluminium alloys among others, widely used in the engineering field for fatigue related applications.

An aspect of paramount importance in the engineering field is the mean axial stress effect, as a large number of structures deal with uniaxial loads. If a multiaxial fatigue method is to be developed, the mean stress effect even in uniaxial fatigue must be properly modelled. So far, these methodologies have been focused on multiaxiality itself, somehow ignoring the uniaxial problem as remarked by Papuga in his review [Papuga, 2011A]. Therefore, one of the specific objectives is to perform a research regarding the influence of mean axial

stresses in axial fatigue. In order to achieve this goal, the following works must be conducted:

- Collect experimental results from the literature regarding uniaxial fatigue with mean loads and postprocess the experimental data in terms of Haigh diagrams, observing the different geometric shapes of ductile and brittle materials for both the tensile and compressive zones.
- Desing and perform an extensive uniaxial fatigue campaign on 34CrNiMo6 steel specimens, including tests on the compressive zone, and obtanining the S-N curves and the axial fatigue limit for each data groups.
- Perform a proper mathematical modelling of the mean axial stress effect searching for a correlation with parameters based on physical considerations (i.e. energetic).
- Incorporate the mean axial stress effect parameters into the proposed multiaxial fatigue original models.
- Validate the mathematical modelling with experimental results on similar ductile materials such as mild and structural steels and aluminium alloys from other researchers.

Amongst the researchers in multiaxial fatigue, there is no unanimous opinion in the mean shear stress effect, there being two schools of thought: one considers that this influence is negligible in the fatigue limit zone, while the other makes that influence dependent upon the ductility of the material. Thus, another of the specific objectives is to perform a study of the influence of mean shear stress on

torsional fatigue. With this objective in mind, the following tasks must be undergone:

- Gather available experimental results from previous works regarding torsional fatigue and postprocess the experimental data in terms of Haigh torsional diagrams, making a distinction between ductile and brittle materials.
- Determine the differences and similarities between the mean axial and torsional stress effect, paying attention to the geometric shapes on the Haigh diagrams.
- Desing and perform an extensive test campaign[1], including mean and variable torsion on 34CrNiMo6 steel specimens obtanining the S-N curves and the torsional fatigue limit for each set of data.
- Perform a proper mathematical modelling of the mean shear stress effect on torsional fatigue searching for a correlation with parameters based on physical considerations (i.e. energetic).
- Incorporate the torsional fatigue modelling through parameters into the proposed multiaxial fatigue original models.
- Validate the mathematical modelling with experimental results on similar ductile materials such as mild and structural steels from other researchers.

Regarding the multiaxial fatigue methods, no one is recognized as clearly superior to the others. This problem is aggravated because in the current

[1] The multi-axial tests were carried out in the LAMEFIP laboratories of ENSAM Bordeaux.

literature there are few comparative analyses between HCF multiaxial fatigue methods, among which the following stand out: [Papadopoulos, 1997], [Wang, 2004], [Papuga, 2011A]. Moreover, the latter has generated a great controversy in the world of fatigue research as some of the methods were not implemented in their latests forms and the way of calculating the amplitude of shear stress did not use the “Minimum Circunscribed Ellipse” method. The last specific objective of this work is to determine which are the multiaxial fatigue methods with the best experimental correlation in the range of "high cycles" or HCF, so that the following works are to be performed:

- Collect the tests used in [Papuga, 2011] and other authors in order to create a database which could be managed by a fatigue calculation program.
- Program all the current methods, including those not included in the Papuga comparison, such as the uniaxial fatigue criteria widely used in the industry and the latest multiaxial fatigue methods such as the one by Vu-Halm-Nadot [Vu, 2010] and Zhang [Zhang, 2010] among others.
- Implement the calculation of the amplitude of the shear stress amplitude with the "Minimum Circumscribed Ellipse" (MCE) methodology, which offers an improvement in the agreement with experimental results for out-of-phase cases over the "Minimum Circumscribed Circumference" (MCC), which is the one used by Jan Papuga in his software.
- Perform a comparative analysis of the multiaxial fatigue models in HCF valid for ductile materials and inferring the necessary features to develop original fatigue models taking into account the most important aspects,

namely the mean axial and torsional stress effects, the phase shift effect and the multiaxiality.

- Compare the most representative and widely used multi-axial fatigue criteria with the ones proposed within this Thesis for the experimental campaign on 34CrNiMo6 steel including axial and torsional tests. Extend the comparison to data of similar ductile materials such as steels and aluminiums from other authors.

1.4. Historical Evolution of Multiaxial Fatigue

In this section there will be a brief historical review of Fatigue with special attention to Multiaxial Fatigue, which is essential to adequately address such a complex problem and in which engineers continue to show conflicting views [Papuga, 2011B], [Susmel, 2011].

The history of fatigue begins with Albert according to several authors [Schütz, 1996], who published in Germany in 1837 the first known tests about the failure in service of lifting chains in the Clausthal iron mines caused by the repetition of small value loads.

The need to study fatigue arose associated with the rapid progression of the railway in the 19th century, with extremely serious accidents such as the one that occurred in Versailles in 1842, caused by a type of rupture totally unknown to engineers and which differed greatly from rupture due to static stresses. The cause of these failures was not immediately recognized, and among the initial explanations were the "crystallization of the material" going from a "fibrous"

and ductile structure to a "crystalline and fragile due to vibrations or terrestrial magnetism, among other probable reasons" [Moore, 1921], [Schütz, 1996].

Between 1858 and 1870, August Wöhler, who worked as a railway engineer in Frankfurt am Oder (Germany), conducted an extensive test campaign, which half a century later remained the most important ever conducted [Moore, 1921]. Wöhler himself perfected his fatigue machines, performing bending, axial and torsional fatigue tests, the latter being biaxial, and therefore the first multi-axial tests.

Whöler drew important conclusions from his work, including the detrimental effect of mean tensile stresses, and fatigue design recommendations for finite life. However, their results were presented in tables and not in the S-N curves that are currently used for design. His contribution has been fundamental in the history of fatigue, not only as a pioneer but also with an approach that could even today be described as modern in much of his work.

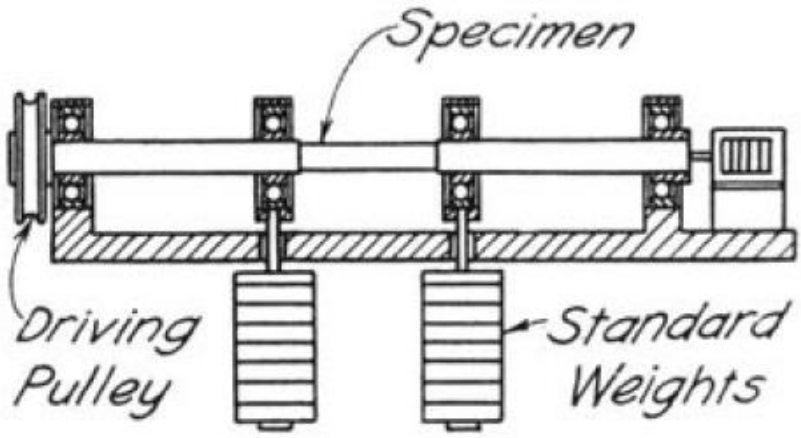

Figure 1-2. *Rotating bending machine used by Wöhler [Moore, 1921]*

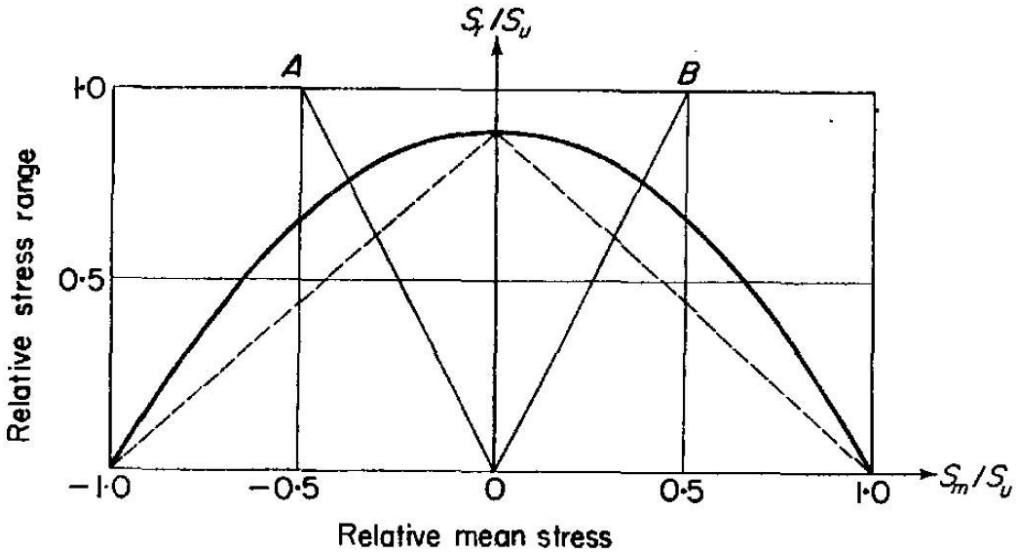

Figure 1-3. *Gerber's diagram [Weibull, 1961]*

Using Wöhler's work, Gerber proposed in 1874 [Gerber, 1874] the first mathematical function to take into account the effect of mean stresses by means of the "Gerber parabola" (1.1), whose objective was not the search for abstract truth, but that its line could be used for mechanical design:

$$\sigma_{\max} = \frac{1}{2} \cdot R \cdot \sqrt{\sigma_{UTS}{}^2 - n \cdot \sigma_{UTS} \cdot R} \qquad (1\text{-}1)$$

This modeling had a great influence on its timing as it showed an excellent fit with the available experimental data [Weibull, 1961], although it was used dogmatically by some authors such as Bauschinger, as quoted in [O'Connor, 1956], who considered it sufficiently proven and presented calculations apparently as experimental results, leading to confusion to other researchers in the fatigue field.

This would be one of the first times in the field of fatigue in which one concept creates confusion, and leads other researchers to consider that behind a mathematical function can be expressed a general fatigue case behavior for all materials.

However, Bauschinger [Bauschinger, 1886] made an excellent contribution to fatigue by introducing the concept of fatigue limit, which has been used so much in Machine Design. However, nowadays the concept of fatigue strength is more frequently used for a certain number of cycles, due to the fact that the behavior of some materials such as bearing steels suffer from a decrease of the strength in the range of the gigacicles, mainly caused by the initiation provoked by internal defects.

In 1903, one of the major advances in fatigue research came about thanks to Ewing and Humphrey's discovery of slip bands under the microscope. This advance meant a transcendental change, as stated in the report of the University of Illinois [Moore, 1924].

In 1910, and using Wöhler data from more than 40 years earlier, Basquin [Basquin, 1910] proposed the first modeling of S-N curves, representing linearly in a logarithmic diagram the amplitude of stress and the number of cycles. This function, although in the author's words "exponential law," is better known as the potential function [Weibull, 1961], and is still used in engineering today.

$$S = b \cdot N^{-a} \tag{1-2}$$

During the 1920s, researchers Moore, Koomer, Howell and Jasper at the University of Illinois, with the collaboration of a major consortium of

companies and public agencies, conducted a series of groundbreaking research, including the effects of axial and torsional mean stresses [Moore, 1923], [Moore 1924], [Moore, 1925]. Using these experimental and other own results on steels, Smith [Smith, 1939] proposed for the first time a law to collect the effect of mean torsion, with a clearly empirical approach, showing a low dependence on mean torsional stresses.

$$\tau_{\max} = \frac{\tau_{-1} \cdot \left(7 \cdot R_{\tau} + 15\right)}{8} \tag{1-3}$$

In 1924, the swede Palmgren presented in a single article the linear relation of sums of damage, known as Palmgren-Miner's law, and his proposal for a four-parameter S-N curve, which allows a better extrapolation. This formulation was popularized by Weibull in the 1950s.

$$S = Se + b \cdot (N + B)^{-a} \tag{1-4}$$

The first multiaxial fatigue theories date back to the 1930s, with pioneering studies by Gough and Pollard [Gough, 1935] in the United Kingdom, and later in the early 1940s by the Japanese Nishihara and Kawamoto [Nishihara, 1945]. Both research teams were the first to perform combined bending-torsion tests without mean stresses. The Gough-Pollard ellipse quadrant (1.5), of eminently empirical origin, and without taking into account the effect of mean stresses, constitutes the first multi-axial formulation of ductile materials:

$$\left(\frac{\sigma_a}{\sigma_{-1}}\right)^2 + \left(\frac{\tau_a}{\tau_{-1}}\right)^2 = 1 \tag{1-5}$$

Subsequently this formulation was generalized by means of the ellipse arch for ductile and fragile materials (1.6).

$$\left(\frac{\tau_a}{\tau_{-1}}\right)^2+\left(\frac{\sigma_a}{\sigma_{-1}}\right)^2\cdot\left(\frac{\sigma_{-1}}{\tau_{-1}}-1\right)+\left(\frac{\sigma_a}{\sigma_{-1}}\right)\cdot\left(2-\frac{\sigma_{-1}}{\tau_{-1}}\right)=1 \qquad (1\text{-}6)$$

This formulation was very useful and successful in experimentally correlating a very extensive test campaign, presented in its final form by Gough and Clenshaw [Gough, 1951]. Figure 1-4 shows the ellipse arc in a continuous line and the ellipse arc in a dotted line.

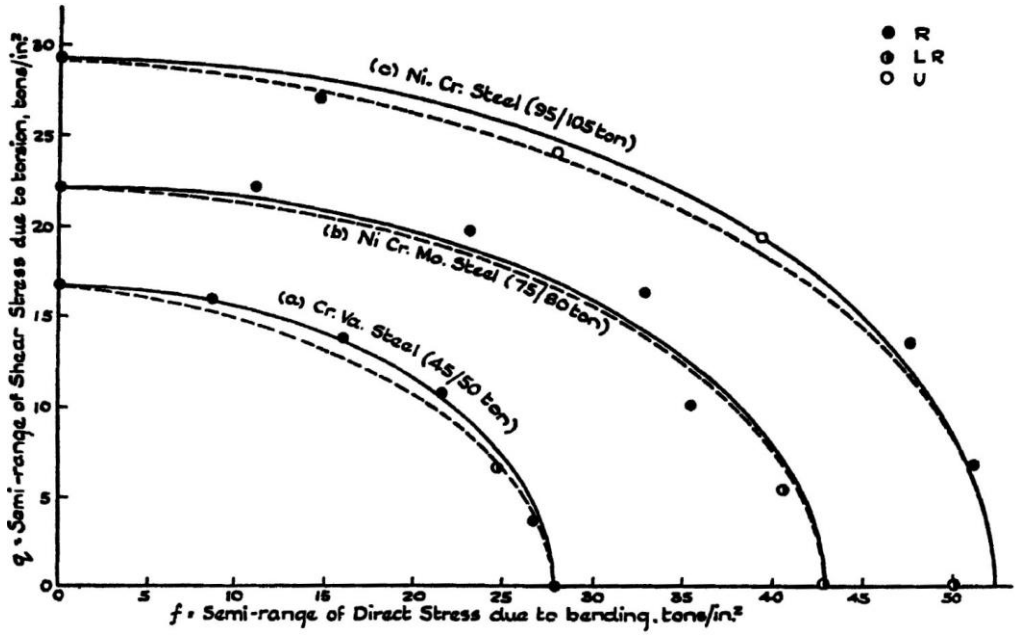

Figure 1-4. *Experimental results of Gough, Pollard and Clenshaw [Gough, 1951]*

In 1939, Orowan [Orowan, 1939] applied the 1903 experimental observations of the slip bands to create the theory of dislocations applied to the field of fatigue. This theory predicts no effect of mean stresses on fatigue strength, and was justified aposteriori with experimental results on extremely ductile ferrous materials. However, this theory did not show a good correlation with current engineering materials.

In 1942 Smith, of the University of Illinois, presents one of the works [Smith, 1942] with the greatest impact in terms of fatigue design, especially concerning mean stresses. Smith compiled and analyzed a large base of experimental results that allowed him to issue the following recommendations regarding ductile materials:

- In tensile axial mean stresses and ductile materials, Goodman's modified line. For compression, it was recommended to use a horizontal line whose height outside the uniaxial fatigue limit at R=-1.
- With respect to the mean torsional stresses: their influence begins to appear for maximum torsional values above 80% of the shear yield stress. This, according to the author, is due to the different criteria used by the authors to determine the yield stress in pure shear. Smith finally points out that the influence of mean shear stresses is negligible for ductile materials when the maximum torsion value is less than the elastic limit of torsion.

These premises remain in force, and are reasonable recommendations for fatigue design. However, they have been used dogmatically by some authors, hindering and delaying the development of new methodologies.

After the Second World War, the first international symposium on metal fatigue was held in Australia in 1946, constituting the first international meeting of experts in Fatigue. Most articles referred to service experience during the Second World War, showing important lessons learned and novel applications in the face of increasing demands in times of war.

However, the most important development could take place in the 1950s. It is at this time when combined bending-torsion tests with mean stresses begin to be carried out, highlighting the experimental campaigns subsidised by NACA and carried out by Findley on steel and aluminium. In the mid-1950s, the available uniaxial and multi-axial test database comprised several aeronautical aluminiums, carbon and low alloy quenched and tempered steels, as well as cast irons, covering to a large extent the entire possible ductility range of engineering metals. Therefore, there was already a sufficient experimental basis for a more complex multi-axial fatigue theory, taking into account the effects of mean axial and torsional stresses.

The first multiaxial fatigue function is proposed by Stulen and Cummings, which reflects that fatigue damage is mainly a consequence of the shear stress amplitude, facilitated by the maximum normal stresses (1.7):

$$\tau_a^*(\varphi,\theta) + \alpha_F \cdot N_{\max}^*(\varphi,\theta) \qquad (1\text{-}7)$$

When this function is applied to the plane of maximum damage, it becomes Findley's critical plane method [Findley, 1959].

At the first International Fatigue Congress in 1956, Findley, Marin (USA) and Crossland (UK) presented respectively the first three multiaxial fatigue methods applicable to a general multiaxial case with mean axial and torsional stresses. The first two authors published their theories supported by a wide range of experimental results and different materials. Marin also applied his method on an extensive collection of experimental results.

In the discussion held during the conference, the researchers on multiaxial fatigue concluded that their theories were obviously incomplete, and that they should be improved in the future. Findley's theory was praised as being dependent on mean shear stresses, which was experimentally supported by the experimental results of Chodorowski, who showed a dependence of mean shear stresses for the cyclic torsion problem even at values below monotonic plasticity.

In the following decades, during the 1970s and 1980s, the development of new methodologies and the publication of experimental results focused primarily on Germany. Thanks to these German researchers, including Baier, Paysan, Nolte and Heidenreich, we can now compare multi-axial theories with experimental results for axial-torsional fatigue with mean axial or torsional stresses.

1.5. Current state of the art

In recent years, it could be said that there are hardly any experimental results from new tests in the literature. This fact, which may seem surprising, is not so when one considers the high cost of an increasingly expensive materials testing

campaign. As an example we could cite those made in France and Italy on Inconel 718, and published in a standardized way to avoid its diffusion [Filippini, 2010], [Bonnand, 2011].

Nor has there been a breakthrough since the 1950s in the development of methodologies. Among the best known: Crossland, Marin, Sines, Findley and Dang Van, only the latter has been developed since the early 70s.

Multiaxial fatigue characterization could be said to be indispensable since there is no method of calculation clearly superior to the others. This problem is aggravated because in the current literature there are only a few samples of comparative analysis between HCF multiaxial fatigue methods, among which the following stand out:

- Papadopoulos in 1997, which mainly addresses his method and compares it with some of the early multi-axial methods with a rather limited experimental base. He also dismisses the mean shear stress effect using the experimental results of 1939 by Smith. [Papadopoulos, 1997].
- Wang in 2003, with a mainly qualitative comparison, in which only the methods of Sines, Gough, Lee and McDiarmid are analysed. [Wang, 2004].
- Papuga in 2011, an ambitious comparison with practically all current methods and an extensive, well-referenced database [Papuga, 2011A].

This last comparison, by the Czech author Jan Papuga, generated a great controversy in the world of fatigue research. On the one hand it showed that some of the advanced methods developed in the early years did not produce

good results (Matake, Dang Van). On the other hand, it showed that methods that did not take into account mean torsional stresses had worse results for tests in which static torsion was applied.

The comparisons between methods are not very profuse, and the last of them, performed in 2011 by Papuga [Papuga, 2011A] on a very extensive database, generated a bitter discussion between this and another researcher, Professor Luca Susmel, who accused him of making this comparison with the sole objective of demonstrating that his method was "the best".

Undoubtedly, the scientific debate has led to great advances, and the field of fatigue cannot be excluded from it. Theories are often presented as what the author thinks the damage represents in fatigue, forgetting their correlation with empirical results.

The sciencific discussion between Papuga and Susmel is undoubtedly one of the most valuable pieces in the Fatigue field. Papuga focused his arguments on experimental results and on publishing all results openly, so that if there was a mistake, it could be amended [Papuga, 2011B]. However, Susmel merely offered a graph showing the benefits of his method without indicating any reference to those tests, and urged the reader to "completely dismiss all observations and conclusions made by Dr. Papuga" [Susmel, 2011].

On the other hand, today there are several open debates regarding Multiaxial Fatigue. One of them is the effect of the mean torsional stresses. Several authors dogmatically defend their lack of influence, even ignoring experimental results

widely recognized and cited in the literature and carried out by excellent research teams.

However, in all available literature there is no cyclic torsion test with mean torsional stresses for ductile quenched and tempered steels with ultimate strength values close to 1200 MPa. On the other hand, there is no recent data from a torsional Haigh diagram sufficiently populated to determine a mathematical law that unequivocally adjusts the data.

1.6. Towards a new multiaxial fatigue method

It seems evident that if there are so many methodologies, it is because none has obtained a clear advantage over the others. The reality is that within the multiaxial fatigue research world there are many particularities with respect to other fields of research, especially a series of "red lines" such as the negligible influence of mean shear stresses, which have been stubbornly defended by some authors [Sines, 1959], [Papadopoulos, 1997], [Susmel, 2011] and therefore contributed to hinder a clear progress in the last 60 years.

As mentioned above, the methods of Marin, Crossland and Findley were presented at the International Fatigue Congress in 1956, and it could be said that slightly revised versions of these methods with their same shortcomings dominate the current landscape. However, as can be deduced from the transcription of the congress, at that historical moment the debate was open and the researchers were fully aware of the shortcomings of their methodologies, which should be expanded in the future [Crossland, 1956B].

Therefore, and as a first premise in mind, the lines of improvement that the authors themselves point out should be considered. For example, Findley admitted that the effect of normal stresses on the critical plane is probably nonlinear, but for practical purposes and taking into account the little improvement in agreement between theory and test data, the linear theory was finally used [Findley, 1959]. Marin openly admitted that his method, being based solely on von Mises stress, was independent of hydrostatic stress, the influence of which had been demonstrated in fatigue. And finally, Crossland's method is independent of the mean shear stress, the effect of which had been demonstrated at the same congress by a researcher in his own department at Bristol University, Chodorowski, who conducted cyclic torsion tests with mean shear stress on the same steel on which Crossland determined the effect of hydrostatic stresses.

In this regard, it is important to clearly document the effects of different types of loads on fatigue experiments. Several of the hypotheses are based on the collection of tests by Sines, who refers to the few tests available at the time, see for example the case of mean torsion together with bending fatigue, later greatly expanded by the tests conducted by German researchers in the 60s and 70s, which are still today ignored by most researchers in Multiaxial Fatigue. Therefore, another premise will be to try to document as many experimental cases as possible, considering simple load cases that allow us to deduce how the materials react to these load states.

In recent years the only serious attempt to adapt a method to the results of a large experimental database has been that of Papuga. Thanks to his efforts, a public database of 407 experiments has been compiled, allowing other

researchers to compare their methods with a common benchmark. By comparing the majority of methods against this database he has managed to discover which is the most important effect on multi-axial fatigue: that caused by the mean stresses. Previously there was a belief that the out-of-phase loading or the way of approaching the method (critical plane or integral methods) had a great influence on fatigue resistance, which has been demystified when comparing against experimental results. In addition, he showed that those methods that have an influence of mean shear stresses perform better than those that do not take them into account for states of loading in which mean torsional stresses exist. Therefore, the lessons learned from Papuga will be followed, especially those concerning the search for a method capable of correctly representing the mean stresses (axial and torsional).

On the other hand, Philosophy has demonstrated (and is therefore applicable to scientific practice) that aprioristic approaches are not adequate for the search for a solution, which has to be sought in an approximate manner through "ways" or reasoning proven through experience. In other words, the assumption of an aprioristic approach such as the following: "the effect of mean stresses on the critical plane is linear", which is a subjective assertion and not proven through experience, can hardly be adjusted to experimental results. Therefore, in order to search for the multiaxial fatigue method of this thesis, a clearly Thomistic approach will be adopted, seeking the correct solution through successive approximative reasoning.

This approach is extremely difficult, and very different from the one that has been followed in most of the papers. Its main difficulty lies in the choice of the variables to be used and in the basic principles from which to start to reach a

solution. In this sense, the principle of energy is a sufficiently solid base and with more than 150 years of solid experience contrasted in Science.

With regard to the selection of the variables that govern the phenomenon, these must be chosen according to the physical problem in question. However, we may be faced with problems such as multicollinearity, the Runge effect, or the low influence of certain variables. Faced with these problems, it is appropriate to apply the philosophical principle known as "Ockham's razor", which implies for practical purposes the elimination of all variables superfluous or with little influence so that the resulting expression is as simple as possible.

The construction of the formula representing multiaxial fatigue shall respect the principles of Dimensional Analysis. On many occasions we find mathematical formulations in engineering, above all of an empirical nature that do not respect the basic rules, and that contain constants with incoherent units. Respecting these norms is a basic premise for the creation of a physical formulation, and will be taken into account for the creation of the method. However, its usefulness does not end there, since we can design tests in which the variables that govern behaviour are related in some advantageous way, so that we can obtain individual and crossed relationships between the different variables that govern the problem.

Finally, the Cartesian concept of analytical geometry will be applied. As Descartes pointed out, "all my physics is geometry." Of course, the representation in the Cartesian plane of the experimental results makes it possible to elucidate what possible forms the damage function would have, and

to help deduce and finally demonstrate whether the proposed approach is the correct one, through correlation with the experimental results.

Chapter 2:

GENERAL ASPECTS OF METAL FATIGUE

CHAPTER 2. GENERAL ASPECTS OF METAL FATIGUE

2.1. Fatigue curves

Within the design of machines, and in particular in the fatigue design for unlimited life, has been used the concept of fatigue limit, first used by Wöhler [Wöhler, 1870], who focused his fatigue studies applied to rail transport in the mid-nineteenth century. Through his observations, he discovered that fatigue strength ceased to decline in the one million cycle environment for ferrous materials. This concept of fatigue limit is still used today in the engineering approach called "stress life".

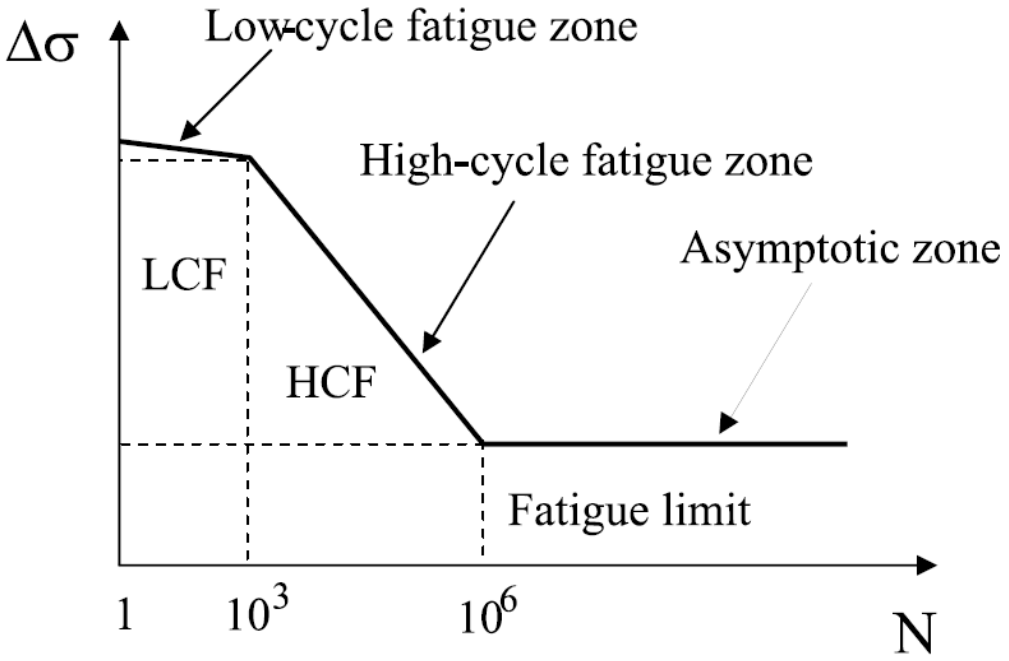

Figure 2-1. *S-N curve with the different fatigue regions [Castillo, 2009]*

However, it is also known that for quenched and tempered steels at high temperature, this fatigue limit exists and does not decrease in VHCF (Very High Cycle Fatigue). The reasons are not fully understood, but as Haibach points out at the 5th VHCF international congress in 2013, it seems to be strongly related to the non-presence of unstable phases, basically residual austenite. Figure 2-2 shows the S-N curves performed by Oguma [Oguma, 2004] of a JIS SNCM439 steel, Japanese equivalent to the North American AISI 4340, superimposed with different tempering temperatures. Above 500 °C, the material has a clearly defined fatigue limit above 1 million cycles.

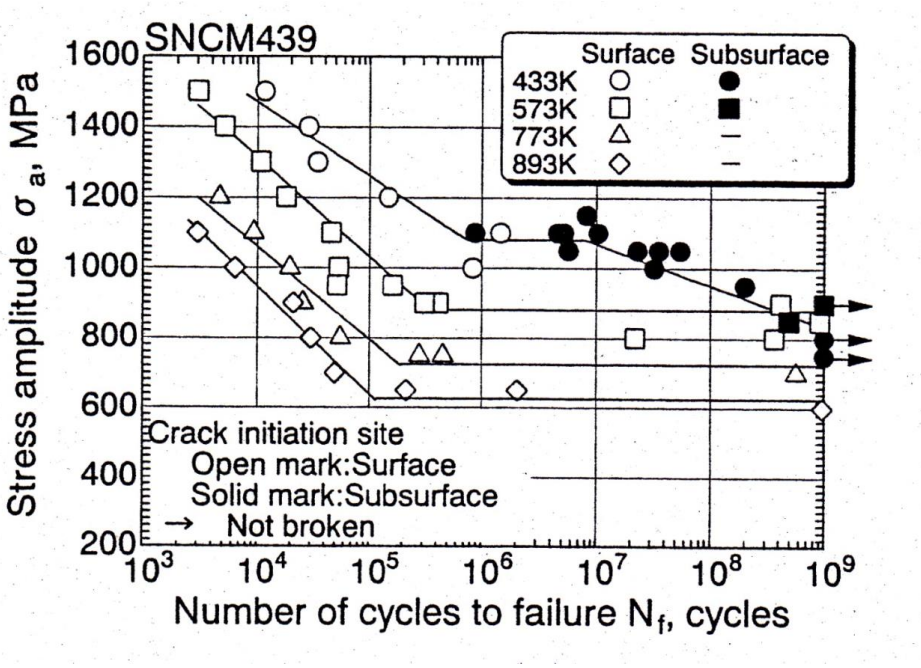

Figure 2-2. *S-N curves of JIS SNCM439 steel at different tempering temperatures [Oguma, 2004]*

The following sections will show the main problems regarding the modelling and estimation of fatigue parameters focusing on low alloy quenched and tempered steels in which the tempering has been carried out at high temperature.

2.2. The fatigue limit

The S-N diagrams of most steels show a sudden change of slope in which the slope becomes abruptly horizontal (Fig.2.3). This level of stress amplitude σ_K at which the "knee" occurs is referred to as the fatigue limit, because no loss of resistance is observed even beyond 10^7 cycles.

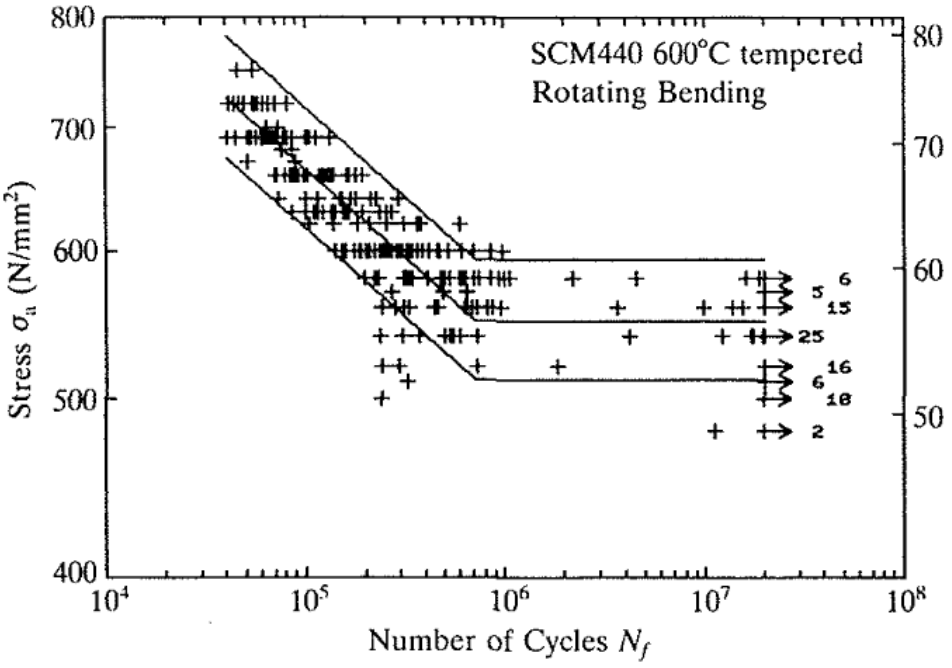

Figure 2-3. *Typical S-N curve in rotating bending showing abrupt knee [Nishijima, 1993]*

Another concept refers to the shape of the S-N curve: the fact that this transition between the limited and infinite life zone is abrupt is related to the averaged effect of several grains. In fact, if the failure occurred only at the grain level, the shape of the slope would be gradual up to the fatigue limit.

The most appropriate way therefore to correlate the fatigue limit with some material property is through parameters that relate the average properties of the microstructure of the material, such as Vickers hardness or ultimate tensile strength at break, which are linearly related to carbon and low alloy steels (Fig. 2.4).

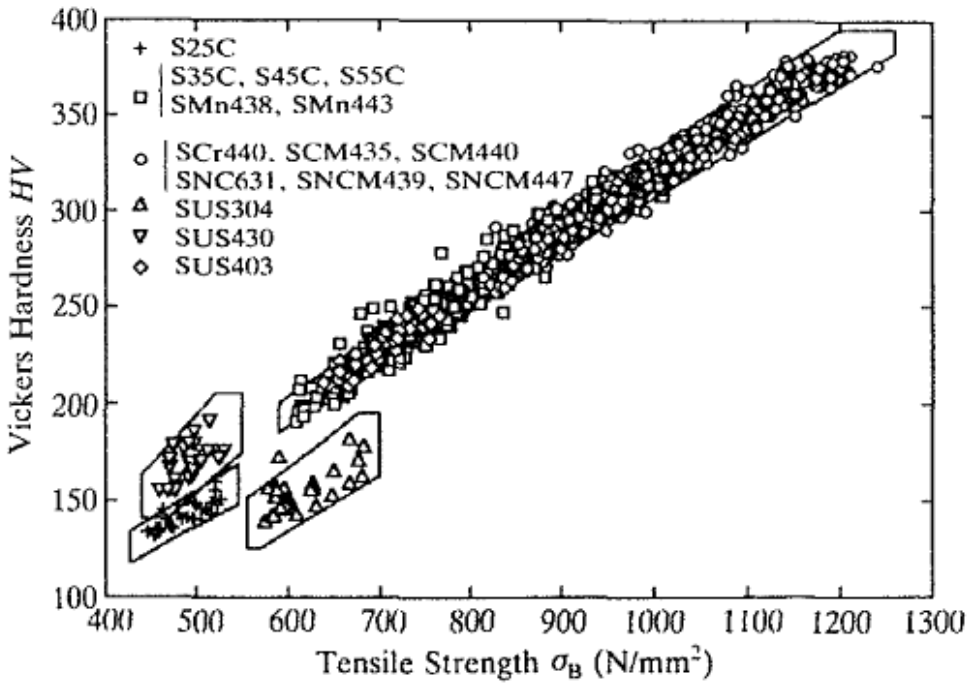

Figure 2-4. *Relationship between ultimate tensile strength and Vickers hardness [Nishijima, 1993]*

For carbon and low alloy steels, NRIM proposes the following ratio (2-1):

$$\sigma_{ut} = 3.12 \cdot HV \tag{2-1}$$

Fig. 2-5 shows the data for 18 low alloy quenched and tempered steels, the class to which the steels studied in the present project belong, and proposes an alternative modelling specific to this type of steels (2-2):

$$\sigma_{ut} = 3.1478 \cdot HV - 1.3496 \tag{2-2}$$

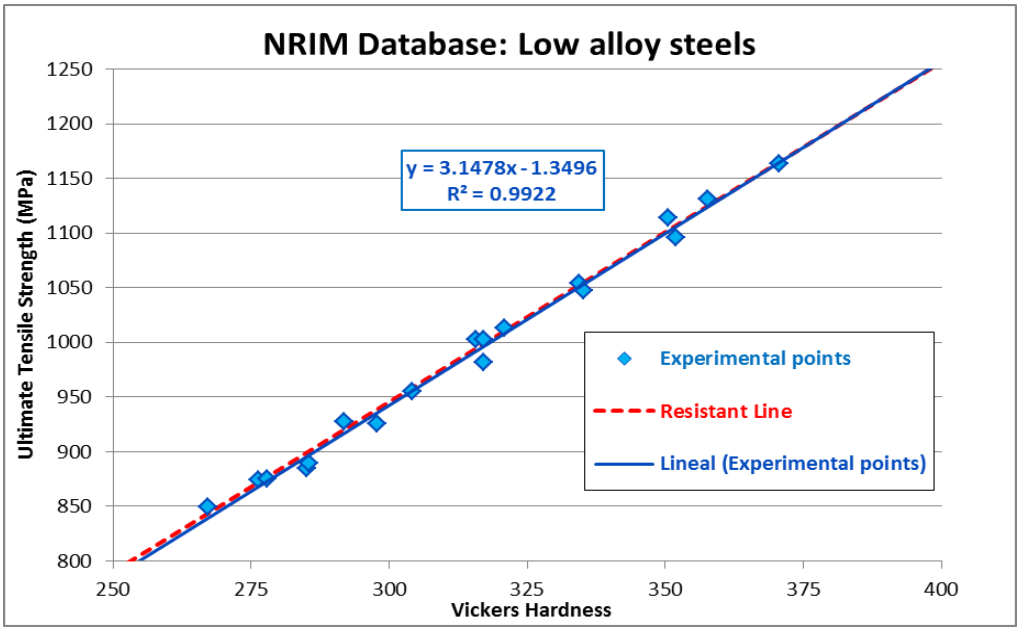

Figure 2-5. *Relationship between ultimate tensile strength and Vickers hardness for 18 low alloy quenched and tempered steels*

2.3. The estimation of the fatigue limit

In the literature there are many formulas that allow to relate the static properties with the fatigue limit. In practice, only expressions using the ultimate strength σ_{uts} and Vickers hardness (HV) are used, with a good correlation with experimental results. However, the correlations with the yield stress show a high dispersion. The explanation offered by some researchers such as Murakami lies in the fact that fatigue is a phenomenon closely linked to the hardness of the matrix, and largely unrelated to monotonic plasticity and its modes of failure.

The main correlations can be found for example in [Nishijima, 1993]. In order to analyse the validity of these, the NRIM quenched and tempered steel data, adjusted by Nishijima modelling, and shown in Table 2-1, will be used:

Table 2-1. *Low alloy quenched and tempered steels and their static and fatigue properties in rotating bending and reverse torsion.*

No.	JIS Steel	Tempering Temperature (ºC)	Static Properties		Rotating Bending			Fully reversed torsion		
			Vickers Hardness (HV)	σ_{ut} (MPa) Tensile strength	A Slope	σ_k (MPa) Fatigue limit	D = logN_k Knee point	A Slope	τ_k (MPa) Fatigue limit	D = logN_k Knee point
1	SCr440	550	334.5	1054.4	0.1047	553.8	5.786	0.0423	383.7	6.423
2	SCr440	600	304.1	954.6	0.0829	507.6	5.993	0.0584	342.7	6.305
3	SCr440	650	276.4	874.0	0.0741	470.4	6.025	0.0349	320.3	6.535
4	SCM435	550	351.9	1095.8	0.1055	566.4	5.831	0.0471	384.4	6.507
5	SCM435	600	317.1	981.6	0.0933	528.4	5.873	0.0427	355.8	6.428
6	SCM435	650	285.1	884.6	0.0876	479.4	5.950	0.0382	325.0	6.420
7	SCM440	550	370.7	1163.5	0.1069	600.5	5.747	0.0545	403.2	6.381
8	SCM440	600	335.2	1047.3	0.1015	553.4	5.802	0.0566	374.2	6.270
9	SCM440	650	297.9	925.7	0.0806	498.7	5.982	0.0533	338.2	6.150
10	SNC631	550	315.7	1002.5	0.0926	556.5	5.874	0.0574	349.0	6.374
11	SNC631	600	291.8	927.1	0.0767	518.0	6.070	0.0474	330.0	6.457
12	SNC631	650	267.2	849.1	0.0754	483.7	6.013	0.0485	304.7	6.440
13	SNCM439	580	350.6	1113.9	0.0990	593.4	5.812	0.0449	396.8	6.422
14	SNCM439	630	317.2	1002.4	0.0891	547.6	5.860	0.0474	365.5	6.297
15	SNCM439	680	278.0	874.7	0.0717	478.9	6.111	0.0309	328.5	6.345
16	SNCM447	580	357.7	1131.3	0.1040	594.0	5.737	0.0574	393.5	6.396
17	SNCM447	630	320.8	1012.8	0.0933	540.5	5.857	0.0470	367.0	6.345
18	SNCM447	680	285.5	889.0	0.0742	475.2	6.094	0.0355	323.5	6.448

A more specific study oriented to the type of steels of the Thesis and focused on the database of Table 2-1 could allow the obtaining of a more adequate value. For this purpose, Figures 2-6 and 2-7 show the statistical distributions of the ratios $\sigma'_{-1}/\sigma_{uts}$ and σ'_{-1}/HV, which adjust with great precision to the Log-Weibull distribution (Largest Extreme Value). The equations (2-3) and (2-4) are proposed in this Thesis:

$$\sigma'_{-1} = 0.5313 \cdot \sigma_{uts} \tag{2-3}$$

$$\sigma'_{-1} = 1.667 \cdot HV \tag{2-4}$$

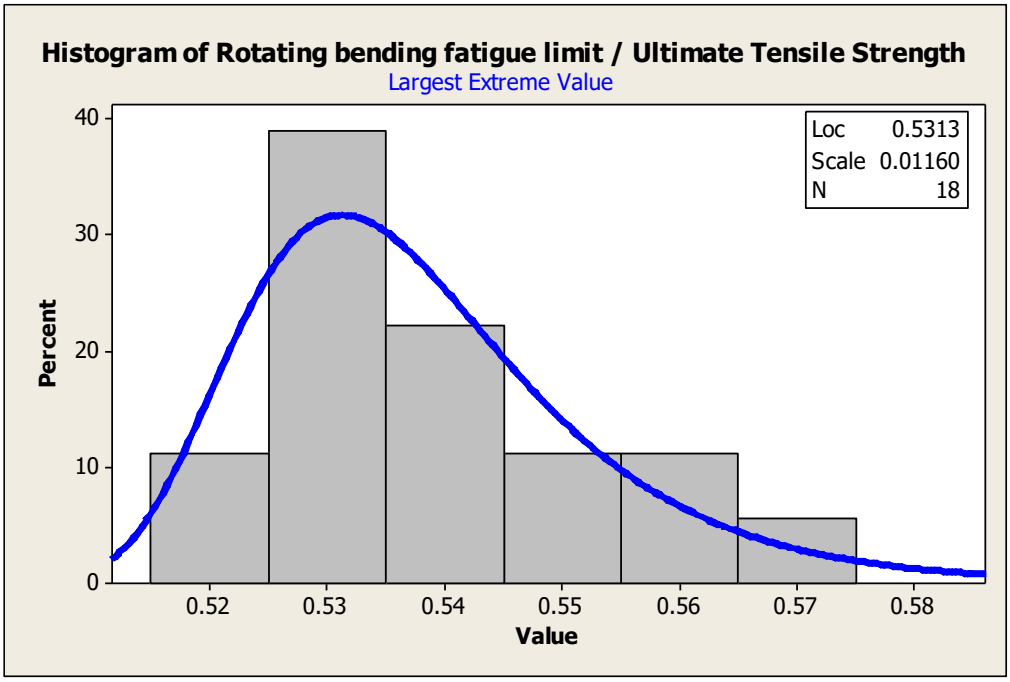

Figure 2-6. *Histogram of $\sigma'_{-1}/\sigma_{UTS}$ and adjustment by Log-Weibull for the 18 quenched and tempered steels contained in NIMS.*

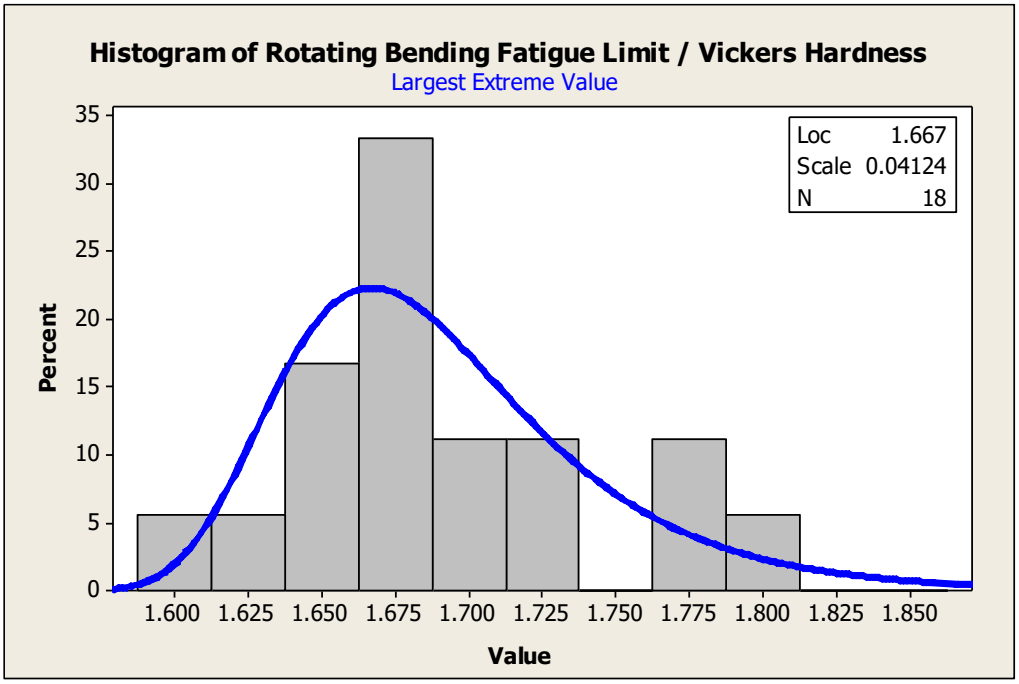

Figure 2-7. *Histogram of $\sigma'_{-1/}$ HV and adjustment by means of Largest Extreme Value for the 18 quenched and tempered steels contained in NIMS.*

2.4. The volumetric fatigue limit

In many steels there is an appreciable decrease in fatigue strength above 10^7 cycles, with a new knee arising around 10^9 cycles. As shown in Fig. 2-8, there could be a new volumetric fatigue limit, in principle capable of reaching unlimited life.

At present, due to the demands of some machines, a new concept has emerged, known as the "very high cycle" fatigue limit, located around 10^9 cycles (Figure 2-8). The phenomena that create this second fatigue limit are mainly caused by

internal material imperfections (mainly inclusions); whereas the causes of the conventional fatigue limit have other causes besides the internal ones: persistent sliding bands (dislocation movement), pores, surface defects, and alpha particles in the case of double-phase Titanium.

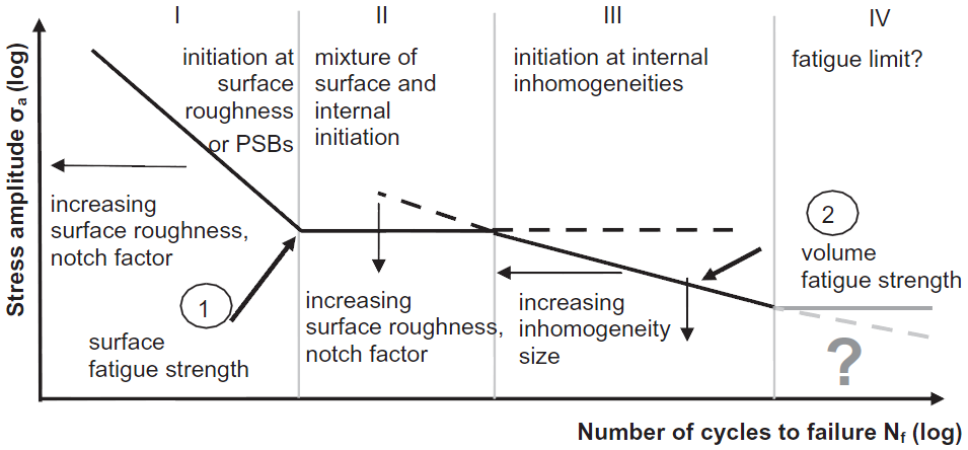

Figure 2-8. *Volumetric Fatigue Limit [Pyttel, 2011]*

The theoretical resistance curves follow a different evolution than the surface resistance. However, in some steels it could be assumed that the quantity and size of these defects is practically negligible, so there could be a surface fatigue limit similar to the volumetric one.

2.5. S-N Curve Models

There are many possibilities to model S-N curves. According to Weibull, the most suitable modelling is the simplest of all those that adequately represent the data. Table -2 shows the most commonly used in literature:

Table 2-2. *Models of S-N curves most used in the literature [Castillo, 2009].*

Model	Functional Form
Wöhler (1870)	$\log N = A - B\Delta\sigma;\ \Delta\sigma \geq \Delta\sigma_0$
Basquin (1910)	$\log N = A - B\log\Delta\sigma;\ \Delta\sigma \geq \Delta\sigma_0$
Strohmeyer (1914)	$\log N = A - B\log(\Delta\sigma - \Delta\sigma_0)$
Palmgren (1924)	$\log(N + D) = A - B\log(\Delta\sigma - \Delta\sigma_0)$
Palmgren (1924)	$\log N = A - B\log(\Delta\sigma - \Delta\sigma_0)$
Weibull (1949)	$\log(N + D) = A - B\log((\Delta\sigma - \Delta\sigma_0)/(\Delta\sigma_{st} - \Delta\sigma_0))$
Stüssi (1955)	$\log N = A - B\log((\Delta\sigma - \Delta\sigma_0)/(\Delta\sigma_{st} - \Delta\sigma))$
Bastenaire (1972)	$(\log N - B)(\Delta\sigma - \Delta\sigma_0) = A\exp[-C(\Delta\sigma - \Delta\sigma_0)]$
Spindel–Haibach (1981)	$\log(N/N_0) = A\log(\Delta\sigma/\Delta\sigma_0) - B\log(\Delta\sigma/\Delta\sigma_0) + B\left\{(1/\alpha)\log\left[1 + (\Delta\sigma/\Delta\sigma_0)^{-2\alpha}\right]\right\}$
Castillo et al. (1985)	$\log(N/N_0) = \dfrac{\lambda + \delta(-\log(1-p))^{1/\beta}}{\log(\Delta\sigma/\Delta\sigma_0)}$
Kohout and Vechet (2001)	$\log\dfrac{\Delta\sigma}{\Delta\sigma_\infty} = \log\left(\dfrac{N + N_1}{N + N_2}\right)^b$
Pascual and Meeker (1999)	$\log N = A - B\log(\Delta\sigma - \Delta\sigma_0)$

The Wöhler model shows a linear resistance loss zone in S-logN. However, all other models use the double logarithmic scale. As for the use of a fatigue limit, only Basquin modelling does not use this parameter. With regard to the transition between the high cycle zone and unlimited life, the Wöhler curve shows an abrupt shape while in the rest of the models it appears smoothed.

There is an alternative modelling, used by Nishijima, that allows an abrupt transition between the high cycle zone and the unlimited life zone on a double logarithmic scale.

As for its use in multi-axial fatigue, Palmgren modelling was successfully used for a 4340 steel of 855 MPa ultimate tensile strength (Fig. 2-9). As can be seen, axial and torsional fatigue limits do not apply for the same number of cycles. Fig. 2-10. shows the difference in percentage with respect to the fatigue limit as a function of the number of cycles.

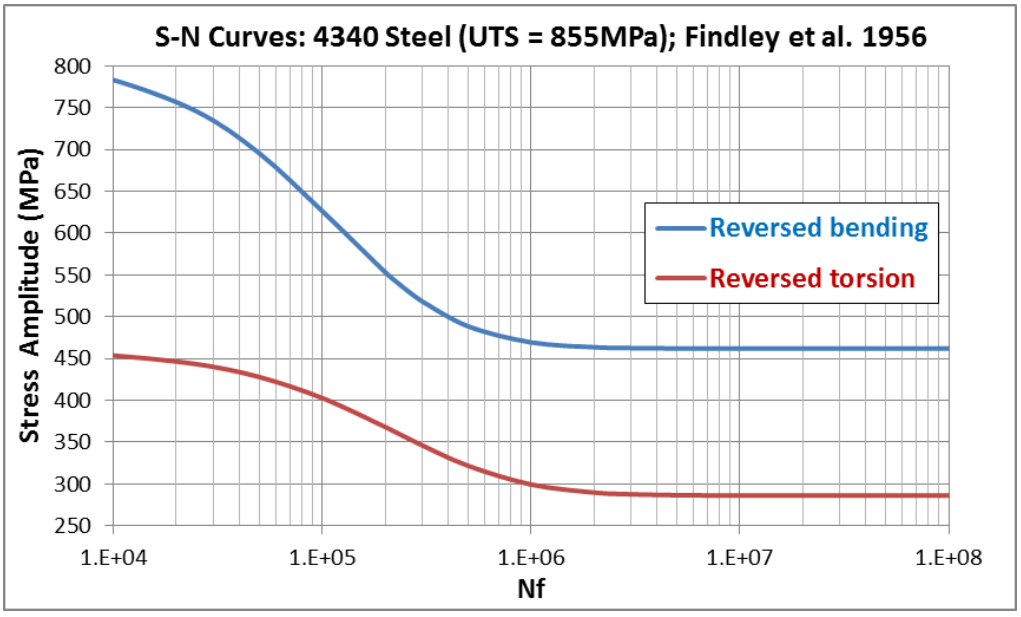

Figure 2-9. *S-N curves of Rotating bending and torsion of a steel 4340 [Findley, 1956]*

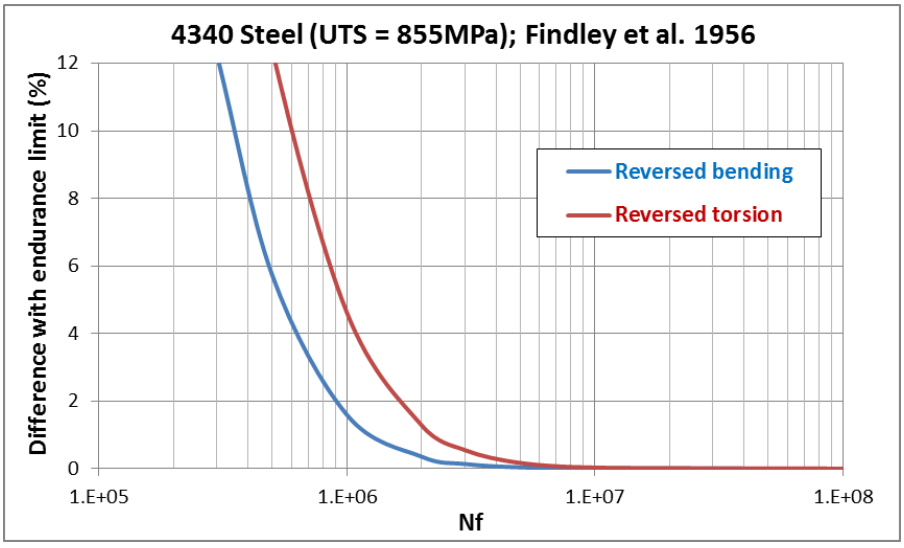

Figure 2-10. *Difference in percentage with respect to the fatigue limit as a function of the number of cycles for an AISI 4340 steel [Findley, 1956].*

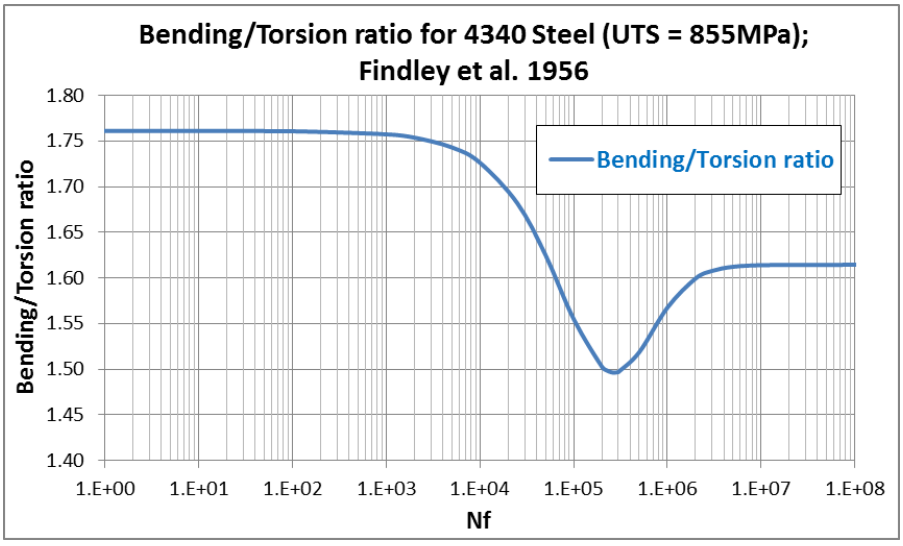

Figure 2-11. *Relationship between axial and torsional fatigue limits as a function of the number of cycles [Findley, 1956].*

The difference in the number of cycles at which the fatigue limit occurs in rotating bending fatigue and torsion is of vital importance, since the factor between axial and torsional fatigue limits appears explicitly as a parameter in many multi-axial methods, and can induce large errors if tests are not performed up to a certain number of cycles.

2.6. The JSME model for S-N curves

This modelling allows a minimum number of specimens to be used to calculate the S-N curve at its inclined part and at the fatigue limit. Basically it consists of using eight specimens in the inclined zone, and with the standard deviation of that zone, to realize a reduced staircase in the zone of unlimited life. This procedure seems to be suitable for multi-axial tests, where the hour-machine cost is very high. The diagram is shown in Figure 2-13, in which an inclined part consisting of 8 specimens can be observed, and a reduced staircase made with 6 specimens and using the standard deviation of the inclined part as a step between different tests.

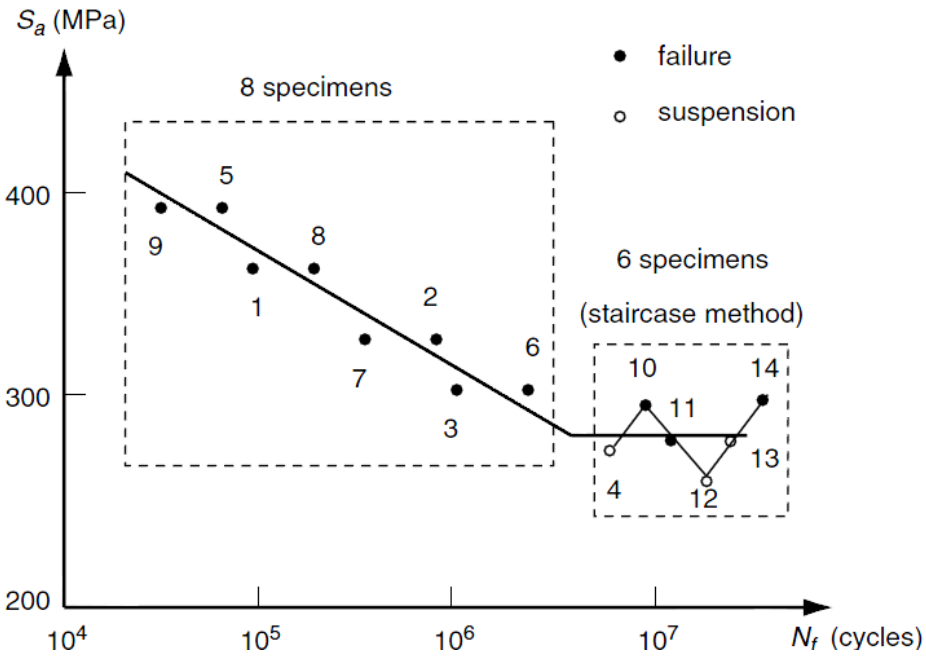

Figure 2-12. *JSME modelling for the realization of S-N curves with 14 specimens.*

2.7. Cyclical yield stress

2.7.1. The concept of monotonic yield stress

The concept of monotonic yield stress is widely used in mechanical engineering: it basically describes the stress from which static plasticity is produced. As described in the section of this Thesis corresponding to the tensile test, this stress is easily determinable in the case of structural steels, which have a very marked influence of the yield, since it can be observed a stress for which the deformation grows without increasing the applied nominal stress. For most ductile steels,

there is also a higher yield stress σ_{yp} upper and a lower yield stress $\sigma_{yp\ lower}$. As an engineering criterion, the lower yield stress is usually adopted as the yield stress σ_{yp}.

On the other hand, there are other materials, such as aeronautical aluminium, hardening and tempering steels at low temperatures or some nickel superalloys such as Inconel 718, whose static stress-strain diagram does not suffer so clearly this phenomenon of yield. In these materials it is very common to use the so-called yield stress with 0.2% plastic deformation $\sigma_{yp\ 0.2}$, which due to the steep slope of the stress-strain curve could be far from the yield stress without plastic deformation σ_{yp}. The development of the technology has allowed the use of gauges with greater precision so it is increasingly common to find data from $\sigma_{yp\ 0.2}$, $\sigma_{yp\ 0.1}$ or even $\sigma_{yp\ 0.05}$. Important differences between these values can be observed in these materials without a marked influence of the yield. However, in conventional structural steels, the error made when using $\sigma_{yp\ 0.2}$ instead of σ_{yp} is low, as when entering static plasticity, curves are generally flat for this type of material.

2.7.2. Cyclical plasticity yield

Just as static plasticity appears from a certain σ_{yp} monotonic stress, cyclic plasticity defines a stress amplitude from which plastic deformations appear. This cyclic stress, called σ'_{yc} must be found by cyclic testing.

The main method used in the literature is the incremental step method, consisting of strain control tests. A total deformation amplitude is fixed, and after stabilization of the cyclic loop a stress amplitude and a plastic deformation

amplitude are obtained. Performing the test for several amplitudes of total deformations, we can obtain the cyclic curve. The real cyclic stress σ'_{yc} is therefore the stress for which there is no plastic deformation amplitude, the deformations being only elastic.

Representing the cyclic curve of deformation amplitudes and stress amplitudes, we can observe that this curve has a very steep slope and without an evident cyclic yield phenomenon, so some authors propose to use cyclic stress with 0.2% plastic deformation $\sigma'_{yc\ 0.2}$, analogous to $\sigma_{yp\ 0.2}$ for the monotonic test. As it will be demonstrated in the following sections, this value may not be close to the real σ'_{yc}, as well as lacking practical utility in engineering.

2.7.3. Ramberg-Osgood's cyclic plasticity model

In order to obtain this cyclic stress, the Ramberg-Osgood expression (2-5 to 2-8) is usually used to adjust the data found by the incremental step method.

$$\varepsilon_a = \varepsilon_{ae} + \varepsilon_{ap} \tag{2-5}$$

$$\varepsilon_{ae} = \frac{\sigma_a}{E} \tag{2-6}$$

$$\varepsilon_{ap} = \left(\frac{\sigma_a}{C'} \right)^{\frac{1}{n'}} \tag{2-7}$$

$$\sigma_a = C' \cdot \varepsilon_{ap}{}^{n'} \tag{2-8}$$

This model implies that there is plastic deformation for any amplitude of stress, so there is strictly no elastic yield stress for which the amplitude of plastic deformation is zero.

Table 2-3. *Incremental passage tests for a steel SNCM 439 hardened and tempered at 630ºC [Nishijima, 1993]*

SNCM439 Q&T 630°C HEAT G								
1			2			3		
ε_{ta}	ε_{pa}	σ_a	ε_{ta}	ε_{pa}	σ_a	ε_{ta}	ε_{pa}	σ_a
1,20E-03	0	226	1,20E-03	0	228	1,20E-03	0	231
2,20E-03	1,00E-04	397	2,20E-03	1,00E-04	399	2,20E-03	2,00E-04	400
3,30E-03	6,00E-04	514	3,30E-03	6,00E-04	515	3,30E-03	6,00E-04	513
4,40E-03	1,30E-03	584	4,40E-03	1,30E-03	584	4,40E-03	1,40E-03	580
5,60E-03	2,20E-03	630	5,60E-03	2,20E-03	630	5,60E-03	2,20E-03	625
6,70E-03	3,10E-03	664	6,70E-03	3,20E-03	664	6,70E-03	3,20E-03	660
7,90E-03	4,10E-03	694	7,90E-03	4,20E-03	693	7,90E-03	4,10E-03	687
9,10E-03	5,20E-03	718	9,10E-03	5,20E-03	718	9,10E-03	5,10E-03	712
1,03E-02	6,20E-03	740	1,03E-02	6,20E-03	740	1,03E-02	6,20E-03	734
1,15E-02	7,30E-03	760	1,15E-02	7,30E-03	760	1,14E-02	7,20E-03	752
1,27E-02	8,30E-03	778	1,27E-02	8,40E-03	778	1,26E-02	8,30E-03	770
1,39E-02	9,40E-03	794	1,39E-02	9,50E-03	795	1,38E-02	9,30E-03	787
1,51E-02	1,05E-02	809	1,51E-02	1,06E-02	809	1,50E-02	1,04E-02	801

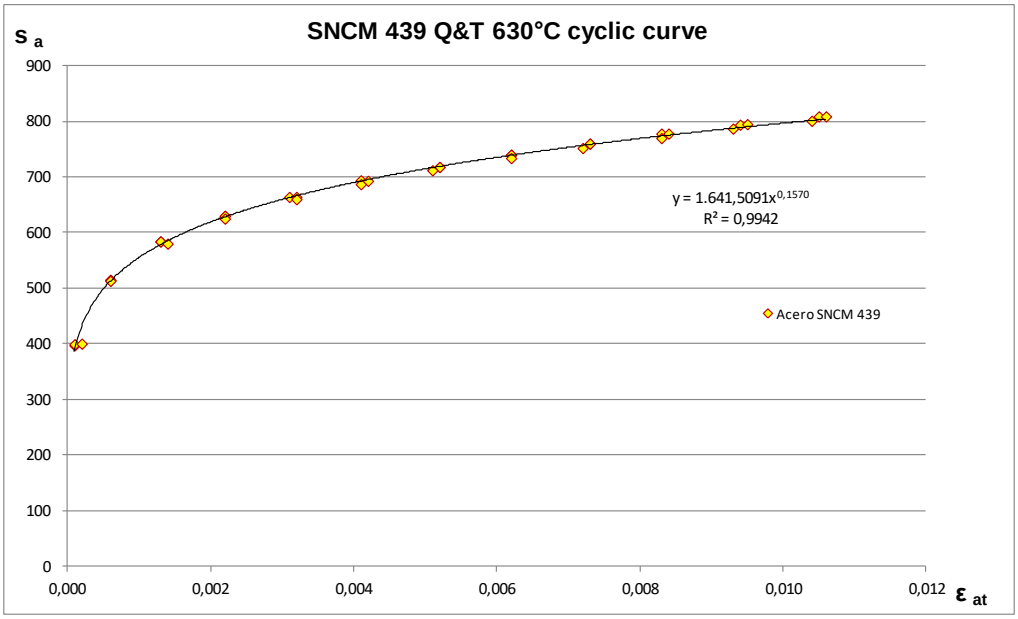

Figure 2-13. *Cyclic curve for a SNCM 439 steel hardened and tempered at 630ºC.*

Table 2.3 shows the incremental step test data for a SNCM 439 steel (JIS equivalent to ISO 34CrNiMo6).

In Figure 2.14 these data are represented in an amplitude diagram of strain amplitude-strain amplitude, together with the Ramberg-Osgood adjustment superimposed on the experimentally obtained points.

The adjustment shows an experimental correlation coefficient R^2=0.9942. However, Ramberg-Osgood's representation implies that plasticity appears for any amplitude of deformation, and there is no real cyclic yield stress. Using the setting values: C'=1641.509 MPa and n'=0.157, the cyclic yield stress at 0.2% would be:

$$\sigma'_{yc0.2} = 1641.509 \cdot 0.002^{0.157} = 618.735 MPa \qquad (2\text{-}9)$$

The usefulness of this concept is however debatable: the value of $\sigma'_{yc\ 0.2}$ implies only the value of the alternating stress for which it is stable with a plastic deformation amplitude of 0.2%, without being a guarantee of unlimited life. In fact, the value of $\sigma'_{yc0.2}$ for this steel is above the fatigue limit, coded at 538 MPa by NIMS [Nishijima, 1993].

On the other hand, unlike the monotonic curve, the value of 0.2% plastic deformation amplitude may show very large differences in stress amplitude with respect to the 0.0% cyclic yield stress due to the much more marked plastic hardening of the cyclic curve.

This excessive plastic deformation makes $\sigma'yc_{0.2}$ a low cycle fatigue criterion. Analysing the extensive NRIM database for steels and aluminiums in LCF, we can obtain the following relationships for steels (equation 2-10) and aluminiums (equation 2-11), shown in Fig. 2-14:

$$\sigma'_{yc0.2} = 0.603 \cdot \sigma_{UTS} \qquad (2\text{-}10)$$

$$\sigma'_{yc0.2} = 0.910 \cdot \sigma_{UTS} \qquad (2\text{-}11)$$

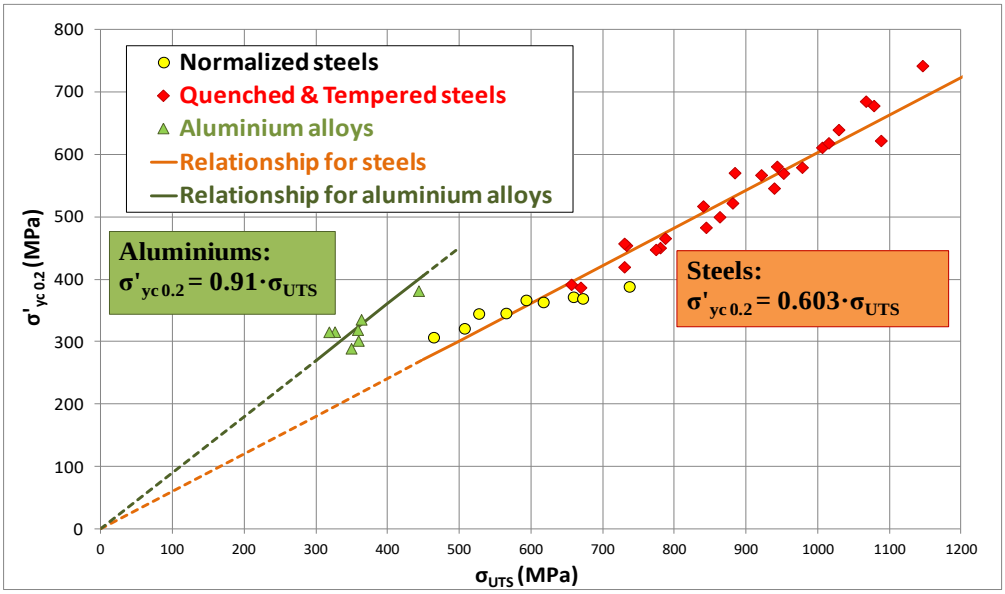

Figure 2-14. *Determination of the LCF parameter $\sigma'_{yc0.2}$ for steels and aluminium alloys*

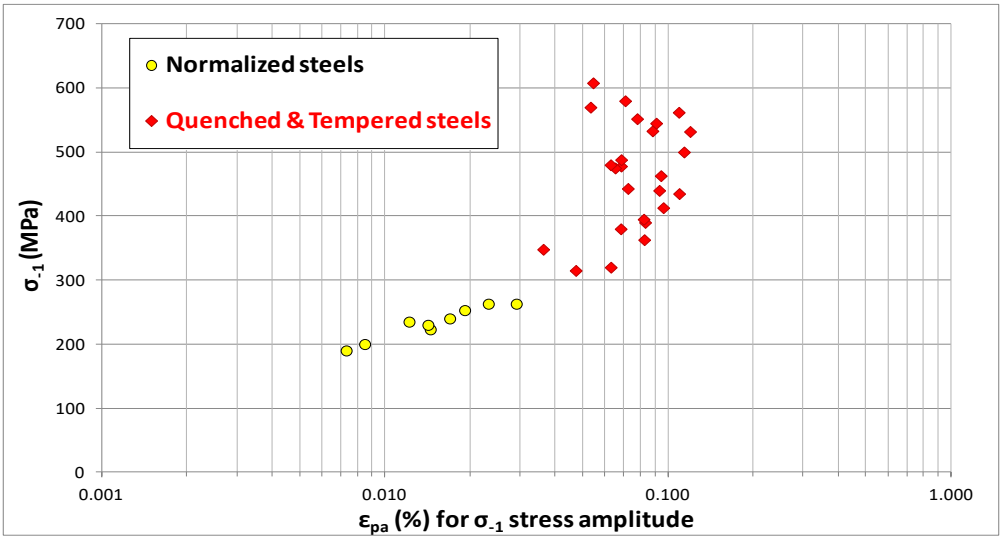

Figure 2-15. *Number of cycles for a cyclic plastic deformation of 0.2%.*

As can be seen in Fig. 2-15, this plastic deformation makes the parameter $\sigma'_{yc0.2}$ a low cycle parameter.

2.7.4. A relevant example chosen from the literature

The Instituto Tecnológico de Aragón (ITA) published in 2011 [Gómez, 2011] monotonous and cyclic tests of steel S355 J2, mainly used in construction and low carbon content.

In Figure 2-16 the monotonic and cyclic curves for the uniaxial test can be observed simultaneously. This material shows cyclic softening, with the cyclic curve is below the monotonic one.

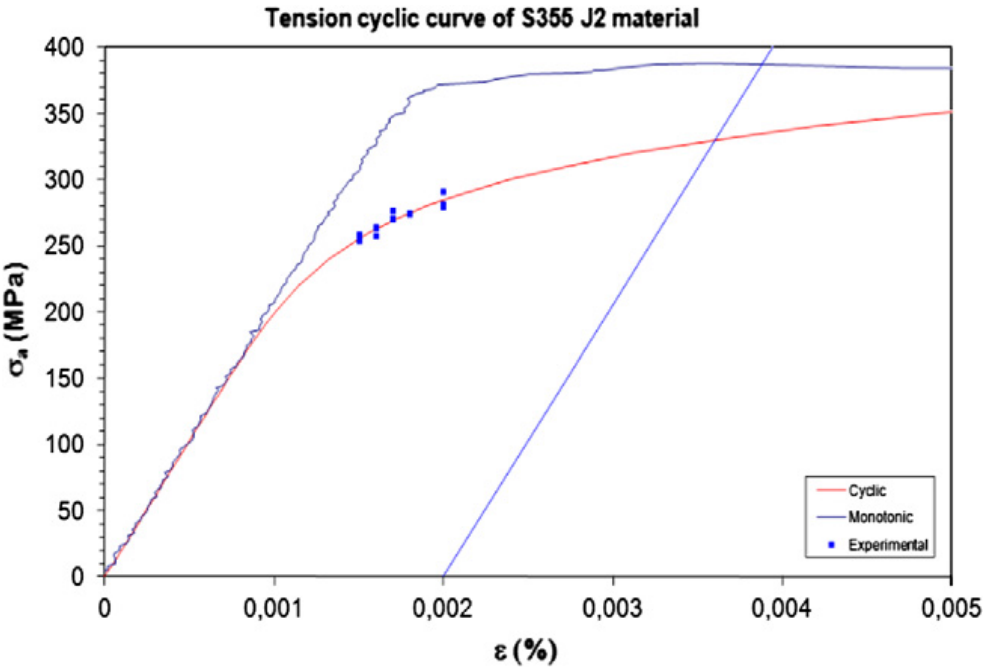

Figure 2-16. *Cyclic and monotonic curves for steel S355J2 [Gómez, 2011]*

Chapter 3:

EFFECT OF AXIAL MEAN STRESSES

CHAPTER 3. EFFECT OF MEAN AXIAL STRESSES

3.1. Introduction

The effect of axial mean stresses is widely documented in the literature. Contrary to the case of mean torsional stresses, there is almost unanimous opinion that they influence even values below the macroscopic yield stress σ_{YP}.

The influence of the mean stress σ_m on the fatigue limit was already observed as one of the main factors influencing the fatigue resistance by Wöhler in 1870 [Wöhler, 1870], who pointed out that the fatigue limit decreased with the increase of the mean stress σ_m.

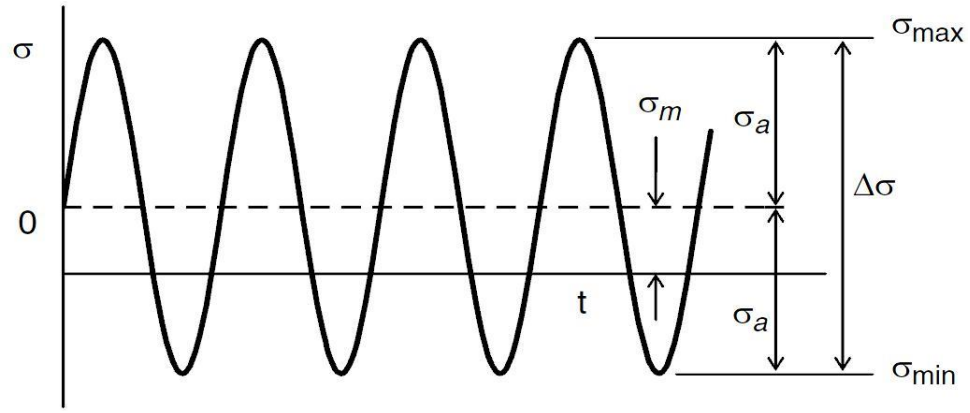

Figure 3-1. *Representation of constant stress tests with mean stresses [Dowling, 2009B]*

The relative importance of axial mean stresses has been particularly noted in Papuga's exhaustive comparison of multi-axial methods in 2011 [Papuga,

2011A], who concluded that the ability to correctly capture the effect of axial mean stresses is a determining factor in the ability of a multi-axial fatigue method. In fact, although virtually all multiaxial methods take into account the influence of axial mean stresses, the way in which they treat the effect of these stresses can differ greatly. With the aim of exposing these differences, throughout this chapter we will also analyse the multiaxial fatigue models, especially the classic ones such as Findley, Crossland, Dang Van and Sines, applied to the case of uniaxial fatigue with mean stresses and being contrasted with an important base of experimental results extracted from the literature.

Historically, a multitude of uniaxial formulations have been proposed to model the effect of mean stresses, most of which use the ultimate tensile strength σ_{UTS} or the yield stress of the uniaxial test σ_{YP} as one of the parameters. These formulas come from generally empirical approaches to correlate groups of tests on certain materials. It is widely accepted in the literature of the fact that there is no general law allowing the effect of the mean stress on the fatigue limit to be related [O'Connor, 1956], [Weibull, 1961].

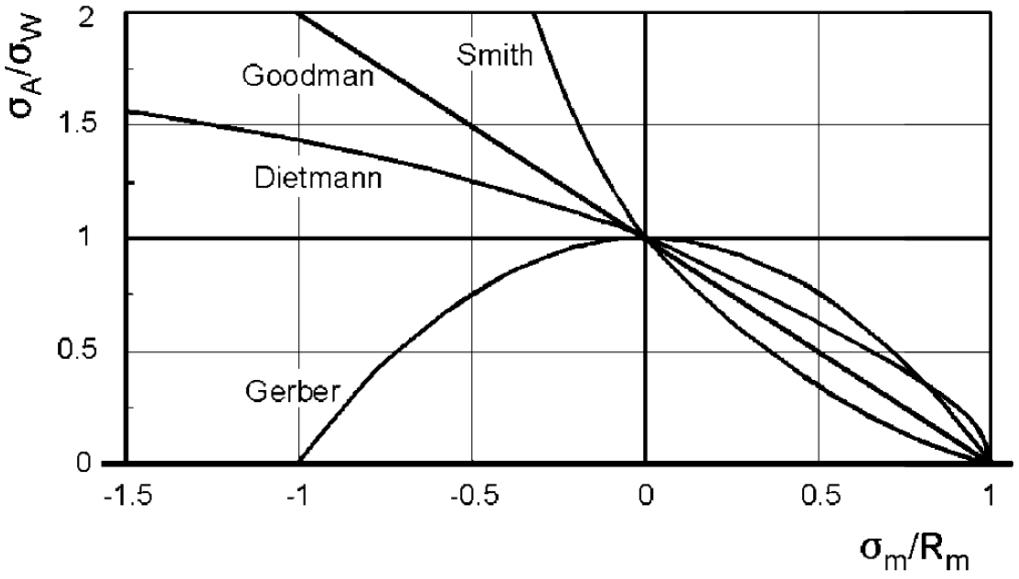

Figure 3-2. *Haigh diagram with the lines of theories not based on fracture or yielding [Lüpfert, 2004].*

Fig. 3-2 shows on a Haigh diagram the main empirical lines coming from theories that do not imply fracture or yielding [Lüpfert, 2004].

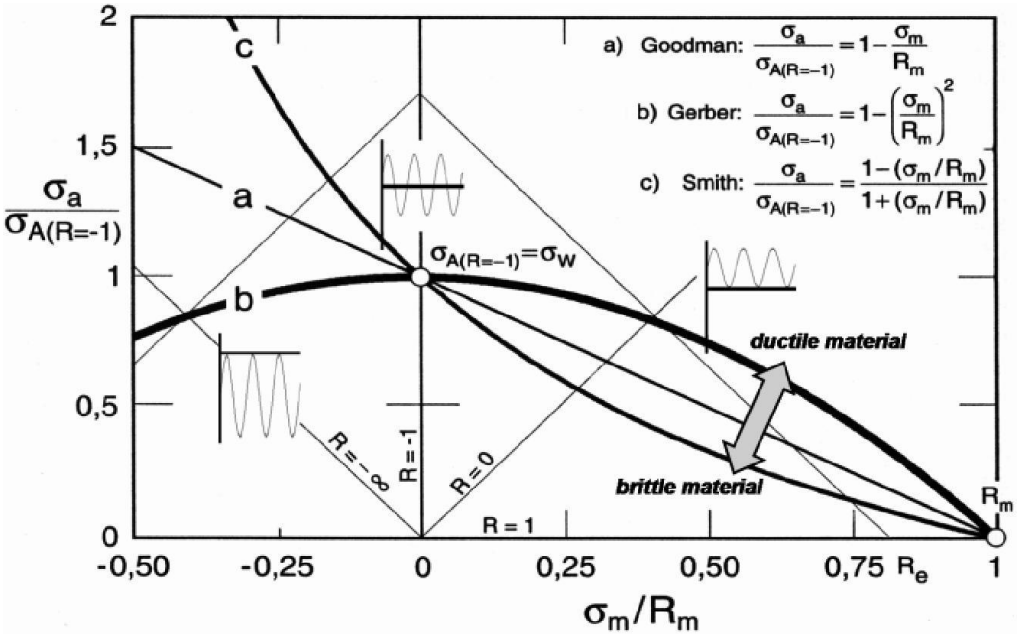

Figure 3-3. *Haigh diagram with different criteria according to ductility [Klubberg, 2011]*

The shape of these lines in the Haigh diagram is indicative of the ductility of the material, as shown in Fig. 3-3, so that it can be used for design as a function of the type of material. For example, the Gerber parabola (concave for any mean stress value) is highly accurate for data on extra-ductile steels; and the Smith line, convex in shape, for fragile castings. However, as will be explained throughout this chapter, some materials that based on their static properties could be considered as relatively ductile, such as some aluminium with hardening particles, have areas with a certain concavity connected to other convex areas, a fact that none of the empirical lines can collect.

These differences in the behaviour of the different materials and the shapes of Haigh's diagrams will be studied in this chapter.

3.2. Uniaxial criteria

3.2.1. Classical uniaxial methods

Historically, the first fatigue tests with mean stresses were performed by Wöhler [Wöhler, 1870]. Based on the experimental results of this, Gerber [Gerber, 1874] proposed in 1884 the following parabolic equation, known as the Gerber line or relationship, equations (3-1) and (3-2):

$$\sigma_{\max} = \frac{1}{2} \cdot R \cdot \sqrt{\sigma_{UTS}{}^2 - n \cdot \sigma_{UTS} \cdot R} \qquad (3\text{-}1)$$

Where n is an experimentally determined constant with an approximate value between 1.33 and 2. The equation (3-1) can be expressed alternatively using the fatigue limit for fully reversed stresses σ_{-1}, equation (3-2):

$$\sigma_a = \sigma_{-1} \cdot \left[1 - \left(\frac{\sigma_m}{\sigma_{UTS}} \right)^2 \right] \qquad (3\text{-}2)$$

As can be seen in equation (3-2), the sign of the mean stress has no influence when σ_m appears squared. This equation was adjusted with great precision to the experimental data available at the time, which were basically limited to rotating bending, and tests with mean compressive stresses were not possible. Gerber deduced that since in rotating bending the failure always occurred in tensile fibres, the fatigue limit would be higher in compression than in tension. Therefore, by proposing a symmetrical method with respect to mean stresses such as the parabola (3-2), the results in compression would be on the safety

side. Thus Gerber's aim was not the quest for abstract truth, but that his line could be used for mechanical design [O'Connor, 1956].

The Gerber line was considered sufficiently tested by Bauschinguer, who used it dogmatically, showing results calculated with the Gerber equation as if they were apparently results of an experimental campaign. As O'Connor and Morrison point out in [O'Connor, 1956], this generated widespread controversy.

In 1899, Goodman [Goodman, 1899] proposed the so-called "dynamic theory", in which it is assumed that vibratory charges produce a stress whose value is twice as high as if the charges had been applied quasi-statically. Thus, the maximum value of the fatigue test R=0 (σ_0) would be half of the ultimate tensile strength σ_{UTS}, which is the only experimental parameter necessary in this criterion. Fig. 3-4 shows Goodman's theory of a Goodman diagram:

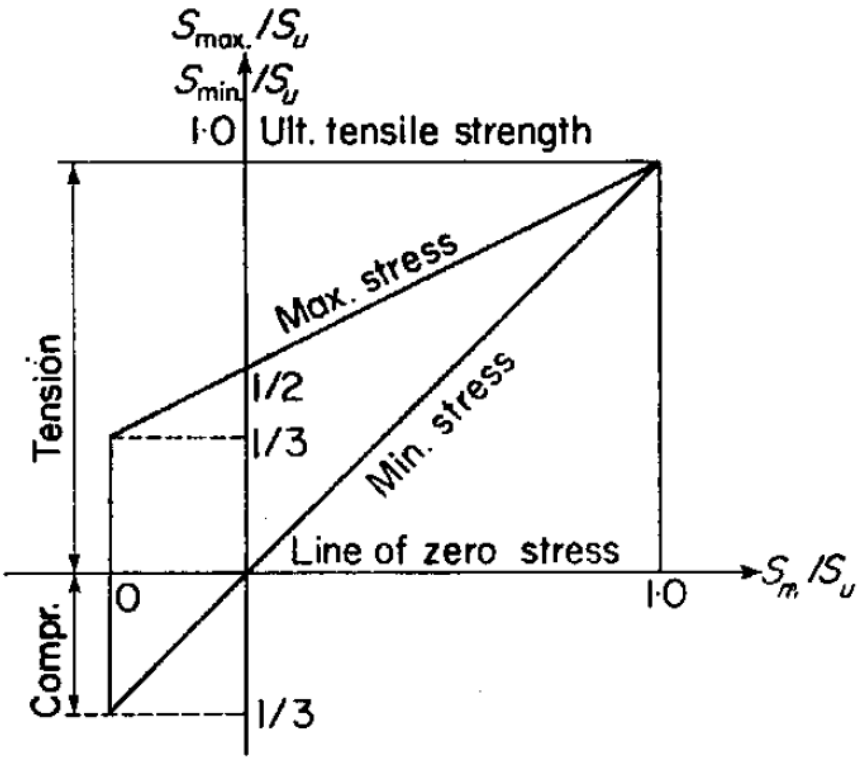

Figure 3-4. *Goodman diagram showing fatigue strength values for R=0 and R=-1 [Weibull, 1961].*

Goodman's dynamic theory can be expressed mathematically by equation (3-3):

$$\sigma_a = \frac{\sigma_{UTS}}{3} \cdot \left(1 - \frac{\sigma_m}{\sigma_{UTS}}\right) \qquad (3\text{-}3)$$

This theory assumes a σ_{-1} fatigue strength value for R=-1 of one third of the ultimate tensile strength, which does not correlate well with the experimental

results on ductile steels, which is usually assumed to be half of the ultimate tensile strength in the absence of experimental data. Goodman himself recognized that "if the assumptions of his theory are justifiable or not, they are an open question", but that "the theory is easy to apply and simple to remember" [Goodman, 1899].

In 1923 Goodman's theory was modified by Haigh [Haigh, 1922] also considering a linear effect of axial mean stresses but replacing the previously quoted value of one third of σ_{UTS} with the data corresponding to the fully reversed uniaxial fatigue test σ_{-1}. The modified Goodman criterion can be expressed by equation (3-4):

$$\sigma_a = \sigma_{-1} \cdot \left(1 - \frac{\sigma_m}{\sigma_{UTS}} \right) \tag{3-4}$$

Some reviews of experimental results for ductile materials, such as the classic paper by Smith [Smith, 1942], the analysis by Susmel [Susmel, 2005] and the most recent collection of ferritic materials [Pallarés, 2018A], show that the overwhelming majority of experimental results stay above Goodman's modified line; and two-thirds between the modified Goodman and Gerber lines. It should be noted that these data are only valid for ductile materials and for specimens without stress concentrators.

In 1923, Soderberg [Soderberg, 1930] made a modification of the modified Goodman linear equation, replacing the ultimate tensile strength σ_{UTS} with the yield strength with the objective of greater conservatism in design, based on the premise that static failure is produced by yielding (3-5):

$$\sigma_a = \sigma_{-1} \cdot \left(1 - \frac{\sigma_a}{\sigma_{yp}}\right) \tag{3-5}$$

Using the linear modelling of modified Soderberg and Goodman, but using as static stress the real fracture stress of the material with Bridgman's correction σ_{fB}, a less conservative modelling is obtained than the two previous ones. This modelling is known as the Morrow criterion [Morrow, 1968], equation (3-6):

$$\sigma_a = \sigma_{-1} \cdot \left(1 - \frac{\sigma_m}{\sigma_{fB}}\right) \tag{3-6}$$

In the event that the value of the actual fracture stress with Bridgman's correction is not available, the following approximation can be used valid for steels with an ultimate tensile strength σ_{UTS} up to 1700 MPa, equation (3.7), as proposed by Dowling in [Dowling, 2009B]:

$$\sigma_{fB}[MPa] = \sigma_{UTS}[MPa] + 345 \tag{3-7}$$

The above criteria were developed for ductile materials. In 1942 Smith [Smith, 1942] published an empirical equation (3-8) that allowed an extraordinarily effective fit for fragile materials. The aim of this line is to be used for designs in which either the material is fragile (e.g. grey castings), or although the matrix of the material is ductile there may be important stress concentrators:

$$\sigma_a = \sigma_{-1} \cdot \frac{1 - \frac{\sigma_m}{\sigma_{UTS}}}{1 + \frac{\sigma_m}{\sigma_{UTS}}} \tag{3-8}$$

The shape of this line represented on a Haigh diagram is convex downward. Fatigue strength therefore increases very rapidly in the compression zone and also decreases very rapidly in the tensile zone.

In 1956 Marin [Marin, 1956] deduced through a balance of energies in static and fatigue cases, the so-called "elliptical relationship" expression. This line obtains a good correlation with the experimental results of extra-ductile materials. Its equation is (3-9):

$$\sigma_a = \sigma_{-1} \cdot \sqrt{1 - \left(\frac{\sigma_m}{\sigma_{UTS}} \right)^2} \tag{3-9}$$

Another commonly used line is Dietmann [Dietmann, 1973], who in the 1970s proposed the relationship represented by the equation (3-10), which shows a high statistical correlation with experimental data, by being located between the Goodman and Gerber lines for most of the R range in axial mean stresses; and by collecting the beneficial effect of mean compressive stresses that is observed in many materials.

$$\sigma_a = \sigma_{-1} \cdot \sqrt{1 - \frac{\sigma_m}{\sigma_{UTS}}} \tag{3-10}$$

All the above theories except Smith's can be summarized in the so-called "Marin generalized relationship", represented by equation (3-11), where parameters *n*, *m* and *f* take different values depending on the method used.

$$\left(\frac{\sigma_a}{\sigma_{-1}}\right)^n + \left(f \cdot \frac{\sigma_m}{\sigma_{UTS}}\right)^m = 1 \tag{3-11}$$

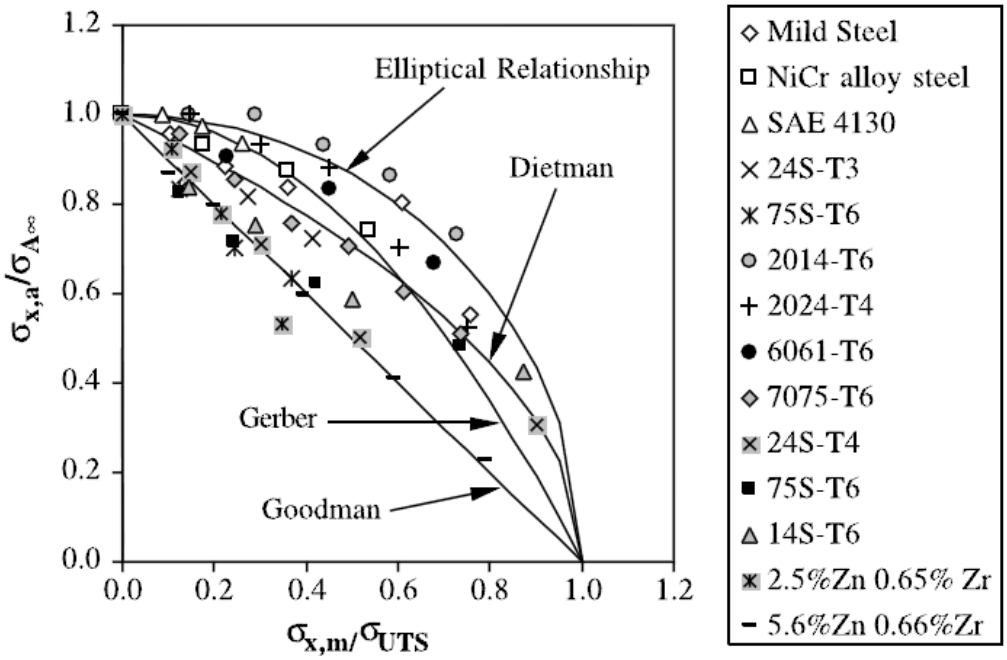

Figure 3-5. *Haigh diagram with lines corresponding to some uniaxial theories about the effect of axial mean stresses [Susmel, 2005].*

With regard to the accuracy of these theories, it could be indicated that no one model is suitable for all types of materials. In some recent studies [Susmel, 2005] it is pointed out that practically all the experimental results are located between Goodman's lines and the elliptical relation (Fig. 3-5).

In addition to the above methods, we could cite Peterson's [Peterson, 1952] method, which uses a cubic relationship for axial mean stresses, and shows a good correlation with experimental results for ductile materials, equation (3-12).

$$\sigma_a = \frac{\sigma_{-1}}{7} \cdot \left(8 - \left[\frac{\sigma_m}{\sigma_{UTS}} + 1 \right]^3 \right) \qquad (3\text{-}12)$$

In order to observe quantitatively the differences between Peterson's method and Gerber and Dietmann classic methods, the three lines on Haigh's diagram are shown for a 25CrMo4 steel [Grün, 1991], whose behaviour could be defined as very ductile. (Fig. 3-6).

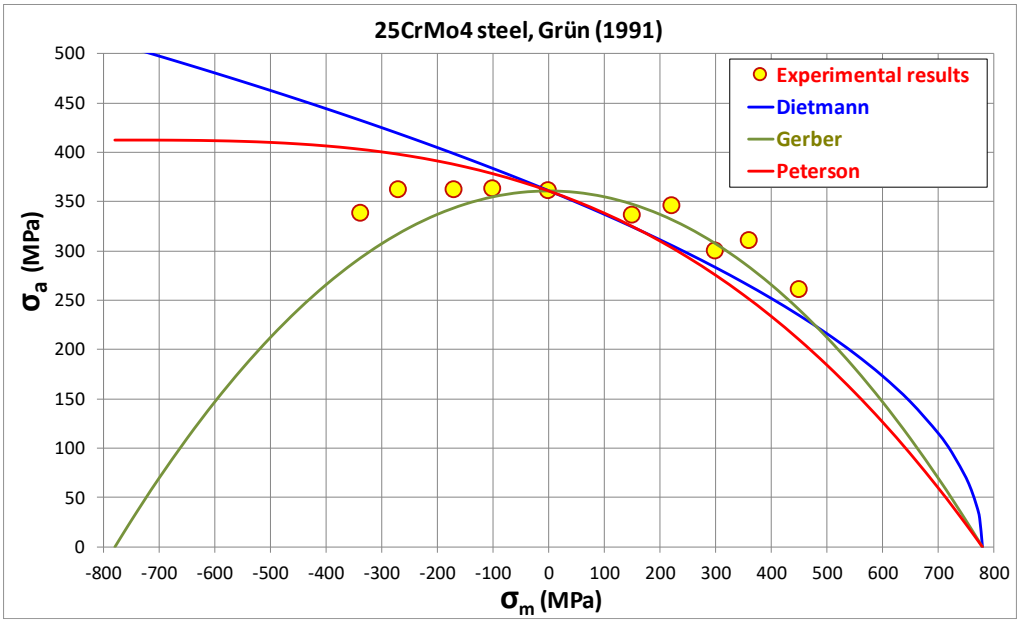

Figure 3-6. *Haigh diagram with experimental results of a 25CrMo4 steel [Grün, 1991] together with Dietmann, Gerber and Peterson lines.*

Regarding the tensile mean stresses, we can observe that Peterson and Dietmann methods have a very similar behaviour, being slightly conservative for experimental data. On the other hand, Gerber's method shows a better correlation, being the best adjustment of the experimental data.

In the case of mean compressive stresses, the Gerber method is symmetrical to the tensile part, being conservative for all experimental results. Peterson's method predicts an increase in fatigue strength, which for a mean compressive stress value of tensile strength, i.e. $\sigma_{m=} -\sigma_{UTS}$, the amplitude of fatigue the material can withstand is 8/7 of the fatigue strength for a fully reversed uniaxial load. The value in the case of the Dietmann line is 2 times the root of the fatigue

limit for fully reversed loads. Both methods, Dietmann and Peterson, are non-conservative for this ductile material.

3.2.2. Advanced uniaxial methodologies

The classical uniaxial theories presented in the previous section are often used to model certain types of materials, as they were not designed to offer a good fit on different types of materials. In order to provide a law that fits a certain range of materials, e.g. steels, it is necessary to use more adjustment data in addition to a static stress, as is the case with classical methods.

- **The Lüpfert method [Lüpfert, 2001]**

This is a formulation with 3 parameters conceived as a generalization of the Dietmann method. The general form of the method is shown in equation (3-13). When parameter p is set to 0.5, Dietmann and Lüpfert methods are equal. The value of parameter n can be found by equation (3-14), by using a second fatigue limit, in this case the fatigue limit for repeated stresses σ_0.

$$\sigma_a = \sigma_{-1} \cdot \left(1 - \frac{\sigma_m}{\sigma_{UTS}}\right)^p \tag{3-13}$$

$$p = \frac{\ln\left(\frac{\sigma_0}{2 \cdot \sigma_{-1}}\right)}{\ln\left(1 - \frac{\sigma_0}{2 \cdot \sigma_{UTS}}\right)} \tag{3-14}$$

As can be seen in Fig. 3-7, thanks to this formulation the effect of the tensile mean stresses can be adequately collected whatever the material, even offering

the possibility of adjusting the method for fragile materials (below Goodman's line), or for ductile materials (above Dietmann's line).

However, a positive influence on fatigue strength is always expected in compressive loads. Therefore, the behaviour of ductile materials such as 25CrMo4 steel shown in Fig. 3-6 cannot be adequately represented.

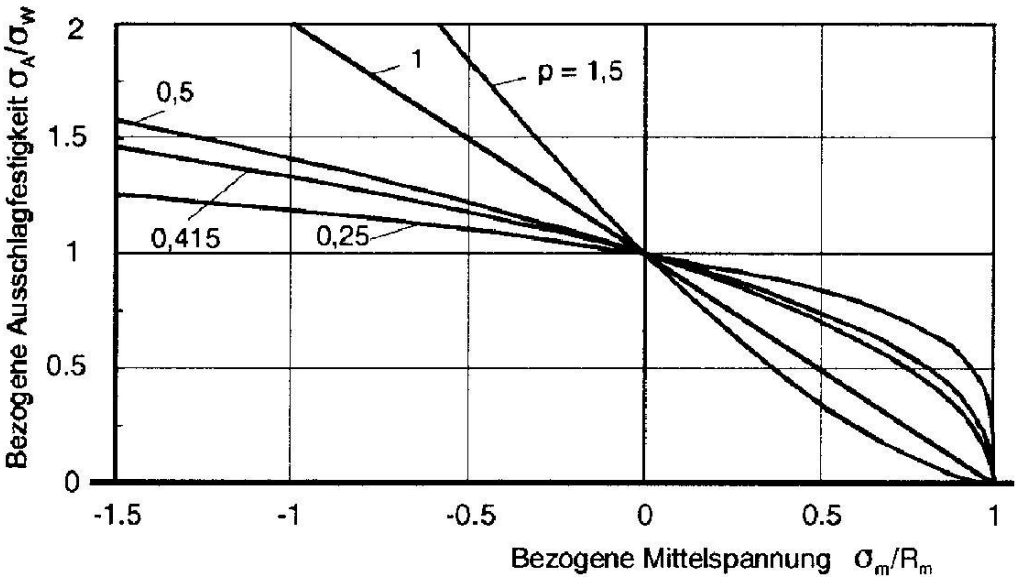

Figure 3-7. *Haigh diagram normalized with different Lüpfert lines depending on the value of parameter p [Lüpfert, 2001].*

The value of parameter *p* recommended by Lüpfert and Spies in [Lüpfert, 2001] for ductile materials is 0.4. In the case of the NRIM list of structural steels [Nishijima, 1993], the value of the *p* parameter takes an average value of 0.43 (Table 3.1), slightly above the Dietmann line (p=0.5) in the tensile part of the Haigh diagram, and slightly below it in the mean compressive stresses region.

In a recent research, a value of the Lüpfert parameter "*p"* equal to 0.52 was used for the modelling of the axial fatigue behaviour in compression for a 1045 normalised steel [Avilés, 2013].

Table 3-1. *Experimental values of Lüpfert parameter p for structural steels NRIM JIS standards [Nishijima, 1993].*

No.	JIS steel	σ_{-1} (MPa)	σ_{UTS}(MPa)	σ_0 (MPa)	*p* Lüpfert
1	S25C	214	489	363	0.35
2	S35C	337	697	524	0.54
3	S45C	409	789	627	0.52
4	S55C	452	850	716	0.43
5	SMn438	418	798	671	0.40
6	SMn443	446	861	705	0.45
7	SCr440	507	956	811	0.40
8	SCM435	510	982	823	0.40
9	SCM440	568	1047	895	0.43
10	SNC631	515	924	815	0.40
11	SNCM439	560	1003	851	0.50
12	SNCM447	555	1013	870	0.43
13	SUS 403	413	727	634	0.46
14	SUS 430	300	494	444	0.50
15	SUS 304	229	614	406	0.30
			Mean value of *p*		**0.43**

- **The Stüssi method [Stüssi, 1955]**

This is a formulation that allows to represent materials whose Haigh diagram is concave, and in which the tensile and compressive strengths are different, as shown in Fig. 3-8.

The method assumes two laws with the same mathematical formulation, which are translated into two curves that are cut in Haigh's diagram. The mathematical formulation of each of the two branches of the Stüssi criterion can be expressed through the equation (3-15)

$$\sigma_a = \sigma_{-1} \cdot \frac{\left(1 - c_1 \cdot \sigma_m\right)}{\left(1 - c_2 \cdot \sigma_m\right)} \tag{3-15}$$

For the adjustment of constants c_1 and c_2 Stüssi proposes to use 2 boundary conditions, which basically mean that for mean stress values equal to the ultimate tensile stress, the stress amplitude is zero, equation (3-16); and that for this mean stress value, the slope in the Haigh diagram is -1, represented by the equation (3-17):

$$\sigma_m = \sigma_{UTS} \Rightarrow \sigma_a = 0 \tag{3-16}$$

$$\sigma_m = \sigma_{UTS} \Rightarrow \frac{d\sigma_a}{d\sigma_m} = -1 \tag{3-17}$$

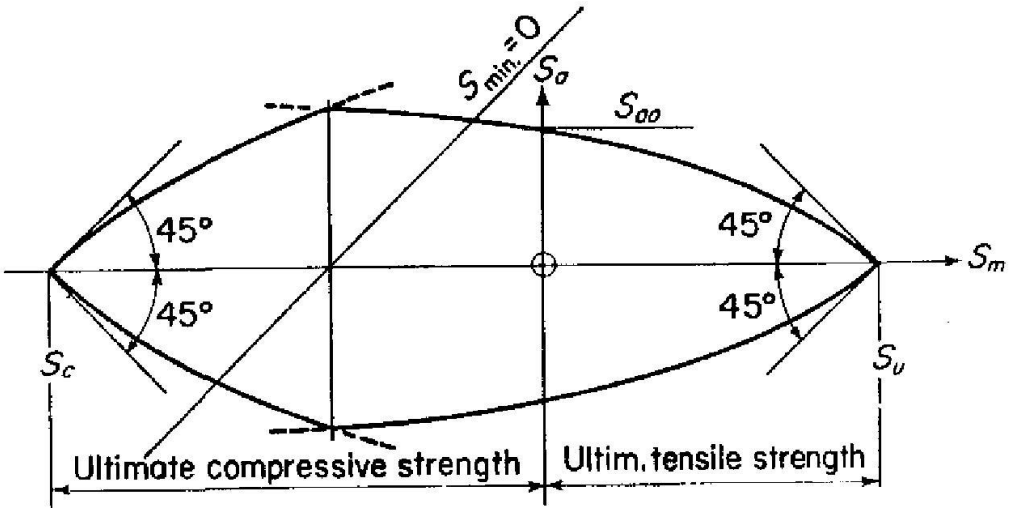

Figure 3-8. *Diagram of Haigh presenting Stüssi's method [Weibull, 1961]*

Similarly, for the compressive part the adjustments of constants c1 and c2 are made using equations (3-18) and (3-19):

$$\sigma_m = \sigma_{UCS} \Rightarrow \sigma_a = 0 \tag{3-18}$$

$$\sigma_m = \sigma_{UCS} \Rightarrow \frac{d\sigma_a}{d\sigma_m} = 1 \tag{3-19}$$

Unlike the Lüpfert method, this method makes it possible to represent ductile materials. However, the data of ultimate resistance to compression, which is relatively difficult to obtain and is offered very rarely in the literature, is necessary. On the other hand, two equations are needed to correctly represent the methodology, making its numerical implementation more complicated.

- **The Bahuaud Method [Brand, 1992]**

This method allows to represent ductile materials with a concave downwards Haigh diagram by means of equation (3-20):

$$\frac{\sigma_a}{\sigma_{-1}} + \frac{1}{\rho} \cdot \left(\frac{\sigma_m}{\sigma_f} \right)^2 + \left(1 - \frac{1}{\rho} \right) \cdot \frac{\sigma_m}{\sigma_f} = 1 \qquad (3\text{-}20)$$

Where σ_f is the real fracture stress in tension and ρ is the relationship between the real fracture stresses in tension and in compression.

The value of the actual tensile fracture stress is not always available, so Bahuaud proposes the following relationship, equation (3-21):

$$\sigma_f = 0.92 \cdot \sigma_{UTS} \cdot (1 + Z_u) \qquad (3\text{-}21)$$

Where Z_u is the reduction of area. On the other hand, Bahuaud demonstrated that the value of the parameter ρ can be correctly represented by the equation (3-22), which relates the fatigue limits totally reversed in alternating torsion τ_{-1} and rotating bending σ'_{-1}.

$$\rho = 3 \cdot \left(\frac{\tau_{-1}}{\sigma'_{-1}} \right) \qquad (3\text{-}22)$$

- **Alternative version of the Bahuaud method with the ultimate tensile strength**

In this Thesis, a modification of the Bahuaud method with the ultimate engineering stress σ_{UTS} instead of the fracture stress is proposed. This way, the method becomes a linear combination of Gerber's and Goodman's methods. The mathematical formulation can be expressed through equation (3-23):

$$\frac{\sigma_a}{\sigma_{-1}} + \frac{1}{\rho} \cdot \left(\frac{\sigma_m}{\sigma_{UTS}} \right)^2 + \left(1 - \frac{1}{\rho} \right) \cdot \frac{\sigma_m}{\sigma_{UTS}} = 1 \qquad (3\text{-}23)$$

Where the value of ρ can be calculated by equation (3-22) if the loads are rotating bending, or equation (3-24) if the loads are pure axial:

$$\rho = 3 \cdot \left(\frac{\tau_{-1}}{\sigma_{-1}} \right) \qquad (3\text{-}24)$$

With these slight modifications to the Bahuaud method, a multitude of ductile materials, such as 25CrMo4 steel tested by Grün [Grün, 1991], can be adequately represented. Fig. 3.9 shows how this method has a better agreement in the compressive part compared to the classical Dietmann and Gerber methods.

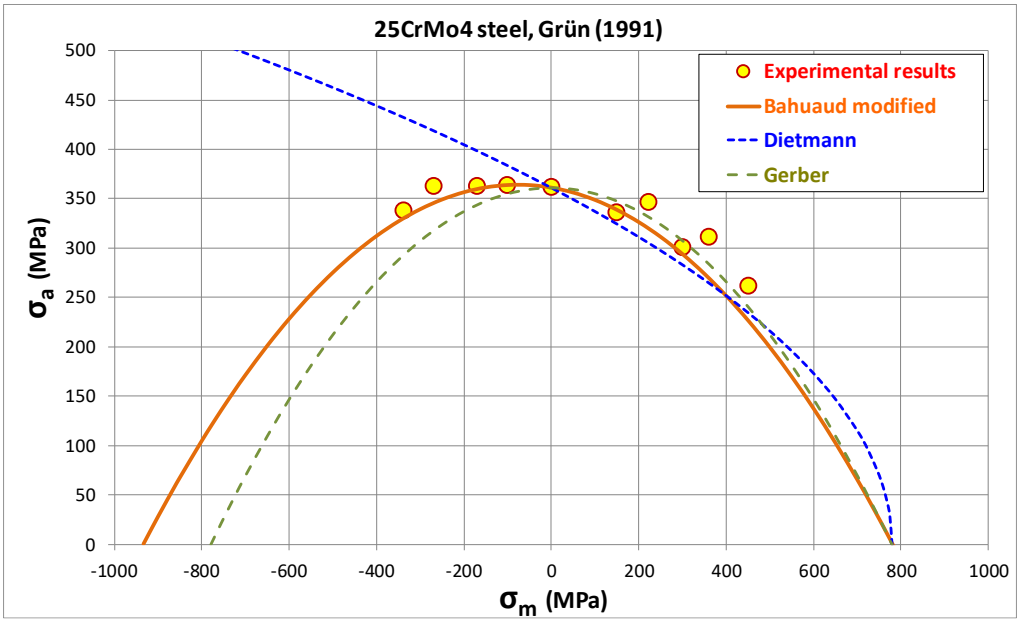

Figure 3-9. *Haigh diagram of a 25CrMo4 steel [Grün, 1991] together with the modified Bahuaud, Dietmann and Gerber lines.*

- **The FKM Guideline [Haibach, 2003].**

The German standard FKM (Forschungskuratorium Maschinenebau) is widely used in Europe for fatigue design, and contains a specific section for the treatment of mean stresses. It should be noted that this methodology does not seek abstract truth but is a suitable method of design.

Fig. 3-10 shows the 4 regions into which this regulation divides the Haigh diagram, each of them showing a different behaviour.

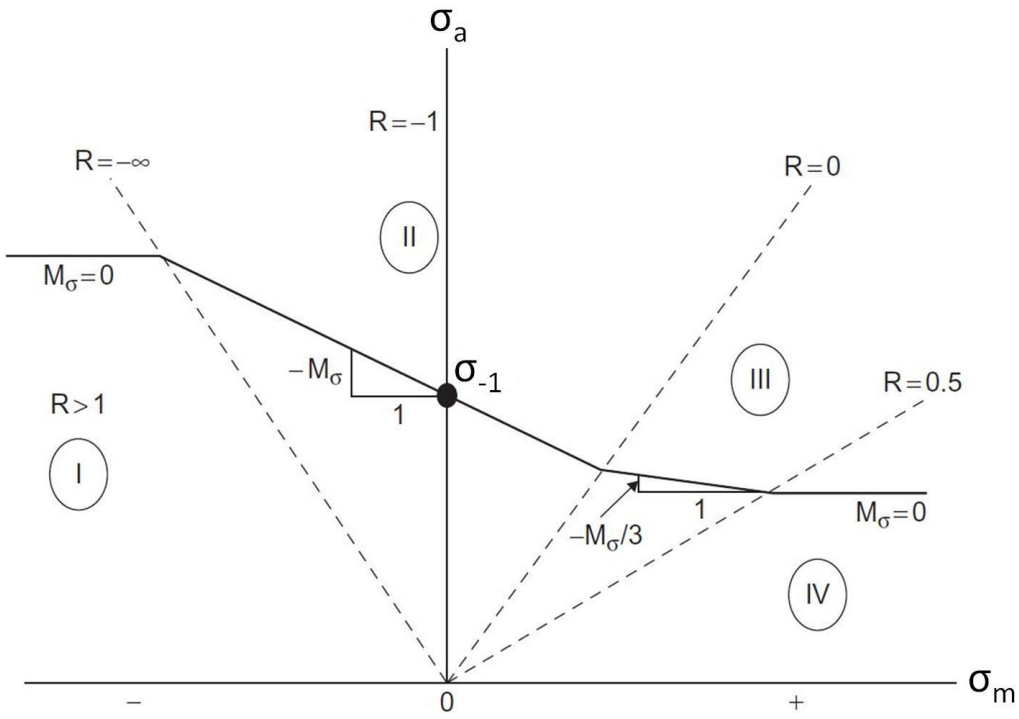

Figure 3-10. *Haigh diagram with representation of the FKM standard, adapted from [Lee, 2012]*

The method captures 4 different regions within the Haigh diagram:

- Region I: For R>1, i.e. fatigue cycles in which the load is always compressive. This region is represented in the Haigh diagram as a horizontal line.
- Region II: This region includes the range -∞<R<0, and is represented as a segment that passes through the data of completely reversed stresses and whose slope M_σ is calculated with the equation (3-25).

- Region III: This region covers the range 0<R<0.5, and is represented by a slope segment $-M_\sigma/3$
- Region IV: For 0.5<R<1 the representation is a horizontal line.

The slope M_σ is calculated through the equation (3-25) and depends on the ultimate engineering stress and on 2 constants a_M and b_M which in turn depend on the type of material, and whose recommended values can be found in table 3.2.

$$M_\sigma = a_M \cdot \sigma_{UTS} + b_M \tag{3-25}$$

Table 3-2. *FKM recommended values for parameters a_M and b_M as a function of material type [Lee, 2012].*

Materials	a_M	b_M
Steel	0.00035	−0.1
Steel casting	0.00035	0.05
Ductile irons	0.00035	0.08
Malleable cast iron	0.00035	0.13
Grey cast iron	0	0.5
Wrought aluminum alloys	0.001	−0.04
Cast aluminum alloys	0.001	0.2

The Haigh diagram of a 30CrNiMo8 ductile steel together with the FKM standard is shown in Fig. 3-11. As it can be seen, the FKM standard is non-conservative in the compressive zone for this ductile material [Rausch, 2011].

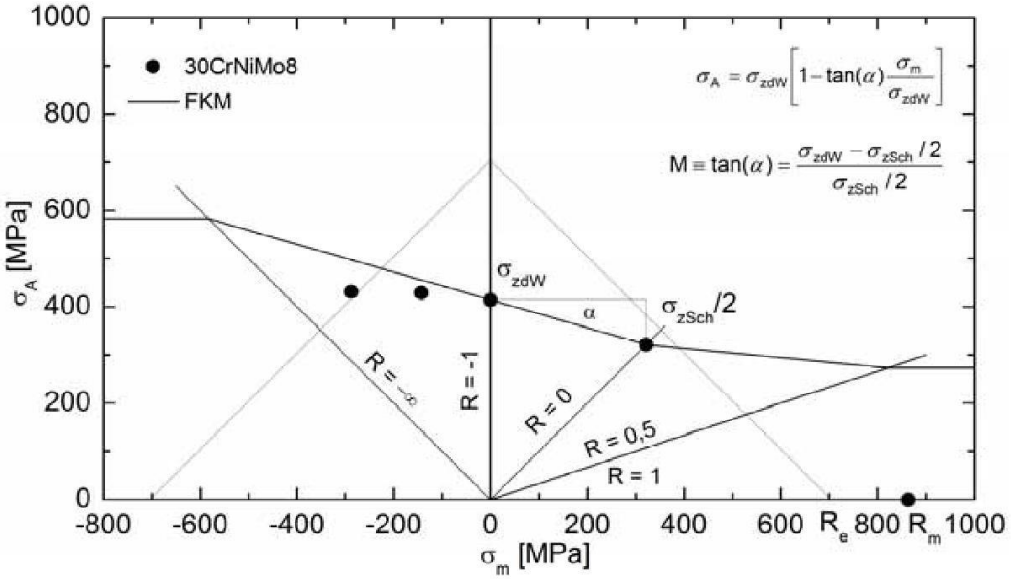

Figure 3-11. *Haigh diagram with representation of the FKM regulation, and experimental data of a 30CrNiMo8 steel [Rausch, 2011].*

3.2.3. Other methodologies of interest

This section will describe several methodologies that explicitly depend on the ratio R between minimum and maximum stress over a fatigue cycle.

- **Jasper's Energy Theory [Jasper, 1923]**

Jasper's method is the first energetic theory of fatigue, and probably the first theory of fatigue based on the physics of the phenomenon, since previously only empirical lines had been proposed without any type of physical foundation except for the *"Goodman's dynamic theory"*.

Jasper proposes that the amount of energy per unit volume per load cycle developed at the fatigue limit for fully reversed stresses should be the same as that developed for the fatigue limit in the case of non-zero mean stresses. This energy is represented in Fig. 3-12 through the shaded area.

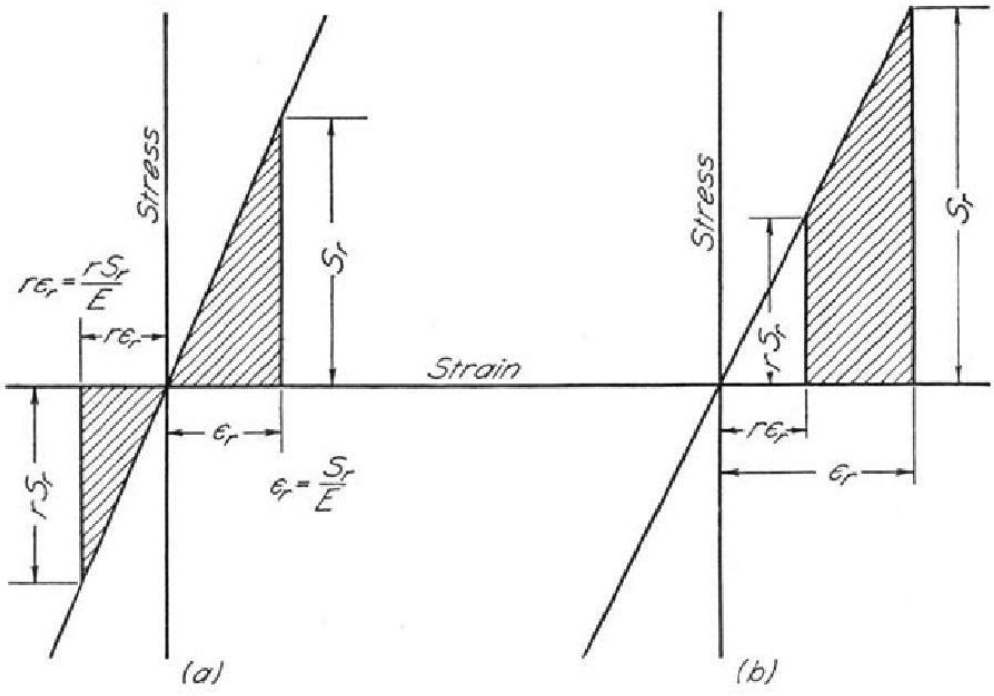

Figure 3-12. *Deformation stress diagrams with energy per cycle (a) completely reversed stresses (b) mean non-zero stress [Moore, 1924].*

The energy for a load case in which the maximum stress is opposite in sign to the minimum stress is described through equation (3-26):

$$W_R = \frac{S_R^2}{2E} + \frac{\left(R \cdot S_R\right)^2}{2E} = \frac{S_R^2 + \left(R \cdot S_R\right)^2}{2E} \tag{3-26}$$

Particularizing for the case of R=-1, equation (3-27):

$$W_{R=-1} = \frac{\sigma_{-1}^2}{E} \tag{3-27}$$

If the amount of energy is the same for a general load case and for the case of reversed loads, then the equation (3-28) is fulfilled:

$$Q = \frac{\sigma_{\max,R}}{\sigma_{-1}} = \sqrt{\frac{2}{1+R^2}} \tag{3-28}$$

For the case in which the maximum stress has the same sign as the minimum stress, and following the same procedure as above, equation (3-29) is arrived at:

$$Q = \frac{\sigma_{\max,R}}{\sigma_{-1}} = \sqrt{\frac{2}{1-R^2}} \tag{3-29}$$

In order to have a single equation governing the fatigue behaviour of the material, Nicholas [Nicholas, 2003] proposed equation (3-30):

$$\sigma_a = \frac{\sigma_{-1}}{\sqrt{2}} \sqrt{\frac{(1-R)^2}{1-R\cdot|R|}} \tag{3-30}$$

- **Moore's line [Moore, 1924]**

This empirical line was proposed by Moore and Jasper to satisfactorily adjust the results of the University of Illinois' extensive fatigue testing campaign on steels.

Fig. 3-13 shows the adjustment of the method with the available experimental results, consisting of equation (3.31):

$$Q = \frac{\sigma_{\max,R}}{\sigma_{-1}} = \frac{R+3}{2} \tag{3-31}$$

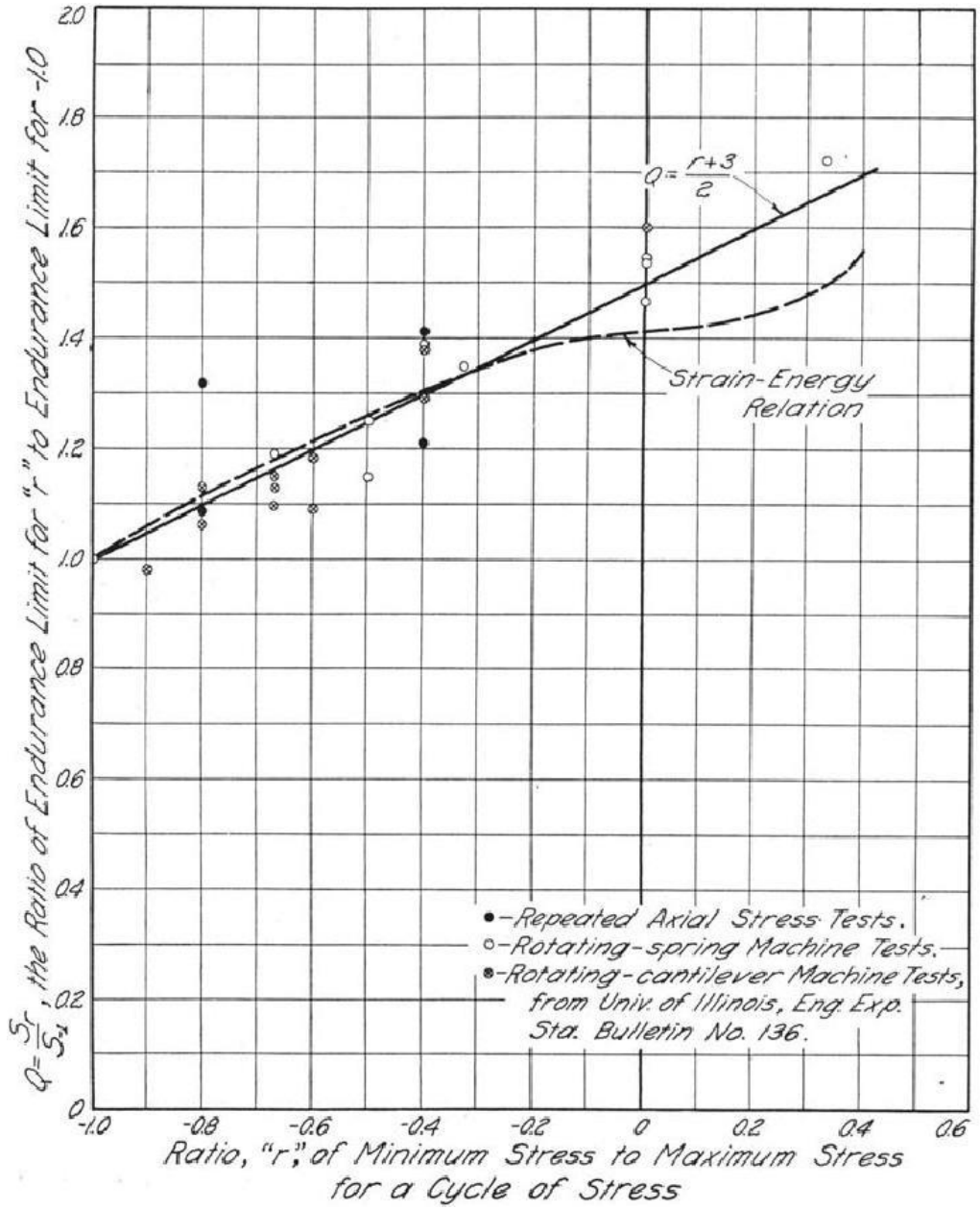

Figure 3-13. *Comparison between Moore-Jasper's empirical method and Jasper's method for experimental results at the University of Illinois [Moore, 1924].*

This method shows a good correspondence with Jasper's energy method for values of R between -1 and 0.2. It is noteworthy that at the time when both methods were formulated in literature there were hardly any tests for R>0 by Haigh, as noted in [Moore, 1924].

Moore's method was designed to adjust results with mean stresses in the bending machine, making it impossible to subject the specimen to a mean compression state. As can be deduced from equation (3-31), the method suffers a numerical incoherence when R=-3, a state with compressive loads.

Figure 3-14 shows Jasper's and Moore's methods on a Haigh diagram together with the experimental results of a 25CrMo4 steel [Grün, 1991].

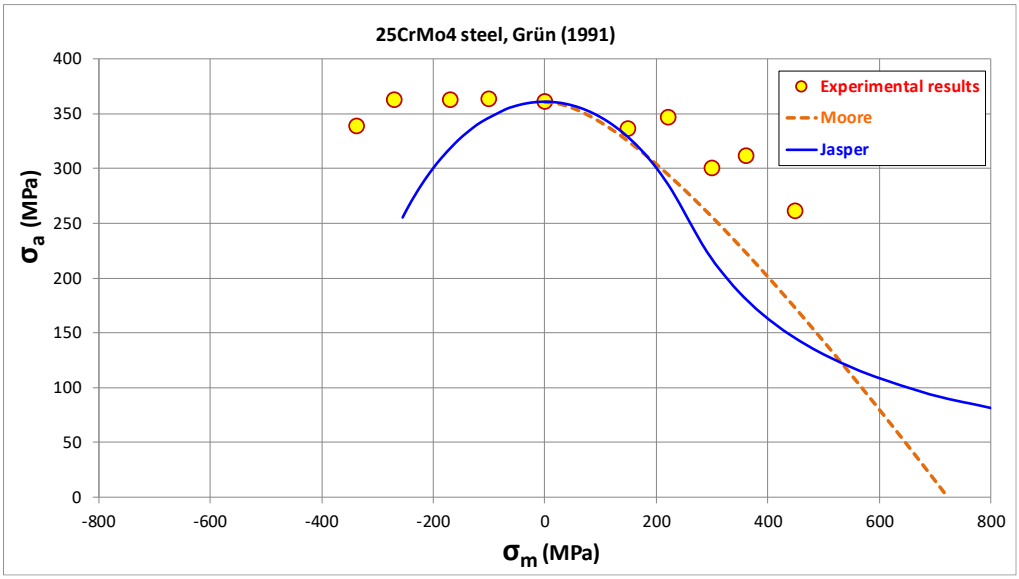

Figure 3-14. *Haigh diagram comparing Moore and Jasper's lines with Grün's experimental results [Grün, 1991].*

It can be observed that Jasper's method shows a concave downward zone in the central part of the Haigh diagram, changing to convex downward for high values of mean tensile stresses. Jasper's line does not intersect with the horizontal axis unlike Moore's line, which shows an intersection with the horizontal axis in this case for a value slightly lower than the ultimate tensile strength σ_{UTS}.

Jasper's method is conservative in the tensile region, and could be considered extremely conservative in the compression zone, as can be deduced from Fig. 3.14, in which a very ductile material is represented.

- **The Nicholas and Maxwell Method [Nicholas, 2002]**

This method is a modification of Jasper's method for adjusting experimental data on an aeronautical titanium. Basically a new parameter α is added which is used as a multiplier on the deformation energy stored in the compressive part of the cycle, as presented in equation (3-32):

$$W_{total} = W_{tensile} + \alpha \cdot W_{compressive} \tag{3-32}$$

Nicholas and Maxwell found that a value of α=0.287 showed a good fit on the Ti-6Al-4V Titanium experimental data for 10^7 cycles, as shown in Fig. 3-15:

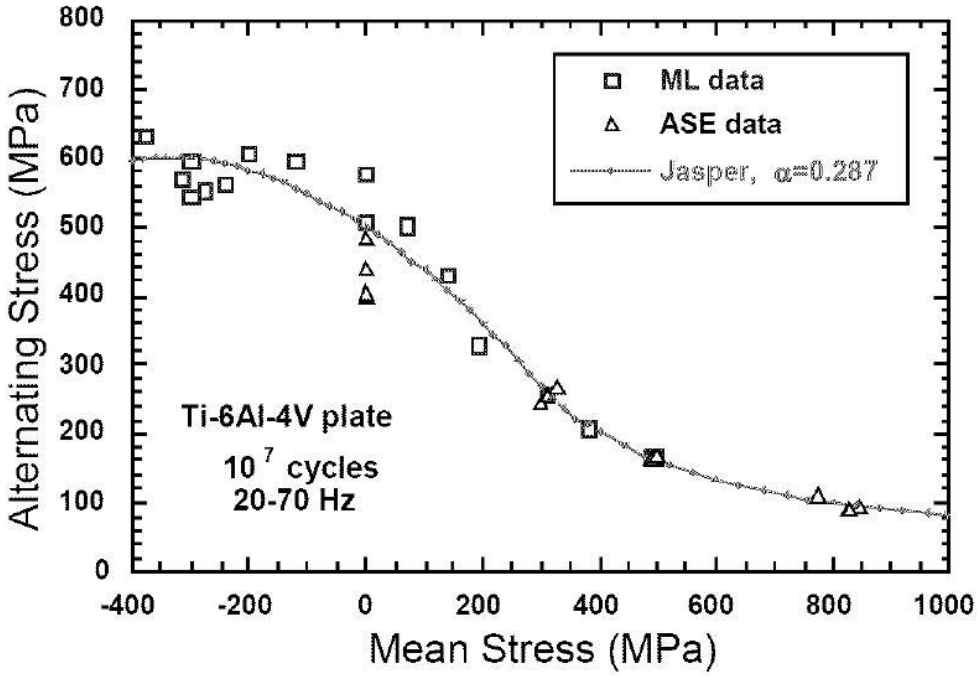

Figure 3-15. *Haigh diagram for Ti 6Al 4V with Jasper's modified equation [Nicholas, 2002].*

- **The Smith-Watson-Topper Method [Smith, 1970]**

The Smith-Watson-Topper (SWT) formulation [Smith, 1970], although defined as a critical plane, and generally used in LCF, can be applied to high cycle fatigue considering stress elasticity. The damage model is based on the hypothesis that life is controlled very early by growth through planes perpendicular to the direction of maximum deformation and normal stress, equation (3-33):

$$\sigma_{n,\max}\frac{\Delta\varepsilon_n}{2}=\frac{\sigma'^2_f}{E}\left(2N_f\right)^{2b}+\sigma'_f\,\varepsilon'_f\left(2N_f\right)^{b+c} \tag{3-33}$$

Assuming elastic stresses and applying this method to the uniaxial case adjusting it for the case of totally reversed stresses can be written using equation (3-34):

$$\sigma_{a,R}=\sigma_{-1}\cdot\sqrt{\frac{1-R}{2}} \tag{3-34}$$

This method is recommended for materials in which the mode of damage is mainly caused by propagation, typical generally of fragile materials, in fact the shape of this methodology in the Haigh diagram is a convex downwards line.

- **The Walker Method [Walker, 1970]**

This formulation is based on the Smith-Watson-Topper formulation but adds an extra parameter called γ that allows a superior adjustment to the SWT method. This function was created to adjust crack propagation data on two types of aluminiums. For the uniaxial case with mean axial stresses, the method can be described through equation (3-35):

$$\sigma_{a,R}=\sigma_{-1}\cdot\left(\frac{1-R}{2}\right)^{1-\gamma} \tag{3-35}$$

Examining equations (3-34) and (3-35) it can be seen that SWT is the particular case of Walker's equation when the parameter γ takes the value of 0.5.

To adjust the value of this parameter in steels the equation (3-36), obtained as best fit by Dowling in [Dowling, 2009A] can be used:

$$\gamma = -0.0002 \cdot \sigma_{UTS}[MPa] + 0.8818 \qquad (3\text{-}36)$$

In the case of aluminium, Dowling [Dowling, 2009A] found that this value could vary between 0.4 and 0.7, not being a direct dependence on the last engineering stress, but is a function of the type of aluminium, as can be seen in Fig. 3-16:

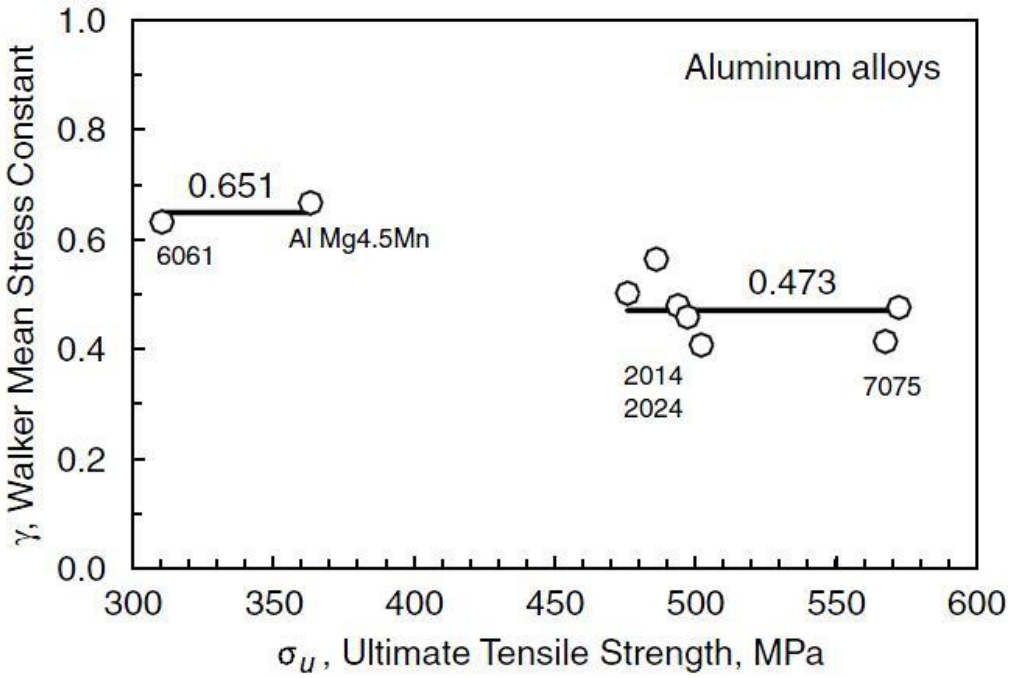

Figure 3-16. *Walker parameter values for different types of aluminiums [Dowling, 2009A]*

For 2000 and 7000 series aluminiums, Walker's optimum constant is close to 0.5, which corresponds to the SWT formulation. On the other hand, for the

aluminium of the 6000 series, the effect of the mean stresses is smaller, taking Walker's parameter a value of approximately 0.65.

When the Smith-Watson-Topper and Walker methods are represented in the Haigh diagram, they show a convex shape. Fig. 3-17 represents both methods together with the Grün experimental data: as can be seen, Walker's method with a parameter γ=0.726 from the application of the equation (3-36) offers a superior fit to the SWT method. Walker's method shows a good correlation with experimental results in the tensile zone. However, the convex downwards shape of the Walker method causes the method to be non-conservative for ductile materials in the compressive part.

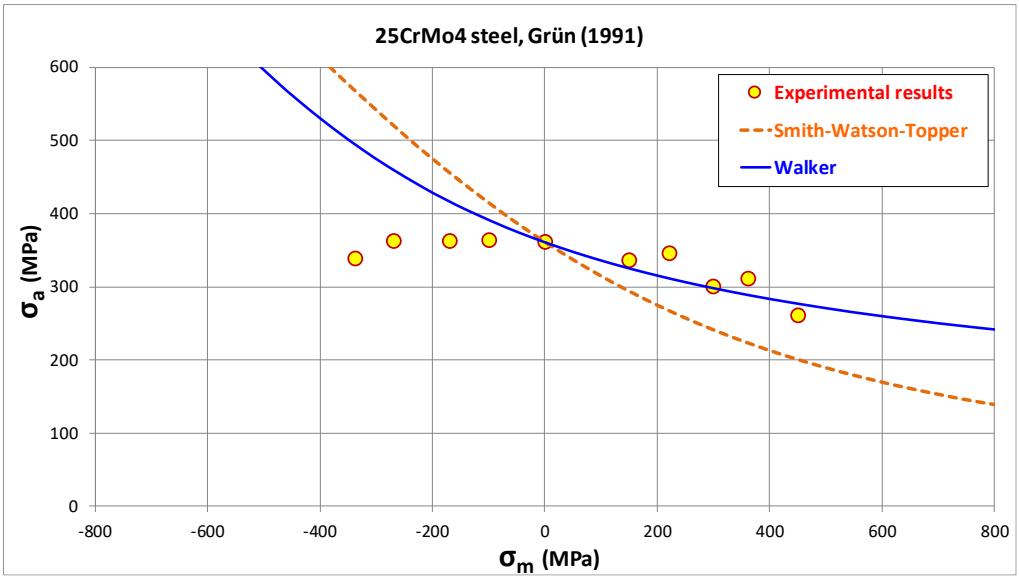

Figure 3-17. *Adjustment of Grün experimental data [Grün, 1991] with the Smith-Watson-Topper and Walker methods*

3.3. Theories about the effect of axial mean stresses

In this Thesis an effort has been made to bring together all known theories about the effect of mean stresses. In literature we can find several examples of compilation of theories in [Marin, 1956], [Woodward, 1956], [Findley, 1959] and [Ukrainetz, 1960]. Basically, they could be summarized in 9 theories, most of which were proposed before the 1960s:

1) The effect of axial mean stresses is related to the energy accumulated in the direction of the main stress [Jasper, 1923], [Delahay, 2003].

2) The effect of the mean stresses could only be due to the damage produced by the maximum stress reached throughout the cycle, the mean stress having no importance by itself [Gough, 1951].

3) There is no fatigue damage with maximum stresses below the proportionality limit [Orowan, 1939], [Freudenthal, 1946].

4) The presence of stress micro-concentrators within the material itself causes similar fatigue behaviour to that of ductile notched materials [Smith, 1942], [Gunn, 1955], [Beretta, 2003].

5) In a theoretical material by von Mises, the effect of normal stresses at the critical plane is quadratic, with no influence of hydrostatic stress. Moreover, by equating the energies produced in N cycles in the case of completely reversed alternating stresses and the case of static stresses superimposed on a variable stress, we arrive at an elliptical relationship between mean and alternating stresses [Marin, 1956].

6) The shape of the R-M diagram could be related to the phenomenon of crack propagation [Woodward, 1956].

7) Normal to flat high amplitude shear stresses allow propagation of a micro crack initiated by shear stresses. This effect is approximately linear in some materials, being clearly non-linear in others [Findley, 1959].

8) The effect of the mean stresses is related to the total stored elastic deformation energy [Froustey, 1992].

9) The increase in the mean normal stresses in materials with defects causes a change in the initiation from surface to interior [Bomas, 2009], [Furuya, 2010].

By themselves, none of these theories is capable of fully explaining the phenomenon of axial mean stresses, or at least not for all types of materials. For example, Gough's theory that damage is caused by maximum stress throughout the cycle has been refuted by some tests, especially those of O'Connor and Morrison on quenched and tempered steel [O'Connor, 1956], which show that it is not only the maximum stress, but also the mean stress that has an influence on fatigue strength. However, Crossland's method, which stipulates that there is no mean stress effect but that it is the maximum stress - in particular, the maximum hydrostatic stress $\sigma_{H,max}$ - that causes the damage, was formulated using only part of these O'Connor data, and ignoring others of vital importance.

Some of these theories are related to each other, and others complement each other. For example, 4) and 7) were related by Findley through the creation of voids. These same theories have also been related through the mechanics of the linear elastic fracture, generalizing this effect not only to the micro-holes but also to the inclusions [Murakami, 2002].

On the other hand, 6) and 7) are clearly related: a normal compressive stress to the plane where a crack has started will tend to slow the propagation and a tensile stress will tend to open the crack.

In the same way, 6) and 9) are related to fatigue of high and especially very high cycles when the initiation takes place fundamentally inside the specimen for high values of mean stress, being the case of titaniums with double phase and steels of very high resistance such as those of bearings.

Additionally, it has been observed that for some materials the shape of the R-M diagram is different depending on the number of cycles. In low cycles (LCF), where propagation is more important, the shape of the R-M curve can vary substantially from high cycles (HCF), where propagation is substantially less important in relative terms.

However, it seems difficult to agglutinate all these theories into a single fatigue theory, since it is possible that the abstract truth about axial mean stresses includes very complex phenomena of monotonic and cyclic plasticity linked and interacting with other phenomena such as the propagation of micro cracks and the relaxation of stresses in very localized areas of the material, such as inclusions or surface defects.

In the following section we will analyse the experimental results collected in the literature that allow to contrast the 9 previously mentioned theories, with the objective of developing a multiaxial fatigue theory that is capable of reflecting the diverse observable aspects in Haigh's diagrams, especially concerning ductile metals.

3.4. Experimental results from literature

3.4.1. Introduction

In this section we will analyse the experimental results of greatest interest in terms of mean stresses. First, the main compilations of experimental results will be presented, including those by Smith, O'Connor and Sines, which had a great impact on the design and creation of multi-axis methodologies. Klubberg's relatively modern collection, which shows experimental results not very well known in the Anglo-Saxon literature, will then be examined.

(a) Smith's collection of experimental results [Smith, 1942]

(b) Results of O'Connor and Morrison steels [O'Connor, 1956]

(c) The compilation of results by Sines [Sines, 1959]

(d) Klubberg's compilation of results [Klubberg, 2011]

The first of these was published in the middle of World War II and had a great impact in terms of fatigue design for ductile materials. Its objective is not the search for the abstract truth of fatigue behaviour, but simple design rules that allow safe designs to be obtained.

The study of the mean stresses of O'Connor and Morrison [O'Connor, 1956] consists of a critical review of experimental results on steels, and a campaign of tests on a ductile steel. Part of these data, especially the almost linear effect of the mean stresses in the elastic range, were used by Crossland himself for the formulation of his method.

The compilation of Sines [Sines, 1959] has had a great influence later on basic research in Fatigue, validating the criteria that argue for a linear effect of mean stresses such as the multi-axial methods of Crossland, Sines or Dang Van.

The Klubberg compilation of results [Klubberg, 2011] contains a multitude of experimental results for structural steels, classical aluminium alloys and nanostructures. This author provides a new point of view focusing mainly on the shape of curves, showing the different types of materials in function of Haigh diagrams with concave, flat, and convex shape.

Subsequently, other experimental results collected from the literature will be analysed, which will be shown according to the type of material, taking into account the following categories of ductile materials: steels and aluminium.

These experimental results will make it possible to identify the possible shortcomings of the first two compilations of results, and will make it easier to understand the different shapes in Haigh's diagrams and to relate them to the different theories explained previously in section 3.3.

3.4.2. Smith's collection of experimental results [Smith, 1942]

The first comprehensive review of a large collection of experimental results was conducted by Smith [Smith, 1942] in the midst of the development of war effort industries. Its objective was undoubtedly to obtain simple and safe design standards for various types of materials depending on their ductile or fragile nature, and taking into account smooth and notched specimens. The importance of Smith's study lies in the subsequent influence it has had on design standards, opting for Goodman's modified line.

Fig. 3-18 shows the results for non-notched ductile materials, namely brass, various aluminiums and steels. The Haigh diagram shows the normalized mean stresses at the ultimate tensile strength. As can be seen, there is a high dispersion of results, so that none of the usual design lines (modified Goodman, Gerber, etc.) would allow a correct representation of all materials. Smith recommended the use of Goodman's line for tension as there are hardly any experimental results below it.

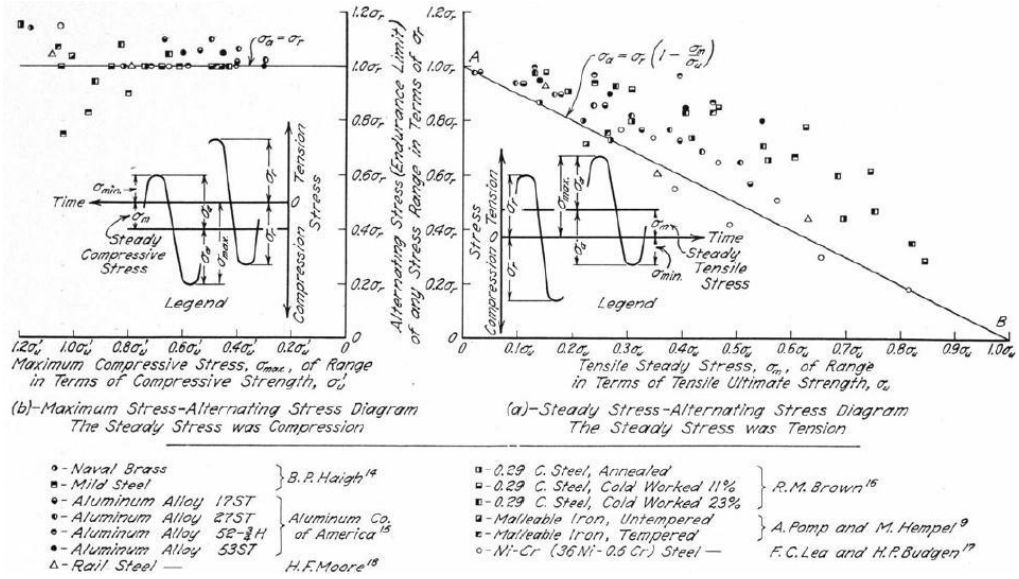

Figure 3-18. *Compilation of Smith results [Smith, 1942] for unnotched ductile materials*

In the compression zone, where there is also a high dispersion, Smith suggested using a horizontal line through the fully reversed fatigue limit. However, it can be observed that some of the materials suffer a loss of strength.

Smith also performed data collection for ductile materials and notched specimens, which are shown in Fig. 3-19. As Smith points out, in the tensile zone there are few differences between figures 3-15 and 3-16, with most experimental results above the modified Goodman line (A-B line). The influence of Smith's work has been very important in terms of mechanical engineering design, as it gave a definitive boost to Goodman's modified line, as this is a suitable criterion for ductile materials and appropriate even in the case of having external stress concentrators.

As for the results in the compressive zone, in this case there is no test in which the fatigue resistance has been reduced with respect to the case of totally reversed stresses, so this line is even more conservative than in the case of smooth specimens.

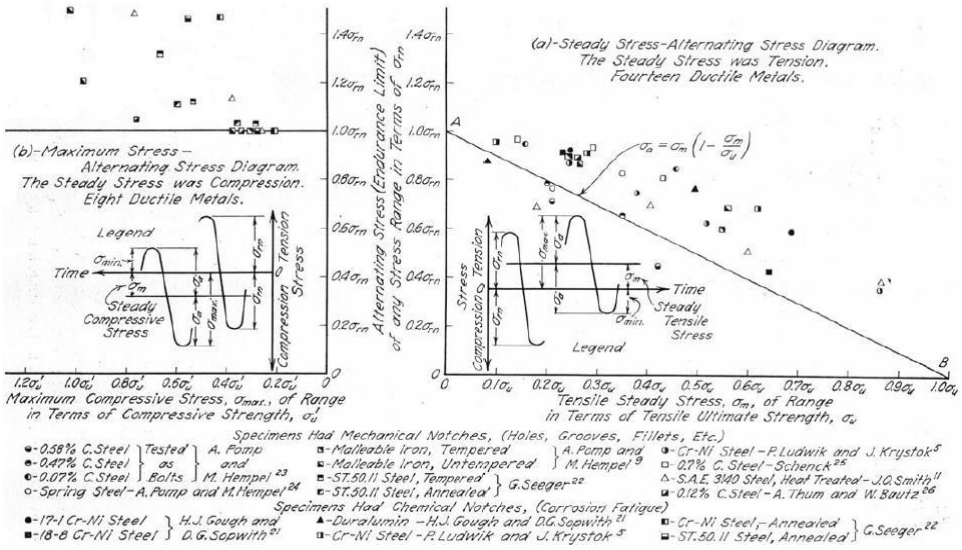

Figure 3-19. *Compilation of Smith results [Smith, 1942] for notched ductile materials*

As for fragile materials, Smith compiled the results of 5 cast irons (fragile) with and without notch. With tensile mean stresses, Smith found that Smith's empirical parable was a more conservative relationship than Goodman's line.

For mean compressive stresses, fatigue strength is always higher than that shown for fully reversed stresses. It is important to note that for cycles with mean compressive stresses in which the maximum stress is also compressive, the results show that there is no longer an improvement in the amplitude of stress that the material is able to withstand, reflected with the horizontal lines in Fig. 3-20 (right image). It is noteworthy that this horizontal line for fatigue cycles with always compressive stresses is recommended by the FKM standard, previously explained in advanced uniaxial methodologies.

According to Smith, "this observation may suggest that fracture due to repeated compressive stress ranges is probably associated with the shear stress range, which is maximum in a plane at 45 degrees from the specimen. The fact that the fracture progresses along an oblique plane through the specimen gives further support to the idea that fatigue fracture can be caused by the range of repeated shear stress.

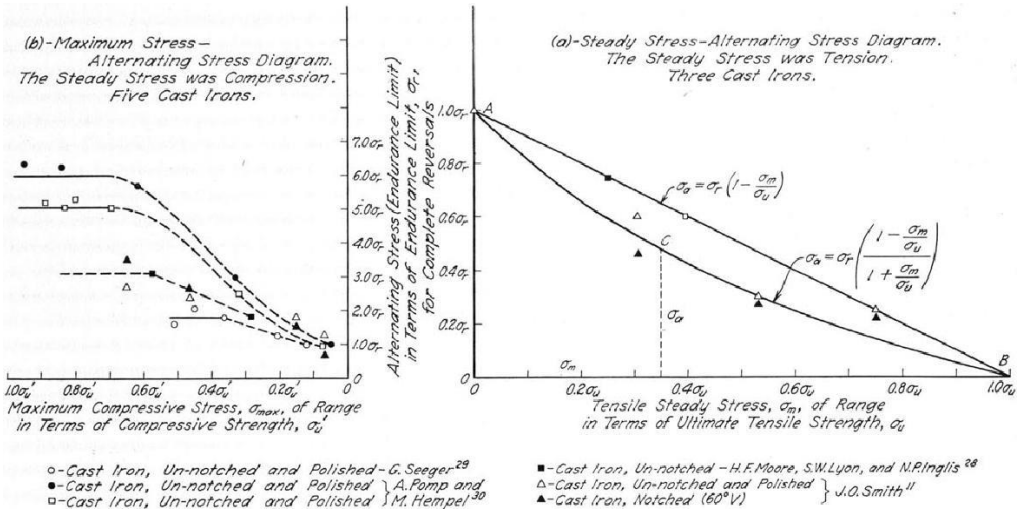

Figure 3-20. *Compilation of Smith results [Smith, 1942] for cast irons (fragile) with and without notch*

3.4.3. The Study of O'Connor and Morrison's of mean stresses on steels [O'Connor, 1956].

In the context of the First International Metals Fatigue Congress, O'Connor and Morrison presented a compilation of axial experiments with mean stresses on steels (Fig. 3-21). The results were presented in a Haigh diagram normalized only with the ultimate tensile strength σ_{UTS}. The intention of the authors was twofold: on the one hand to show that fatigue limits cannot be normalized in a single way with σ_{UTS}, and on the other hand to show that - as with Smith- results - there is no single experimental line (modified Goodman, Gerber, etc.) that is capable of adjusting the effect of mean stresses for all materials.

After analysing the data, these researchers concluded that there are 2 typical shapes of Haigh's diagram:

- Haigh diagram symmetrical and with an approximately parabolic shape, behaving similarly in tension and compression and both mean stresses (positive and negative) exerting the same damage, following to a large extent the predictions of Gerber's parabola. This family of curves includes Haigh's tests on low-carbon steels, although O'Connor and Morrison point out that there are many similar results in the literature.

- Highly asymmetrical Haigh diagram, "crossing the vertical axis of zero mean stresses at a considerable angle and in the mean compression zone there is no sign of reversing the slope". In other words, this type of Haigh diagrams always shows an increase in fatigue strength at mean compressive loads.

The authors show great concern in this regard, as they consider that the differences between the two behaviours do not seem justified by the differences between the materials, citing as an example the discrepancies between Haigh's and Gough's results from apparently similar materials.

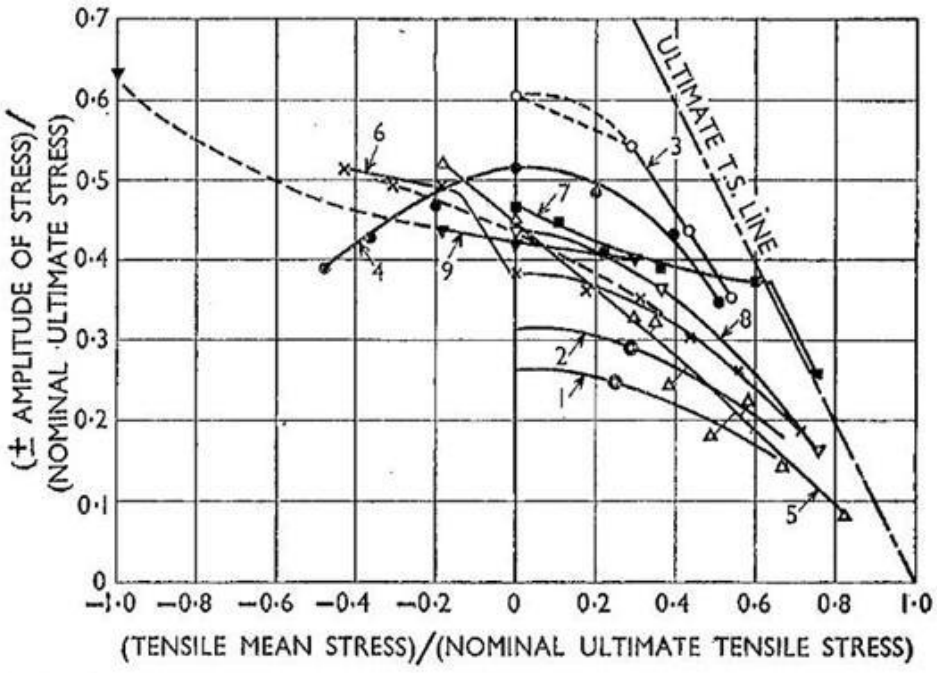

1, 2. J. Bauschinger, axle steel and wrought iron respectively.
3. J. H. Smith, 3¼ per cent nickel steel.
4. B. P. Haigh, 0·13 per cent carbon steel.
5. E. C. Lea and H. P. Budgen, 3½ per cent nickel-chromium steel (8×10^6).
6. R. M. Brown, 0·3 per cent carbon steel (12×10^6).
7. H. J. Gough and W. A. Wood, 0·12 per cent carbon steel.
8. W. J. Trapp and R. T. Schwartz, SAE 4340 (1·8 per cent nickel-chromium-molybdenum) steel.
9. W. N. Findley, SAE 4340 steel.

Figure 3-21. *Haigh diagram normalized with compilation of experimental results of O'Connor and Morrison steels [O'Connor, 1956].*

Taking into account these discrepancies, and in order to resolve the uncertainty, these same researchers tested a NiCrMo steel before several values of mean

axial stresses including compression, for which they designed a specimen and a clamping mechanism to ensure compression.

Fig. 3-22 shows the results in both nominal and real stresses (calculated by reducing or increasing the area if necessary). It should be noted that this diagram is of the second type indicated above, with an asymmetrical diagram in which fatigue strength increases with compressive loads. In addition, the shape of the Haigh diagram is concave although with an approximately linear behaviour within the elastic range.

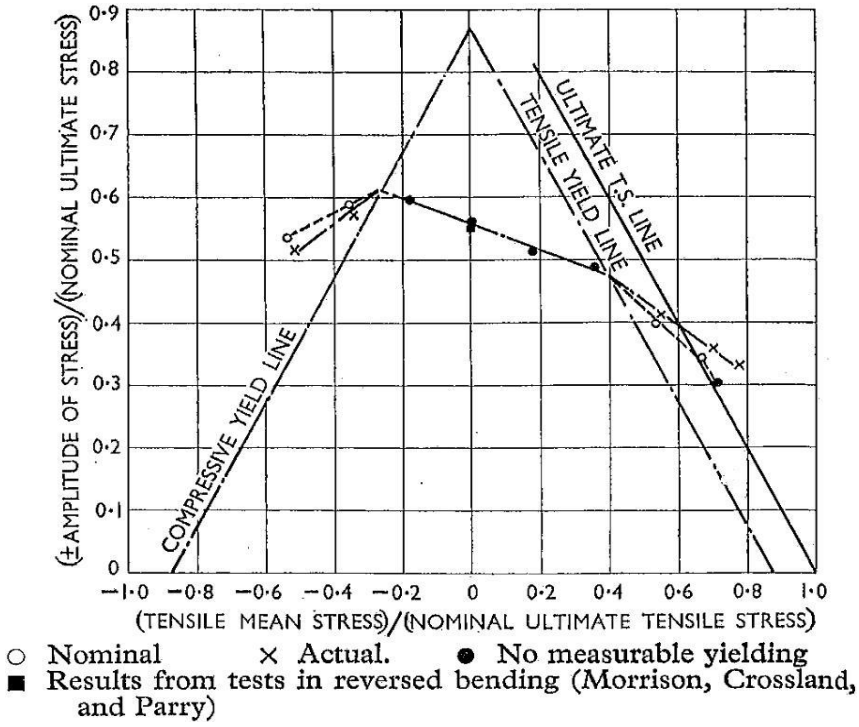

Figure 3-22. *Haigh diagram normalized the experimental results of O'Connor and Morrison [O'Connor, 1956].*

Another aspect pointed out by the authors is the possibility of 3 discontinuities in behaviour, reflected in changes of slope in the curve, when the stress thresholds of yield in tension, yield in compression, and ultimate tensile strength (σ_{UTS}) are exceeded.

Fig. 3-23 shows the experimental results together with some of the uniaxial criteria explained in previous sections.

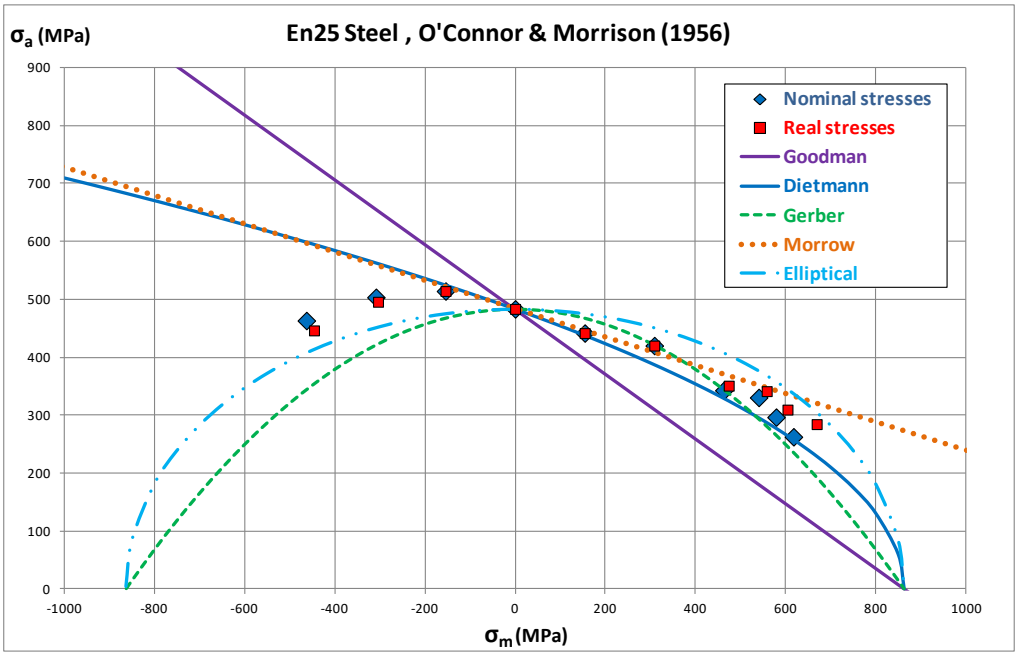

Figure 3-23. *Haigh diagram normalized the experimental results of O'Connor and Morrison and some of the most used uniaxial criteria [O'Connor, 1956].*

None of the uniaxial methods can be said to have a good experimental correlation for all cases of mean stresses. It could be pointed out that the Dietmann and Morrow methods adequately adjust the tensile part data for

nominal and real stresses respectively. However, in mean compression they predict a continuous increase in fatigue resistance that is not endorsed by the experimental results, and therefore Dietmann and Morrow are not conservative for mean compressive stresses.

For mean compressive stresses, the most suitable methods appear to be Gerber and above all the elliptical ratio, which being conservative allows a good fit throughout the entire compression range. The Gerber method, on the other hand, increases its conservatism as the value of the mean compressive loads increases.

Also noteworthy is the following fact, defined as surprising by O'Connor and Morrison, who found no evident signs of plasticity in any specimen subjected to axial mean stresses in which the yield stress would not have been overcome. However, for mean compressive loads in which the compressive yield stress was not exceeded, plasticity phenomena appeared. This fact was evidenced for the point with the highest fatigue strength (5% above the fatigue limit without mean stresses). Although the authors of the article do not give any possible answer, this fact could be related to the overcoming of the fatigue limit, which as many sources in the literature point out is the cyclical yield stress. Therefore, phenomena related to cyclic plasticity, intrinsically different from monotonic plasticity phenomena, could appear when overcome.

3.4.4. The collection of experimental results from Sines [Sines, 1959]

Sines chose a series of experimental results on steels and aluminium in which a perfect axial load in compression had been assured, shown in Fig. 3-24, concluding that the effect of the mean stresses is approximately linear. Thus, by

obtaining the slope of the line in the Haigh diagram (using for example 2 tests) it would be possible to determine its effect.

The diagram shown by Sines involuntarily shows – pointed out by the author - a linear dependence of the normalized mean stress on the yield stress. This linearity is maintained for mean stresses that practically reach the yield stress of the material in tension and compression, thus ensuring plasticity at some point in the cycle in both cases.

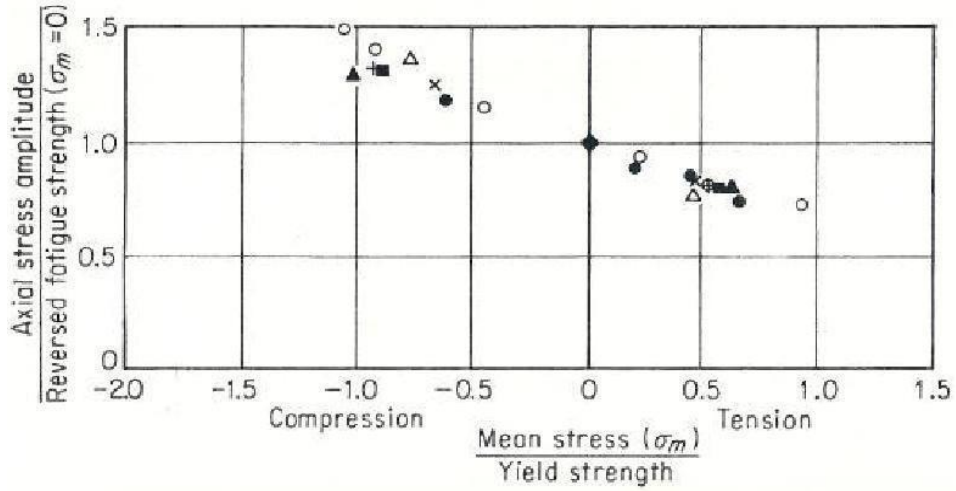

Material	Fatigue strength, psi	Yield, psi	Source
× 24 ST aluminum	± 26,000	48,000	Newmark [16]
○ 0.41C steel	± 36,000	55,000	Nishihara [18]
+ 0.65C steel	± 38,000	57,000	Nishihara "
△ 0.44C steel	± 33,000	57,000	Nishihara "
● Duralumin	± 17,000	32,000	Nishihara [17]
■ Mild steel	± 26,000	38,000	Roš [21]
▲ Mild steel	± 37,000	47,000	Roš "

Figure 3-24. *Normalized Haigh diagram showing results compiled by Sines [Sines, 1959] for steels and aluminiums.*

This compilation of results gave a definitive impulse to the idea that the effect of mean stresses was linear, and giving experimental support to the methods of Sines, Crossland and others later developed such as that of Dang Van.

Although the experimental campaigns of Smith, Sines and O'Connor have had a definite influence on fatigue modelling, and its linear influence, there are subsequent experimental results showing that linear modelling may not be suitable for all materials, especially structural steels and aluminium.

3.4.5. Klubberg's collection of experimental results

This compilation of results is the most current and includes several types of materials: structural steels, classical and nanostructured aluminium alloys, and cast irons, attempting to cover the whole spectrum between ductile and fragile materials, and different Haigh diagram shapes. Many of these experimental results are of great value as they are practically unknown outside Germany, and others were presented for the first time in this comparison.

The most ductile materials according to these authors show a concave downwards Haigh diagram, as can be seen in Fig. 3-25:

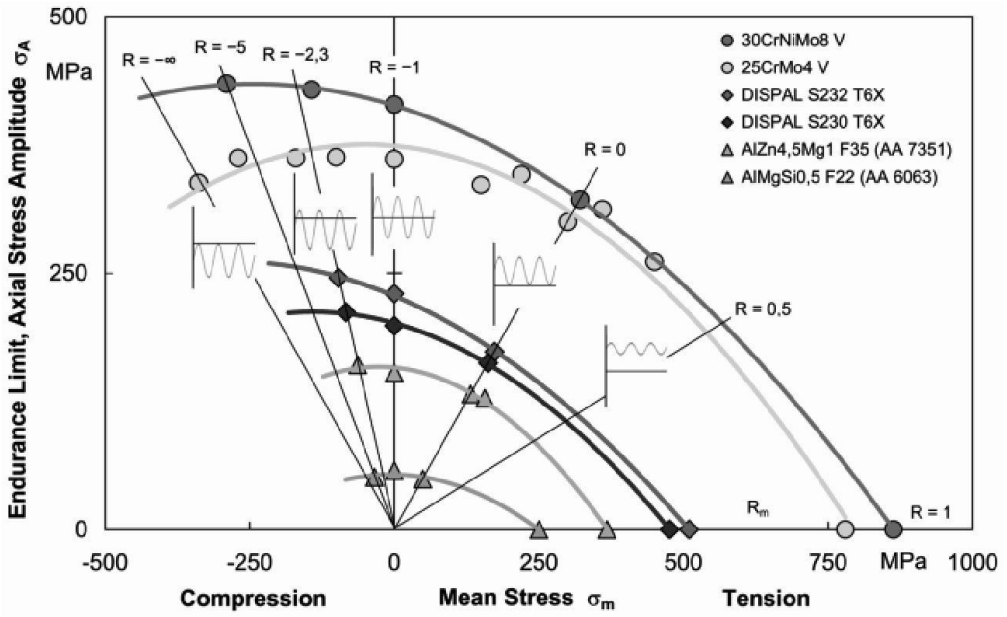

Figure 3-25. *Haigh diagram showing the effect of mean stresses for ductile materials [Klubberg, 2011]***.**

Among the materials analysed in Fig. 3-25 is 25CrMo4 steel which has been shown in the comparison of uniaxial methods. In addition, another structural steel and 4 aluminium alloys are presented together. The shape of the Haigh diagram is concave in all cases, but this does not mean that there cannot be an increase in fatigue strength in the mean compression zone, which is noticeable in the case of aluminium alloys.

It should be noted that the results shown by Klubberg for the steels 25CrMo4 and 30CrNiMo8 show a certain similarity to those presented by O'Connor and Morrison: a concave Haigh diagram with a decreasing slope as the mean compressive stresses become more important.

This comparison also shows other semi ductile materials, mainly nanostructured aluminium alloys, in which the influence of the mean stresses follows approximately a linear influence, adjusting to Goodman's modified line, as can be seen in Fig. 3-26.

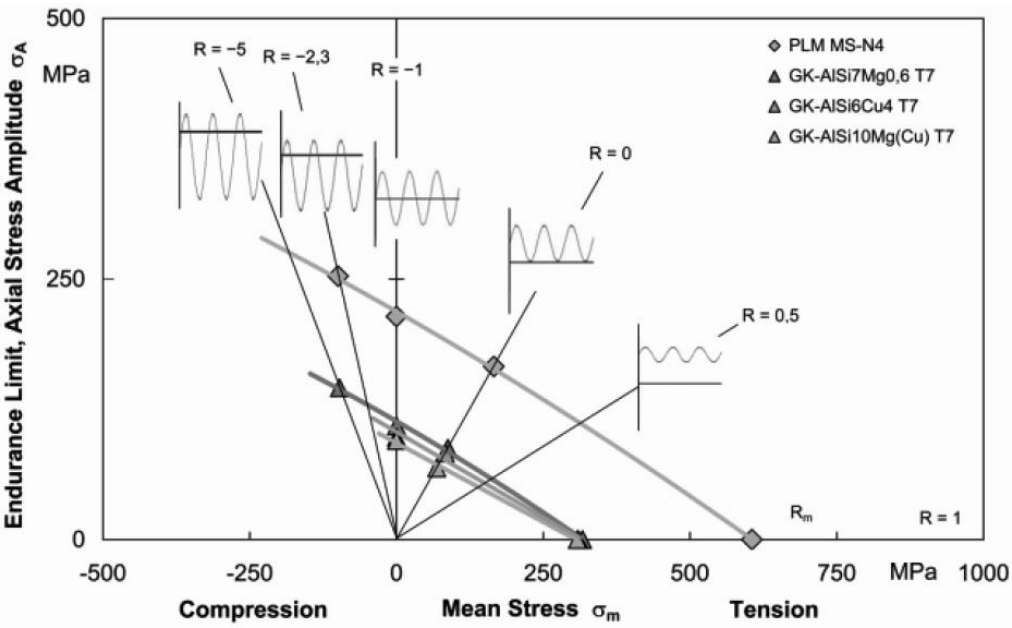

Figure 3-26. *Haigh diagram showing the effect of mean stresses for semi ductile materials [Klubberg, 2011].*

It should be noted that these aluminium alloys contain a higher percentage of silicon than those showing a concave diagram. Silicon is an element known to fragilize materials, which would explain this change in behaviour.

Finally, materials are shown with a convex downwards diagram in Figure 3-27. These are basically cast irons and show a good agreement with the experimental campaign of Smith [Smith, 1942].

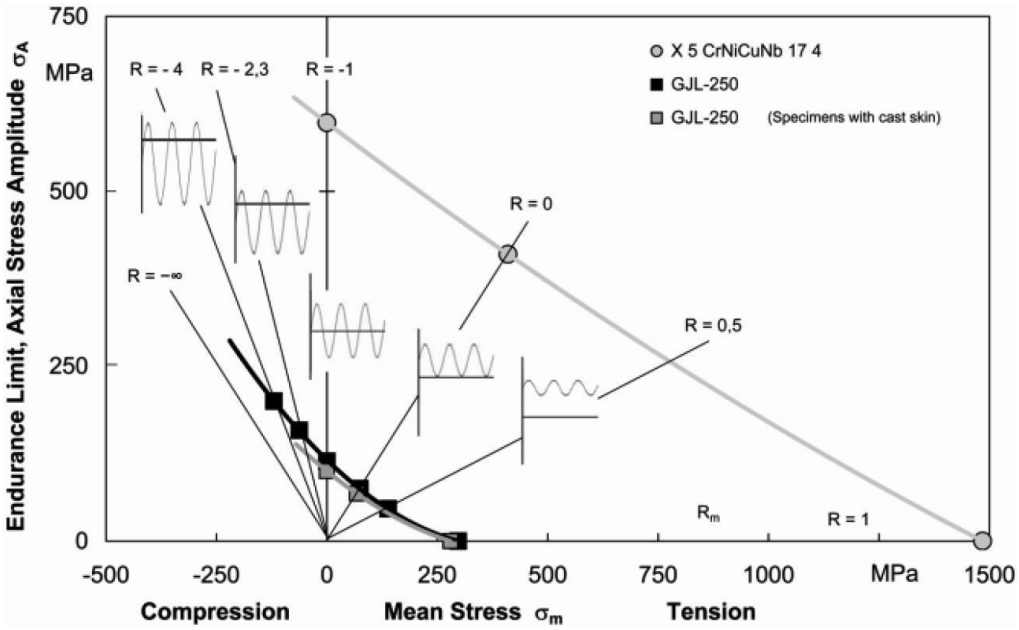

Figure 3-27. *Haigh diagram showing the effect of mean stresses on brittle materials [Klubberg, 2011].*

3.4.6. Other experimental results of ductile steels

In 1960 Ukrainetz [Ukrainetz, 1960] investigated the effect of axial mean stresses on the tensile axial mean problem and the effect of torsional mean stresses on torsional fatigue strength. For this purpose, it chose a 0.1% carbon steel, extremely ductile, being in fact the most ductile material for which uniaxial and multi-axial fatigue data have been found. This material also has 2

characteristics that make it especially attractive for study with the aim of drawing conclusions for the development of a multi-axial fatigue method:

- The metallographic study revealed that this steel can be considered isotropic, with a random orientation of the grains and defects, which are also very small and without angular shapes that could create important internal concentrators.
- The relationship between fully reversed axial and torsional fatigue limits is approximately the root of 3, which coincides with the theoretical value of von Mises' theory.

In addition, it is similar to Haigh and Gough steels in which O'Connor and Morrison [O'Connor, 1956] had observed negligible differences in behaviour.

The Ukrainetz results, which can be seen in Fig. 3.28, are above the Gerber line, and show a cut with the vertical axis as it passes through $\sigma_{m=0}$ approximately horizontally. Among the lines represented in Fig. 3.28, the one corresponding to the elliptical relationship shows a better experimental correlation.

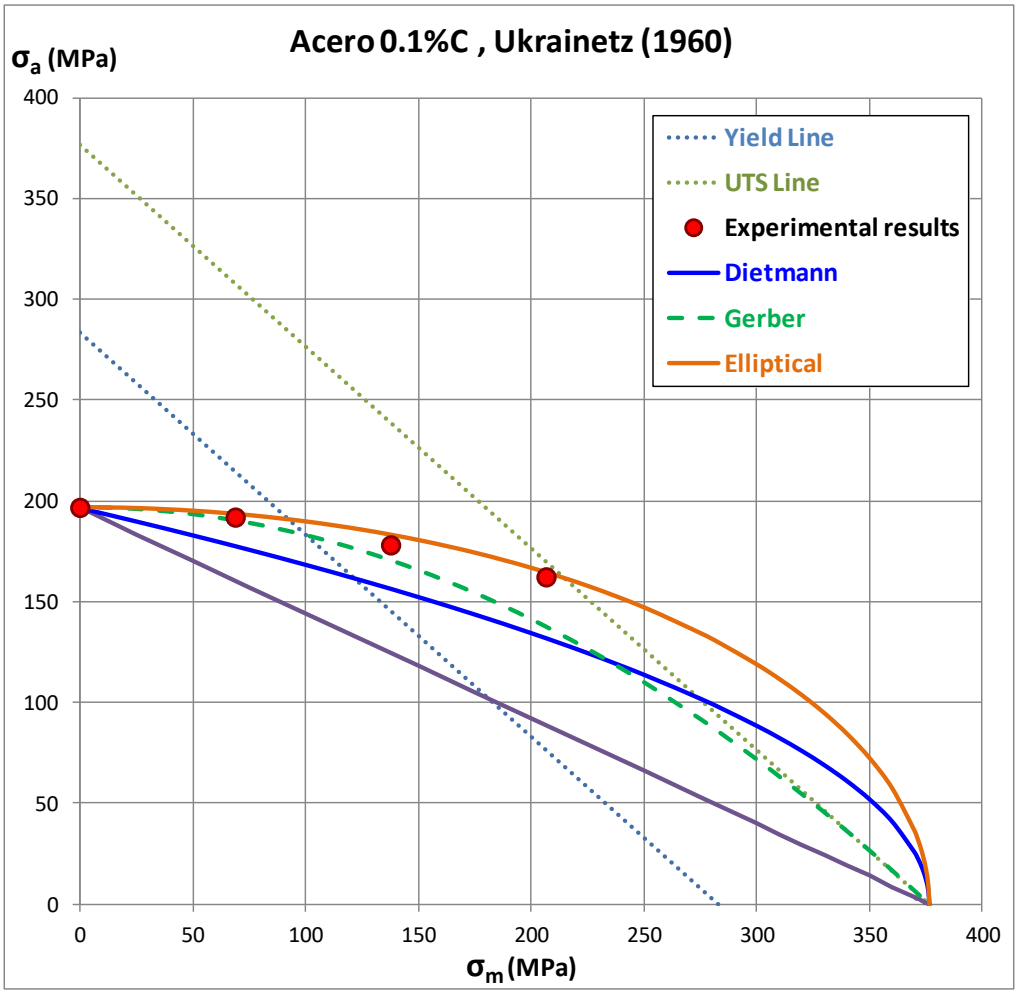

Figure 3-28. *Haigh diagram with experimental results of Ukrainetz 0.1C ductile steel [Ukrainetz, 1960].*

These results support experimentally the Marin theory, which indicates that for a von Mises material there is no influence of hydrostatic stresses, and there is an elliptical relationship between the von Mises equivalents of amplitude stress and mean stress.

3.4.7. Other experimental results of aluminium

In 1956, and also within the International Congress of Multiaxial Fatigue, Woodward, Gunn and Forrest [Woodward, 1956] showed the very extensive experimental campaign of axial fatigue with mean stresses on aluminium. In most cases Haigh's diagram had a concave shape and was between the lines of modified Goodman and Gerber. Only DTD363A aluminum shows a diagram with a "non-orthodox" shape, being convex and below the modified Goodman line. This fact is explained by the authors due to the importance of internal concentrators that act as micro-notches.

Only 2 aluminiums were analysed with mean compressive stresses, which are shown in Fig. 3-29. In both the fatigue strength increases with increasing compressive loads, but the shape is different in both cases.

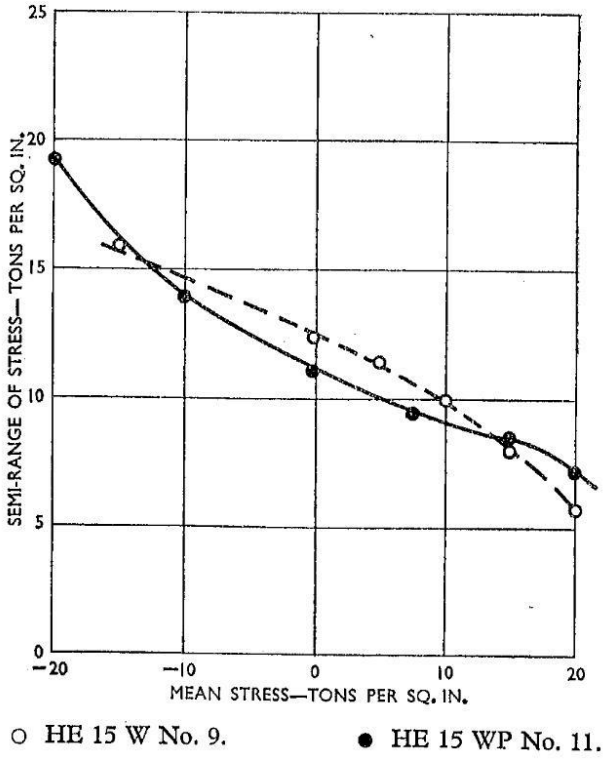

Figure 3-29. *Haigh diagram with experimental results of two Woodward aluminiums [Woodward, 1956].*

The failure criterion to represent the data in Fig. 3-29 is the total rupture of the specimen: because of this, in the case where the Haigh diagram is convex (aluminium HE 15W No.9), the number of cycles devoted to propagation is very different from that of aluminium with a concave Haigh diagram, which would support Woodward's theory that the shape of the Haigh diagram is related to propagation. In Fig. 3-30 the differences between the two aluminiums can be seen on an S-N diagram:

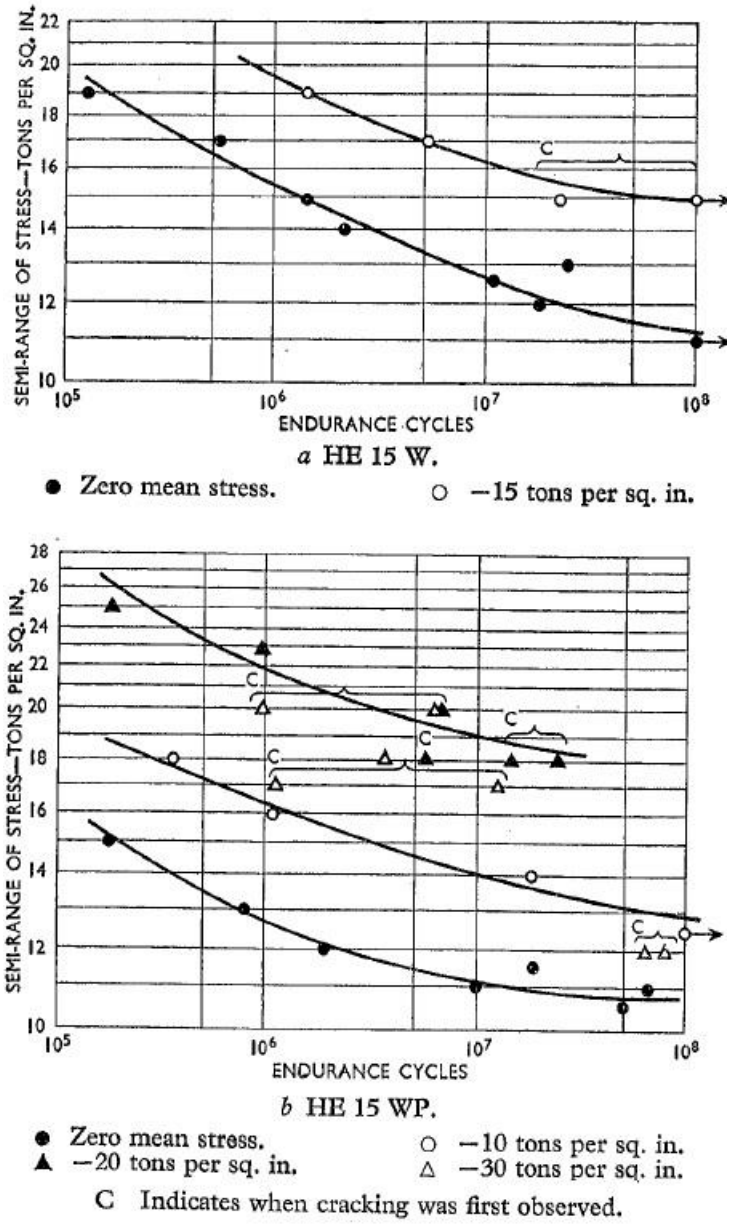

Figure 3-30. *S-N curves for Woodward aluminiums in compression showing initiation and rupture [Woodward, 1956].*

In 1977 Sochava [Sochava, 1977] presented the experimental results of a D16T aluminium (Russian GOST standard), very similar to ASTM 2024 T6. The interest of these results lies in the fact that it is the only one in which the ultimate tensile strength has been found in tension and compression, with 45% greater resistance to compression. As can be seen in Fig. 3.31, the R-M diagram shows a symmetry with respect to a mean stress value of approximately 200 MPa in compression.

It can also be observed that this classical ductile aluminium alloy behaves quite similarly to other ductile ferrous materials in which fatigue strength begins to decrease in compression, although as can be observed, in aluminium this slope change occurs for relatively higher compressive stresses.

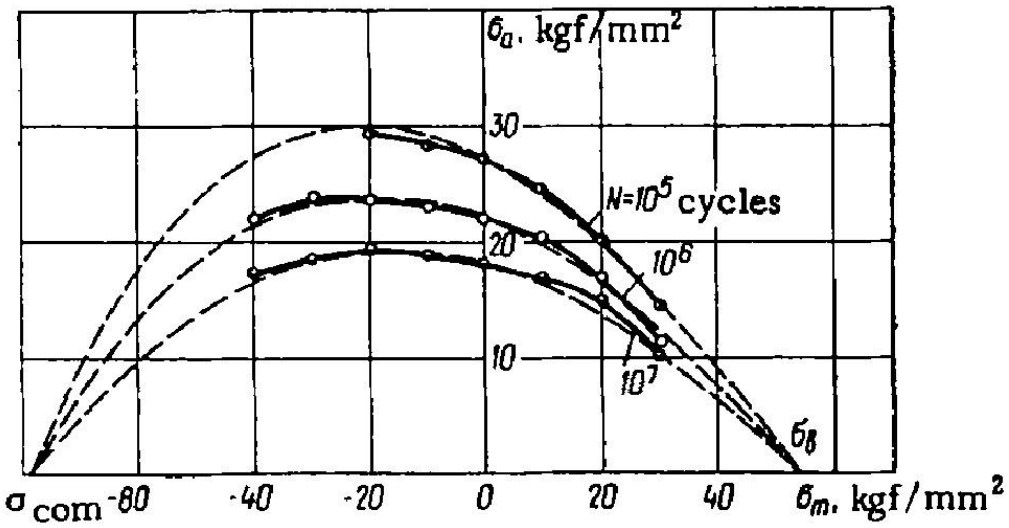

Figure 3-31. *Haigh diagram with experimental results of a D16T aluminium [Sochava, 1977].*

3.5. Further investigation on the shape of the Haigh diagram

In this section, the shape of the Haigh axial diagram will be analysed taking into account data gathered from the literature, including 82 experimental results on ferritic materials (steels and cast irons and aluminium alloys). The materials, number of tests and references are presented in Table 4-3.

Table 3-3. *Fatigue tests used in the characterization of the axial Haigh diagram shapes [Pallarés, 2018A]*

Material	No. of tests	Reference
0.1% C Steel	4	[Ukrainetz, 1960]
0.13 Carbon Steel	4	[Gough, 1924]
0.29 Carbon Steel	6	[Forrest, 1962]
AISI 4130 Steel	7	[Grover, 1951]
AISI 4340 Steel	5	[Trapp, 1953]
En25 Steel	10	[O'Connor, 1956]
30NiCrMo8 Steel	4	[Klubberg, 2001]
25CrMo4 Steel	10	[Grün, 1991]
SAE 52100 Steel	5	[Bomas, 2009]
GJL-250 cast iron	5	[Klubberg, 2009]
EN-GJV-450 Cast iron	6	[Rausch, 2011]
D16T aluminium	9	[Sochava, 1977]
Aluminum 7351	4	[Beiss, 2008]
Aluminum 6063	3	[Beiss, 2008]

In Figure 3-32, the ferritic materials from Table 4-3 are represented in a normalized Haigh axial diagram. The mean axial stress σ_m is expressed as a fraction of the ultimate tensile strength σ_{uts}, and is plotted as an abscissa; the axial stress amplitude σ_a is expressed as a fraction of the fully reversed axial fatigue limit σ_{-1} and is plotted as an ordinate [Pallarés, 2018A].

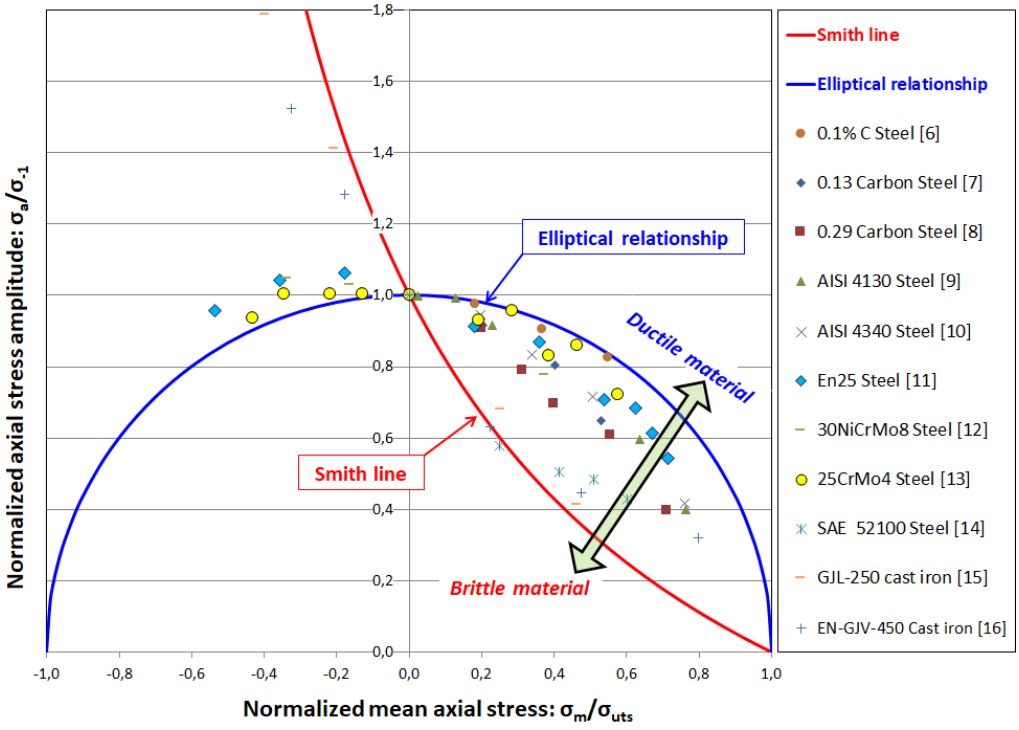

Figure 3-32. *Axial Haigh diagram with experimental results for ferritic materials with the extreme lines of behaviour [Pallarés, 2018A].*

It must be noted that the shape of these lines in the Haigh diagram is indicative of the ductility of the material. The majority of the results lie within the Smith and elliptical lines for all the range of static loads. Therefore, those lines represent the extremes of behaviour for the mean axial stress effect [Pallarés, 2018A].

The elliptical relationship, proposed in [Marin, 1956], is symmetrical for tensile and compressive static loads, presents a concave downward shape for any mean stress value, and has a good agreement with extra-ductile materials without

internal stress raisers as the 0.1% Carbon Steel of [Ukrainetz, 1956]. The elliptical formulation predicts the compressive loads as damaging as the tensile loads, without any increase in fatigue strength for moderate compressive static loads.

The Smith line, whose shape is convex downward, was devised as an empirical criterion to adjust the results of brittle materials. This formulation predicts an important increase of the fatigue strength for compressive static loads. The shape is therefore non-symmetrical. This criterion highly accurate to data on brittle cast irons as the ones presented in Figure 3-32 with a hard and fragile matrix sometimes reinforced by the presence of compounds of silicium with inclusions of different types acting as severe internal notches.

The experimental results on ductile metals for the compressive side of the Haigh diagram will be presented next. The work by O'Connor and Morrison [O'Connor, 1956] was the first investigation with a machinery able to correctly apply compressive loads, showing a detrimental effect on the fatigue strength for high compressive mean stresses. Later investigations confirmed this fact, as it is shown in Figure 3-33, where the results on 6 ductile steels and aluminium alloys from Table 4-3 are presented in a Haigh diagram, showing non-symmetrical concave downward shapes. However, the effect of the compressive mean stresses could be nearly as damaging as the tensile mean stresses, as it takes place for the 25CrMo4 steel, which is regarded as very ductile due to the low carbon content.

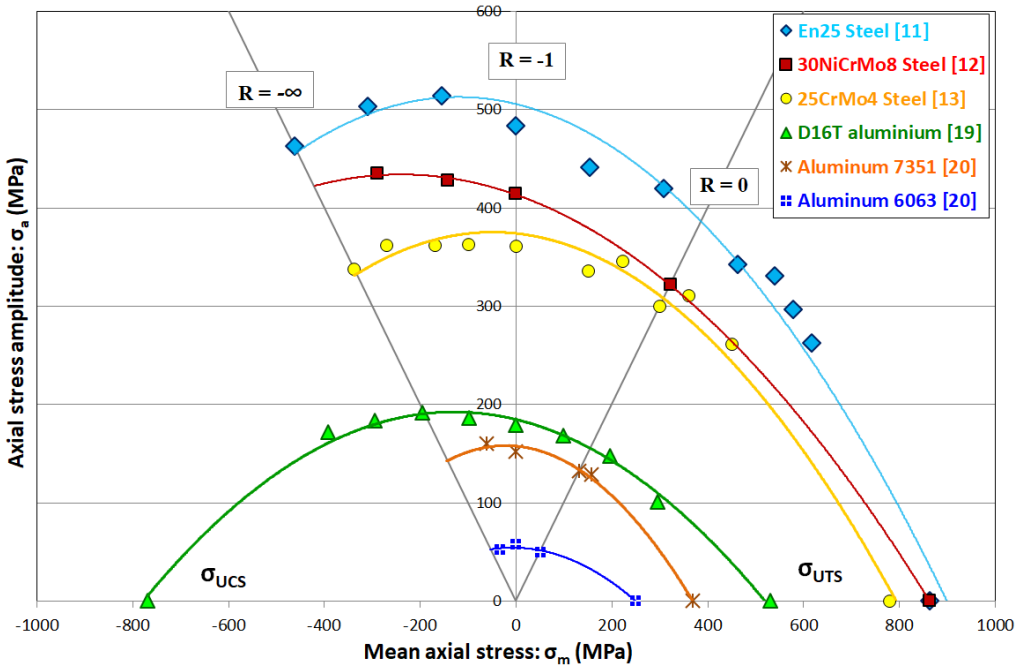

Figure 3-33. *Axial Haigh diagram with experimental results in compression for ductile materials [Pallarés, 2018A].*

3.6. Discussion

3.6.1. Haigh diagram shape

Regarding the shape of the Haigh diagram as a function of the type of material: In extra-ductile materials with hardly any internal stress concentrators, the Haigh diagram presents a symmetrical shape, being the compressive static loads as damaging as the tensile loads (Figure 3-32). The Marin method, which is based on a quadratic effect of the mean axial stresses, presents an excellent agreement for this extra ductile materials, as the 0.1% carbon steel of

[Ukrainetz, 1960], exerting equal damage in static tension and compression, and therefore the resulting R-M diagram is concave downward and symmetrical.

In most structural steels (e.g. quenched and tempered steels, carbon steels), and in untreated aluminium, the diagram is concave downward although it does not show symmetry with respect to mean zero stress. Mean compressive stresses have a positive influence on fatigue strength up to a certain value, from which resistance begins to decrease with the increase in static compressive stress. This type of materials comprehends the majority of the steels and aluminium alloys, as shown in Figures 3-32 and 3-33.

In extra fragile matrix materials and with internal stress raisers, the fatigue failure changes and the diagram is completely convex downward, as it is shown in Figure 3-32 for the grey cast irons. This fatigue behaviour can be modelled through the empirical Smith line for design purposes. The multiaxial fatigue models examined within this Chapter are unable to correctly represent a convex downward shape.

3.6.2. Theories of the effect of mean stresses

Gough's theory states that mean stresses by themselves do not have any effect, noting that it is the maximum stress that controls the fatigue damage. As it has been demonstrated within this chapter, this hypothesis does not seem to agree with experimental results on ductile materials, especially for the extra ductile metals showing a symmetrical Haigh diagram. In those cases, it would be necessary to extend the theory to the maximum stresses in absolute value,

especially for the high mean loads approaching the ultimate tensile and compression strengths.

Findley's theory seems suitable for ductile materials such as NiCrMo steels where the effect of the mean normal stresses is approximately linear within the elastic range. On the other hand, according to Findley's theory, a beneficial effect of mean compression stresses on fatigue strength should be taken as a general rule, contradicting some experimental results on extra ductile materials.

Marin's theory, based on energy considerations, fits isotropic extra-ductile materials with great precision and with a weak influence of internal stress raisers. It should be noted that this method is unable to be adapted to other type of materials, as the fatigue ratio κ is fixed to $\sqrt{3}$, which corresponds to a von Mises material. The Froustey method corrects this aspect, being able to be adapted to other type of materials with different fatigue ratios. However, for both methods, the axial Haigh diagram is symmetric.

The theory of Freudenthal and Orowan, which is based on structural damage once the elastic limit has been exceeded, should be expanded to take into account the peculiarities of the fatigue damage. On the one hand, this damage can be located in a microscopic stress raiser without the elastic stress being exceeded in the nominal section. On the other hand, it should be taken into account not only monotonous plasticity but also cyclic plasticity, which differ in their effect once the elastic limit has been exceeded. In this sense, Gunn's proposal tries to explain the behaviour of a material with internal inclusions by comparison with ductile notched materials, both developing concentrated fatigue plasticity [Gunn, 1955].

3.6.3. Modelling of axial mean stresses:

By carrying out a synthesis exercise regarding the factors in the modelling of axial mean stresses in order to obtain an adequate function that represents the effect of the same, three key aspects could be highlighted:

- The ductility of the material matrix
- Internal concentrators and their severity
- Anisotropy of the matrix and inclusions

These 3 factors seem to be related to each other. A material with an extremely ductile matrix will have greater ability to plasticize locally before a stress concentrator. This fact is well known and documented as for example in Peterson [Peterson, 1952]: In soft steels such as very low carbon steels, sensitivity to notching can be extremely low for size defects of manganese sulphide inclusions.

On the other hand, polycrystalline materials are usually macroscopically isotropic despite the fact that the monocrystals of which they are formed are anisotropic. This is because the random orientations of each of these monocrystals are globally balanced, being macroscopically isotropic. However, many polycrystalline materials show a marked anisotropy due mainly to manufacturing processes (i.e. forging process).

Finally, it should be noted that no empirical method has achieved to have a good agreement with ductile materials, and therefore a much more refined and physically based method should be developed [Pallarés, 2018A].

Chapter 4:

EFFECT OF MEAN TORSIONAL STRESSES

CHAPTER 4. EFFECT OF MEAN TORSIONAL STRESSES

4.1. Introduction

The effect of mean torsional stresses on fatigue strength is a controversial issue in the engineering world, with research groups having conflicting views on their influence. However, a detailed study of the available data in the literature indicates that the degree of influence of the mean shear stress is dependent on the type of material tested. In any case, it can be stated that this influence is less than that of mean normal stresses, especially in ductile materials.

A widespread hypothesis in the literature is that the average torsional stress does not influence the torsional fatigue strength, provided the yield point in cutting is not reached. This theory is based on Smith's research in the 1930s and 1940s [Smith, 1939], [Smith, 1942] and is also reflected in Sines' 1959 book [Sines, 1959]. For example, some of the most widely used multi-axial fatigue analysis methods, such as those of Sines [Sines, 1959], Crossland [Crossland, 1956A] or Dang Van [Dang Van, 1973] do not take into account the influence of these methods, regardless of the material being analysed.

However, as mentioned above, there are numerous studies documenting an appreciable influence of the mean shear stress on torsional fatigue [Gough, 1951], [Findley, 1953], [Chodorowski, 1956], [Marquis, 2000], [Lempp, 1977] and [Brune, 1991]. As a result, other methods take into account average torsional stresses. The first methodologies to assume this hypothesis, in the 1950s, were those of Marin [Marin, 1956] and Findley [Findley, 1959], or more

recently those of Liu-Zenner [Liu, 1993] or Papuga [Papuga, 2009] among others. This difference in approach has been reflected in the literature, with various comparative studies, some of which conclude that there is no influence of mean shear stress, such as those by Papadopoulos et al. [Papadopoulos, 1997] and Davoli et al. [Davoli, 2003].

In this Thesis, special attention is paid to this aspect, making an exhaustive study of the experimental data on fatigue behaviour for different materials available in the literature, contrasting them with the main multiaxial fatigue analysis theories available.

The effect of mean torsional stresses will be studied next from a mathematical point of view, addressing the shape of the Haigh torsional diagram and analysing the relationship between mean axial and torsional stresses.

Additionally, a complete test campaign has been performed on 34CrNiMo6 steel with quenching and tempering treatment, which has been used as a basis for the development of the method proposed in this Thesis. The experimental results are shown and furtherly analysed in Chapter 7.

4.2. Historical review of the effect of the mean torsional stresses

Research on this topic dates back to 1924 when McAdam [McAdam, 1924] concluded that the mean torsional stress has no influence on the fatigue limit, proposing the equation (3-1), in which the torsional stress range is kept constant with the load ratio in torsion R_τ:

$$\tau_{max} = \frac{2 \cdot \tau_{-1}}{(1 - R_{\tau})} \tag{4-1}$$

Moore and Jasper [Moore, 1924], [Moore, 1925] took advantage of their own experimental campaign to conclude that the repeated torsional fatigue limit τ_0 is 1.93 times the fully reversed torsional fatigue limit τ_{-1}. This means a decrease of 3.5% in fatigue strength for a repeated torsional fatigue loading compared with the fully reversed torsional loading, leading to a weak effect of the mean shear stresses on the torsional fatigue limit.

In 1939, Smith [Smith, 1939] performed torsional fatigue tests with mean stresses on an SAE 3140 steel in two different states: hot-rolled; and quenched and tempered. From these tests Smith determined that in this material the torsional fatigue limit is not affected as long as the maximum shear stress along a cycle does not exceed the shear yield stress.

Smith presented a model to fit the data, and included tests beyond the torsional yield strength, through linear equation (4-2), which predicts a 6.25% decrease in fatigue strength for the repeated torsion case ($R_\tau = 0$).

$$\tau_{max} = \frac{\tau_{-1} \cdot (7 \cdot R_{\tau} + 15)}{8} \tag{4-2}$$

Furthermore, these tests show a certain beneficial effect of the mean torsional stresses in terms of the alternating torsion that the material can withstand within the elastic range (Figure 4-1); this beneficial effect can be observed even in tests

exceeding the torsional elastic limit. As it will be studied later, this supposed beneficial effect is very debatable and is in contradiction with the rest of the results obtained by other researchers.

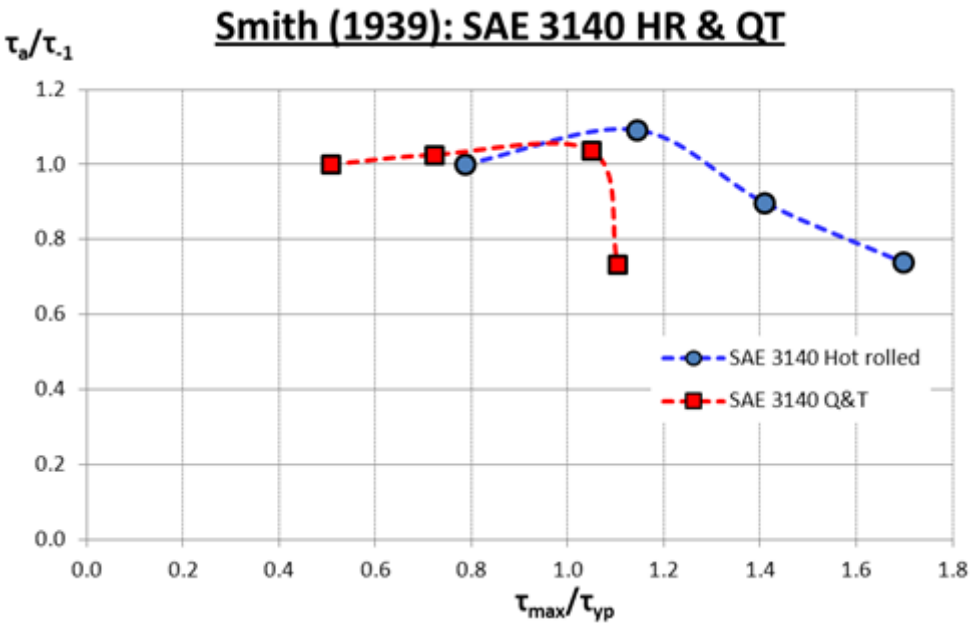

Figure 4-1. *Torsional fatigue tests with mean shear stresses on SAE 3140 steels [Smith, 1939]*

Three years later, Smith [Smith, 1942] collected a large number of experimental results on various metals, including steels, aluminium, copper etc. and generalised the hypothesis that mean torsional stresses do not influence the torsional fatigue strength in unnotched specimens. In fact, in the compilation of results performed by Smith shown in Figure 4-2, the beneficial effect of mean torsional stresses already mentioned can only be observed in an appreciable way in the tests performed by Smith himself on 3140 steel and bronze.

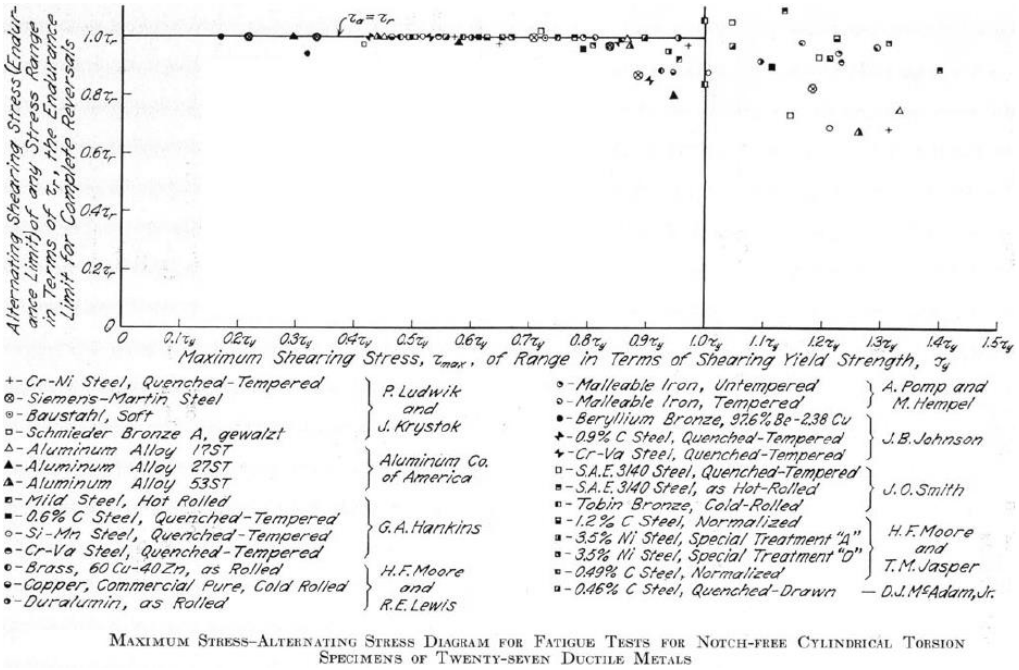

Figure 4-2. *Collection of torsional fatigue tests with mean shear stresses on several ductile materials [Smith, 1942]*

Smith's work has influenced later works extensively, as summarised by Sines [Sines, 1939], who is cited by Papadopoulos et al. [Papadopoulos, 1997] to have stated that the effect of mean shear stress is negligible for fatigue lives above 10^6 cycles, where the fatigue limit usually occurs, provided that the torsional yield strength is not exceeded. For lower fatigue lives, the slope of the torsional fatigue line in a Haigh-like τ_m–τ_a diagram is negative. This hypothesis is in accordance with equation (4-1) for the case of the torsional fatigue limit, and is represented schematically in Figure 4-3a [Papadopoulos, 1997].

The Sines-Papadopoulos hypothesis shows the influence of a mean (static) torsional stress as a function of life. The mean torsional stress has an important influence for lives in the field of Low Cycle Fatigue (10^4 cycles and below), progressively decreasing its importance until lives around 10^6 cycles, in which the mean torsional stress no longer has any influence (Figure 4-3a).

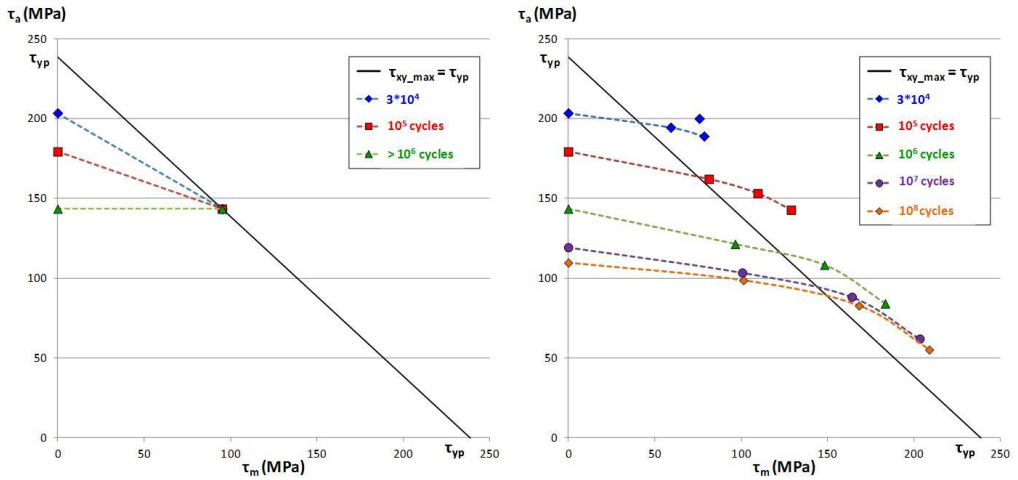

Figure 4-3. *Aluminium 76S-T61 torsional Haigh diagrams*

a. *Sines–Papadopoulos hypothesis [Papadopoulos, 1997],* ***b.*** *experimental results by Findley [Findley, 1953]*

In 1953 Findley conducted multi-axial tests on aircraft aluminium 76S T61 with solid specimens [Findley, 1953], which included a wide variety of stress states. His results, shown in Figure 4.3b depict a dependence on the mean shear stress, also for maximum shear stresses below the elastic limit in torsion. For stresses exceeding the yield strength, the plastic correction described in [Nadai, 1931] was applied.

Furthermore, it should be noted that the mean shear stress effect is maintained over lives in excess of 10^6 cycles. Findley developed its critical plane multiaxial fatigue method, which is sensitive to mean torsional stresses.

In 1951, Gough [Gough, 1951] published in its final form a large number of experimental results of multi-axial fatigue, from which he concluded that the effect of mean torsional stresses was negligible. However, McDiarmid in [McDiarmid, 1985], based on the same results published by Gough, concludes that there is a certain influence of these mean stresses. In fact, it can be observed for example that the reduction in amplitude τ_a reaches 7% for R_τ=0 in S65A steel, without the maximum shear stress exceeding the torsional yield stress in this case (Figure 4-4).

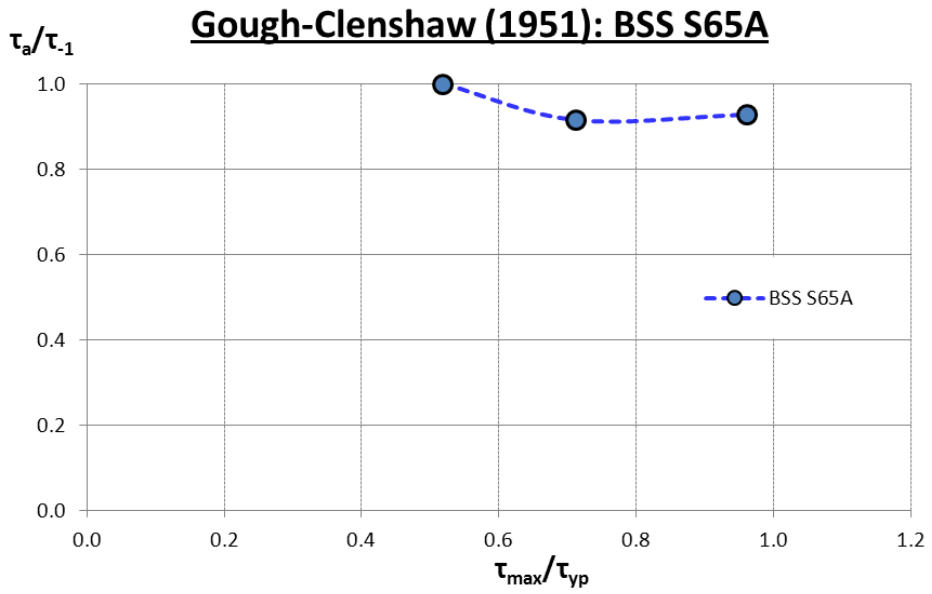

Figure 4-4. *Experimental results of torsional fatigue on S65A steel presented in final form by Gough and Clenshaw [Gough, 1951]*

In the International Conference on Fatigue of 1956, the research group of the University of Bristol presented a multiaxial fatigue campaign on En25 NiCrMo quenched and tempered steel. Chodorowski was in charge of the torsional fatigue campaign [Chodorowski, 1956], and derived several conclusions:

- The mean torsional stresses reduce the torsional fatigue limit, even for maximum shear stresses below the shear yield strength (Fig. 4-5)
- The influence of mean shear stresses in the cyclic torsional amplitude is approximately linear from load ratios ranging from R_τ=-1 (fully reversed torsion) to R_τ=0 (repeated torsion), even for mean shear stresses exceeding the elastic limit (Figure 4-6)
- The inclusions and their effect on the anisotropic behaviour of the material affect could affect the torsional fatigue limit with the increase of the mean torsional stress.

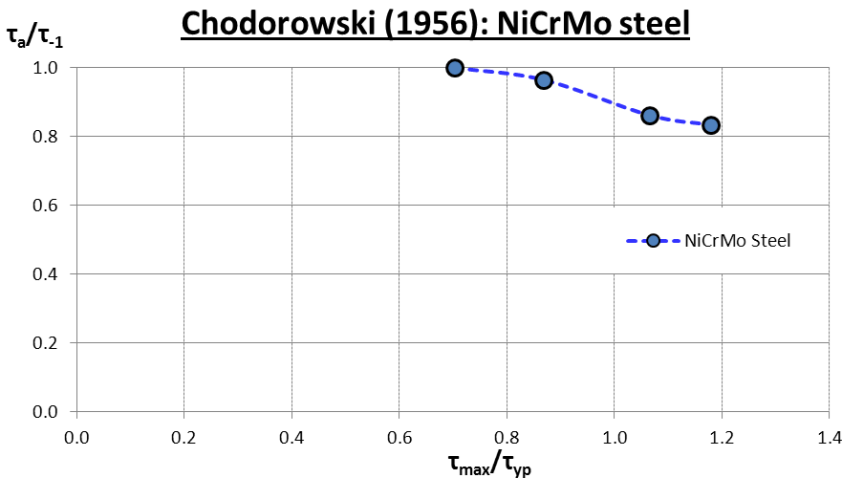

Figure 4-5. *Torsional fatigue campaign on En25 steel [Chodorowski, 1956]. Mean stresses normalized with the torsional yield strength*

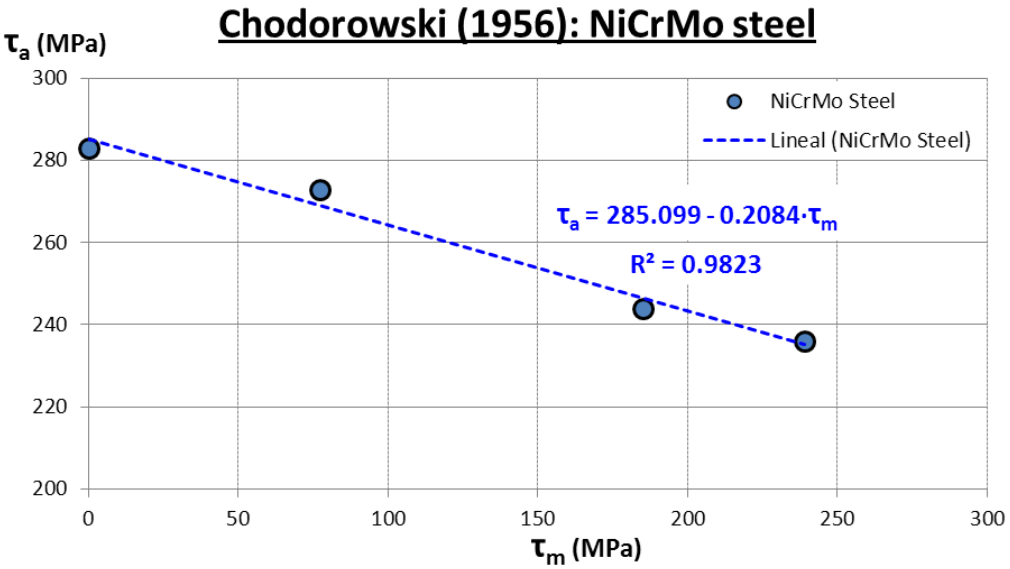

Figure 4-6. *Linear influence of the mean shear stress and its correlation for the fatigue data on En25 steel [Chodorowski, 1956]*

In 1960, Ukrainetz studied of the influence of mean axial and torsional stresses [Ukrainetz, 1960]. The last hypotheses presented at the First International Congress on Metal Fatigue of 1956 were verified, including those proposed by Chodorowski and Smith.

A 0.1% C steel was tested with tubular specimens at several mean torsional levels, obtaining a good experimental correlation with Smith's hypothesis: the mean torsional stresses did not reduce the torsional fatigue limit for lives above 10^6 cycles (Figure 4-7).

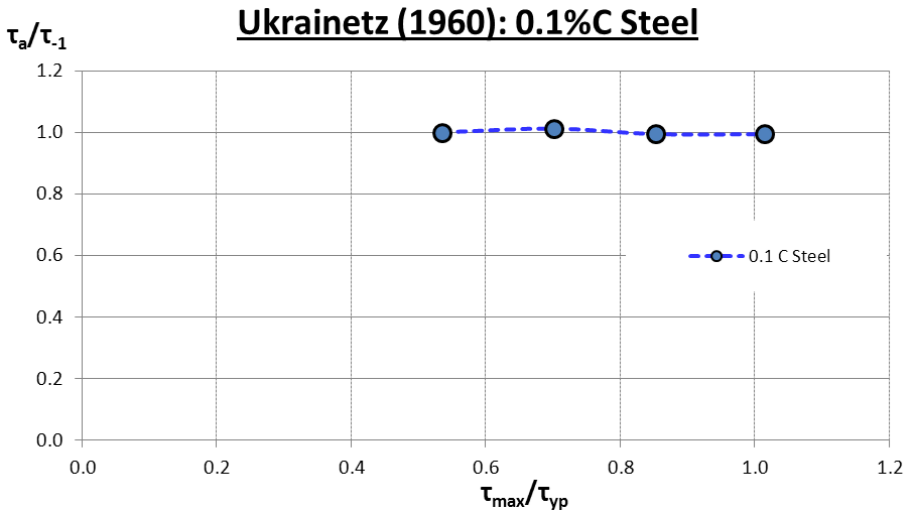

Figure 4-7. *Independence of the mean torsional stress for a 0.1% Carbon steel [Ukrainetz, 1960]*

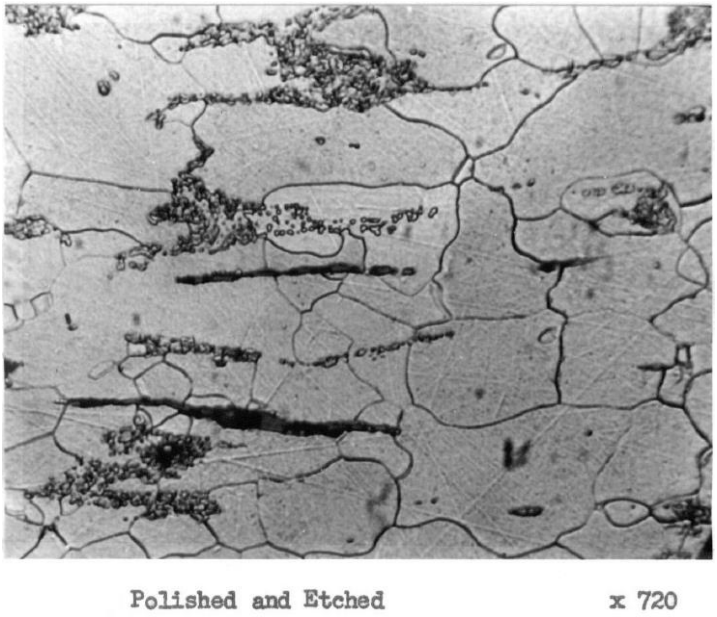

Figure 4-8. *Microstructure of the 0.1% C steel [Ukrainetz, 1960]*

The microstructure of this 0.1% carbon steel was analysed, and an extremely ductile ferritic microstructure was observed, with globular perlite, equiaxial grain and manganese sulphide inclusions aligned with the axis of the specimen (Figure 4-8). In the steel analysed by Chodorowski the inclusions are also aligned longitudinally, however the microstructure is sorbitic, substantially harder than the ferritic of 0.1% C steel.

In 1963, a theory was presented by Yokobori [Yokobori, 1963] concerning the effect of mean torsional stresses. According to this hypothesis, the influence is determined by the microstructure and the dimensions of the defects or inclusions. Its influence can be expressed through equation (4-3):

$$\frac{\tau_a}{\tau_{-1}} = 1 - \eta \cdot \frac{\tau_m}{\tau_{yp}} \qquad (4\text{-}3)$$

The variation in mean torsional stresses according to Yokobori is therefore linear and dependent on a material-dependent constant η. This linear influence shows a good agreement with the experiments of Chodorowski. Through the coefficient η different behaviours of a material with respect to the mean torsional stresses can therefore be modelled.

In the 1970s and 1980s, several German researchers addressed the problem of average torsional stresses. Baier published experimental results [Baier, 1970] on two steels: CK35 and 34CrMo4. The fatigue strength in torsion decreased with mean torsional stresses in the two groups of tests presented by this author. However, it should be noted that in both tests the torsional yield strength was exceeded.

In 1973, the German researcher Issler performed a multiaxial fatigue campaign on St35 steel [Issler, 1973], which, due to its low carbon content and consequent high ductility, is comparable to that used by Ukrainetz in 1960. Issler's results are consistent with those of Ukrainetz, showing minimal influence of static torsion as long as the elastic limit in torsion is not exceeded. Taking into account these experimental results, Issler formulated his multiaxial fatigue method by neglecting the effect of average torsional stresses.

In 1977, Lempp used the same test equipment as Baier and Issler, and determined an influence of the mean torsional stresses for a 42CrMo4V steel even below the shear yield strength [Lempp, 1977].

In the 1980s, Heidenreich [Heidenreich, 1984] and Bhongbhibhat [Bhongbhibhat, 1986], obtained experimental results indicating an influence of mean torsional stress but exceeding the shear elastic limit.

In 1991, Wang and Miller [Wang, 1991] conducted tests on a NiCrMo steel in the range of 10^4-10^6 cycles, and with various levels of mean torsional stresses. These authors determined that the influence of mean torsional stress was not negligible, and modelled it through equation (4-4):

$$\tau_a = 675 \cdot e^{\frac{-\tau_m}{823}} \cdot N_f^{-0.063} \qquad (4\text{-}4)$$

Representing this mathematical equation in a Haigh torsional diagram (Figure 4-9) it is observed that the correlation of Wang and Miller's experimental results is similar to the results obtained by Findley, which were in clear contrast to

Sines-Papadopoulos hypothesis which states the negligible influence of mean torsional stresses.

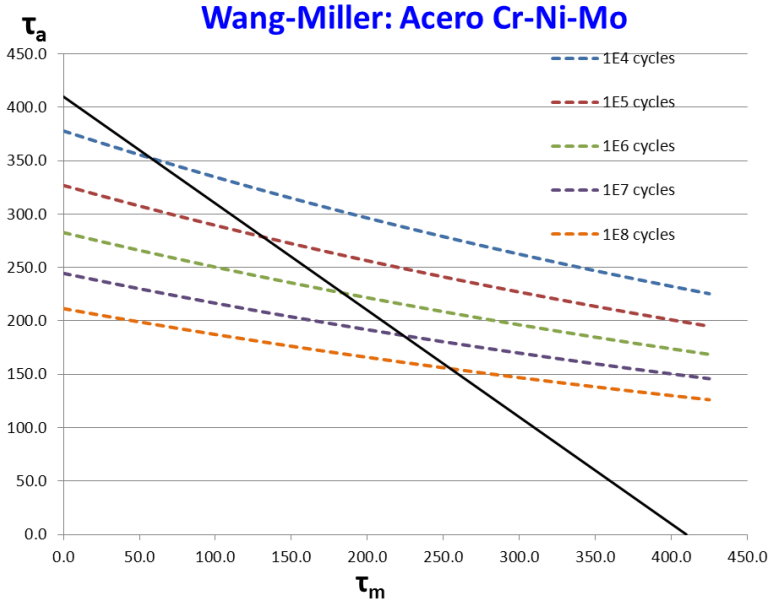

Figure 4-9. *Wang-Miller modelling of torsional fatigue [Wang, 1991]*

In the JSMS Databook [JSMS, 1996], a single experimental result of torsional fatigue with mean torsional stresses was published. In this case, the elastic limit in shear is exceeded with a significant decrease in the fatigue limit for R_τ=0.

In 1999, Lüpfert [Lüpfert, 1999] studied a 20MnCr5 steel, with a 12% decrease in the torsional fatigue limit compared to R_τ=-1 for a maximum stress of 5% below the yield strength in shear.

In 2003, Davoli et al. [Davoli, 2003] conducted tests on hardened and tempered 39NiCrMo3 steel in order to demonstrate that mean torsional stresses do not

affect the fatigue limit in torsion. The results provided show a clear influence of the average torsional stresses, with a 5% drop in the torsional amplitude stress for a maximum shear stress value of 95% of the shear limit value.

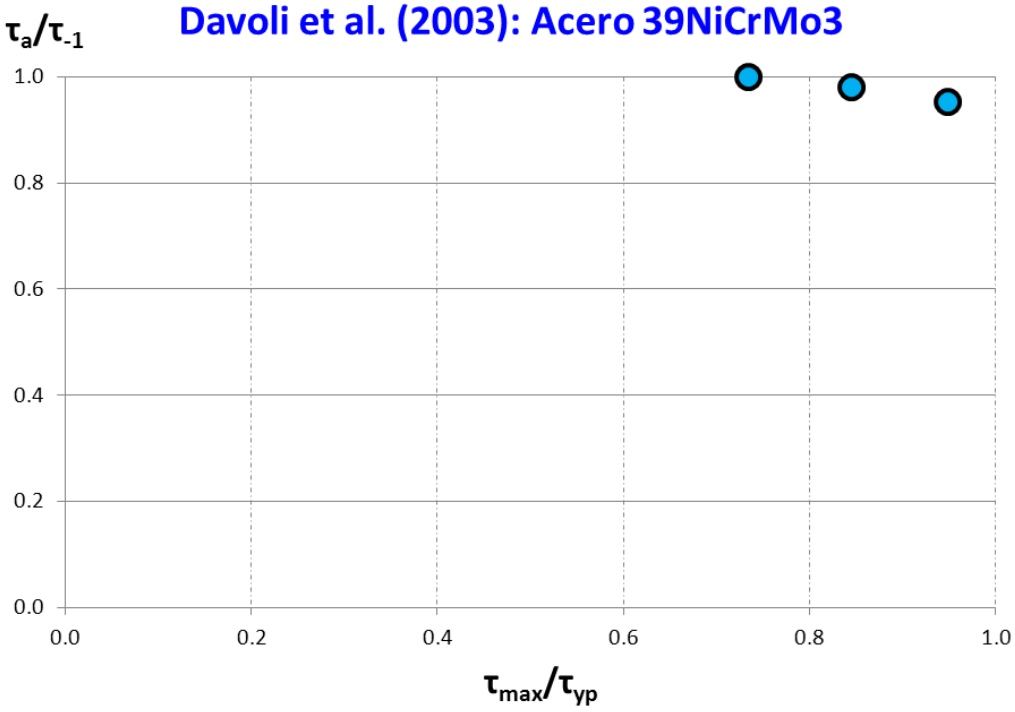

Figure 4-10. *Haigh torsional diagram for a 39NiCrMo3 steel [Davoli, 2003]*

Rausch published in 2011 experimental results on an EN-GJV-450 cast iron [Rausch, 2011], whose behaviour is extremely fragile. The results show the greatest influence of the mean torsional stresses, with a decrease of the fatigue limit in torsion of 32% for values of 30% for a maximum stress of 66% of the yield strength in shear.

4.3. Review of relevant results from the literature

The effect of mean torsion in the torsional fatigue limit is reviewed and summarized next. Given the dispersion of published experimental results, some of which are contradictory, in this work we have made a detailed compilation and review of the most relevant tests carried out in the last 70 years, and which are summarized in Tables 4-1 and 4-2. The databases are commonly used as reference in the literature for the development and comparison of methods of analysis of multi-axial fatigue in high cycle regime (HCF).

Table 4-1. *Torsional fatigue tests on aluminiums and steels [Pallarés, 2018B]*

Material	No. of tests	Reference
1.2C normalized steel	2	[Moore, 1924]
3.5C Ni steel treat. A	2	[Moore, 1924]
3.5C Ni steel treat. B	2	[Moore, 1924]
3.5C Ni steel treat. D	3	[Moore, 1924]
0.49C normalized steel	3	[Moore, 1924]
0.49 C sorbitic steel	2	[Moore, 1924]
CrNi Steel treat. D	3	[Moore, 1925]
1.2C sorbitic steel	2	[Moore, 1925]
SAE 3140 H.R. steel	4	[Smith, 1939]
SAE 3140 Q&T steel	4	[Smith, 1939]
14S-T Aluminum	5	[Sauer, 1948]
BSS S65A steel	3	[Gough, 1951]
Aluminum 76S T61	12	[Findley, 1953]
En25T NiCrMo steel	8	[Chodorowski, 1956]
0.1 C Steel	4	[Ukrainetz, 1960]
CK 35 steel	2	[Baier, 1970]
34CrMo4 Steel	2	[Baier, 1970]
St 35 steel	3	[Issler, 1973]

42CrMo4V steel	2	[Lempp, 1977]
34Cr4 steel	2	[Heidenreich, 1984]
42CrMo4 steel	2	[Bhongbhibhat, 1986]
JIS SCM440 steel	2	[JSMS, 1996]
20MnCr5 steel	2	[Lüpfert, 2001]
39NiCrMo3 steel	3	[Davoli, 2003]
VDSiCr spring steel	4	[Mayer, 2015]
34CrNiMo6 steel	5	[Pallarés, 2018B]

Table 4-2. *Torsional fatigue tests on cast irons [Pallarés, 2018B]*

Material	**No. of tests**	**Reference**
Cast iron	3	[Smith, 1942]
Special cast iron	4	[Smith, 1942]
Ni-Mo cast iron	5	[Smith, 1942]
GGG60 cast iron	2	[Grubisic, 1979A]
GGG40 cast iron	2	[Grubisic, 1979B]
GRP500 nodular cast iron	2	[Marquis, 2001]
EN-GJV-450 cast iron	2	[Rausch, 2011]
EN-GJS-400-18-LT cast iron	2	[Tovo, 2014]

The aim of this created database is to compare groups of torsional fatigue experiments altogether so that conclusions regarding the behaviour could be inferred for different types of materials.

Eighty-eight experimental results for 26 different steels and aluminium alloys with unnotched specimens for lives above 10^6 cycles have been collected (Table 4-1), including all the experimental results known by the authors, which are represented in the normalized diagram of Figure 4-11, which is shown in the same way as the classic and influential work of [Smith, 1942].

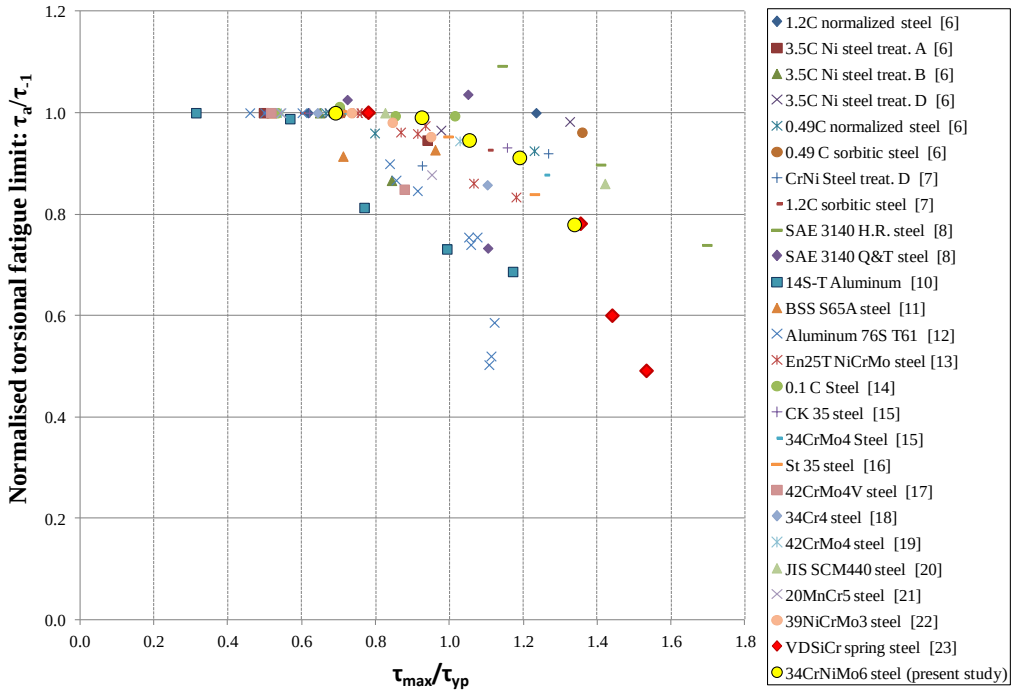

Figure 4-11. *Normalized maximum shear stress-alternating shear stress diagram, 25 steel and aluminium alloys represented [Pallarés, 2018B]*

As it can be observed in Figure 4-11, the mean shear stress effect take place for values of maximum shear stress exceeding 80% of the shear yield strength. As remarked by some authors [Findley, 1959], the way of representing the experimental results can lead to misleading conclusions. In Figure 4-11, the fully reversed torsional fatigue limits are included within the graphic, so that an impression of the negligible effect of mean shear stresses could be created.

According to the Sines-Papadopoulos hypothesis, the mean shear stress effect is negligible as long as the shear yield strength is not exceeded. In order to

clearly show the influence of mean shear stress for the experiments in the elastic range, a diagram is created showing only the experimental results in which the maximum shear stress is below the shear yield strength (Figure 4-12):

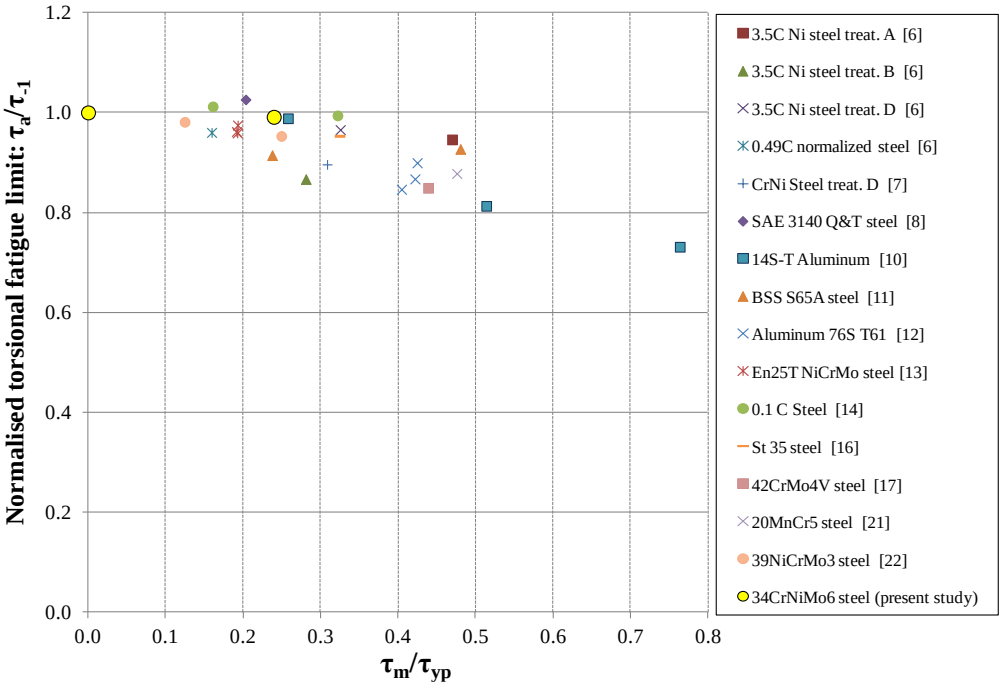

Figure 4-12. *Mean-shear-stress effect, represented only the tests in which the maximum shear stress is below the torsional yield strength [Pallarés, 2018B]*

As it can be seen in Figure 4-12, the overwhelming majority of the tests lie bellow the fully reversed torsional fatigue limit.

In order to investigate the shape of the Haigh torsional diagram, the experimental results will be compared to the classic methods, namely the Smith, Goodman, Gerber and elliptical lines.

The Gerber line in torsion, equation (4-5), shows a horizontal slope with the intersection of the axis of ordinates, and a concave downward shape.

$$\tau_a = \tau_{-1} \cdot \left(1 - \left(\frac{\tau_m}{\tau_{uss}} \right)^2 \right) \tag{4-5}$$

The elliptical relationship for torsion, represented in equation (4-6), shows also a horizontal slope in the intersection with the axis of ordinates, but the mean shear stress effect is slightly less pronounced than the one predicted by the Gerber line.

$$\tau_a = \tau_{-1} \cdot \sqrt{1 - \left(\frac{\tau_m}{\tau_{uss}} \right)^2} \tag{4-6}$$

The Goodman line for torsion, equation (4-7), represents a linear influence of the mean shear stress on the torsional fatigue strength. Its influence is higher than in the Gerber and elliptical lines.

$$\tau_a = \tau_{-1} \cdot \left(1 - \frac{\tau_m}{\tau_{uss}} \right) \tag{4-7}$$

In case that the static shear strength τ_{uss} is not available, the estimated static shear strength is calculated by means of equation (4-8), based on the collection of data gathered in [McAdam, 1924].

$$\tau_{uss}^{s} \approx 0.75\, \sigma_{uts} \tag{4-8}$$

Regarding the shape of the Haigh torsional diagram, Mayer et al. [Mayer, 2015] recently found that the mean-shear-stress effect on a VDSiCr spring steel could be modelled through Gerber's parabola in the torsional Haigh diagram. The same idea was proposed by Sauer [Sauer, 1948] for a 14S-T aluminium alloy. It should be noted that the VDSiCr spring steel is a semi ductile material, due to the large size of the inclusions and the high value of hardness of the matrix.

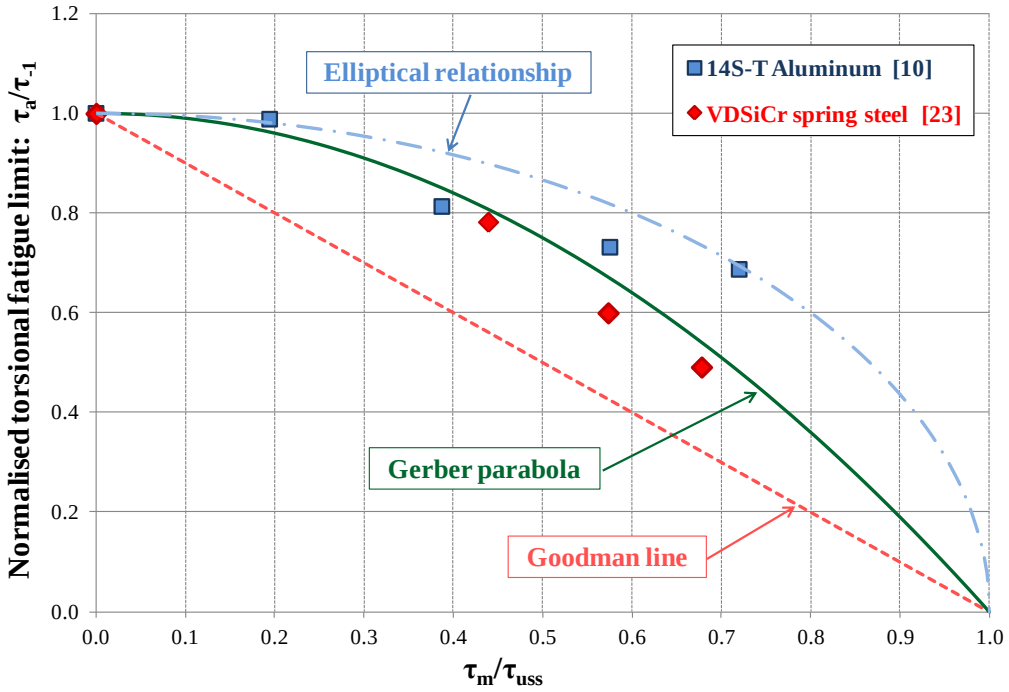

Figure 4-13. *Normalized torsional Haigh diagram with the experimental results of a 14S-T aluminium alloy and a VDSiCr spring steel [Pallarés, 2018B]*

In order to observe the shape in the Haigh torsional diagram for the aluminium alloys and steels, all the data of Table 4-1 is represented altogether in a

normalized Haigh torsional diagram with the elliptical, Gerber and Goodman lines (Figure 4-14):

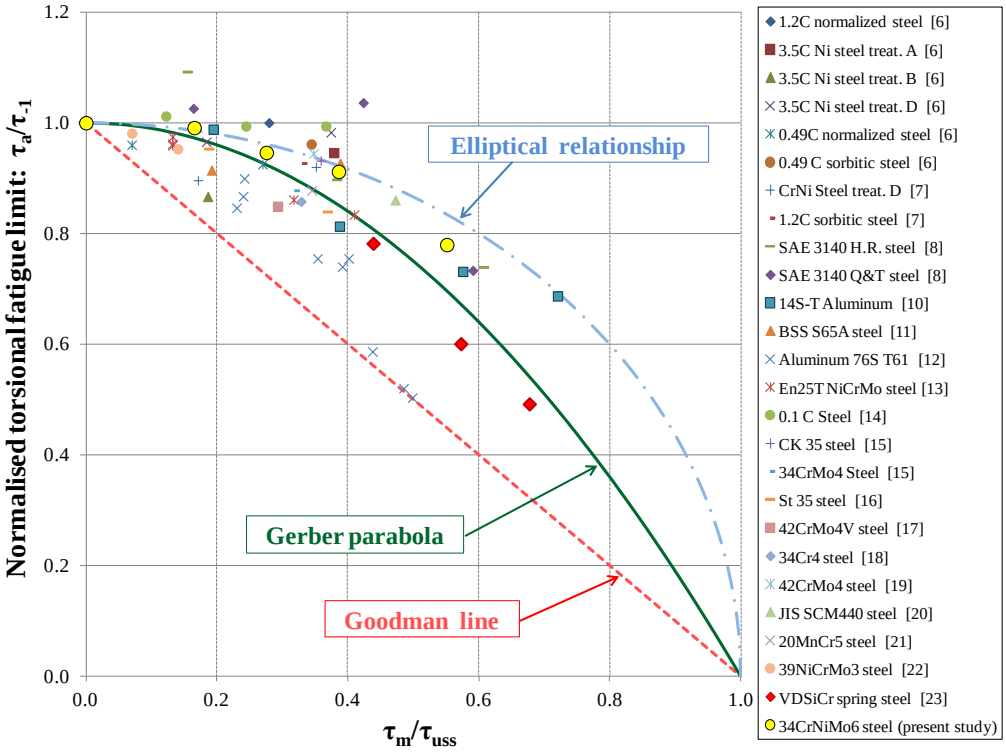

Figure 4-14. *Normalized torsional Haigh diagram, 25 different steel and aluminium alloys represented and the 34CrNiMo6 of this work [Pallarés, 2018B]*

As it can be observed in Figure 4-14, the Gerber lines lies in the middle of the scatter for aluminium alloys and steels, whereas the elliptical relationship allows to fit the most ductile materials, and the Goodman relationship appears to be very conservative for the majority of the experimental data. It should be noted that only 53.4% of the results lie between Gerber and Goodman lines; whereas

for the axial fatigue problem, other authors as [Susmel, 2005] have found that approximately 90% of the results lie between the Goodman and Gerber lines. Thus, it can be said that the mean stress effect is weaker in torsion than in axial for ductile materials.

In order to analyse the behaviour of cast irons, the data of Table 4-2 will be represented altogether in a Haigh torsional diagram (Figure 4-15) with some of the already mentioned classic lines. In order to obtain the estimated ultimate torsional strength, the equation (4-9) proposed in [Marin, 1952] will be used.

$$\tau_{uss}^{s} \approx \sigma_{uts} \tag{4-9}$$

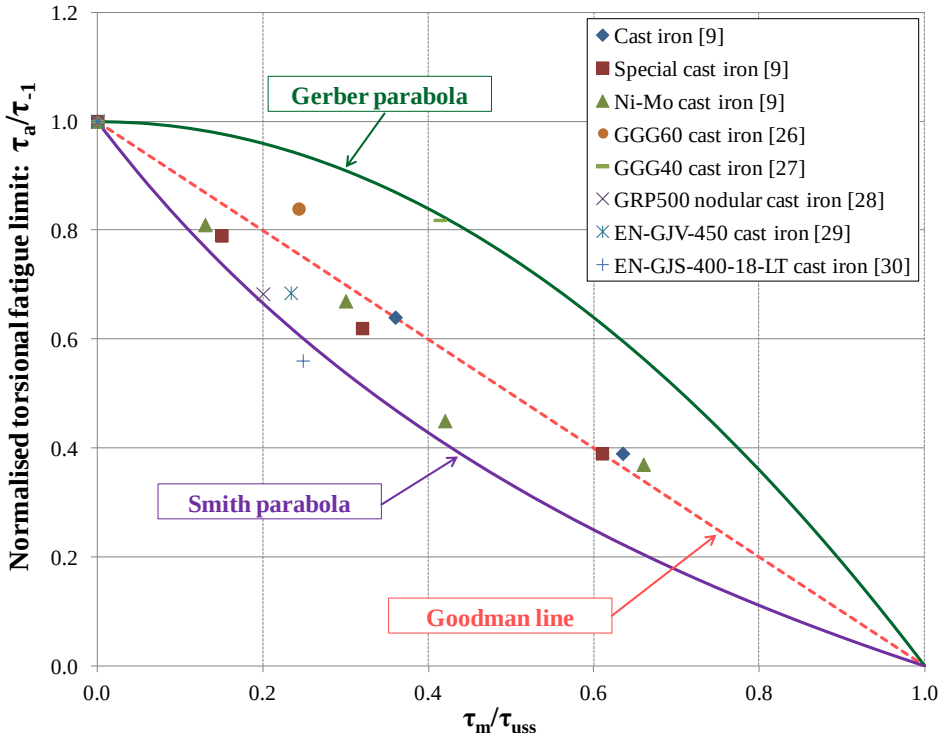

Figure 4-15. *Normalized Haigh torsional diagram showing eight different cast irons [Pallarés, 2018B]*

Equation (4-9) assumes that the ultimate strength in shear is approximately equal to the ultimate tensile strength, by using the Worst Principal Stress criterion, which is commonly used in brittle materials. This type of static failure of cast irons implies a brittle fracture for quasi-static loads.

As the fatigue failure changes in cast irons, the design for torsional fatigue must be much more conservative than the classic engineering design using ductile materials. As it can be seen in Figure 4-15, some of the results for cast irons lie below the Goodman line.

Smith's conclusions in [Smith, 1942] remark on the great impact of mean torsional stresses in fragile materials due to the presence of severe inclusions acting as internal notches. The Smith line, equation (4-10) was recommended for design purposes. The same line was recommended for the axial fatigue of this type of brittle materials.

$$\tau_a = \tau_{-1} \cdot \frac{\left(1 - \frac{\tau_m}{\tau_{uss}}\right)}{\left(1 + \frac{\tau_m}{\tau_{uss}}\right)} \tag{4-10}$$

Therefore, it can be concluded that the mean stress effect is lower in torsion than the axial mean stress effect for ductile materials, but is strong in torsion and axial for cast irons, which are considered to be fragile materials.

4.4. Relationship between mean axial and torsional stresses

The mean stress effect in axial and torsion has been compared from the pioneering work of [Smith, 1942] to infer conclusions for mechanical design purposes. Findley in the final form of his method [Findley, 1959] compares both effects from a theoretical point of view, by applying his method to different load cases, and comparing with experimental results. Findley led to the conclusion that the mean shear stress effect takes place, being weaker than the mean axial stress effect for ductile materials.

Papadopoulos in his review of methodologies [Papadopoulos, 1997] compares the mean axial and torsional stress effects for different methods, discarding the methods which take into account the mean shear stress effect. The reaction of Zenner et al. arrived 3 years later in [Zenner, 2000], where a review of experimental data is presented, and arriving to the same conclusions as Findley.

Zenner states that a parameter must be defined in order to compare the mean stress effects. In that sense, the sensitivity to axial mean stresses M_σ is defined as the average slope in the Haigh axial diagram, reflecting the influence of an axial mean stress on the axial stress amplitude drop. This parameter can be calculated by using two fatigue limits, namely σ_{-1} and σ_0, by means of equation (4-11), defined in [Zenner, 2000]:

$$M_\sigma = \frac{\sigma_{-1} - \frac{\sigma_0}{2}}{\frac{\sigma_0}{2}} \qquad (4\text{-}11)$$

Similarly, the sensitivity to mean torsional stresses is defined by means of equation (4-12):

$$M_\tau = \frac{\tau_{-1} - \frac{\tau_0}{2}}{\frac{\tau_0}{2}} \tag{4-12}$$

Modern design rules, such as the FKM Guideline [Haibach, 2003], [Lee, 2012], takes into consideration the effect of mean shear stresses in torsional fatigue for design purposes, and compares the mean stress sensitivities in axial and torsion. The mean shear stress effect for ductile steels is approximately 58% of the effect of axial static stresses in the pure axial fatigue loading case. This is expressed through equation (4-13), which presents the relationship between the slopes of the Haigh diagram axial and the torsional diagrams, M_σ and M_τ respectively:

$$M_\tau = \frac{M_\sigma}{\sqrt{3}} \tag{4-13}$$

A mean stress sensitivity that is higher in axial than in torsion was also reported in [Findley, 1989], and in a recent paper by Mayer et al. for a VDSiCr spring steel [Mayer, 2016]. The results in torsion for the latter report could be fitted by the Gerber line in the Haigh torsional diagram, as shown in Figure 4-13.

Zenner, using data from [Brune, 1991], show a dependence of the mean torsional stresses on the ultimate tensile strength (σ_{uts}), as it can be seen in Figure 4-6 [Zenner, 2000].

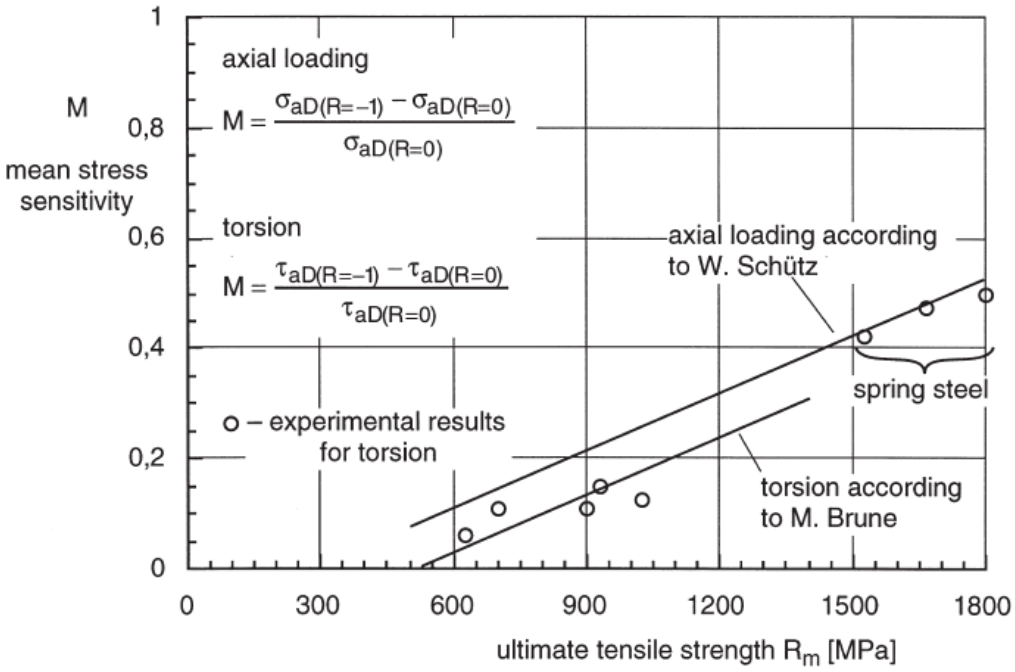

Figure 4-16. *Sensitivities to mean axial and torsional stresses [Zenner, 2000]*

According to Figure 4-6, the mean stress sensitivity is higher for high strength steels, which usually contain a hard matrix of martensite with large inclusions acting as internal stress raisers. In any case, for a given steel, the mean stress effect is higher in axial than in the torsional fatigue case.

4.5. Effect of mean shear stress in multiaxial fatigue models

Amongst the multiaxial fatigue methods, the Marin method, which is based on stress invariants [Marin, 1956]; the Findley critical-plane method presented in its final version [Findley, 1959] and the energetic approach that is based on the method of Froustey [Froustey, 1992] will be considered. These methods take into account the effect of mean shear stresses in the torsional fatigue case, and can be expressed easily through analytic formulations for the torsion case.

The Marin method is based on stress invariants, and can be expressed through equation (4-14):

$$\left(\frac{\sqrt{3}\cdot\sqrt{J_{2,a}}}{\sigma_{-1}}\right)^2+\left(\frac{\sqrt{3}\cdot\sqrt{J_{2,m}}}{\sigma_{uts}}\right)^2\le 1 \qquad (4\text{-}14)$$

where $\sqrt{J_{2,a}}$ and $\sqrt{J_{2,m}}$ are the amplitude and the mean value of the square root of the second invariant of the stress deviator, and σ_{-1} is the fully reversed fatigue strength in bending or tension. For pure torsion tests, it can be expressed as follows:

$$\tau_a \le \frac{\sigma_{-1}}{\sqrt{3}}\cdot\sqrt{1-\left(\frac{\sqrt{3}\cdot\tau_m}{\sigma_{uts}}\right)^2} \qquad (4\text{-}15)$$

As given by equation (4-15), the Marin method is sensitive to the mean shear stress, and is represented by an ellipse in the Haigh torsional diagram. The von Mises relationship is conserved; therefore, the ratio between the fully reversed axial (σ_{-1}) and the fully reversed torsional fatigue limit (τ_{-1}) is equal to $\sqrt{3}$, which

cannot be used as a general rule, since mild steels usually present a fatigue ratio $\kappa = \sigma_{-1}/\tau_{-1}$ near 1.5 [Papuga, 2011A].

The Froustey and Laserre method is based on energetic considerations. When this method is applied to the pure torsion case, analytic equation (4-16) is derived:

$$\tau_a \leq \tau_{-1} \cdot \sqrt{1 - \left(\frac{\kappa \cdot \tau_m}{\sigma_{uts}} \right)^2} \tag{4-16}$$

Equation (15) is an ellipse in the Haigh torsional diagram τ_m–τ_a. A visual inspection of the terms indicates that the derived formula is similar to that of Marin, but the experimental fatigue ratio κ is taken into account instead of the von Mises relationship.

The Findley method is a critical plane approach that is based on the plane that maximises the damage function as given by:

$$f(\varphi,\theta) = \tau_a{}^*(\varphi,\theta) + \alpha_F \cdot N_{\max}{}^*(\varphi,\theta) \tag{4-17}$$

Findley's method can be applied analytically to pure torsion tests (4-18):

$$\tau_a \leq \frac{\sqrt{\lambda_F{}^2 \cdot \alpha_F{}^2 + \lambda_F{}^2 - \alpha_F{}^2 \tau_m{}^2} - \alpha_F{}^2 \cdot \tau_m}{1 + \alpha_F{}^2} \tag{4-18}$$

The constants α_F and λ_F depend on the value of the fatigue ratio $\kappa = \sigma_{-1}/\tau_{-1}$. When κ is equal to 2.0, which corresponds to the Tresca criterion, α_F becomes 0.0, so

that the mean shear stresses produce no effect on the torsional fatigue strength. For materials that follow the Rankine maximum principal stress criterion, that is: $\kappa \approx 1$, the predicted influence of the mean shear stress is very high. This theory explains the fact that the influence of mean stress is small for the torsion of ductile metals, but is strong for the torsion of cast irons.

Some methods do not take into account the mean shear stress effect, as the Crossland stress invariant method, and other methodologies such as the ones based on the mesoscopic theory, namely the Papadopoulos integral method [Papadopoulos, 1997] and the Dang Van critical plane method [Dang Van, 1973].

4.6. Discussion

After a careful analysis of the entire experimental database, it can be inferred that the mean shear stresses do have an influence on the torsional fatigue strength, especially on certain types of materials and for high mean torsional loadings.

The experimental tests used by the authors who neglect the effect of mean shear stresses are mainly those collected in [Smith, 1942]. This hypothesis can be applied as long as the maximum shear stress is below the shear yield strength with a good agreement on ductile steels as the ones of [Ukrainetz, 1960] and [Davoli, 2003]. However, some of the original results by Smith [Smith, 1942] are in clear disagreement with later experimental results, showing in 2 different

tests a beneficial effect of mean shear stresses. This particular effect could have been provoked by the testing equipment of that era.

The effect of mean torsional stresses for maximum stresses bellow the torsional yield strength has been clearly demonstrated in a number of tests on ductile steels and aluminium alloys, namely in [Findley, 1953], [Chodorowski, 1956], [Lempp, 1977], [Wang, 1991] and [Lüpfert, 2001].

In fact, the tests by Davoli on a quenched and tempered ductile steel [Davoli, 2003], which are intended to demonstrate the non-influence of mean torsional stresses, and exclusively in the case of steels, end up demonstrating the mean shear stress effect. Indeed, the steel analysed in those tests features an aeronautical quality and therefore it is largely free of the defects as non-metallic inclusions that various microstructural theories relate to the influence of mean torsional stresses. In spite of all experimental evidence, the article by Davoli recommends the use of methods independent of the mean shear stress in cases of pure torsion, such as the Papadopoulos or Crossland method.

In order to develop the multiaxial fatigue limit, it should be noted that sensitivity to mean shear stresses is one of the features that lacks the Crossland method, considered as the of the most successful multiaxial fatigue method in the industry. Crossland himself mentions in [Crossland, 1956B] that his theory of multi-axial failure must be complemented in the future in various aspects, such as mean shear stresses. In fact, the team from the University of Bristol, to which Crossland and Chodorowski amongst others belonged, thoroughly analysed En25 steel and found an influence of mean shear stresses. Both Crossland's theory and Chodorowski's tests were presented at the 1956 International Fatigue

Conference. In the discussion in London of this conference, Findley and other authors remarked on the lack of adequacy of Crossland method to represent behaviour under mean torsional stresses.

Once the need for the development of a multiaxial fatigue taking into account mean shear stresses is justified taking into account the experimental results collected from the literature, the emphasis must be focused on the way of modelling this effect.

The elliptical relationship agrees well with a great deal of tests on ductile materials, especially for maximum shear stresses below the torsional yield strength. Moreover, this way of modelling agrees with the hypothesis of no fatigue damage for the elastic range, as the slope for zero mean shear stresses of the ellipse is horizontal in a Haigh diagram.

However, other ways of modelling the mean shear stresses have been collected in the literature. Chodorowski found an approximately linear effect up to values of R=0, even for stresses exceeding the elastic shear strength. Therefore, it seems coherent to use the repeated torsional fatigue limit as the data to be used in the multiaxial fatigue method to be adjusted in any case. If this value is not available, it could be obtained by means of the Zenner empirical relationship.

Moreover, it should be noted that the mean axial and shear stress effects appear to be related. Both effects are weak for extra-ductile materials, and strong for brittle materials such as cast irons. Moreover, the effect appears to be stronger for mean axial stresses in any type of material.

By examining the fatigue tests on the most ductile material found in the literature, the 0.1% C steel [Ukrainetz, 1960], it can be inferred that even with a negligible effect of mean shear stresses, the mean axial stress effect plots a symmetrical axial Haigh diagram, leading to the conclusion that at least two different sources of mean stresses effect should be differentiated. In this milestone of the Thesis, the author considers that the volumetric strain energy W_H, which does not take place in torsion, could be one of the sources of fatigue damage, whereas the distortion strain energy W_D appears exclusively in the pure torsional fatigue tests.

Finally, it should be noted that the pure torsion fatigue tests are scarce within the literature, and the modelling of the behaviour for this loading case is difficult as long as most of the authors have performed a few series of tests. Considering that the mean shear stress effect is the second effect in terms of fatigue damage [Papuga, 2011A], it must be incorporated into the method. Therefore, a pure torsional fatigue campaign with several groups of tests is needed to create a mathematical modelling of the mean torsional stresses.

Chapter 5:

MULTIAXIAL FATIGUE METHODS

CHAPTER 5. MULTIAXIAL FATIGUE METHODS

5.1. Introduction

The way of dealing with the multiaxial fatigue problems has its origin in the 1930's with the empirical method of Gough and Pollard [Gough, 1935]. It was devised specifically for bending and torsion combined loads, and did not take into account the mean stress effect.

After World War II, a better comprehension of the fatigue problem was demanded by the aeronautic industry. Thus, a number of large testing campaigns of multiaxial fatigue were performed in the early 1950's, including bending and torsional loadings with mean axial and torsional stresses. Soon afterwards, the researchers in the fatigue field realized that the classic theories of fatigue were unable to explain the results when a mean stress was applied [Findley, 1953], and the race for the development of multiaxial fatigue methods began. The overwhelming majority of those methods were presented in the International Conference on Fatigue of Metals in 1956, with the presentation of the Marin energetic method [Marin, 1956], the empirical method by Crossland [Crossland, 1956A] and an early version of the Findley critical plane method [Findley 1956]. A great number of multiaxial fatigue methods have been developed since; some of them will be presented here.

The daily experience in the engineering field tells us that the multiaxial fatigue methods are not widespread in the engineering practice. In turn, some classic methods are applied currently, specially modifications of the von Mises stress

to be adapted to fatigue problems in which the main loads are uniaxial. In this chapter, some classic fatigue methods were presented together with the more advanced multiaxial fatigue methods.

Multiaxial fatigue calculation methods are usually divided into three types [Papuga, 2011A]: Critical Plane Analysis (CPA), Integral Analysis (IA), and Ilyushin Deviatoric Space Analysis (IDSA).

- Ilyushin deviator space analysis (IDSA): These criteria are generally based on an analysis of the load path envelope analysed in the 5-dimensional Ilyushin deviator space. They are also known in the literature as "methods based on invariant stresses" or "global approach methods". They can be based on empirical considerations, such as that of Crossland [Crossland, 1956A], or on energy balances [Marin, 1956], [Froustey, 1992].

- Critical Plane Analysis (CPA): The method basically consists of examining different planes that pass through the point to be evaluated to find the one with the highest value of a damage function that is supposedly responsible for the onset of cracks. This damage function is generally based on empirical considerations. Different types of planes are used for damage assessment:

    - MSSR (Maximum Shear Stress Range): The failure takes place in the plane with the highest amplitude value of the shear stress, which is the critical plane. Afterwards, the damage function of

the method is applied. Usually, there are several planes in which the maximum shear stress amplitude takes a value close to maximum value. Therefore, the damage function is evaluated in those planes taking a value of 99.9% of the maximum shear stress amplitude.

  - MD (Maximum Damage): The method searches for the plane with the highest damage parameter, which is normally a function of the amplitude of shear stress and the normal stress to the critical plane.
  - CPD (Critical Plane Deviation): We first look for a fracture plane defined by some hypothesis, and then we look for the critical plane with a certain inclination with respect to the fracture plane, where the damage parameter is maximum.
  - MVM (Most Variance Method): Developed by Susmel [Susmel, 2010] for joint application with its critical plane method, the plane with the greatest variance of the maximum shear stress amplitude is sought. This method is validated for parts with notch and random loads [Susmel, 2012].

- Integral Analysis (IA): The damage parameter or its individual components are integrated on all planes at the point to be examined.

Of the 3 types of methods, those of integral analysis (IA) are those which require the greatest computational load, an order of magnitude higher to critical plane methods and two orders with respect to the IDSA methods, without demonstrating in any case an improvement in the correlation with experimental

results. In this sense, it is of special interest that the researcher Jan Papuga, creator of a method of critical plane and another of integral analysis, fervently recommends using the critical plane in his paper of 2008 [Papuga, 2008]. Therefore, an exhaustive study of the methods of integral analysis will not be carried out.

Critical plane methods have an implicit advantage in showing the orientation of the initial nucleated crack. IDSA-type methods are better from a computational point of view, but they are based solely on the analysis of the stress tensor at each point, so they are not able to predict the orientation of the crack.

A particular case of the multiaxial fatigue method is that of Susmel-Lazzarin [Susmel, 2002], also known as MWCM: Modified Wohler Curve Method, which has been improved over the years with abundant experimentation, and addressing practically all possible casuistry in multi-axial fatigue, even with notched parts and random loads.

Within the HCF methods, there are some that can be applied not only to unlimited life, but also to medium cycle fatigue. Among them are Susmel's critical plane [Susmel, 2002], [Susmel, 2012], and those of the IDSA type derived from Crossland, such as those of Cristofori [Cristofori, 2008] and Mamiya [Mamiya, 2011], which have been validated in the range $2 \cdot 10^3$-$2 \cdot 10^6$ cycles.

5.2. Classic fatigue methods

These methods have been developed ad-hoc in order to solve specific fatigue problems in which the multiaxiality does not take a great importance. The author of the Thesis found that these methods are being used in the engineering practice in the aeronautic field, namely in the design and calculations of rotating parts in the aviation jet engines. Those methods, although developed in the late years, have their origin in the classic theories shown in Figure 5-1.

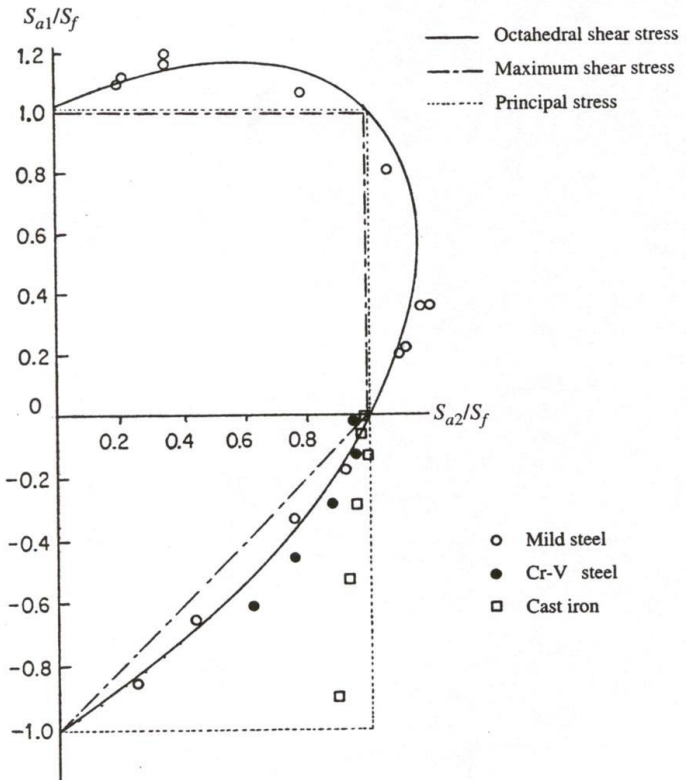

Figure5-1. *Classic yield theories together with fatigue experimental results by Sawert shown in [Sines, 1959]*

The most commonly used classical yield methods, the von Mises and Worst Principal Stress (both signed) are used with mean stress correction methods such as Goodman and Walker in order to be applied to the multiaxial fatigue problem. Numerically, it involves calculating the equivalent von Mises stress or the worst principal stress (Rankine theory).

In this sense, Figure 5-1 is representative of the biaxial behaviour of these methods under static loads, which can be extrapolated to cyclic loads: the application of Worst Principal or Rankine has a non-conservative trend for ductile materials in torsion. In fact, in the above figure Rankine's criterion would be non-conservative in torsion even for iron casting. The von Mises line has a better agreement with torsional loads, with Tresca's criteria being the most conservative in all cases.

These methods consist of simulating a cycle, and storing the maximum and minimum of the Worst Principal or von Mises stresses (both methods with sign). After finding these two extreme values, the value of Stress Ratio R is obtained. From this value we move through the Haigh diagram to R=0 by means of Full Range, real Walker or Walker 0.5 (Smith-Watson-Topper) in the case of -1<R<0 and Goodman for the case of 0<R<1.

In the case of mean compression stresses, the correction of R is carried out horizontally, seeking extreme conservatism.

As shown in Figure 3-5 of the chapter dealing with mean axial stresses, ductile materials are usually located between the Gerber and Dietmann lines, and few

materials are located below the Goodman line, so these classical methods seek above all conservatism in the treatment of mean stresses.

Thus, as can be seen in Figure 5-2, the fatigue limits σ_0 obtained by corrections of R based on Full Range for -1<R<0 and Goodman for 0<R<1 will in theory always be located above the real value of σ_0. The Gerber parabola is shown as an example of the typical behaviour of a ductile metal.

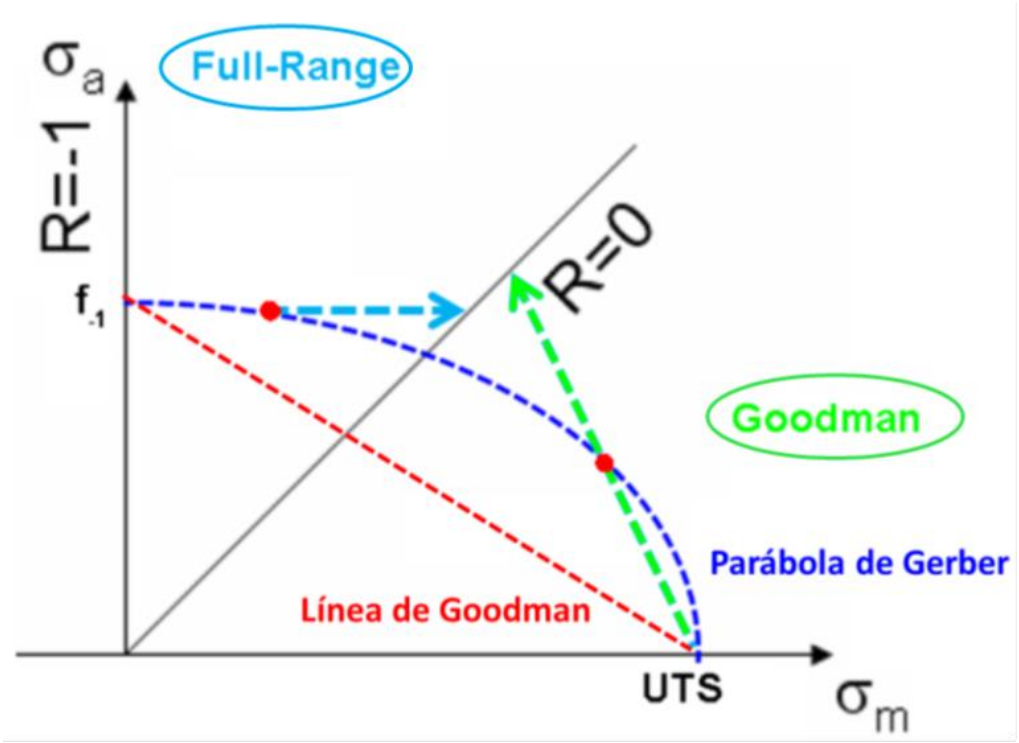

Figure 5-2. *Stress correction methods used in the classic methods presented within this Thesis*

The classic methods that will be defined in this section are the 6 combinations of using von Mises and Worst Principal along with R corrections at -1<R<0 for Full Range, Walker and Smith-Watson-Topper, which uses a value of the Walker parameter equal to 0.5. In the compression region, Goodman's R correction is used in all cases. As a note of clarification, the real Walker exponent can be obtained from two fatigue limits, such as σ_{-1} and σ_0. In this case Walker's exponent m_{Walker} would have the following form:

$$m_{Walker} = \frac{\log\left(\frac{\sigma_0}{\sigma_{-1}}\right)}{\log 2} \tag{5-1}$$

The notation of the methods' names begins with the equivalent stress used (Worst Principal or von Mises); followed by the stress correction for -1<R<0 (Full range, Walker or SWT); and followed by the stress correction for 0<R<1, which in all cases is the modified Goodman method. Therefore, 6 different methods will be presented in this section.

Therefore, all the Goodman stress corrections for 0<R<1 for the different methods can be expressed through equation (5-2) for the Worst principal equivalent stress and equation (5-3) for the von Mises stress:

$$2 \cdot \left(\frac{\sigma_{UTS} \cdot \sigma_{1,a}}{\sigma_{UTS} + \sigma_{1,a} + \sigma_{1,m}} \right) \leq \sigma_0 \tag{5-2}$$

$$2 \cdot \left(\frac{\sigma_{UTS} \cdot \sqrt{3}\sqrt{J_{2,a}}}{\sigma_{UTS} + \sqrt{3}\sqrt{J_{2,a}} + \sqrt{3}\sqrt{J_{2,m}}} \right) \leq \sigma_0 \qquad (5\text{-}3)$$

The formulation for the 6 methods in the -1<R<0 range is presented next.

5.2.1. Worst Principal Full Range-Goodman

$$\sigma_{1,\max} \cdot \left(1 - \frac{\sigma_{1,a}}{\sigma_{1,\max}} \right) \leq \sigma_0 \qquad (5\text{-}4)$$

5.2.2. Von Mises Full Range-Goodman

$$\sqrt{3} \cdot \sqrt{J_{2,\max}} \cdot \left(1 - \frac{\sqrt{J_{2,\min}}}{\sqrt{J_{2,\max}}} \right) \leq \sigma_0 \qquad (5\text{-}5)$$

5.2.3. Worst Principal Walker-Goodman

$$\sigma_{1,\max} \cdot \left(1 - \frac{\sigma_{1,a}}{\sigma_{1,\max}} \right)^{m_{Walker}} \leq \sigma_0 \qquad (5\text{-}6)$$

5.2.4. Von Mises Walker-Goodman

$$\sqrt{3} \cdot \sqrt{J_{2,\max}} \cdot \left(1 - \frac{\sqrt{J_{2,\min}}}{\sqrt{J_{2,\max}}} \right)^{m_{Walker}} \leq \sigma_0 \qquad (5\text{-}7)$$

5.2.5. Worst Principal SWT-Goodman

$$\sigma_{1,\max} \cdot \sqrt{\left(1 - \frac{\sigma_{1,a}}{\sigma_{1,\max}}\right)} \leq \sigma_0 \qquad (5\text{-}8)$$

5.2.6. Von Mises SWT-Goodman

$$\sqrt{3} \cdot \sqrt{J_{2,\max}} \cdot \sqrt{\left(1 - \frac{\sqrt{J_{2,\min}}}{\sqrt{J_{2,\max}}}\right)} \leq \sigma_0 \qquad (5\text{-}9)$$

5.3. Methods based on stress invariants

They are also known as advanced global approach methods. They use stress invariants in the 5-dimensional Ilyushin field (IDSA) to estimate fatigue damage. They may have clearly empirical approaches, such as the Crossland method [Crossland, 1956A] or based on energy balances, such as the Marin [Marin, 1956] and Froustey [Froustey, 1992] methods.

5.3.1. Marin

Marin's method [Marin, 1956] was presented at the first International Fatigue Congress in 1956 along with an extensive database compiled by the author, consisting of 289 fatigue limits from 23 test series. This method can be generally expressed by equation (5-10). Its physical interpretation is a balance of the

distortion energy W_D between the uniaxial static case and the totally reversed uniaxial fatigue case without mean stresses.

$$\left(\frac{\sqrt{3}\cdot\sqrt{J_{2,a}}}{\sigma_{-1}}\right)^2+\left(\frac{\sqrt{3}\cdot\sqrt{J_{2,m}}}{\sigma_{UTS}}\right)^2\leq 1 \qquad (5\text{-}10)$$

This method requires only fully reversed axial fatigue strength σ_{-1} and ultimate tensile strength σ_{UTS}. For the particular case of pure torsion, it can be defined by the expression (5-11), which is an ellipse in the torsional Haigh diagram. Therefore, Marin's criterion predicts that the limit on torsional fatigue depends on a static shear stress, although this dependence is relatively low for small values of the mean shear stress.

$$\tau_a \leq \frac{\sigma_{-1}}{\sqrt{3}}\cdot\sqrt{1-\left(\frac{\tau_m}{\sigma_{UTS}/\sqrt{3}}\right)^2} \qquad (5\text{-}11)$$

As can be seen after examining the equation (5-11), Marin's method uses the von Mises ratio, and therefore the ratio between the fully reversed axial fatigue limits (σ_{-1}) and the fully reversed torsional fatigue limit (τ_{-1}) is assumed to be equal to $\sqrt{3}$. For the case of uniaxial stresses with mean stresses, the application of the method leads to the elliptical relationship, equation (5-12):

$$\sigma_a \leq \sigma_{-1}\cdot\sqrt{1-\left(\frac{\sigma_m}{\sigma_{UTS}}\right)^2} \qquad (5\text{-}12)$$

In the above formula it is clearly observed that this method is unable to distinguish between the effect of a static tensile and compressive stress, because the value of σ_m is squared.

5.3.2. Froustey

Another widely used method is that of Froustey [Froustey, 1992], which is based on a balance of total deformation energy. The application of this method to the case of torsional fatigue with mean shear stresses leads to the analytical formula of equation (5-13):

$$\tau_a \leq \frac{\sigma_{-1}}{\kappa} \cdot \sqrt{1 - \left(\frac{\tau_m}{\sigma_{UTS} / \kappa} \right)^2} \qquad (5\text{-}13)$$

Which, like Marin's method, is also an ellipse in the torsional Haigh diagram, but using the experimental relationship $\kappa = \sigma_{-1}/\tau_{-1}$ instead of the theoretical relationship of von Mises. The application of the Froustey method to the case of axial fatigue with mean axial stresses leads to the same elliptical relationship as the Marin method, equation (5-12). Therefore, the Froustey criterion shows a symmetrical Haigh diagram, without distinguishing between mean tensile or compressive stresses.

5.3.3. Sines

This high cycle fatigue criterion was formulated by Sines in the late 1950's [Sines, 1959] and is still one of the most widely used today. It can be formulated as follows:

$$\sqrt{J_{2,a}} + \kappa \cdot \sigma_{H,m} \leq \lambda \tag{5-14}$$

The parameters κ and λ can be obtained from tension and torsion tests:

$$\kappa = \left(3\sigma_{-1} / \sigma_0\right) - \sqrt{3} \tag{5-15}$$

$$\lambda = \tau_{-1} \tag{5-16}$$

This method is independent of mean shear stresses, a hypothesis put forward by Smith [Smith, 1942]. With respect to mean axial stresses, this criterion predicts a linear influence of the same, increasing fatigue strength in compression and decreasing in tension.

However, by applying this method to reverse bending, the following expression is inferred:

$$\kappa = \frac{\sigma_{-1}}{\tau_{-1}} = \sqrt{3} \tag{5-17}$$

That is the relationship of von Mises, a criterion of special application in ductile materials. This implies that Sines' criterion considers this factor to be the same for all materials, when experimental evidence shows that this factor varies

between 0.5 (ductile metals, Tresca ratio) and 1 (brittle metals). Therefore, the Sines criterion will not be suitable for materials that deviate from the value of that factor.

The safety zone of the Sines method can be expressed as follows when compared against the uniaxial fatigue limit with R=-1:

$$k \cdot \sqrt{J_{2,a}} + \left(6 \cdot \frac{\sigma_{-1}}{\sigma_0} - k \cdot \sqrt{3} \right) \cdot \sigma_{H,m} \leq \sigma_{-1} \tag{5-18}$$

5.3.4. Crossland

Crossland's criterion was presented at the International Fatigue Congress in 1956 [Crossland, 1956A] along with numerous tests conducted by the University of Bristol including the effect of mean axial stresses [O'Connor, 1956], and the effect of mean torsional stresses [Chodorowski, 1956] on a quenched and tempered NiCrMo steel with En25T denomination.

This method differs from that of Sines only in the influence of hydrostatic stress, which in the Crossland criterion appears with its maximum value, while Sines uses the mean value of the hydrostatic stress.

$$\sqrt{J_{2,a}} + \kappa \cdot \sigma_{H,\max} \leq \lambda \tag{5-19}$$

By means of two tests the two parameters κ and λ can be found. Unlike the Sines criterion, depending on the choice of these tests, different values will be obtained for the constants. Using bending and torsion the parameters can obtained as follows:

$$\kappa = \left(3\tau_{-1} / \sigma_{-1}\right) - \sqrt{3} \tag{5-20}$$

$$\lambda = \tau_{-1} \tag{5-21}$$

This criterion is independent of mean torsional stresses, despite having been formulated using experimental data from a steel sensitive to mean shear stresses [Chodorowski, 1956]. In the section on authors' responses to the 1956 International Congress, Crossland pointed out that his method should be updated in future work to take account of mean torsional stresses [Crossland, 1956B].

On the other hand, the effect of the mean normal stresses is taken into account through a linear influence of the maximum hydrostatic stress, which predicts a beneficial effect on fatigue strength for uniaxial compressive static loads, and detrimental for mean tensile loads.

The safety zone of the Crossland method can be expressed as follows when compared against the uniaxial fatigue limit with R=-1:

$$k \cdot \sqrt{J_{2,a}} + \left(3 - k \cdot \sqrt{3}\right) \cdot \sigma_{H,\max} \leq \sigma_{-1} \tag{5-22}$$

5.3.5. Kakuno-Kawada

The Kakuno-Kawada method [Kakuno, 1979] is an extension of the Sines and Crossland methods. The damage function contains the mean hydrostatic stresses and amplitude, and the adjustment is performed with three tests: the uniaxial at R=-1 and R=0 and the torsional at R=-1. In this way the advantages of the Sines method can be used for the adjustment in axial mean stresses, but without

imposing the von Mises ratio between fully reversed axial and torsional fatigue limits.

This method therefore has a linear influence of the mean axial stresses, being adjusted for the uniaxial test R=0. On the other hand, it is independent of the mean torsional stresses.

The safety zone of the Kakuno-Kawada method can be expressed as follows when compared against the uniaxial fatigue limit with R=-1:

$$a \cdot \sqrt{J_{2,a}} + b \cdot \sigma_{H,m} + c \cdot \sigma_{H,a} \leq \sigma_{-1} \qquad (5\text{-}23)$$

5.3.6. Altenbach-Zolochevski

The Altenbach-Zolochevski [Altenbach, 1994] function is basically an extension of the Kakuno-Kawada method to take into account the mean torsional stresses through the mean value of the von Mises stress. Four tests are required: uniaxial and torsion R=-1 and R=0. The effect of the mean axial and torsional stresses is linear.

The safety zone of the Altenbach-Zolochevski method can be expressed as follows:

$$a \cdot \sqrt{J_{2,a}} + b \cdot \sqrt{J_{2,m}} + c \cdot \sigma_{H,m} + d \cdot \sigma_{H,a} \leq \sigma_{-1} \qquad (5\text{-}24)$$

5.3.7. Vu-Halm-Nadot

The Vu-Halm-Nadot criterion [Vu, 2010] is a purely empirical method that attempts to improve Crossland's method, especially in terms of collecting the influence of the out-of-phase loading. In addition, it tries to avoid the use of the Minimum Circumscribed Circle (MCC) due to its high computational cost. For this purpose, the integral is carried out throughout the cycles of the distortion energy, and through multipliers depending on the ultimate tensile strength of the material, corrections are applied depending on the phase difference according to the scheme shown in Figure 5-3.

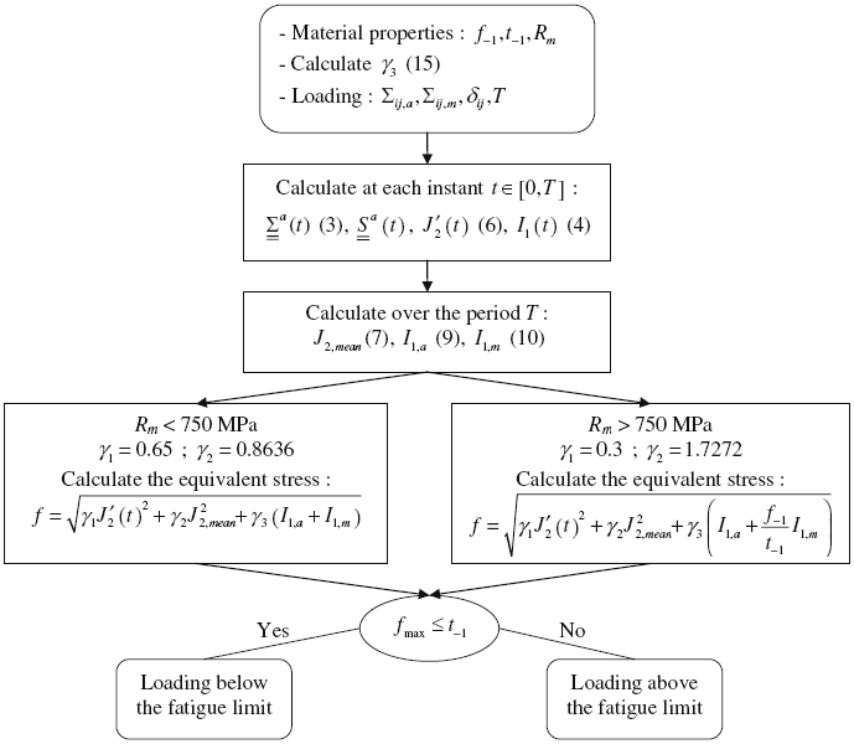

Figure 5-3. *Application scheme of the Vu-Halm-Nadot method [Vu, 2010].*

This method divides materials into high and low strength, and uses parameters based on this criterion. In addition, a damage parameter for fragile materials deduced from the Papuga method is used.

The safety zone of the Vu-Halm-Nadot method can be expressed by equations (5-25) and (5-26) when compared against the uniaxial fatigue limit with R=-1. For a material whose ultimate stress is less than 750 MPa (σ_{UTS}<750 MPa), equation (5-25) shall be used:

$$k \cdot \sqrt{0.65 \cdot \left(\sqrt{J'_{2,\max}}\right)^2 + 0.8636 \cdot \left(\sqrt{J'_{2,mean}}\right)^2 + \left(\frac{\tau_{-1}^{\,2} - \frac{\sigma_{-1}^{\,2}}{3}}{\sigma_{-1}}\right) \cdot \left(I_{1,a} + I_{1,m}\right)} \leq \sigma_{-1} \qquad (5\text{-}25)$$

For a material whose ultimate stress is greater than 750 MPa (σ_{UTS} >750 MPa), the safety zone can be expressed by equation (5-26):

$$k \cdot \sqrt{0.3 \cdot \left(\sqrt{J'_{2,\max}}\right)^2 + 1.7272 \cdot \left(\sqrt{J'_{2,mean}}\right)^2 + \left(\frac{\tau_{-1}^{\,2} - \frac{\sigma_{-1}^{\,2}}{3}}{\sigma_{-1}}\right) \cdot \left(I_{1,a} + k \cdot I_{1,m}\right)} \leq \sigma_{-1} \qquad (5\text{-}26)$$

5.3.8. Matsubara-Nishio

This method is one of the most recently published [Matsubara, 2013]. Its damage function uses the square root of the amplitude of the second invariant of the deviator tensor measured by the Li method, along with a new parameter called S_{max}. This parameter is calculated looking for the maximum normal amplitude in all the possible points that pass through the plane. The maximum value of this normal amplitude stress is S_{max}.

Matsubara-Nishio's criterion is expressed as follows:

$$\sqrt{J_{2,a}} + \frac{\sigma_{-1}}{\sqrt{3}\cdot\left(\sigma_f - \sigma_{-1}\right)} S_{\max} \leq \frac{\sigma_{-1}\cdot\sigma_f}{\sqrt{3}\cdot\left(\sigma_f - \sigma_{-1}\right)} \tag{5-27}$$

And comparing it against the uniaxial fatigue limit R=-1, we arrive at the following expression:

$$\sqrt{3}\cdot\left(1-\frac{\sigma_{-1}}{\sigma_f}\right)\cdot\sqrt{J_{2,a}} + \frac{\sigma_{-1}}{\sigma_f}\cdot S_{\max} \leq \sigma_{-1} \tag{5-28}$$

The application of this method is complicated because it uses the fracture stress of the material σ_f, a data whose availability in the literature is relatively scarce.

5.4. Critical Plane Methods

Critical plane methods look for a plane in which the crack nucleates and propagates in stage 1. This plane is usually one close to the maximum shear stress range (MSSR), but there are other formulations based on maximum damage (MD). Although the functions are generally of empirical origin, the concept of the critical plane is based on experimental observations.

According to the microstructural theory described by Susmel [Susmel, 2002], if a homogeneous polycrystalline material is available, some of the grains will be adequately oriented so that it suffers failure by persistent slip bands (PSB), created by variable shear stresses. The critical plane concept in fatigue was first used by Stulen and Cummings [Stulen, 1954] and furtherly developed by

Findley and others. The case for an isotropic polycrystalline material in described in [Papadopoulos, 1997] and shown in Figure 5-4.

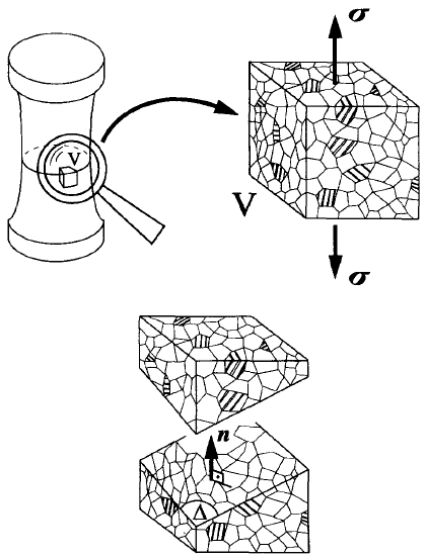

Figure 5-4. *Critical plane concept in an isotropic polycrystalline material [Papadopoulos, 1997].*

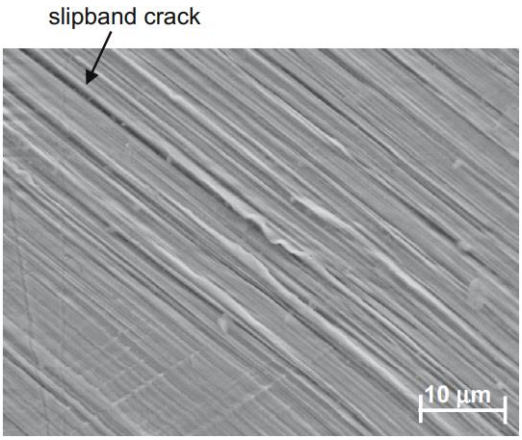

Figure 5-5. *Persistent fatigue-induced slip bands. [Chan, 2010]*

Figure 5-5 shows the slip bands that some crystals (grains) suffer due to cyclic deformation.

These persistent sliding bands create intrusions and extrusions on the glass surface that due to processes such as oxidation prevent the reversibility of the process. Therefore, at some point a micro crack is generated, as shown in Figure 5-6.

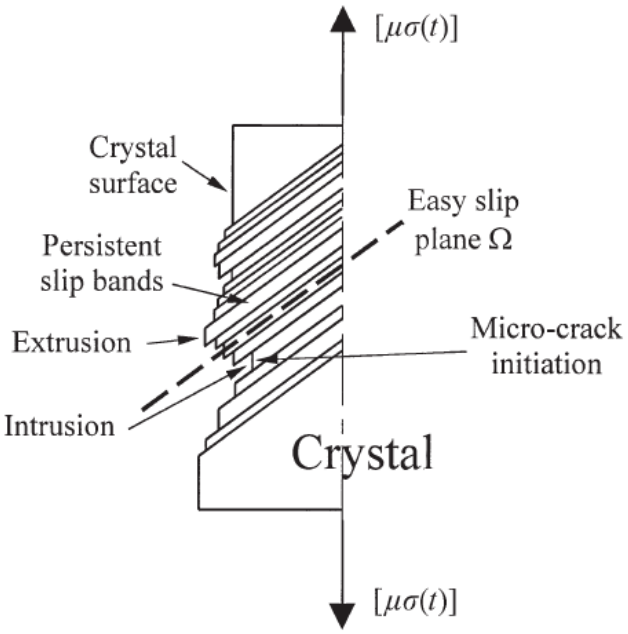

Figure5-6. *Formation of a crack by intrusions and extrusions [Susmel, 2002]*

For critical plane theories to function properly, the material must be polycrystalline to find a random direction in which shear stress causes damage.

Figure 5-7 shows a real case of the application of the Susmel method to a broken fatigue specimen: the orientation of the crack practically coincides with the

theoretical one when finding a suitable orientation of one of the grains in which the micro crack begins.

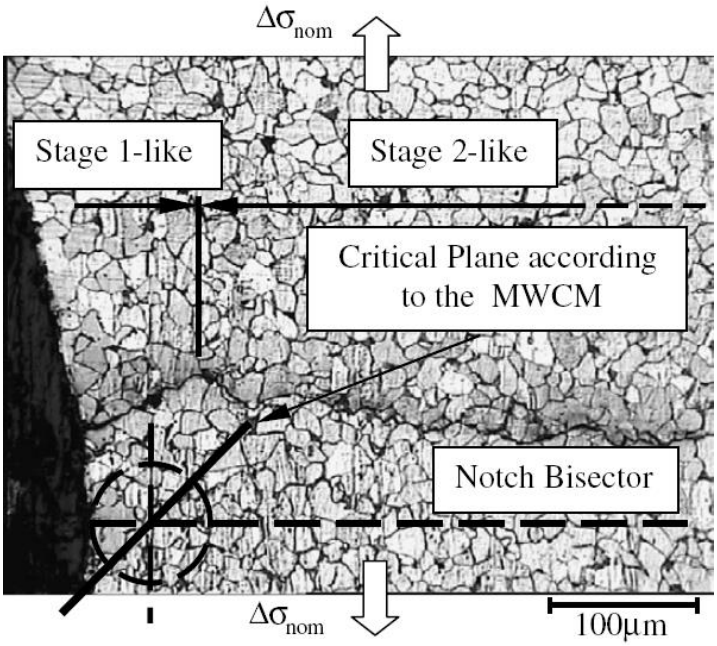

Figure 5-7. *Actual and calculated initiation orientation of the Susmel method [Susmel, 2007]*

Susmel's method uses the maximum shear stress amplitude, so that the orientation of the crack in initiation and propagation in stage 1 has a good experimental correlation. However, these methods do not cover propagation in stage 2.

The critical plane must be searched taking into account one of the two previous criteria. Basically, MSSR methods will search for the maximum amplitude of the shear amplitude, select all planes within 99.9% of the maximum shear

amplitude, and select the one with the maximum normal stress, as described in [Susmel, 2011]. In the methods of maximum damage (MD) the process is substantially simpler and with lower computational cost, not having to make a previous selection of planes "candidates" to critical plane.

The measurement of the amplitude of shear stress is a controversial issue, as several publications in the literature, including [Meggiolaro, 2011B], [Gonçalves, 2004], [Li, 2009], [Araujo, 2011] and [Papuga, 2005] strongly recommend the use of the Minimum Circumscribed Ellipse (MCE) ahead of the Minimum Circumscribed Circle (MCC), especially in the case of non-proportional (out-of-phase) loads.

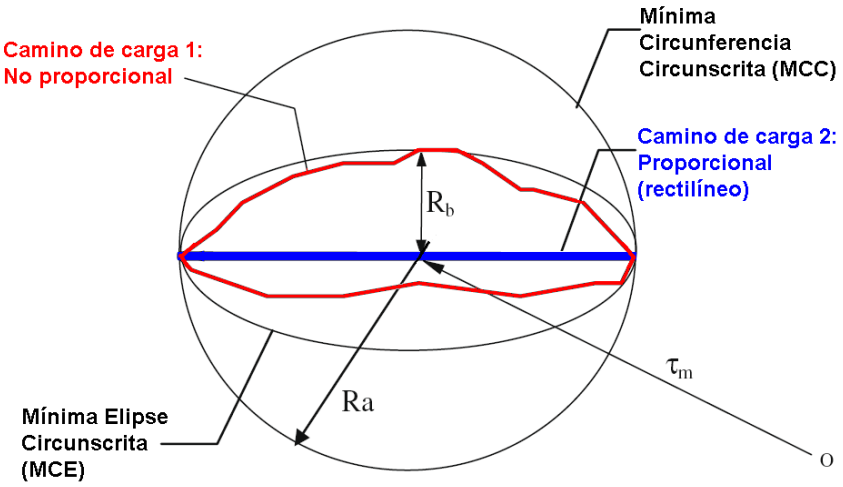

Figure 5-8. *Measurement of load paths by the MCC and MCE. Adapted from [Li, 2009]*

As shown in Figure 5-8, the MCC offers the same shear amplitude value for non-proportional load paths as for proportional load cases.

Therefore, in the case of the Minimum Circumscribed Circle, the shear stress amplitude will be described by the formula (5-29):

$$\tau_a = R_a \tag{5-29}$$

The shear amplitude for the case of the Minimum Circumscribed Ellipse equation (5-30):

$$\tau_a = \sqrt{R_a{}^2 + R_b{}^2} \tag{5-30}$$

Thus, with the MCE an extra damage is obtained with respect to the MCC for non-proportional loading paths that seems to be more in line with the experimental results. A proof of this improvement is the fact that applying the MCE over the Crossland method gives results similar to those of Papadopoulos [Papadopoulos, 1994] for all cases in the database which will be analysed in the next section. Although the Papadopoulos method is not analysed in this comparison due to its very high computational cost, the results obtained here can be compared with those obtained by Papuga in [Papuga, 2011A]. Therefore, in the comparison presented in the following chapter, the MCE will be used.

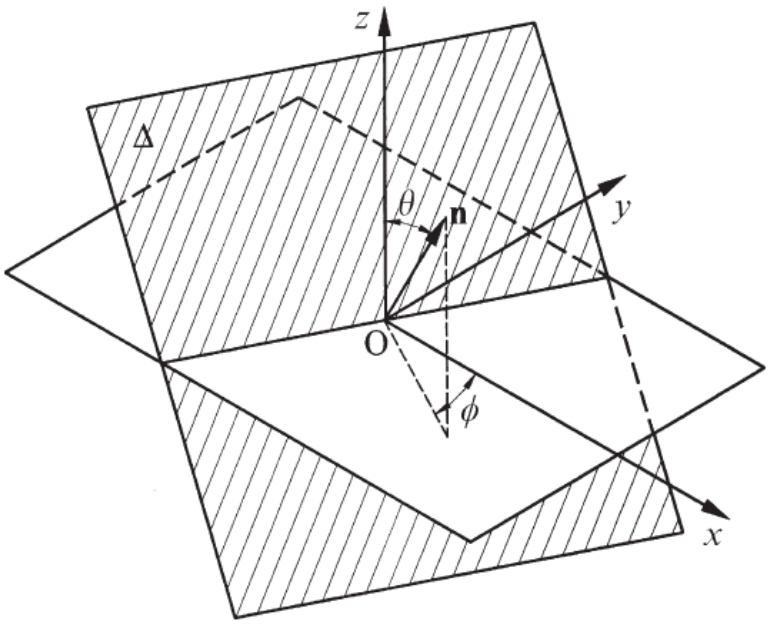

Figure 5-9. *Spherical coordinates used to search for the critical plane [Susmel, 2002]*

With regard to the search for the critical plane, the usual formulation presented by Papuga in his doctoral thesis [Papuga, 2005] will be used. Basically, two spherical coordinates Φ and θ will be used, and a search will be carried out that in this case, as it has scientific purposes, will be using a step of 1º.

The main critical plane methods are described next. Some of them will be furtherly analysed in the next chapter and the agreement with experimental results will be compared against other IDSA methods and classic methodologies.

5.4.1. Stulen-Cummings (MD)

The method of Stulen-Cummings [Stulen, 1954] uses as critical plane π that in which the next quantity is maximum:

$$\pi = Max\left(\frac{\tau_a}{\beta - \alpha \cdot N_{\max}} \right) \tag{5-31}$$

Where α and β are material constants:

$$\alpha = 2 \cdot \frac{\tau_{-1}}{\sigma_{-1}} \tag{5-32}$$

$$\beta = \tau_{-1} \tag{5-33}$$

Once the orientation of the critical plane is known, the damage function is evaluated. The safe zone of the Stulen & Cummings method as a function of the uniaxial fatigue limit R=-1 is:

$$2\sqrt{k-1} \cdot \tau_a + \left(2-k\right) \cdot N_{\max} \leq \sigma_{-1} \tag{5-34}$$

This method shows a non-linear dependence of axial and torsional mean stresses.

5.4.2. Findley (MD)

An early version of Findley's method was presented at the 1956 International Fatigue Congress [Findley, 1956] along with the methodologies of Marin and Crossland. It was subsequently improved in a late work by Findley [Findley,

1959]. It uses the same damage function as the Stulen-Cummings method, but unlike the Stulen-Cummings method, in the Findley method the critical plane is the one in which the damage function is maximum.

As cited in [Papuga, 2011A], planes defined in maximum damage (MD) show a better agreement with experimental results of out-of-phase loads than MSSR-type methods.

In the words of the method's own author, *"this theory explains the fact that the influence of mean stress is small for torsion and stronger for bending of ductile materials but strong for torsion and bending of cast irons"* [Findley, 1959].

Although the damage function is defined in linear terms, being of the Maximum Damage (MD) type, the influence of the mean normal and torsional stresses is slightly non-linear.

The safety zone of the Findley method with respect to the uniaxial fatigue limit under fully reversed conditions (R=-1) is exactly the same as that of the Stulen-Cummings method equation (5-34), although the failure plane is different and therefore there is a difference between the results of both methods.

$$2\sqrt{k-1}\cdot\tau_a+\left(2-k\right)\cdot N_{\max}\le\sigma_{-1} \qquad (5\text{-}35)$$

5.4.3. Matake (MSSR)

The Matake method [Matake, 1977] uses the Maximum Shear Stress Range (MSSR) as the critical plane. Unlike the Dang Van method, which uses the maximum hydrostatic stress, the Matake method uses as a damage parameter

the maximum normal stress at this plane of maximum shear. Further analysis and comparison will help to shed light on the suitability of these two parameters. This method shows an independence of the torsional fatigue limit from a static superimposed torsional stress. However, the mean torsional stress can influence other states of loading.

The safety zone of the Matake method with respect to the uniaxial fatigue limit in "fully reversed" conditions (R=-1) is as follows:

$$k \cdot \tau_a + (2-k) \cdot N_{\max} \leq \sigma_{-1} \tag{5-36}$$

5.4.4. Yokobori

Yokobori's method [Yokobori, 1963] uses the maximum shear as a critical plane. Once the orientation of the plane is located, the same damage function is evaluated as in the Stulen-Cummings, Findley and Matake methods:

$$2\sqrt{k-1} \cdot \tau_a + (2-k) \cdot \sigma_{\max} \leq \sigma_{-1} \tag{5-37}$$

5.4.5. Dang Van Method (MSSR and MD)

Dang Van's method [Dang Van, 1973] is one of the first to be developed after the 1950's classic multiaxial fatigue methods. It is also the best known and most implemented method in commercial solutions [Papuga, 2005]. The critical plane is both the maximum shear stress amplitude and the maximum damage [Papuga, 2011A].

A linear combination of maximum shear amplitude and maximum hydrostatic stress is used as damage parameter. This method is independent of the mean shear stresses for any state of loading. The effect of the mean normal stresses is collected through a linear influence of the maximum hydrostatic stress, similar to the Crossland method.

The safety zone of the Dang Van method with respect to the uniaxial fatigue limit in "fully reversed" conditions (R=-1) is as follows:

$$k \cdot \tau_a + (3 - k \cdot 1.5) \cdot \sigma_{H,\max} \leq \sigma_{-1} \tag{5-38}$$

5.4.6. McDiarmid (MD)

The method of McDiarmid was first developed as a MSSR critical plane [McDiarmid, 1991], being finally developed as a MD critical plane method [McDiarmid, 1994]. This criterion is based on the use of an extensive experimental database, being of empirical type. In addition to the fatigue limits σ_{-1} and τ_{-1} used by the already mentioned methods, the McDiarmid method uses the ultimate tensile strength σ_{UTS} in order to have better performance under normal static superimposed loads.

The safety zone of the McDiarmid method with respect to the uniaxial fatigue limit under fully reversed (R=-1) conditions is as follows:

$$k \cdot \tau_a + \frac{\sigma_{-1}}{2 \cdot \sigma_{UTS}} \cdot N_{\max} \leq \sigma_{-1} \tag{5-39}$$

5.4.7. Robert (MD)

Robert's critical plane method [Robert, 1992] is defined as maximum damage (MD). It really is a natural evolution of the Findley method, but a separate treatment of mean and variable normal stresses is performed. In addition, in order to take into account the effect of the mean normal stresses, a uniaxial fatigue limit is used to adjust the method for conditions of R=0: σ_0.

This method has been criticized in some articles such as Papadopoulos [Papadopoulos, 1997] for having a dependence on mean shear stresses. This fact appears as a consequence of being dependent on a mean normal stress defined in a plane that may not be that of maximum shear stress amplitude, as it is defined in the maximum damage.

The safety zone of Robert's method with respect to the uniaxial fatigue limit in "fully reversed" conditions (R=-1) is as follows:

$$2\sqrt{k-1}\cdot\tau_a+(2-k)\cdot N_a+\left(2\cdot\frac{\sigma_{-1}}{\sigma_0}-\sigma_0\cdot\frac{k-1}{2\sigma_{-1}}-(2+k)\right)\cdot N_m\le\sigma_{-1} \quad (5\text{-}40)$$

5.4.8. Zhang-Yao Method (MSSR)

Zhang-Yao's Critical Plane Method [Zhang, 2010] is one of the latest methods published in literature. The same article also contains experimental tests relating to the aeronautical aluminium LY12CZ. This method is defined as other methods, such as the ones by Matake and Susmel-Lazzarin, using the maximum shear stress range plane (MSSR).

Like Robert's method, it uses the mean normal stresses and amplitude separately, but in this case, being of the MSSR type, there is no dependence on the mean shear stress. Another difference with Robert's method is that to take into account the effect of mean normal stresses, the equivalent Goodman stress is used in its formulation, a criterion defined as "conservative" in [Zhang, 2010].

The safety zone of the Zhang-Yao method with respect to the uniaxial fatigue limit under fully reversed (R=-1) conditions is as follows:

$$k \cdot \sqrt{\tau_a^{\,2} - \tau_a \cdot \frac{\sigma_a}{1-\frac{\sigma_m}{\sigma_{ut}}} + \frac{\tau_{-1}^{\,2}}{\sigma_{-1}^{\,2}} \cdot \left(\sigma_{-1} + 2 \cdot \tau_a\right) \cdot \frac{\sigma_a}{1-\frac{\sigma_m}{\sigma_{ut}}}} \leq \sigma_{-1} \quad (5\text{-}41)$$

5.4.9. Susmel-Lazzarin Method (MSSR)

Susmel's Critical Plane Method was devised in 2002 [Susmel, 2002], but later developments have been presented [Susmel, 2003], [Susmel, 2005], [Susmel, 2008], [Susmel, 2011], [Susmel, 2012]. In the analysis of the next chapter, the latest version of the method is used, together with the procedure proposed by Papuga to estimate the influence coefficient *m* of normal stresses [Papuga, 2011b].

This method, of the MSSR type, has as damage parameters the normal amplitude and mean stresses, as well as Robert, Zhang-Yao and Papuga. However, this method establishes two basic considerations regarding normal stresses:

Not all of the mean normal stress contributes to opening the micro cracks generated by a shear stress. Therefore, a value of *m* is defined which determines the influence as a function of the material (Figure 5-10).

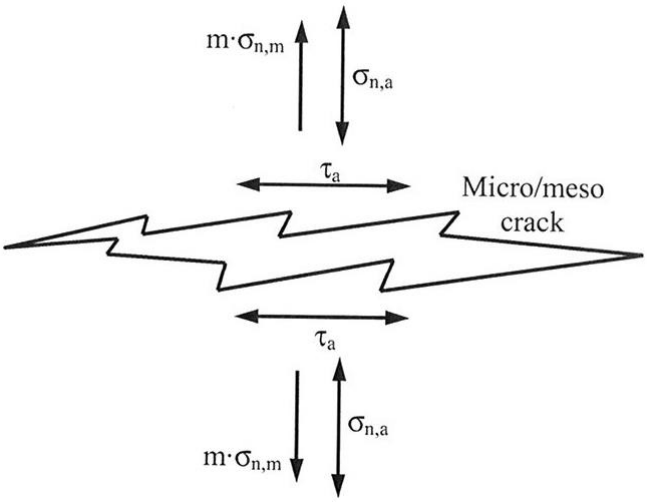

Figure 5-10. *Influence of normal stresses and the m parameter [Susmel, 2008]*

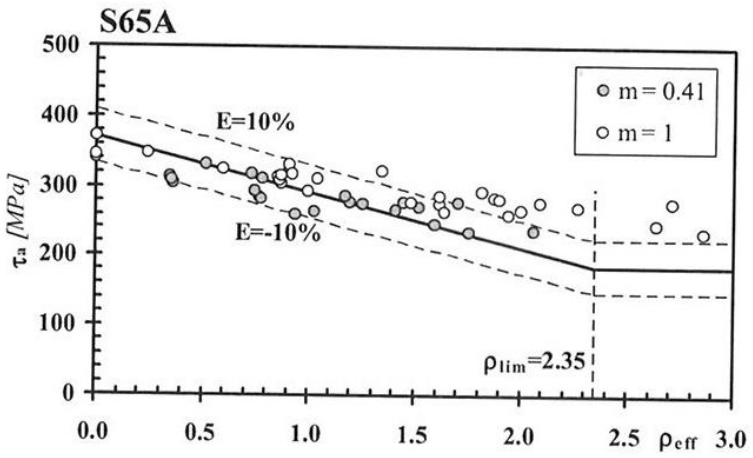

Figure 5-11. *Improvement of experimental results [Susmel, 2008]*

The use of a value other than 1 considerably improves the correspondence with experimental results (Figure 5-11). This way of dealing with mean stresses is based on the experimental observations of Kaufman and Topper, which showed that from a certain threshold value of the mean normal stress, the damage in fatigue does not increase. This threshold value is called σ_{lim} and depends on the characteristics of the material, and its effect can be seen in Figure 5-12.

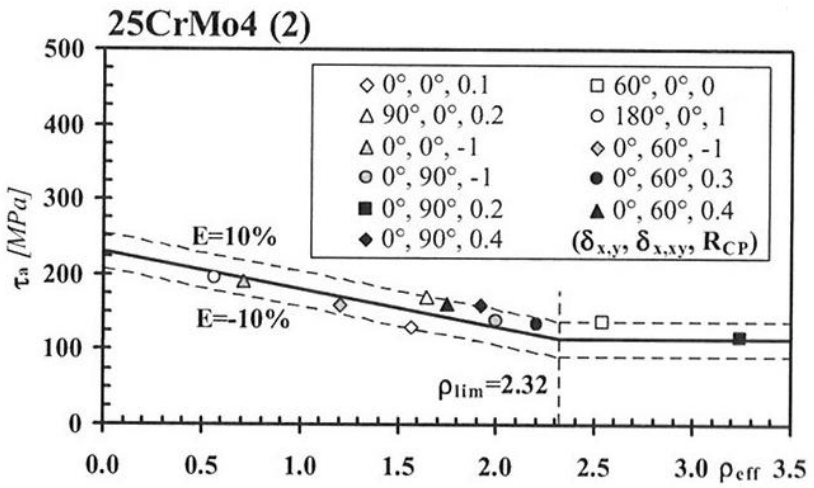

Figure 5-12. *ρ_{lim} value that determines the maximum damage threshold of normal stresses [Susmel, 2008]*

On the one hand, the value of the influence coefficient *m* of normal stresses, which can vary between [0,1] will be defined according to the value proposed by Papuga in [Papuga, 2011B]:

$$m = \frac{2 \cdot \tau_{-1} - \frac{\sigma_0}{2}}{2 \cdot \tau_{-1} - \sigma_{-1}} - 1 \qquad (5\text{-}42)$$

The value of ρ_{lim} that determines the threshold at which an increase in normal stresses does not cause greater fatigue damage can be found with the formula proposed in [Susmel, 2008]:

$$\rho_{\lim} = \frac{\tau_{-1}}{2 \cdot \tau_{-1} - \sigma_{-1}} \qquad (5\text{-}43)$$

The safety zone of the Susmel method with respect to the uniaxial fatigue limit under "totally reversed" conditions (R=-1) is as follows:

$$k \cdot \tau_a + \sigma_{-1} \cdot (1 - 0.5 \cdot k) \cdot Min\left(\frac{\sigma_a + m \cdot N_m}{\tau_a}; \rho_{\lim} \right) \leq \sigma_{-1} \qquad (5\text{-}44)$$

5.4.10. Papuga (MD)

Papuga's critical plane method was first defined in [Papuga, 2008] and later optimized in [Papuga, 2009]. This method is defined in maximum damage plane. It shares great similarities with Robert's, as it is defined in the maximum damage, uses the mean normal stresses and amplitude, and also takes advantage of a uniaxial fatigue limit in R=0.

The main difference with Robert's method is that the damage function varies depending on ductility. The Papuga method is defined in two sections, the boundary being defined at κ=1.155.

The safety zone of the Susmel method with respect to the uniaxial fatigue limit under "totally reversed" conditions (R=-1) is as follows:

$$\sqrt{a_{Pap}\cdot {\tau_a}^2 + b_{Pap}\cdot\left(\sigma_a + \frac{\tau_{-1}}{\sigma_0}\cdot\sigma_m\right)} \le \sigma_{-1} \qquad (5\text{-}45)$$

Where a_{Pap} and b_{Pap} are two material constants that are defined in sections according to the value of κ. For values of κ less than 1.155 (extra-fragile materials) equations (5-46) and (5-47) should be used:

$$a_{Pap} = 0.5\cdot\left(\kappa^2 + \sqrt{\kappa^4 - \kappa^2}\right) \qquad (5\text{-}46)$$

$$b_{Pap} = \sigma_{-1} \qquad (5\text{-}47)$$

For values of κ greater than 1.155 the equations (5-48) and (5-49) will be used:

$$a_{Pap} = \left(\frac{4\cdot\kappa^2}{4+\kappa^2}\right)^2 \qquad (5\text{-}48)$$

$$b_{Pap} = \frac{8\cdot\sigma_{-1}\cdot\kappa^2\cdot\left(4-\kappa^2\right)}{\left(4+\kappa^2\right)^2} \qquad (5\text{-}49)$$

5.5. Discussion

Analysing the characteristics of the methods previously mentioned, we can resolve that the method to develop must have certain characteristics that allow it to be effective against those already present in the literature.

5.5.1. Computational cost

In terms of computational cost, there is an obvious advantage of global approach or invariant based methods. Its computational cost is 2 orders of magnitude lower than the integral methods, and at least one order of magnitude lower than the critical plane methods.

With respect to critical plane methods, those defined as maximum damage (MD) are preferable. By using a function of this type, the computational cost is lower than in MSSR methods, in which a second optimization in the normal stresses has to be made once the planes with maximum shear stress amplitude have been chosen. Through the use of a critical plane in maximum damage (MD) together with an adequate algorithm of search of planes as for example the one described by Weber in [Weber, 1999], the process can be very advantageous from the computational point of view.

Integral methods would be discarded due to their high computational cost, an order of magnitude higher than that of critical plane methods, as noted in [Papuga, 2005] and [Papuga, 2009]. On the other hand, in the review of methods presented by Jan Papuga in [Papuga, 2011A], there does not seem to be much

difference between averaging the damage (integral methods) and maximizing the damage (critical-plane methods).

5.5.2. Influence of mean normal stresses

Many experimental results from the literature show that the influence of the mean normal stresses is greater in fragile materials than in ductile materials, a fact that should undoubtedly reflect the method to be developed.

Other methods use empirical relationships such as Goodman, Gerber, etc. which are not suitable for all types of materials, and which make use of the ultimate tensile strength at break σ_{UTS}. This parameter, which represents the highest engineering stress the material can withstand in a tensile test, is related in steels to Vickers hardness [Nishijima, 1993], which is in turn a measure of the resistance of the matrix to local deformation [Murakami, 2002].

The method to be developed should take into account that for most engineering materials, mean compressive stresses increase fatigue strength, and that tensile stresses are detrimental in terms of the variable stress that the material is able to withstand.

5.5.3. Influence of mean torsional stresses

The effect of mean torsional stresses on cyclic torsion is known in many materials, among which are all kinds of engineering materials, such as quenched and tempered steels [Chodorowski, 1956], cast irons [Rausch, 2011], and aluminiums [Findley, 1953]. The damage may be due to the fact that the plane in which the crack starts is not the maximum shear stress amplitude.

Invariant methods based on energy balances such as those of Marin and Froustey take this effect into account through the balancing of distortion energy, resulting in a torsional Haigh diagram with an elliptical damage function. The multiaxial critical plane fatigue methods defined in maximum damage (MD) also capture this effect.

However, invariant methods that do not explicitly use the mean second invariant value of stresses are not sensitive to mean torsional stresses. The critical-plane methods MSSR and Dang Van are also not sensitive to mean shear stresses in the case of pure torsion.

Many experimental results from the literature show that the influence of the mean normal stresses is greater in fragile materials than in ductile materials, a fact that should undoubtedly reflect the method to be developed.

5.5.4. Effect of Phase Shift

Critical plane methods defined in maximum damage (MD) take into account the effect of phase shifting more accurately than the maximum shear amplitude (MSSR) methods according to the review by Papuga [Papuga, 2011A].

Another aspect that can improve the accuracy of the methods for out-of-phase loads is the use of alternative ways of measuring the shear stress amplitude different from the Minimum Circumscribed Circle (MCC). Among the alternatives we can find the method of the Minimum Circumscribed Ellipse (MCE) or the Moment of Inertia (MOI), the latter exclusive for use in critical

plane methods. However, the MCE can be used to improve global approach methods (based on invariants) to improve response to out-of-phase loads.

5.5.5. Ability to use for finite life

One of the main advantages of methods based on stress invariants is that they can be easily adapted for use in finite life [Cristofori, 2008]. Although this is not the aim of this Thesis, it must be taken into account that further development of an IDSA method would allow its use for finite life calculation, adding an important added value to being able to be used in a much larger life range.

With respect to the critical plane methods, their adaptation to their use for finite life implies for practical purposes the adoption of a value of sensitivity to normal stresses at the critical plane for the whole range of life, an arbitrary hypothesis not confirmed by the experimental results.

SECTION II

Research work performed

Chapter 6:

ANALYSIS AND DISCUSSION OF MULTIAXIAL FATIGUE METHODS

CHAPTER 6. ANALYSIS AND DISCUSSION OF MULTIAXIAL FATIGUE METHODS

6.1. Experimental database

The analysis and discussion of the experimental agreement of multiaxial fatigue methods will help to infer which methodologies are the most interesting for the development of a multi-axial calculation criterion, and which features must be incorporated into the developed method.

In the current literature there are few comparative analyses between HCF multiaxial fatigue methods, among which the following stand out: [Papadopoulos, 1997]. [Wang, 2004]. [Papuga, 2011A].

- Papadopoulos in 1997, which mainly addresses his method and compares it with some of the early multi-axial methods with a rather limited experimental base [Papadopoulos, 1997].
- Wang in 2003, with a mainly qualitative comparison, in which only the methods of Sines, Gough, Lee and McDiarmid are compared [Wang, 2004].
- Papuga in 2011, an ambitious comparison with virtually all current methods and an extensive, well-referenced database [Papuga, 2011A].
- This last comparison, by the author Jan Papuga, generated a great controversy in the world of fatigue research. On the one hand it showed that some of the advanced methods developed in the early years did not

produce good results (Matake, Dang Van). However, one of the most recognized methods today, Luca Susmel's method or "Modified Wöhler Curve Method" had not been implemented in its latest version in this comparison. The world's most prestigious magazine on fatigue, the International Journal of Fatigue, opened a discussion [Susmel, 2011] and [Papuga, 2011B] in which author Luca Susmel defended results of extraordinary quality for his method implemented in the latest versions.

In order to analyse the main multiaxial fatigue methods, a large database of multiaxial fatigue tests has been compiled. The original starting point was the Papuga database [Papuga, 2011A], which is available at www.pragtic.com and consists of 407 experiments.

The database compiled is very extensive, with different types of materials: aluminium, ferrous materials (various types of steels, cast irons, etc.) and Ti-6Al-4V titanium. Therefore, the spectrum of materials is covered according to their ductility: fragile, semi-ductile, ductile, extra-ductile. In addition, it contains a wide variety of biaxial load states, including mean normal and tensile stresses, and load combinations. The main multiaxial fatigue methods have been programmed and applied on this extensive database, summarized in Table 6-1.

Table 6-1. *Database of tests by Papuga [Papuga, 2011A]*

Group name	Material	No. of tests	Reference
BAB	Ck35 steel	11	[Baier, 1970]
BAI	34CrMo4 steel	15	[Baier, 1970]
BER	39NiCrMo3 steel	3	[Davoli, 2003]
BKL	SAE 52100 steel	9	[Bomas, 2009]
DEL	Ti-6Al-4V	2	[Delahay, 2004]
DUB	30NCD16 steel	23	[Dubar, 1992]
EMM	St60 steel	8	[El Magd, 1977]
FI6	76S-T61 aluminium	14	[Findley, 1953]
FI7	76S-T61 aluminium	14	[Findley, 1953]
FI8	76S-T61 aluminium	13	[Findley, 1953]
FLA	30NCD16 steel	12	[Froustey, 1989]
FLB	30NCD16 steel	13	[Froustey, 1989]
GGH	S65A steel	27	[Gough, 1950]
GPA	0.1%C steel	5	[Gough, 1935]
GPB	3.5%NiCr steel	5	[Gough, 1935]
GPC	Silal cast iron	5	[Gough, 1935]
GPD	Cast steel	5	[Gough, 1937]
GPE	CuCr cast iron	5	[Gough, 1937]
GPF	Inoculated cast iron	5	[Gough, 1937]
GPH	NiCr cast iron	5	[Gough, 1937]
GPI	0.4%C steel (normalised)	5	[Gough, 1951]
GPJ	0.4%C steel (spheroidised)	5	[Gough, 1951]
GPL	0.9%C steel (pearlitic)	5	[Gough, 1951]
GPM	3/3.5%Ni steel (45/50 ton)	5	[Gough, 1951]
GPN	CrVa steel (45/50 ton)	5	[Gough, 1951]
GPO	3.5% NiCr steel (low impact)	5	[Gough, 1951]
GPP	NiCrMo Steel (75/80 ton)	5	[Gough, 1951]
GPQ	NiCr steel (95/105 ton)	5	[Gough, 1951]

GPR	Nicrosilal cast	5	[Gough, 1951]
HEG	GGG60 cast iron	4	[Heidenreich, 1979]
HEI	34Cr4 steel	14	[Heidenreich, 1983]
HRZ	34Cr4 steel	18	[Heidenreich, 1984]
HZ	34Cr4 steel	2	[Heidenreich, 1976]
ISS	St35 steel	18	[Issler, 1973]
LEM	42CrMo4 steel	10	[Lempp, 1977]
MI	25CrMo4 steel	15	[Mielke, 1980]
MPA	30NCD16 steel	3	[Morel, 2002]
MPB	XC18 cast iron	3	[Morel, 2002]
MPC	FGS800-2 cast iron	4	[Morel, 2002]
NKC	Grey cast iron	8	[Nishihara, 1945]
NKD	Duralumin	2	[Nishihara, 1945]
NKH	Hard steel	10	[Nishihara, 1945]
NKM	Mild steel	8	[Nishihara, 1945]
NOL	C35N steel	2	[Nolte, 1973]
PAY	34Cr4 steel	3	[Paysan, 1970]
SIB	XC48 cast iron	16	[Simbürger, 1975]
TAK	25CrMo4 steel	11	[Troost, 1987]
ZHA	LY12CZ aluminium	15	[Zhang, 2010]

Therefore, this database can be used not only to analyse the overall precision of the different methods in all tests, but also to analyse individual effects, such as those of axial and mean shear stresses, which according to various researchers [Papadopoulos, 1997] and [Papuga, 2011A] are fundamental for a method to be accurate in multi-axial calculations. Therefore, the following aspects will be analysed within the present chapter of the Thesis:

1. Overall results for the entire test sample
2. Effect of multi-axiality without mean stresses or phase shifts
3. Effect of Phase Shift
4. Effect of axial mean stresses
5. Effect of mean torsional stresses

Firstly, the overall performance of the different methods will be analysed for the entire test sample, which includes all possible biaxial load types, without discriminating the individual effects.

In later stages, each of the above effects will be analysed individually. It should be noted that the effect of mean torsional stresses is a controversial issue even among leading researchers in multi-axial fatigue, as previously indicated in the chapter on mean torsional stresses. Among others, Sines and Papadopoulos maintain that their influence is null. However, some methods such as Marin, Findley, Robert and Papuga take into account the effect of mean torsional stresses.

The procedure for calculating the error is defined in the same way as [Papadopoulos, 1997] and [Papuga, 2011A]:

$$Index\_of\_error(\%) = \frac{\sigma_{-1}(load) - \sigma_{-1}(material)}{\sigma_{-1}(load)} \cdot 100 \qquad (6\text{-}1)$$

Thus, a positive value indicates that the method is conservative, predicting a failure that never occurred. On the other hand, a negative value indicates non-conservative behaviour.

In general, a centred distribution is sought, with an average value close to zero, and a variance as low as possible, which indicates a scarce dispersion of the results, see the following figure:

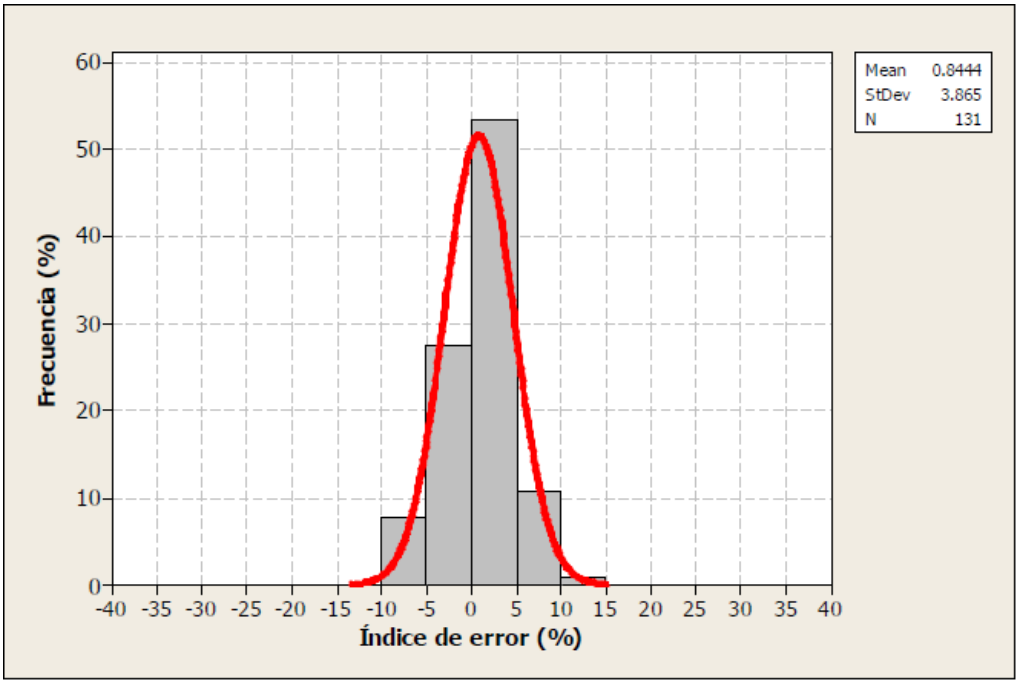

Figure 6-1. *Ideal error distribution of a multi-axial method*

The figure above shows an error distribution with a mean value centred and slightly displaced towards the conservative zone (0.844%), and a very low dispersion, with a standard deviation (StDev) of the error of 3.865%.

The value of N refers to the number of experiments that have been taken into account. The greater the number of tests taken into account, the higher the reliability of the analysis.

6.2. Overall results for the entire test sample

These results indicate the overall performance of the methods taking into account the entire database, which concerns 422 experiments, covering a large number of different stress states. In many of the experiments, the effects of phase shift and mean stresses appear mixed, however many of the experiments only contain biaxiality itself, like the tests performed by Gough and Pollard. Table 6-2 shows the global results of the different methods. All the individual distributions for the entire sample are shown in Figures 6-2 to 6-21.

- **Classic methods:**

Among the classic methods we find a great dispersion, much higher than the multiaxial methods. This generalised dispersion in results is greater in von Mises than in Worst Principal. On the other hand, with equal treatment of the effect of mean stresses, von Mises tends to be more conservative than Worst Principal.

Another noteworthy fact is that the use of any criterion with Walker 0.5 (Smith-Watson-Topper) shifts the distribution of results to the non-conservative zone, especially in the case of Worst Principal.

Within the classic methods, the option of von Mises combined with the real exponent of Walker and Goodman offers with a centred distribution and with a good percentage of cases in the range [-15%,15%], reaching 59.2% of cases in this margin of error.

Table 6-2. *Global results for the entire database (422 tests)*

Criterio	Valor medio del error	Desviación estándar del error	Porcentaje de resultados en el rango [-40%,40%]	Porcentaje de resultados en el rango [-15%,15%]	Porcentaje de resultados en el rango [-5%,5%] *"Ajustados"*	Porcentaje de resultados en el rango [-5%,-40%] *"No-conservadores"*	Porcentaje de resultados en el rango [+5%,+40%] *"Conservadores"*
Worst Principal Full Range-Goodman	3.13	34.55	82.7	40.0	13.3	22.0	47.4
Von Mises Full Range-Goodman	20.25	46.94	74.2	24.2	7.1	17.3	49.8
Worst Principal Walker real-Goodman	-11.62	28.00	86.0	56.6	27.3	46.9	11.8
Von Mises Walker real-Goodman	3.17	40.68	86.0	59.2	33.9	24.4	27.7
Worst Principal Walker 0.5-Goodman	-16.33	26.95	85.1	45.3	16.8	58.8	9.5
Von Mises Walker 0.5-Goodman	-2.28	39.79	87.0	55.7	21.8	47.2	18.0
Sines	-4.94	12.99	99.1	76.1	36.7	43.8	18.5
Crossland	-4.51	10.21	98.8	85.8	52.1	37.0	9.7
Marin	-2.54	12.41	98.1	82.2	45.0	34.1	19.0
Vu-Halm-Nadot	-2.86	9.57	99.5	86.7	57.1	30.6	11.8
Dang Van MSSR	0.82	11.31	99.3	84.8	47.9	25.1	26.3
Dang Van MD	0.86	11.31	99.3	84.8	47.6	25.1	26.5
Matake	6.61	15.37	96.0	76.5	42.9	14.0	39.1
Findley	8.60	14.80	95.0	73.9	43.6	9.7	41.7
McDiarmid MSSR	-7.39	12.04	97.9	76.3	32.0	52.6	13.3
McDiarmid MD	-5.80	11.50	98.3	79.1	35.5	47.4	15.4
Robert	4.14	9.59	99.5	88.2	48.8	12.6	38.2
Zhang Yao	-2.77	9.67	99.3	88.9	56.9	30.1	12.3
Susmel	1.87	7.97	99.8	92.7	58.1	13.7	28.0
Papuga	-0.43	6.03	100.0	97.2	66.6	18.0	15.4

- **Advanced "global approach" methods:**

In general, this type of methods exhibits a slight trend towards non-conservative results. Evidently, the dispersion of global-type methods is substantially less than that of classical methods, with Crossland and Vu-Halm-Nadot standing out in this respect.

It is noteworthy that Marin's criterion, which only requires uniaxial tests (σ_{-1} and σ_{UTS}), and not requiring torsional tests when considering the von Mises ratio between uniaxial and torsional fatigue limits, obtains results more adjusted to experimental tests than the Sines method, which uses up to 3 different tests, namely τ_{-1}, σ_{-1} and σ_0.

The Vu-Halm-Nadot method obtains the best results among the global approach methods, ahead of Crossland and even surpassing many of the critical plane methods. However, it has a high computational cost and its purely empirical basis is based on a numerical optimization for 127 of the experiments used in this database [Vu, 2010].

- **Critical Plane Methods:**

It should be noted that the method with the best correlation with the experimental results is the Papuga critical plane method. The quality of the distribution is excellent, with a small variance and a very centred value, although very slightly inclined towards non-conservatism (-0.4%).

The Susmel method also obtains excellent results, with a centred distribution whose average value is in the conservative zone (1.87%), and above all with a

dispersion lower than that of other critical plane methods. In this sense, it should be noted that the Susmel method offers excellent performance when used in the last of its versions, in which different influence coefficients of mean normal stresses are used depending on the material. In the original Papuga comparison [Papuga, 2011A] this value was set at 0.35, reducing the overall performance of the method. In the open discussion in [Papuga, 2011B] and [Susmel, 2011], Papuga offers a way to calculate this coefficient explicitly, which is the one used in this comparison.

On the other hand, Dang Van's method, the most implemented in commercial programs, has a focused distribution but a greater dispersion in results than Susmel and Papuga's methods. The scatter in the Dang Van results is similar to that of the Crossland method, which also uses maximum hydrostatic stress. The methods most adjusted to experimental results: Papuga, Susmel, Robert, Zhang Yao, use as damage parameter the amplitude and mean value of normal stress to the critical plane, instead of the maximum normal stress or hydrostatic stress.

The use of the maximum normal stresses at the critical plane (Matake, Findley, McDiarmid) does not seem to bring benefits with respect to the use of the maximum hydrostatic stress (Dang Van), in fact the methods based on maximum normal stresses show a greater dispersion in the results.

On the other hand, the use of maximum damage (MD) planes slightly displaces the distributions towards the conservative part. This fact is practically negligible in Dang Van's method, but it is evident in McDiarmid's method; and also between the Matake (MSSR) and Findley (MD) methods, the latter two having a very similar formulation.

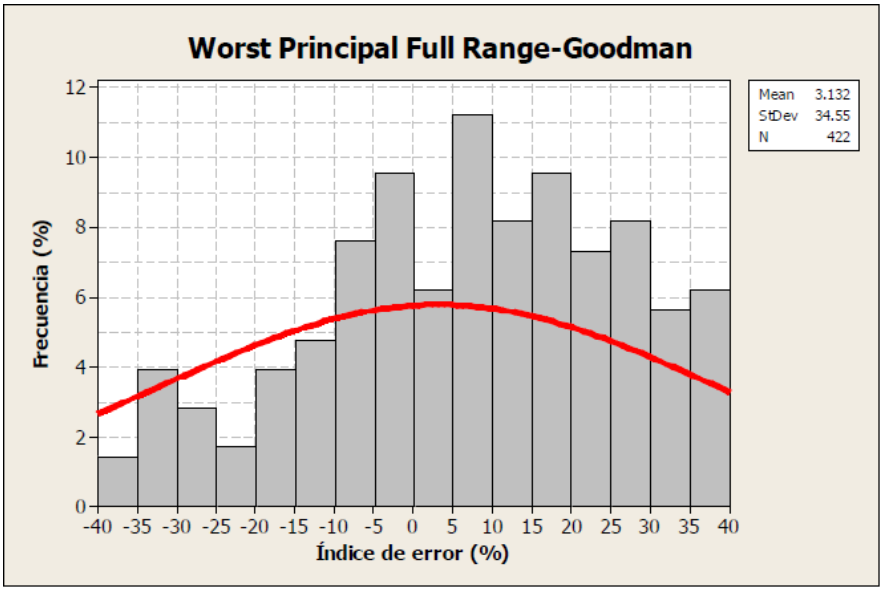

Figure 6-2. *Error distribution of Worst Pr. FR-Goodman for the entire sample*

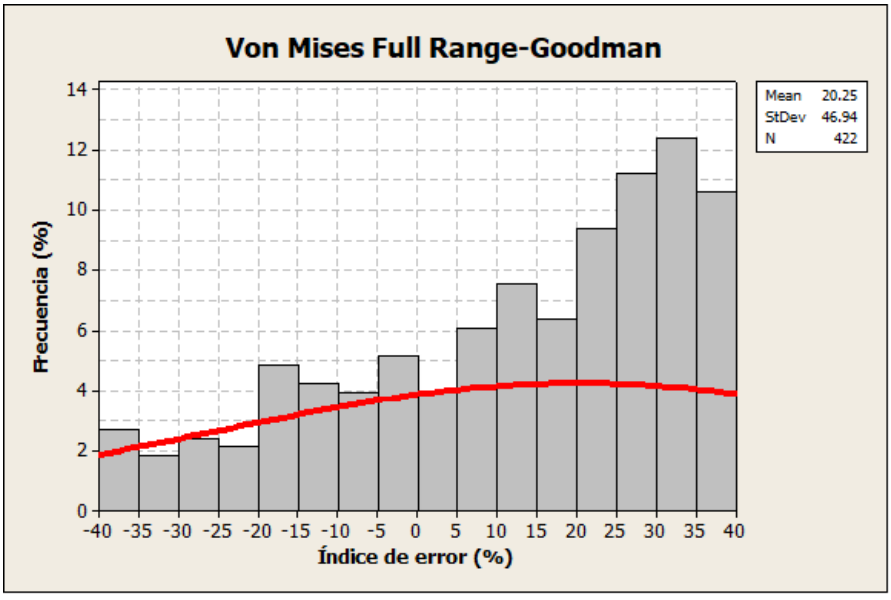

Figure 6-3. *Error distribution of von Mises FR-Goodman for the entire sample*

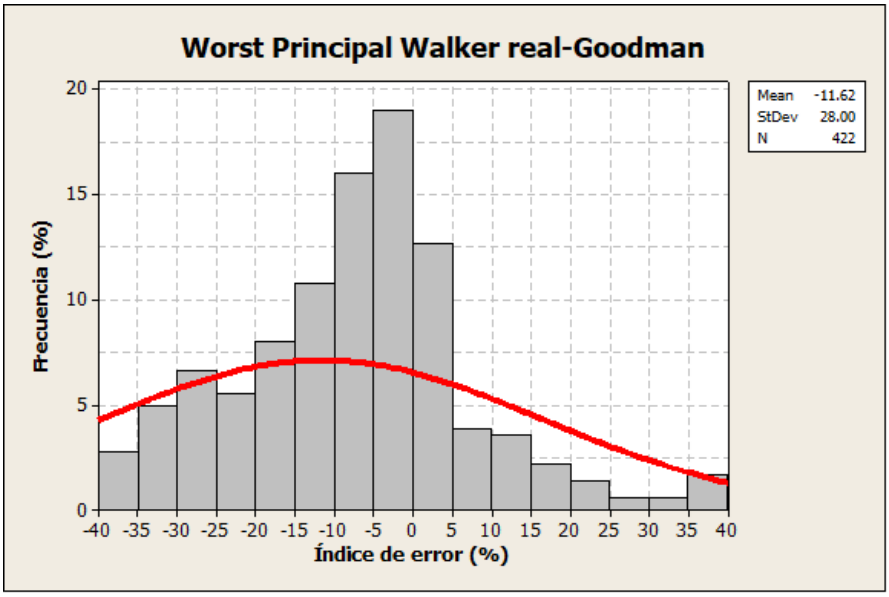

Figure 6-4. *Error distribution of Worst Principal Walker R.-Goodman for the entire sample*

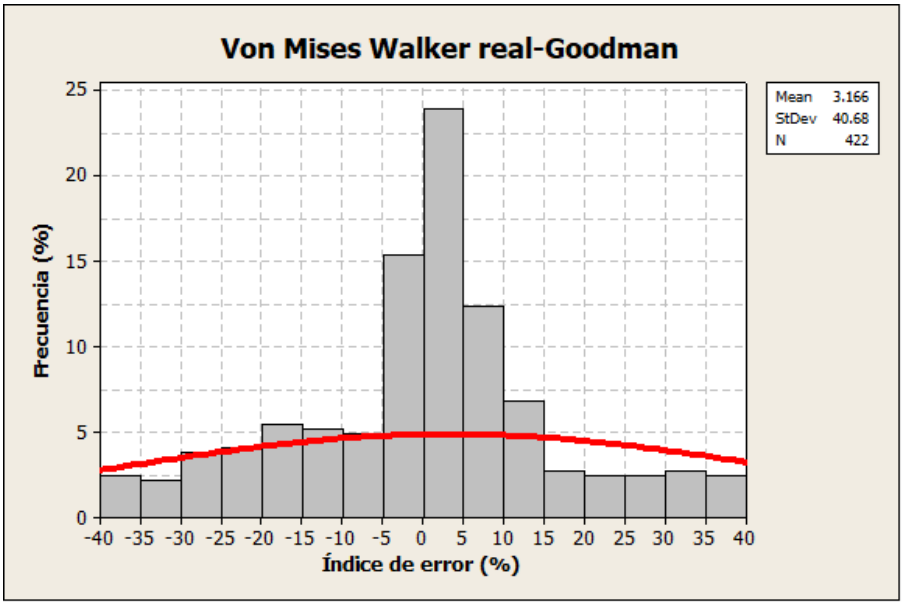

Figure 6-5. *Error distribution of von Mises Walker R.-Goodman for the entire sample*

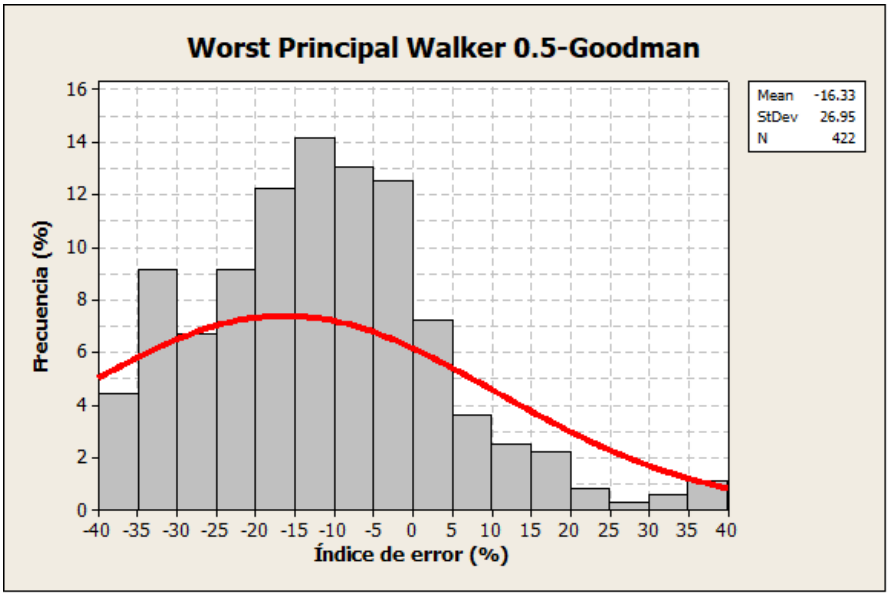

Figure 6-6. *Error distribution of Worst Pr.Walker 0.5-Goodman for the entire sample*

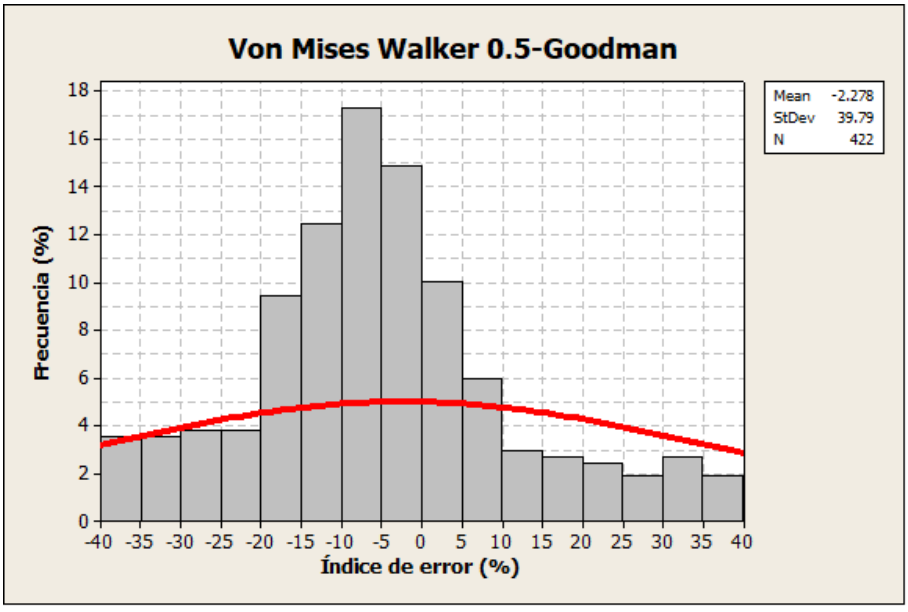

Figure 6-7. *Error distribution of von Mises Walker 0.5-Goodman for the entire sample*

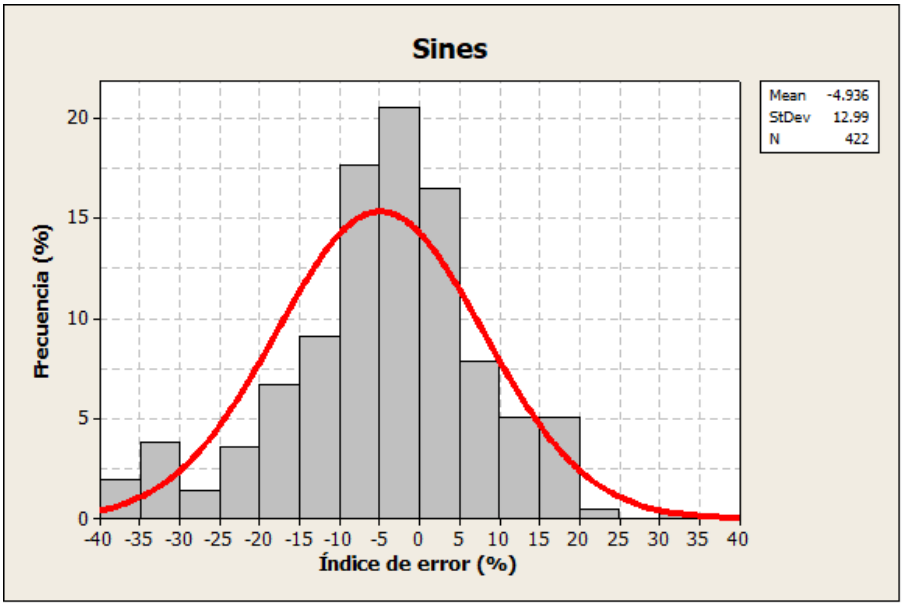

Figure 6-8. *Error distribution of Sines for the entire sample*

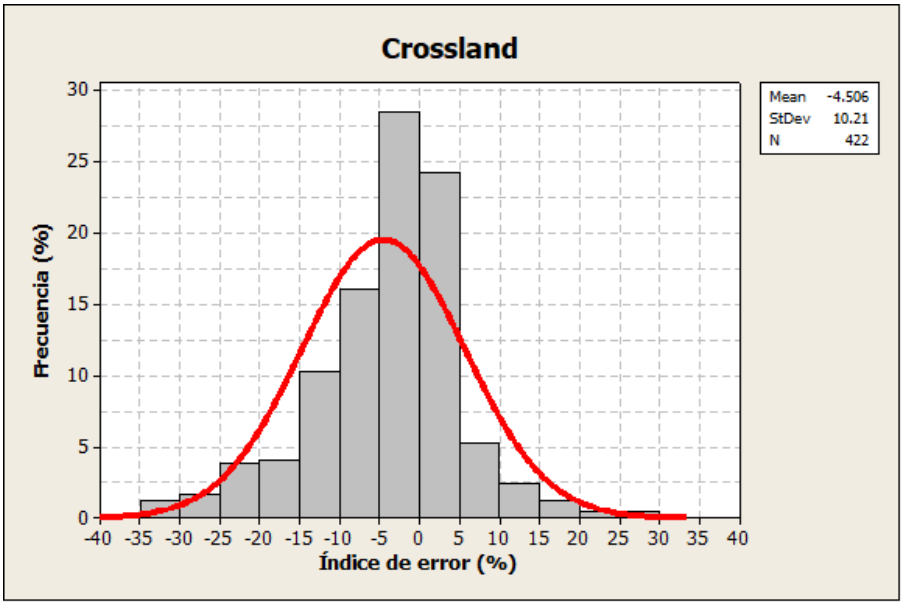

Figure 6-9. *Error distribution of Crossland for the entire sample*

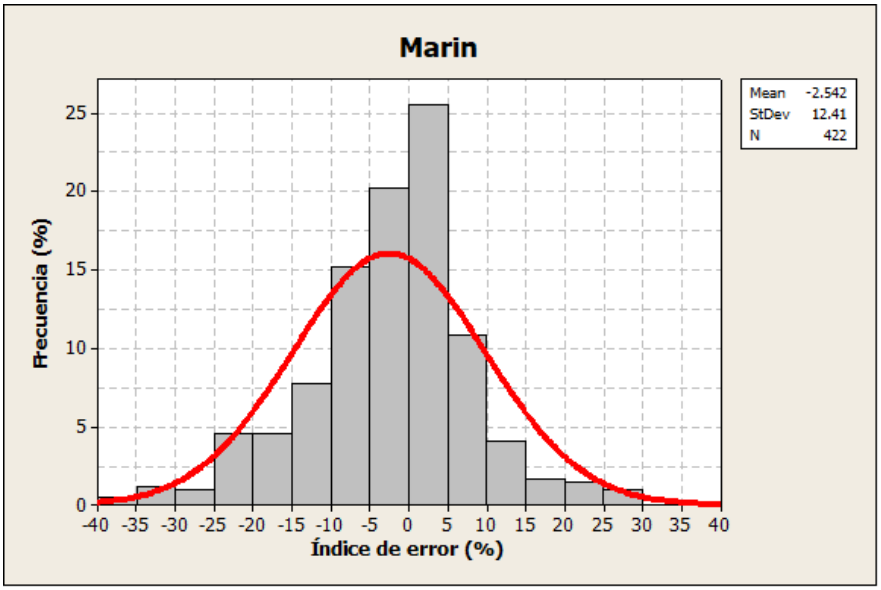

Figure 6-10. *Error distribution of Marin for the entire sample*

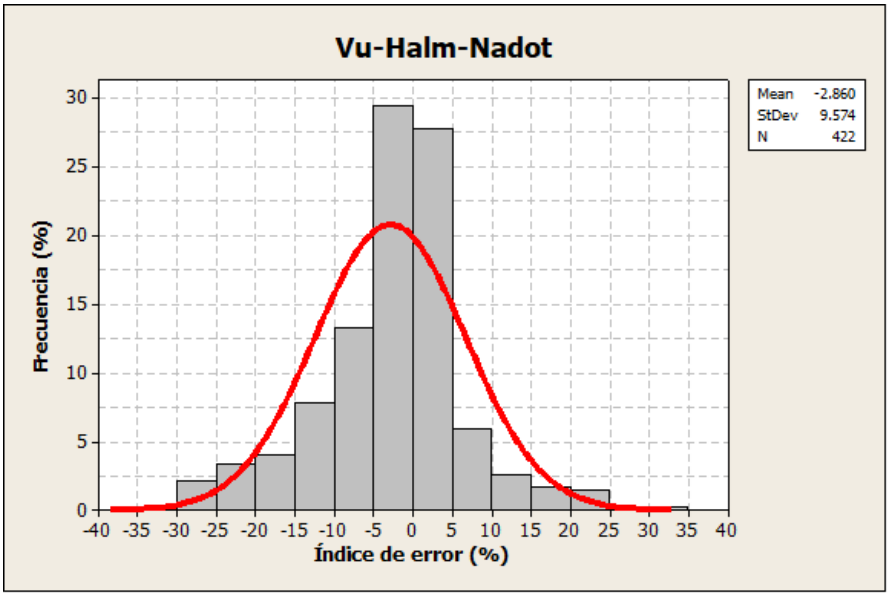

Figure 6-11. *Error distribution of Vu-Halm-Nadot for the entire sample*

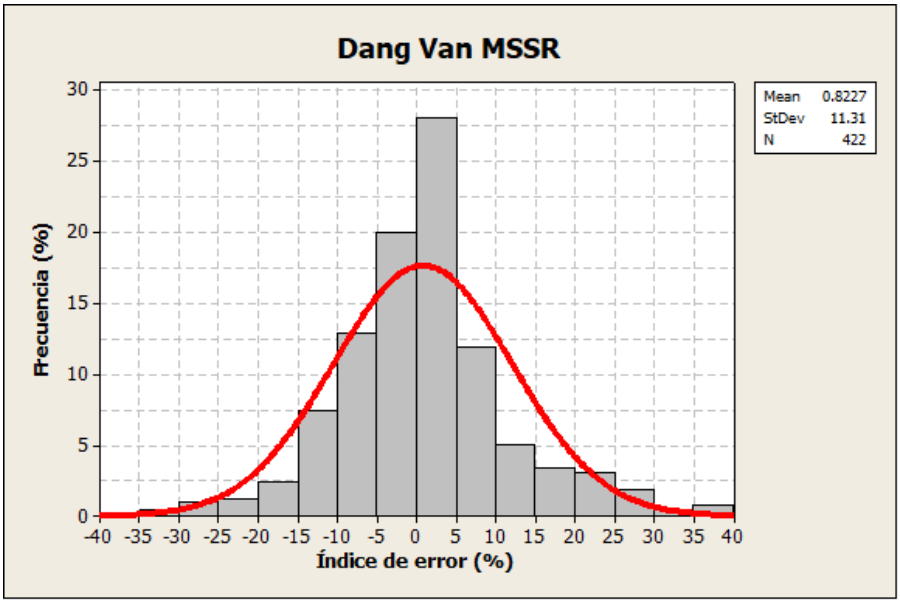

Figure 6-12. *Error distribution of Dang Van MSSR for the entire sample*

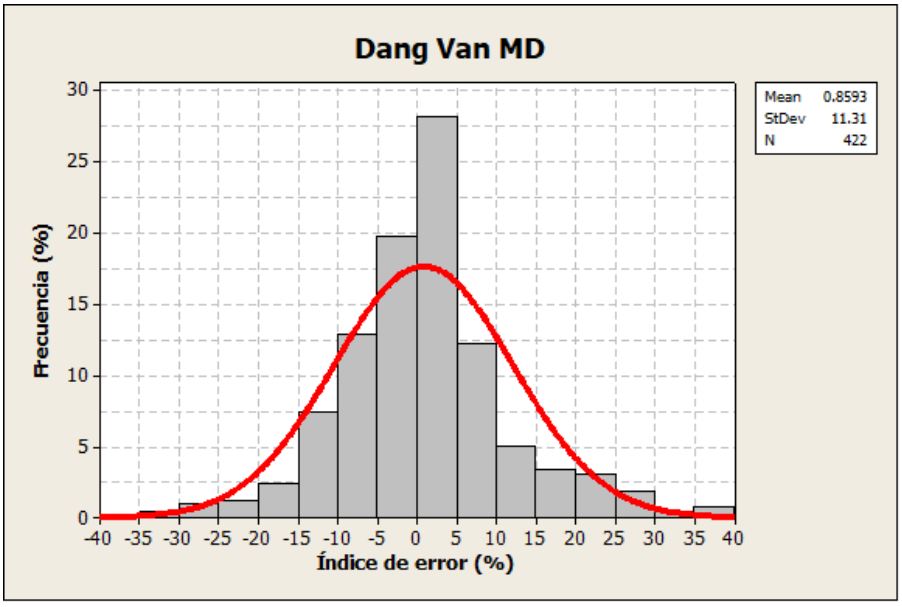

Figure 6-13. *Error distribution of Dang Van MD for the entire sample*

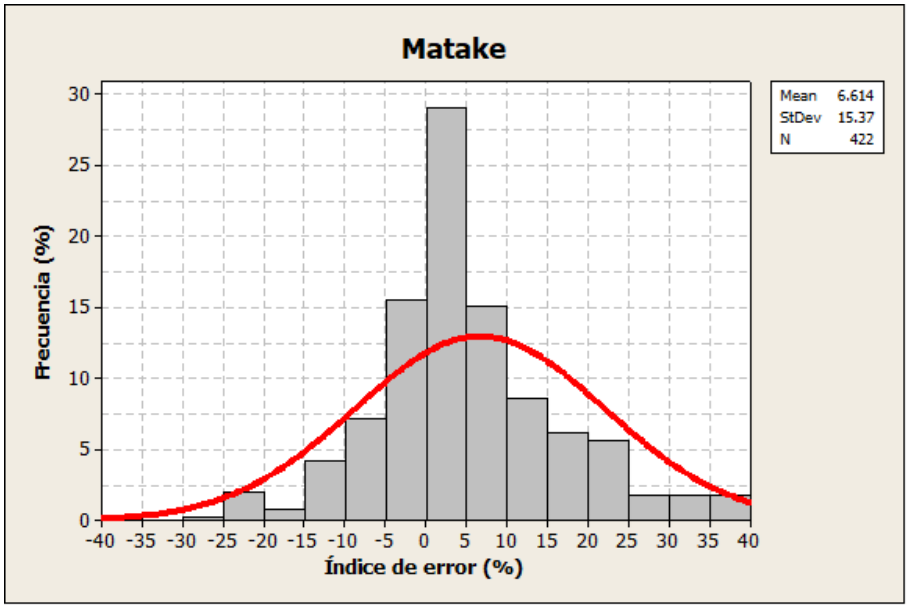

Figure 6-14. *Error distribution of Matake for the entire sample*

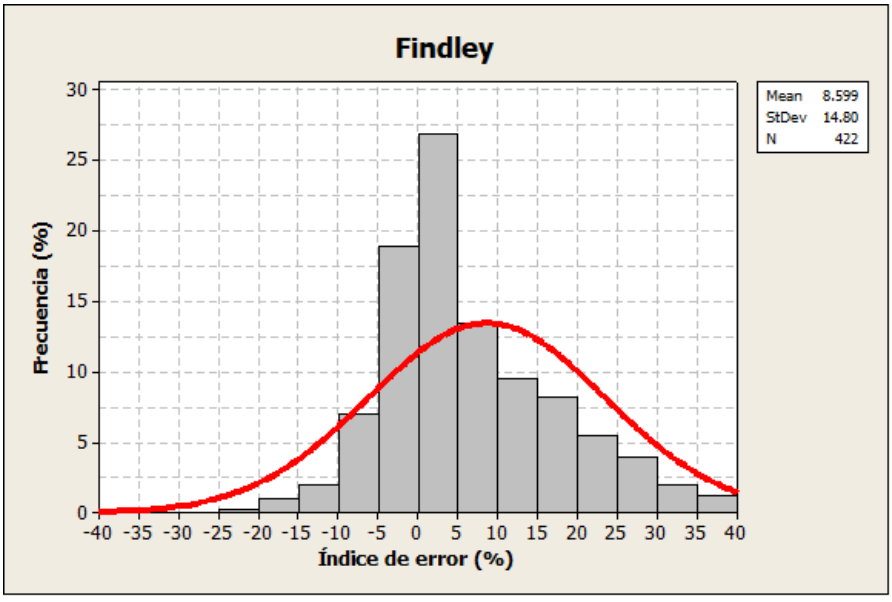

Figure 6-15. *Error distribution of Findley for the entire sample*

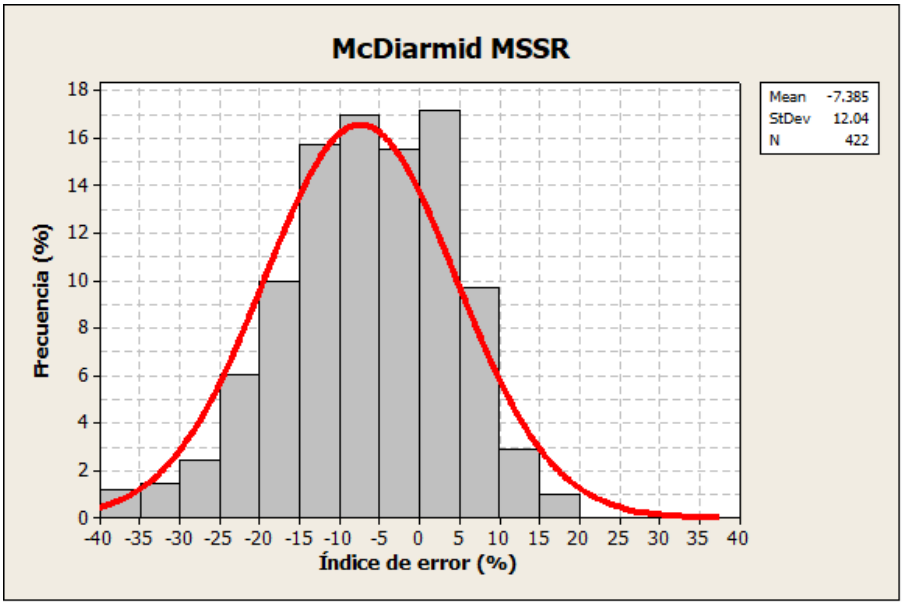

Figure 6-16. *Error distribution of McDiarmid MSSR for the entire sample*

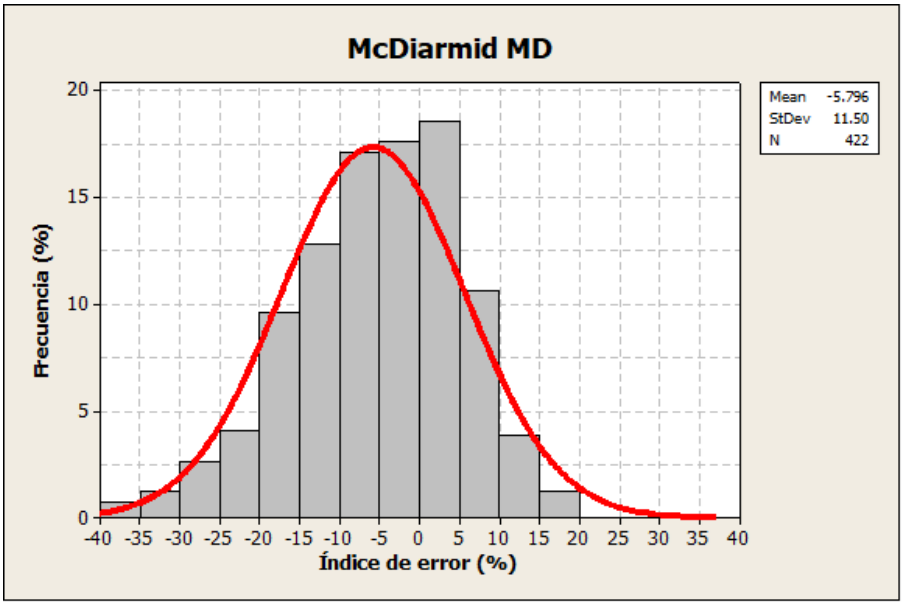

Figure 6-17. *Error distribution of McDiarmid MD for the entire sample*

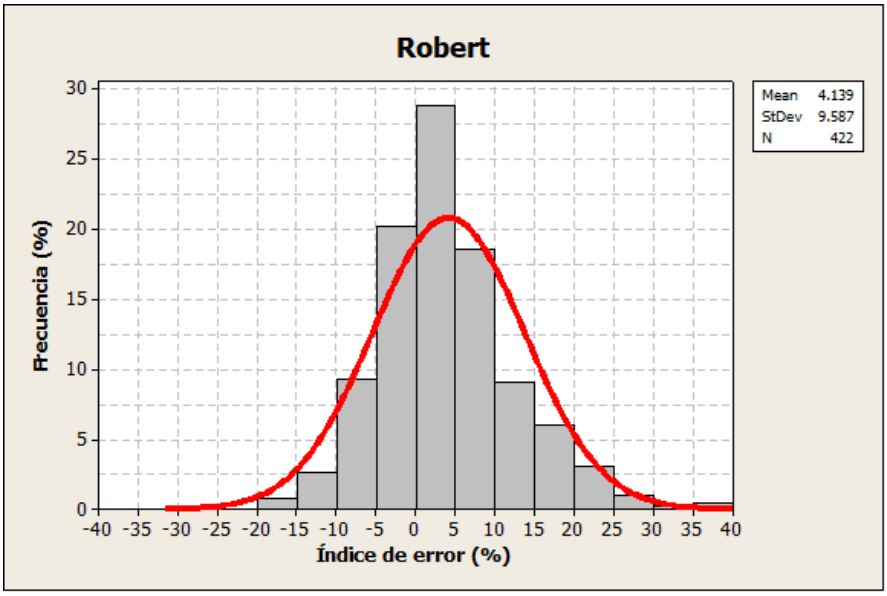

Figure 6-18. *Error distribution of Robert for the entire sample*

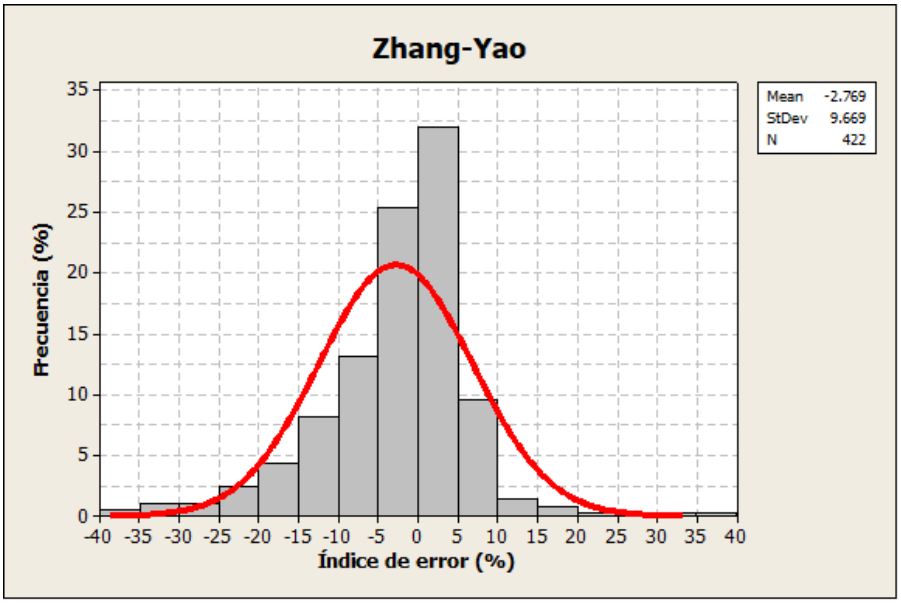

Figure 6-19. *Error distribution of Zhang-Yao for the entire sample*

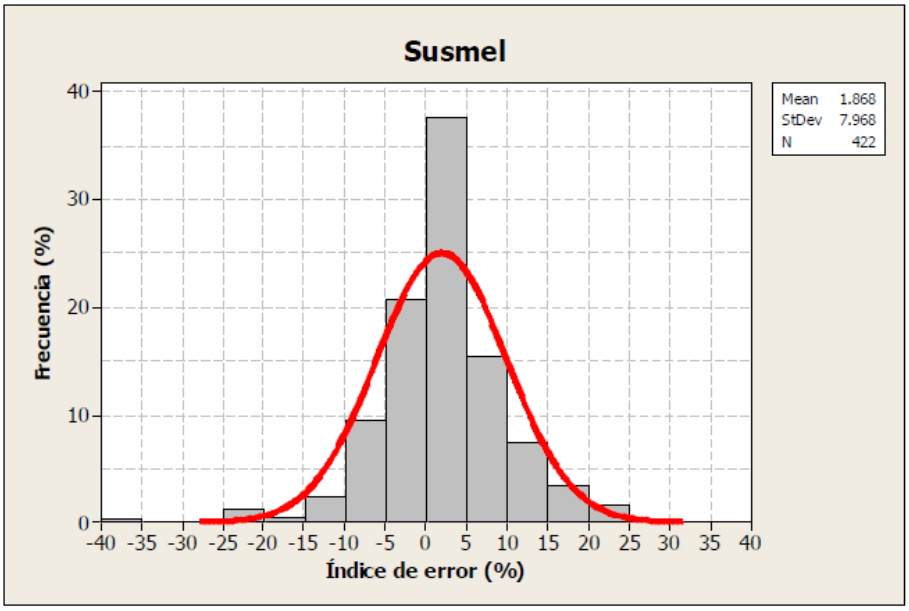

Figure 6-20. *Error distribution of Susmel for the entire sample*

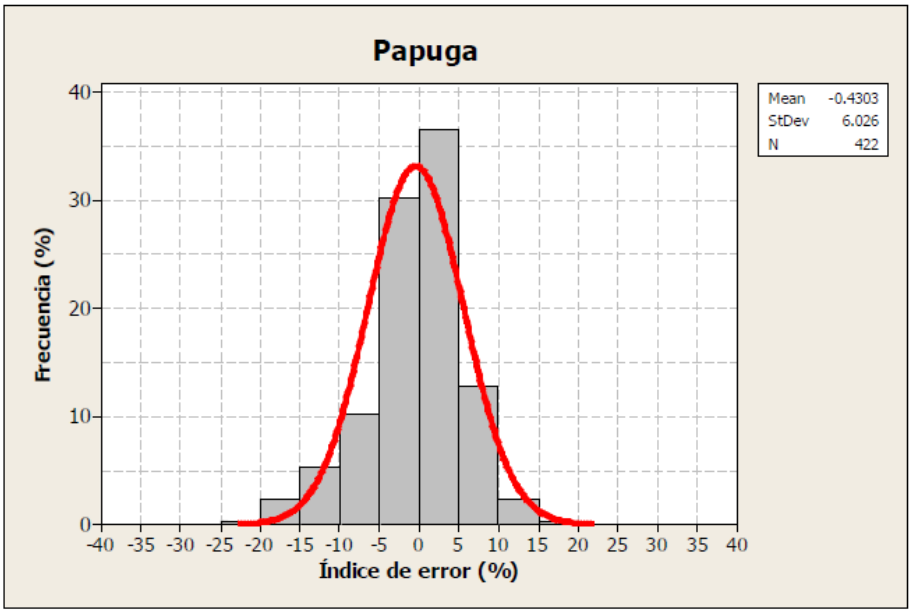

Figure 6-21. *Error distribution of Papuga for the entire sample*

6.3. Study of multi-axiality without other effects

In this section only those experiments in which there is no mean stress or phase difference between axial and torsional stresses will be taken into account. Therefore, the load paths will be proportional and without the effect of mean stresses of any kind, with only axial and torsional variable stresses in phase and without mean components.

These results indicate treatment of multi-axiality without any added effect. Therefore, a good distribution in the results is to be expected. A large deviation in them could indicate that the method has intrinsic deficiencies for the treatment of multi-axiality itself.

The number of experimental tests with these characteristics is 134 out of 422 in the global sample, which are presented altogether in Table 6-3. Although the number of data is lower, it is large enough to draw certain conclusions.

- **Classic methods:**

The multiaxiality without phase shift and mean stress effects can be treated adequately by applying Von Mises with sign, provided that Walker's exponent is available. The results of this method are the same as those of Marin's advanced global method in the case of proportional loads and without average stresses.

The use of Worst Principal has a tendency towards the non-conservative zone, no doubt created by the fact that the torsion line in this criterion moves away from those of Tresca and Von Mises, which follow the ductile materials.

Table 6-3. *Obtained results for multiaxiality without other effects (134 tests)*

Criterio	Valor medio del error	Desviación estándar del error	Porcentaje de resultados en el rango [-40%,40%]	Porcentaje de resultados en el rango [-15%,15%]	Porcentaje de resultados en el rango [-5%,5%] *"Ajustados"*	Porcentaje de resultados en el rango [-5%,-40%] *"No-conservadores"*	Porcentaje de resultados en el rango [+5%,+40%] *"Conservadores"*
Worst Principal Full Range-Goodman	19.29	14.71	98.3	33.6	8.2	7.5	79.1
Von Mises Full Range-Goodman	35.68	15.15	92.2	4.5	0.0	0.0	75.4
Worst Principal Walker real-Goodman	-8.63	8.16	100.0	79.9	37.3	62.7	0.0
Von Mises Walker real-Goodman	3.92	6.91	100.0	94.0	67.9	2.2	29.9
Worst Principal Walker 0.5-Goodman	-15.65	10.40	99.8	50.0	14.2	84.3	0.7
Von Mises Walker 0.5-Goodman	-4.06	10.71	100.0	83.6	30.6	56.7	12.7
Sines	-9.41	11.53	100.0	76.1	38.1	59.0	3.0
Crossland	-0.40	3.70	100.0	100.0	82.8	11.2	6.0
Marin	3.92	6.91	100.0	94.0	67.9	2.2	29.9
Vu-Halm-Nadot	-0.56	3.43	100.0	100.0	83.6	11.2	5.2
Dang Van MSSR	1.73	4.01	100.0	100.0	75.4	6.0	18.7
Dang Van MD	1.77	4.02	100.0	100.0	74.6	6.0	19.4
Matake	2.54	3.97	100.0	100.0	72.4	2.2	25.4
Findley	1.77	4.02	100.0	100.0	74.6	6.0	19.4
McDiarmid MSSR	-5.29	10.01	100.0	84.3	41.8	45.5	12.7
McDiarmid MD	-4.10	9.75	100.0	86.6	46.3	39.6	14.2
Robert	1.77	4.02	100.0	100.0	74.6	6.0	19.4
Zhang Yao	1.57	3.16	100.0	100.0	85.1	2.2	12.7
Susmel	0.90	3.85	100.0	100.0	80.6	7.5	11.9
Papuga	1.15	3.17	100.0	100.0	86.6	2.2	11.2

Using any criteria with Walker 0.5 shifts the distribution of results to the non-conservative zone, especially in the case of Worst Principal. The use of Full-Range, on the other hand, has a conservative effect.

- **Advanced "global" methods:**

The performance of these methods under conditions of proportional loads with mean zero stresses is very close to experimental results, with the only exception of Sines, which seems to suffer from an intrinsic deficiency to deal with biaxial problems even without mean stress and out-of-phase loads, with very non-conservative effects and a high scatter.

The Crossland and Vu-Halm-Nadot methods give very similar results and are very much in agreement with the experiments: their error distributions are centred and they suffer little dispersion. Both methods have 100% of the results in the error range [-15%,15%] under these loading conditions, and more than 80% in the range [-5%,+5%], which gives an idea of their excellent behaviour.

- **Critical Plane Methods:**

All critical-plane methods offer excellent correlation with experimental results, with the sole exception of McDiarmid methods, which suffer from non-conservative behaviour and high dispersion.

The methods of Dang Van, Matake, Findley, Robert, Zhang-Yao, Susmel and Papuga have a similar performance, with 100% of the experiments having an error in the range [-15%,15%]. The Papuga method seems to be the most adjusted to the experiments, but the difference in this case with respect to the

other methods is negligible, so the reasons for its superior performance should be sought in individual effects that will be analysed in the following sections.

The error distributions of the different methods for multi-axial stress conditions with no effect of mean stresses or phase shift in the range [-40%,+40%] are shown in Figures 6-22 to 6-41, covering 134 experiments in each case:

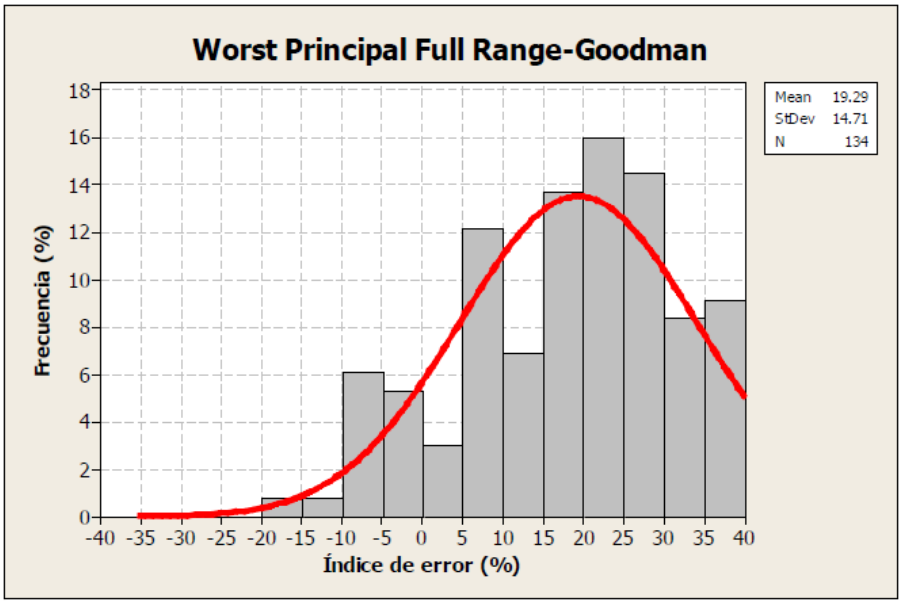

Figure 6-22. *Error distribution of Worst Principal FR-Goodman in multiaxiality*

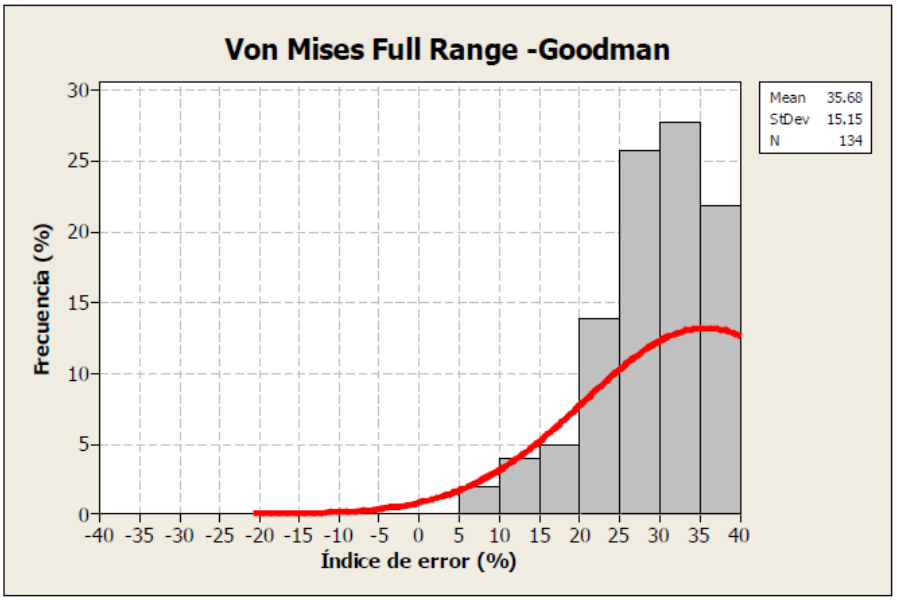

Figure 6-23. *Error distribution of von Mises FR-Goodman in multiaxiality*

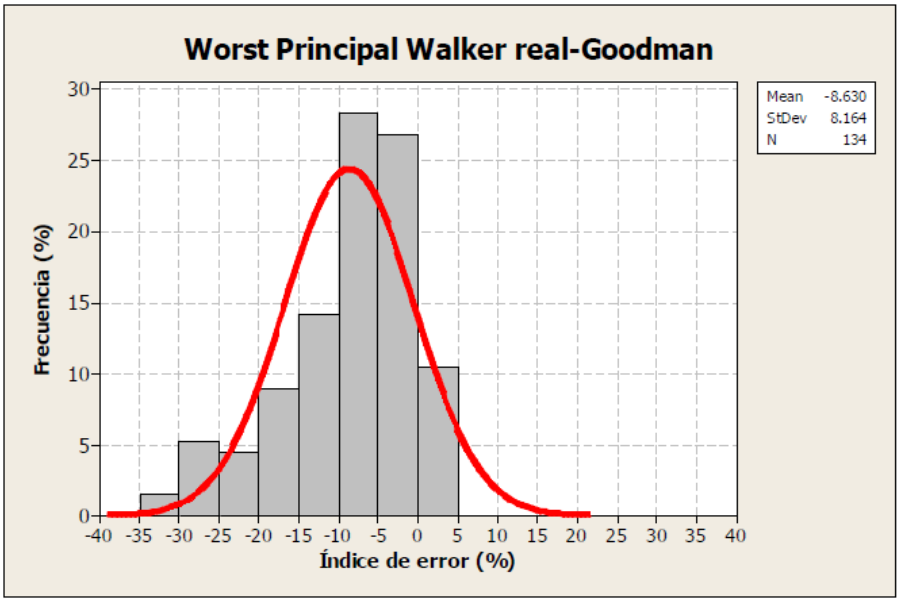

Figure 6-24. *Error distribution of Worst Principal Walker R.-Goodman in multiaxiality*

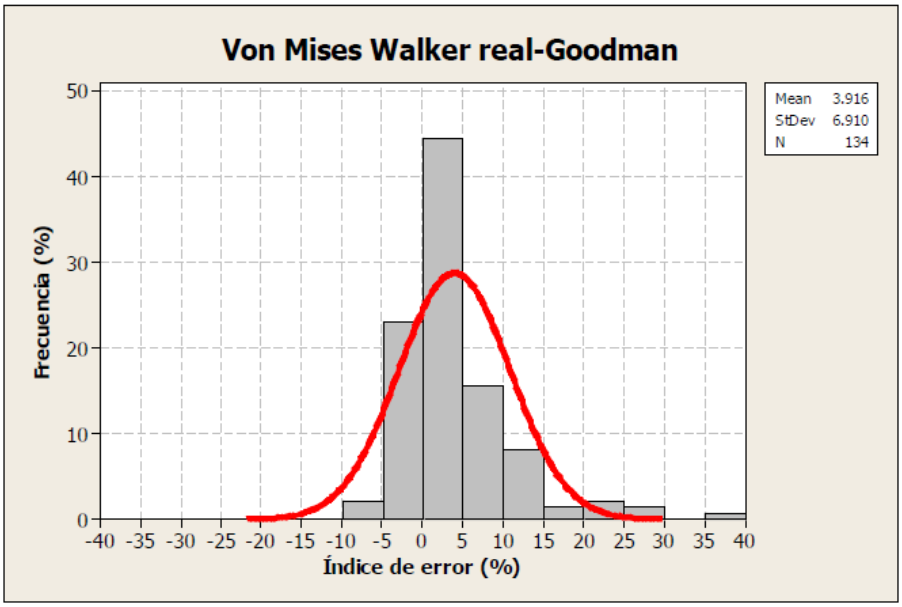

Figure 6-25. *Error distribution of von Mises Walker R.-Goodman in multiaxiality*

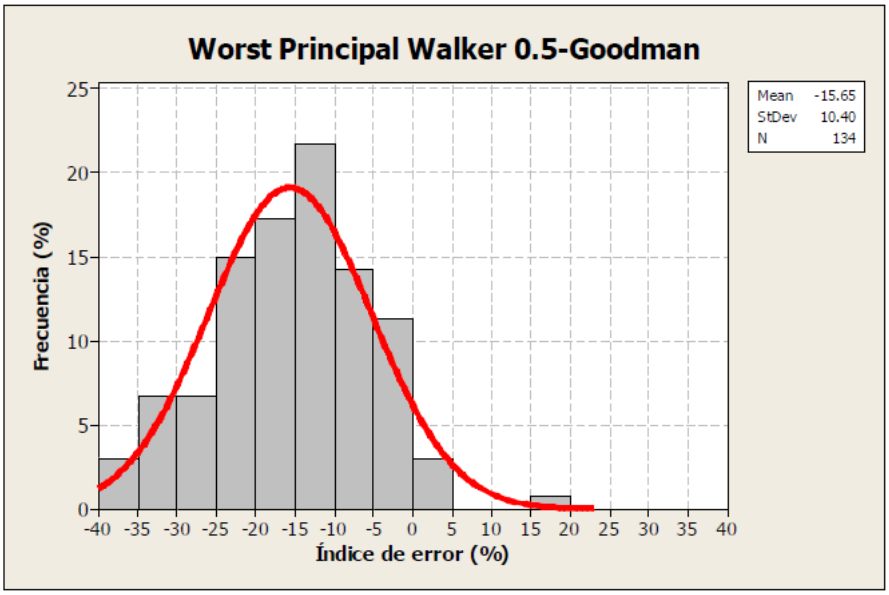

Figure 6-26. *Error distribution of Worst Principal Walker 0.5-Goodman in multiaxiality*

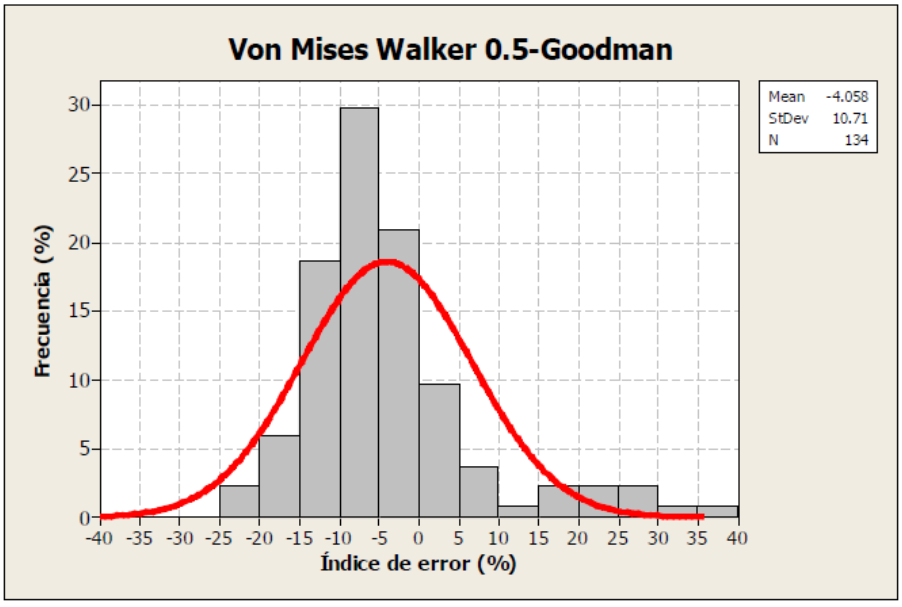

Figure 6-27. *Error distribution of von Mises Walker 0.5-Goodman in multiaxiality*

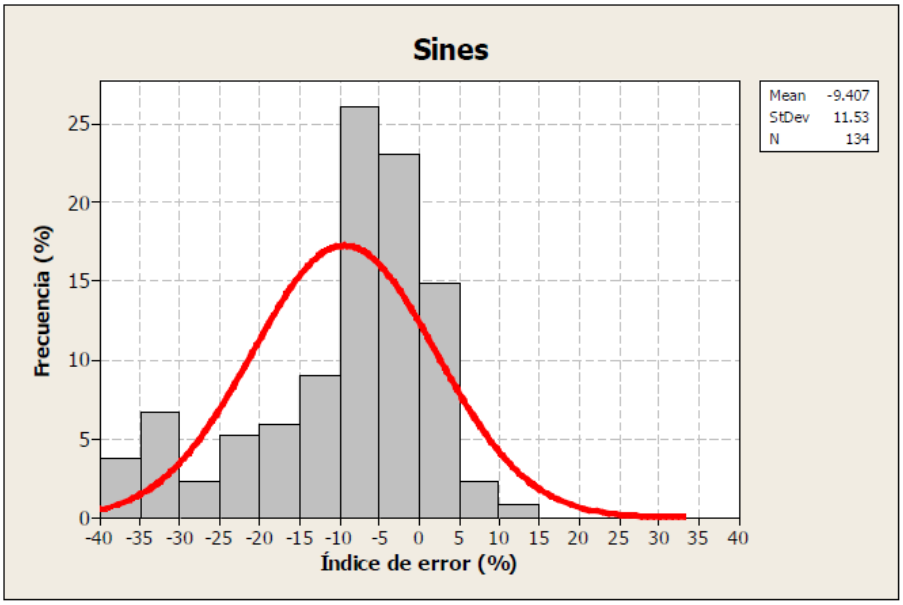

Figure 6-28. *Error distribution of Sines in multiaxiality*

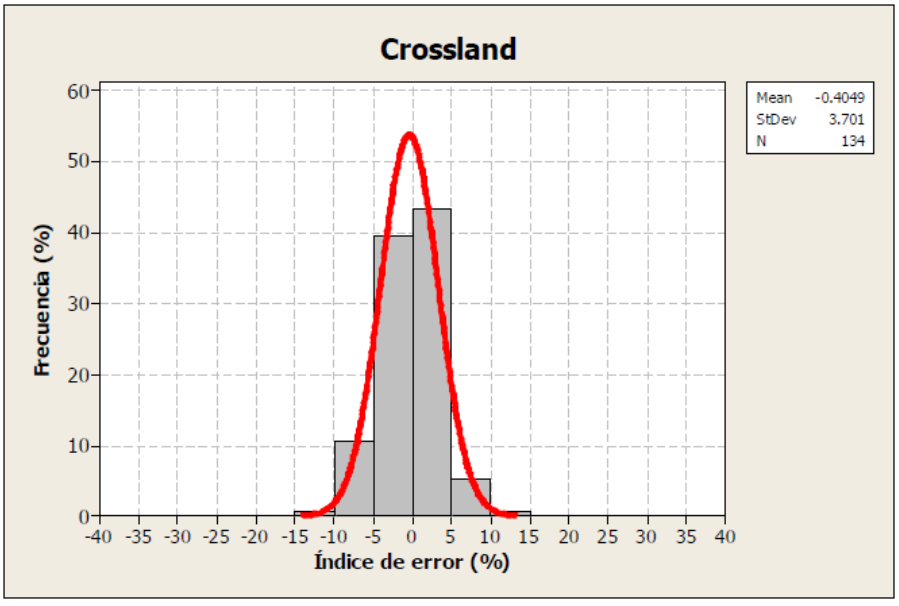

Figure 6-29. *Error distribution of Crossland in multiaxiality*

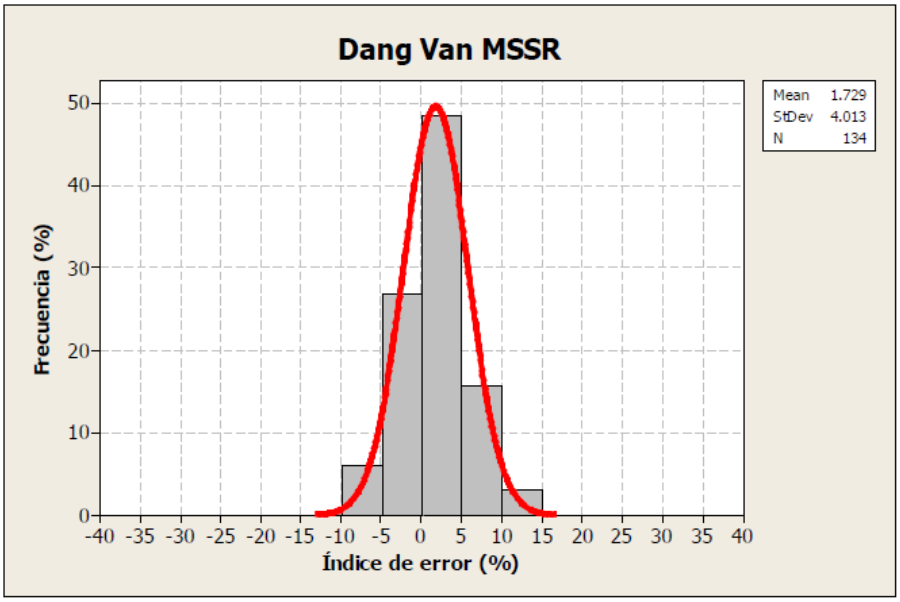

Figure 6-30. *Error distribution of Marin in multiaxiality*

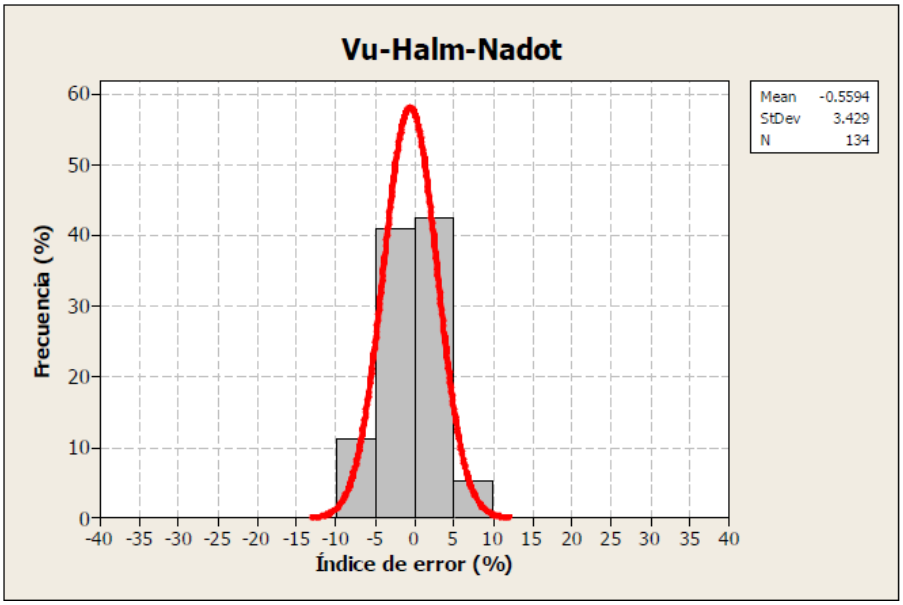

Figure 6-31. *Error distribution of Vu-Halm-Nadot in multiaxiality*

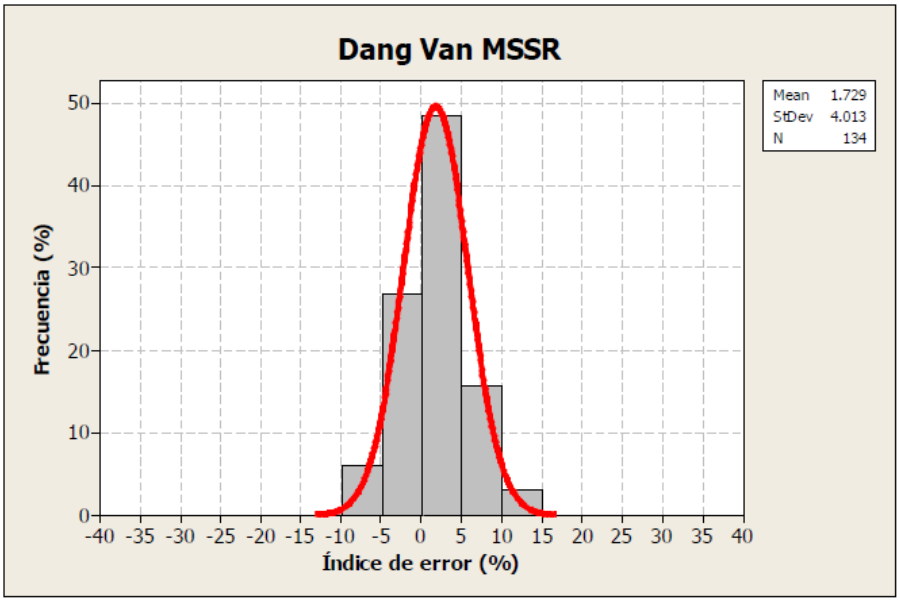

Figure 6-32. *Error distribution of Dang Van MSSR in multiaxiality*

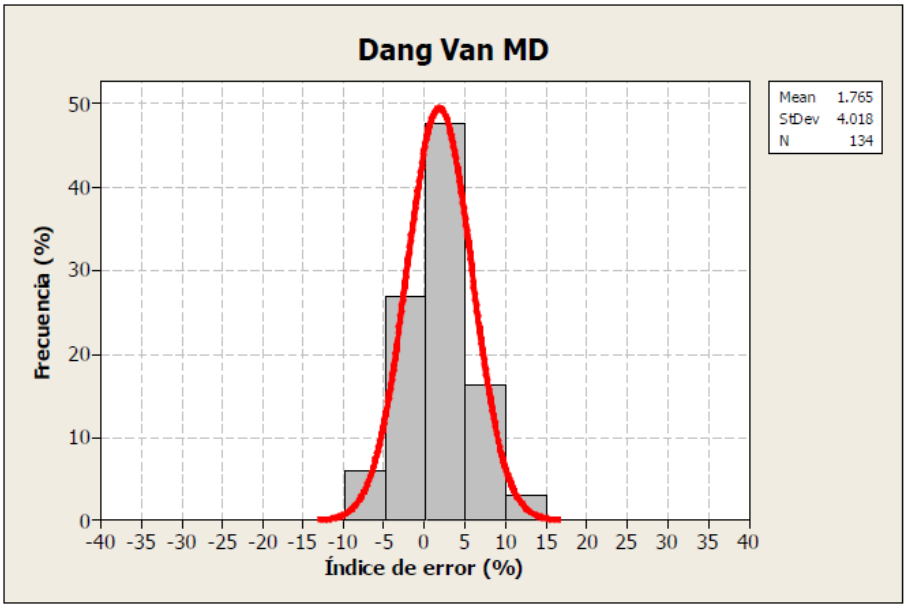

Figure 6-33. *Error distribution of Dang Van MD in multiaxiality*

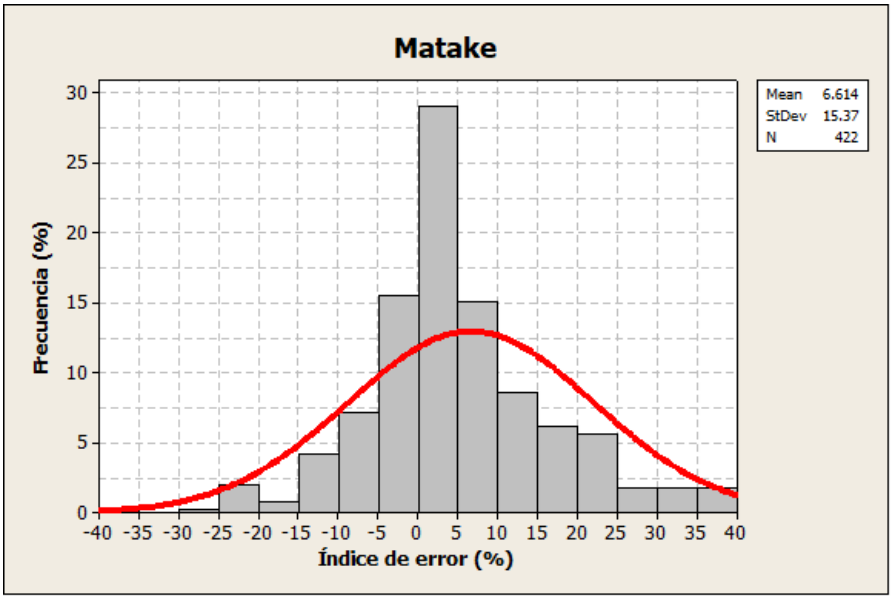

Figure 6-34. *Error distribution of Matake in multiaxiality*

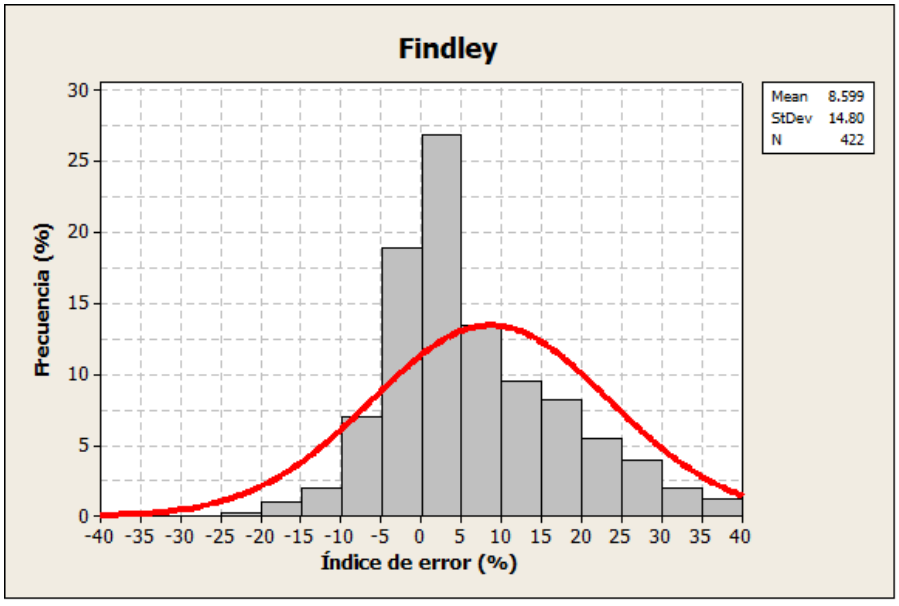

Figure 6-35. *Error distribution of Findley in multiaxiality*

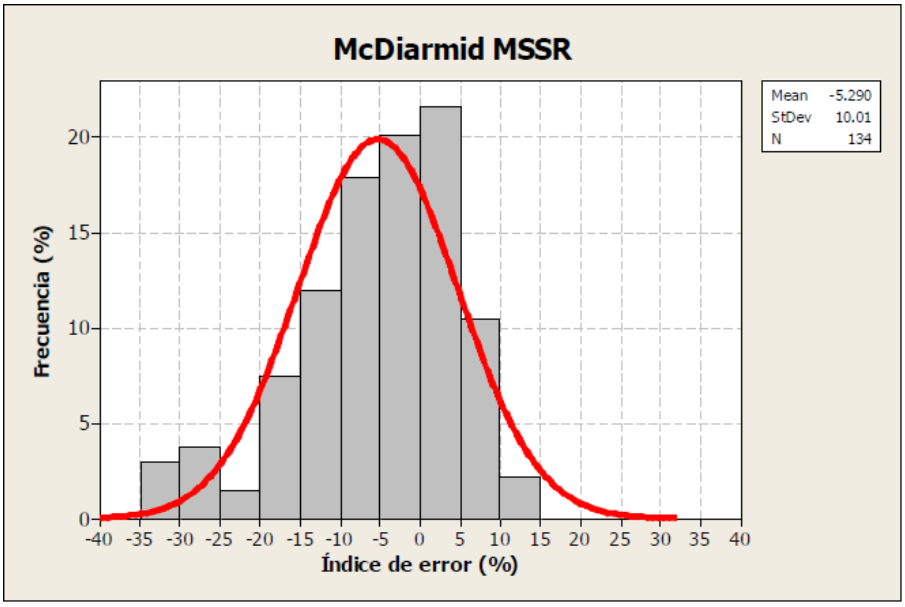

Figure 6-36. *Error distribution of McDiarmid MSSR in multiaxiality*

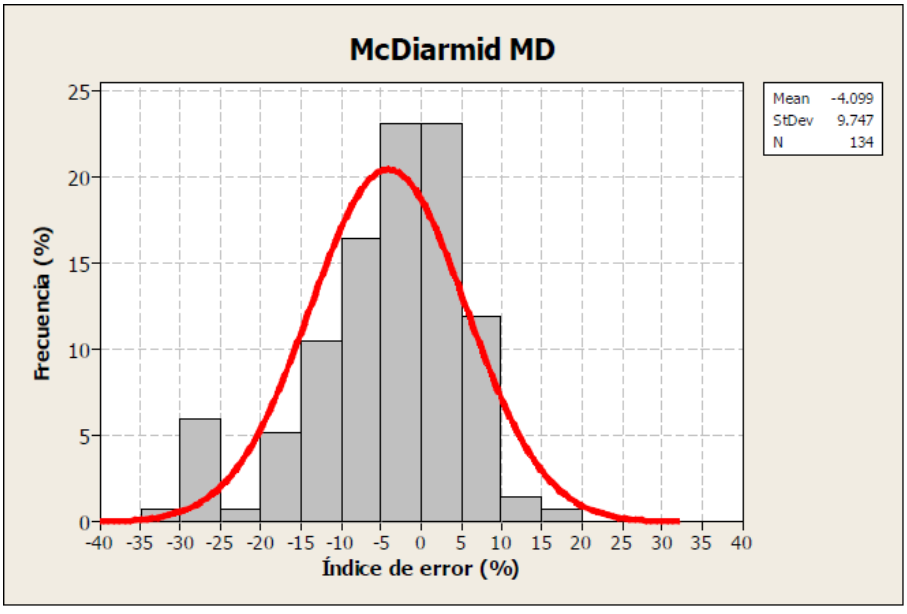

Figure 6-37. *Error distribution of McDiarmid MD in multiaxiality*

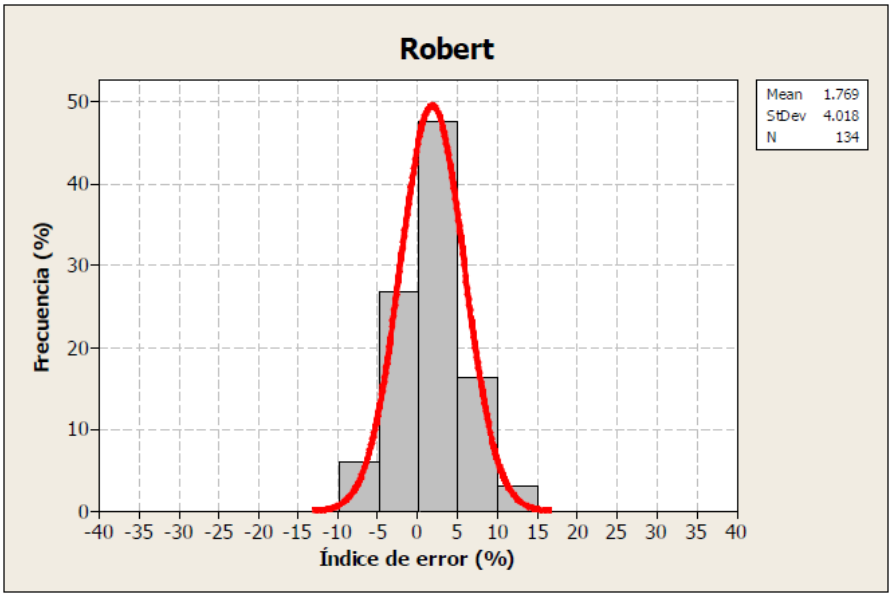

Figure 6-38. *Error distribution of Robert in multiaxiality*

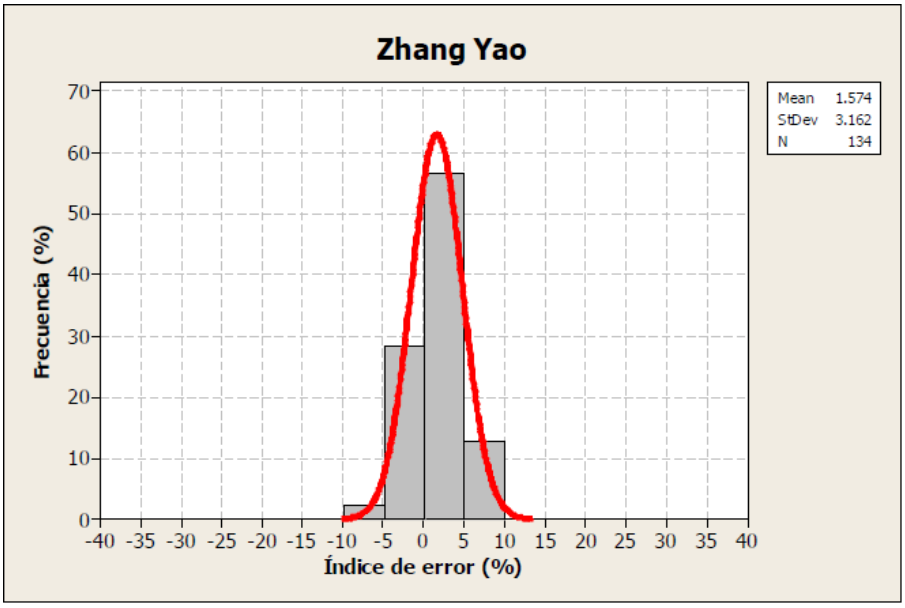

Figure 6-39. *Error distribution of Zhang-Yao in multiaxiality*

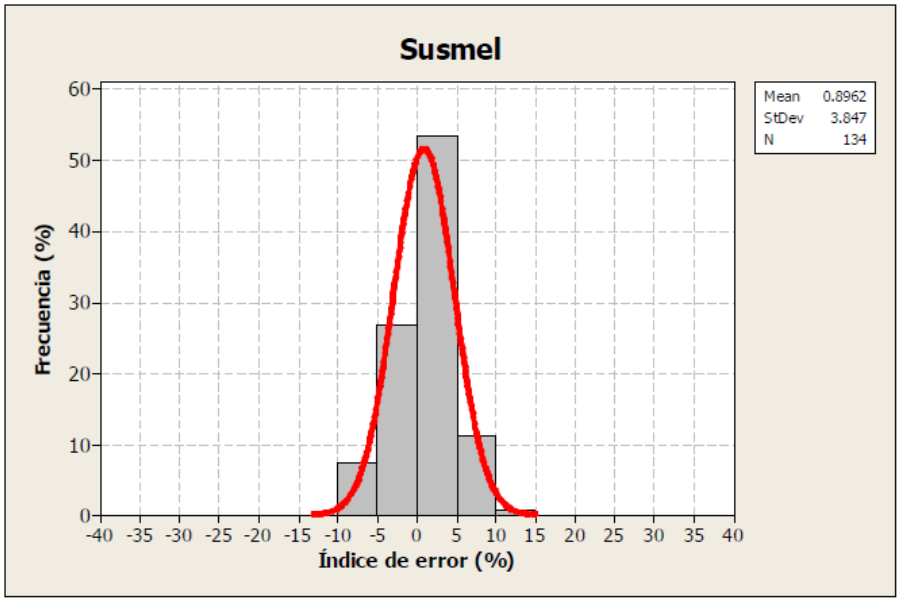

Figure 6-40. *Error distribution of Susmel in multiaxiality*

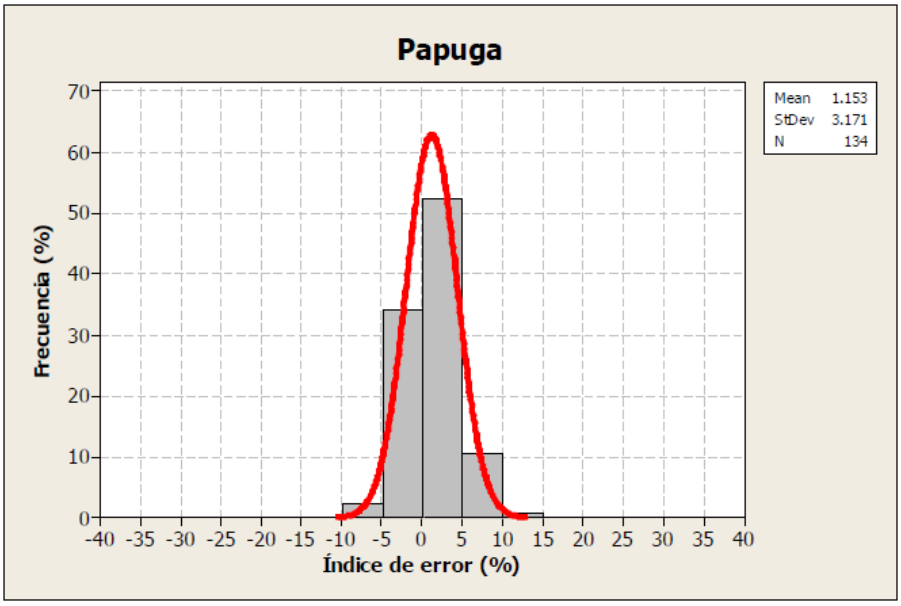

Figure 6-41. *Error distribution of Papuga in multiaxiality*

6.4. Study of the effect of the phase shift

In this section, only those experiments in which there is no axial or torsional mean stress, but there is a phase sift between the axial and torsional stresses, will be taken into account. The effect of the phase between axial and torsional loads is widely cited in the literature as a key factor taking decisive importance in the calculation of life in multi-axial fatigue [Papadopoulos, 1997], [Papuga, 2011A].

In this case, 52 experimental data will be available. The sample is small compared to other groups of tests, but it seems sufficient if we consider that studies such as Papadopoulos [Papadopoulos, 1997] use only a small fraction of the tests presented here. All the results are summarized in Table 6-4.

Another novelty presented by this study is the use of the CSM instead of the CSM used by Papuga in [Papuga, 2011A], which in various publications [Li, 2009], [Araujo, 2011], [Meggiolaro, 2011A] is recognized as more suitable for non-proportional load paths. Moreover, in Papuga's thesis [Papuga, 2005] it is pointed out that the Minimum Circumscribed Ellipse (MCE) has a much more profound physical meaning than the Minimum Circumscribed Circle (MCC).

- **Classic methods:**

The standard deviation of the error in these methods is lower than that of the overall of all the experiments, which implies that this is not the effect that most influences the great dispersion of results that suffer.

Table 6-4. *Obtained results for phase shift effect without mean stress (52 tests)*

Criterio	Valor medio del error	Desviación estándar del error	Porcentaje de resultados en el rango [-40%,40%]	Porcentaje de resultados en el rango [-15%,15%]	Porcentaje de resultados en el rango [-5%,5%] *"Ajustados"*	Porcentaje de resultados en el rango [-5%,-40%] *"No-conservadores"*	Porcentaje de resultados en el rango [+5%,+40%] *"Conservadores"*
Worst Principal Full Range-Goodman	3.05	18.83	96.2	57.7	23.1	36.5	36.5
Von Mises Full Range-Goodman	17.53	24.11	92.3	46.2	19.2	13.5	59.6
Worst Principal Walker real-Goodman	-20.97	12.06	94.2	30.8	11.5	82.7	0.0
Von Mises Walker real-Goodman	-9.87	15.85	96.2	55.8	28.8	61.5	5.8
Worst Principal Walker 0.5-Goodman	-27.13	13.31	84.6	17.3	9.6	75.0	0.0
Von Mises Walker 0.5-Goodman	-16.89	17.05	94.2	38.5	9.6	82.7	1.9
Sines	-6.64	9.91	100.0	86.5	26.9	61.5	11.5
Crossland	2.23	7.71	100.0	92.3	57.7	15.4	26.9
Marin	6.97	12.76	96.2	88.5	46.2	7.7	42.3
Vu-Halm-Nadot	0.09	7.17	100.0	94.2	65.4	19.2	15.4
Dang Van MSSR	-3.20	8.41	100.0	88.5	44.2	44.2	11.5
Dang Van MD	-3.17	8.40	100.0	88.5	44.2	44.2	11.5
Matake	3.82	11.99	96.2	90.4	51.9	15.4	28.8
Findley	0.91	7.05	100.0	96.2	57.7	17.3	25.0
McDiarmid MSSR	-7.90	10.84	100.0	73.1	15.4	69.2	15.4
McDiarmid MD	-7.36	10.76	100.0	75.0	15.4	67.3	17.3
Robert	0.91	7.05	100.0	96.2	57.7	17.3	25.0
Zhang Yao	2.88	9.08	98.1	92.3	63.5	11.5	23.1
Susmel	2.23	7.05	100.0	96.2	67.3	9.6	23.1
Papuga	0.39	5.17	100.0	100.0	65.4	15.4	19.2

The classic methods exhibit a non-conservative trend using the real Walker exponent or the value 0.5; instead using Full-Range they can be shifted into the conservative zone.

It should be noted in this case that Worst-Principal together with Walker 0.5 is an extremely non-conservative solution.

- **Advanced methods of global approach:**

The difference in behaviour between the different methods is evident in the fact that while Crossland and Vu-Halm-Nadot exhibit a centred distribution with little dispersion, the Sines and Marin methods have respectively a non-conservative and conservative behaviour, with an increase in dispersion.

The correlation of experimental results with Vu-Halm-Nadot is excellent, among other reasons because its authors created the method with the intention of addressing the effect that the displacement of axial and torsional stresses creates in different materials depending on their strength. While in low strength steels (C35, mild steels) the phase difference increases the fatigue limit; in high strength steels (42CrMo4, 30NCD16) the fatigue limit decreases due to the phase difference.

- **Critical Plane Methods:**

McDiarmid's methods offer an extremely non-conservative solution and high dispersion, even at maximum damage.

Dang Van's method, which uses the maximum hydrostatic stress, suffers from a non-conservative behaviour. The Matake method, which uses the maximum

normal stress at the plane of maximum shear stress amplitude, shows a conservative trend but a high dispersion. In contrast, Findley's method, which also uses maximum normal stress, but in this case to a plane of maximum damage, offers excellent results, with low dispersion and a centred error distribution. Robert's method, also defined in the Maximum Damage plane, offers the same results as Findley's, suggesting that separation into normal mean and alternating components does not have an extra beneficial effect on using only the maximum normal stress in this case.

As a conclusion, it seems key to use the maximum normal stress in a plane in the maximum damage for the computation of the damage caused by the phase shift. This is also the case with Papuga. The method best suited to experimental results among the MSSR is that of Susmel, undoubtedly due to the use of the factor of influence of normal stresses, which also allows to collect to some extent the effect of phase difference.

The individual distribution of errors in the range [-40%, +40%] is presented in Tables 6-42 to 6-61.

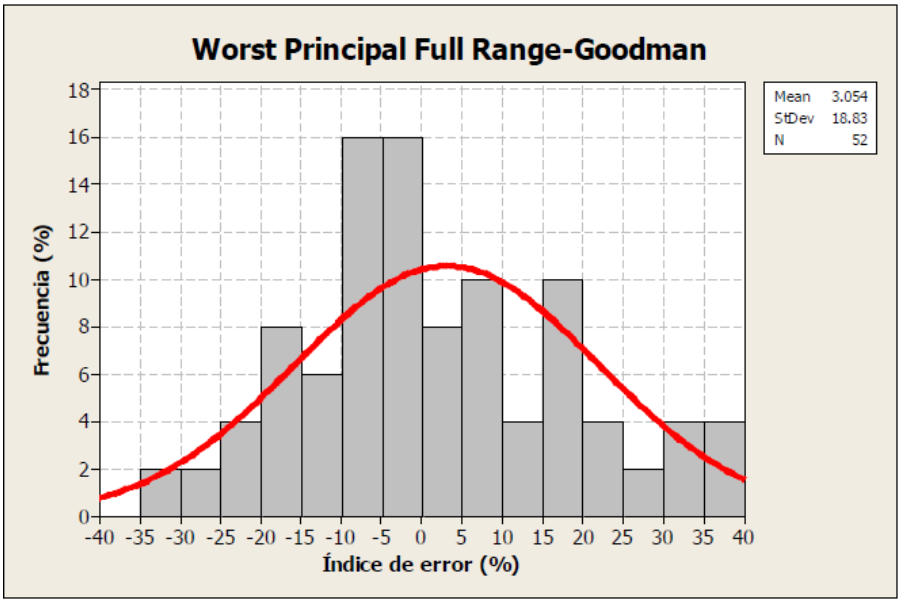

Figure 6-42. *Error distribution of Worst Principal FR-Goodman for phase shift effect*

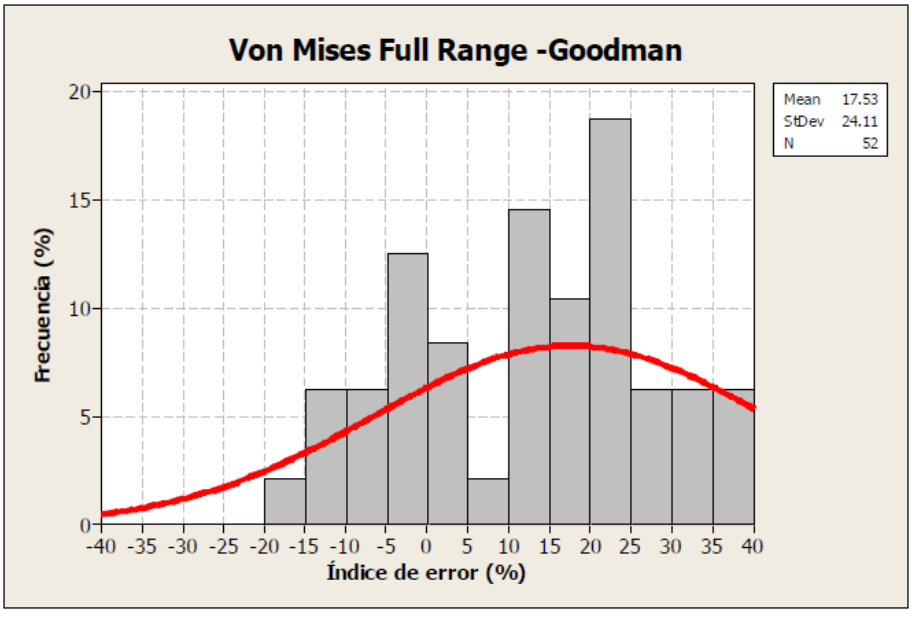

Figure 6-43. *Error distribution of von Mises FR-Goodman for phase shift effect*

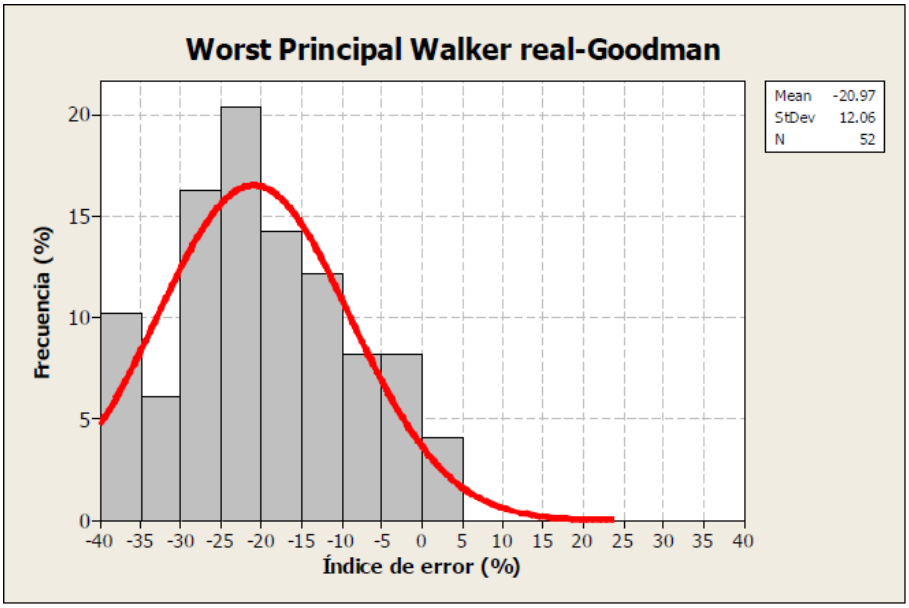

Figure 6-44. *Error distribution of Worst Pr. Walker R.-Goodman for phase shift effect*

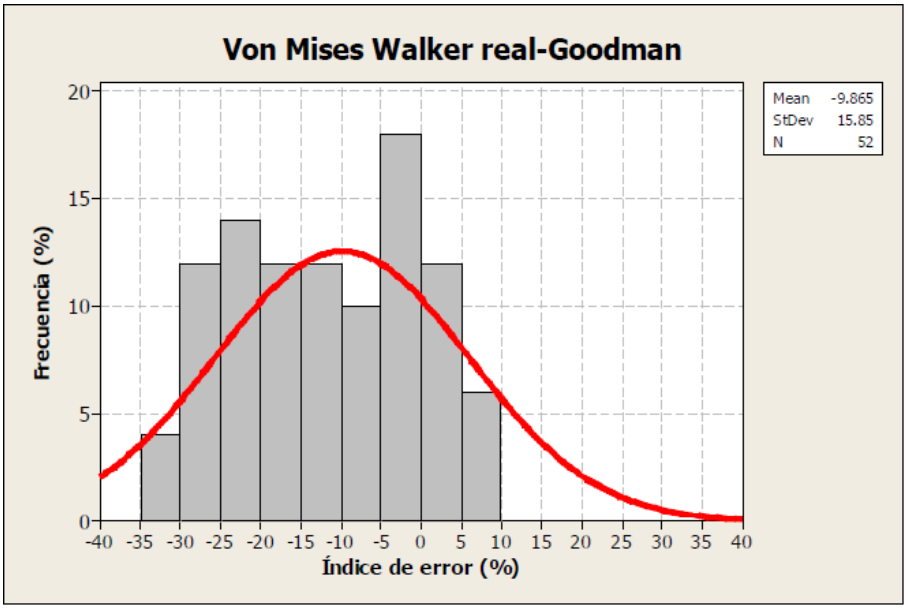

Figure 6-45. *Error distribution of von Mises Walker R.-Goodman for phase shift effect*

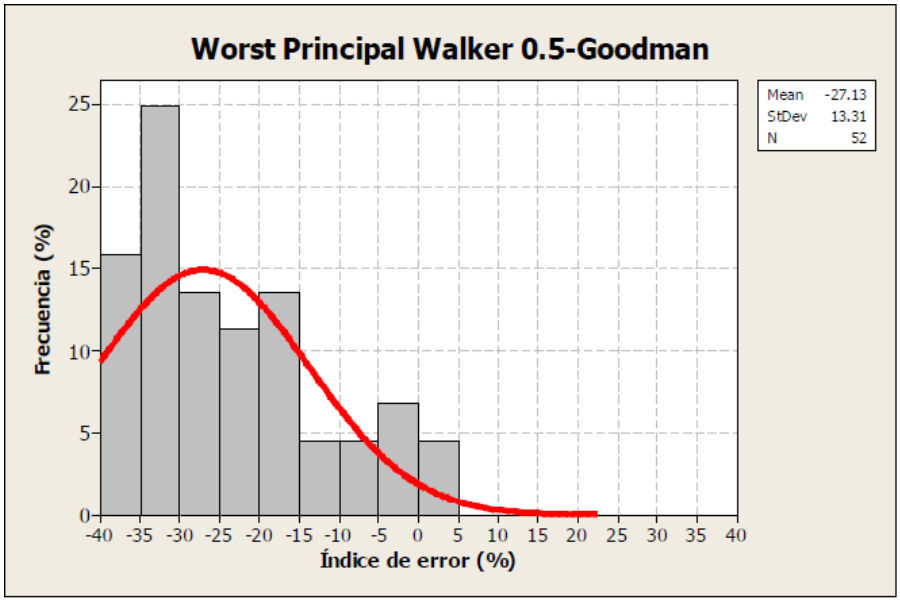

Figure 6-46. *Error distribution of Worst Pr. Walker 0.5-Goodman for phase shift effect*

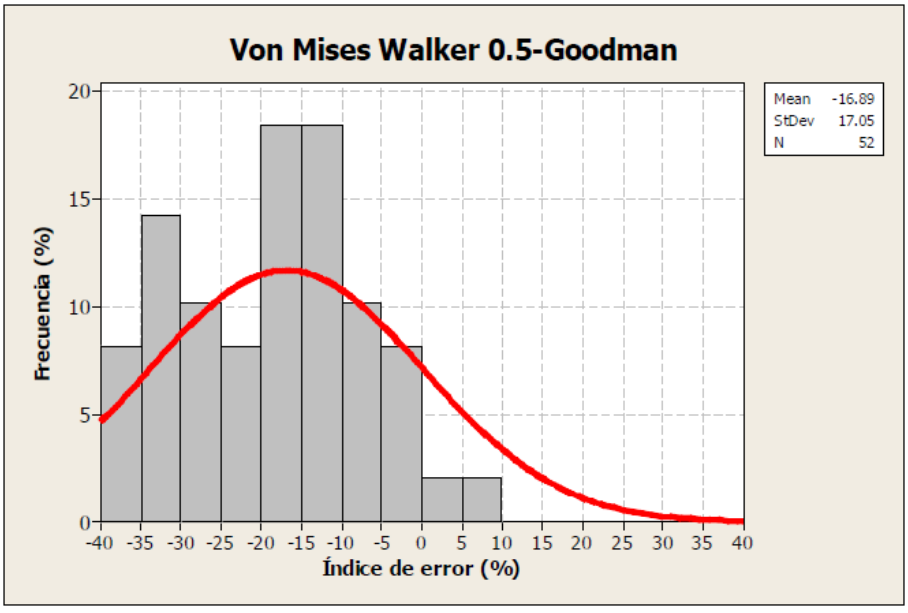

Figure 6-47. *Error distribution of von Mises Walker 0.5-Goodman for phase shift effect*

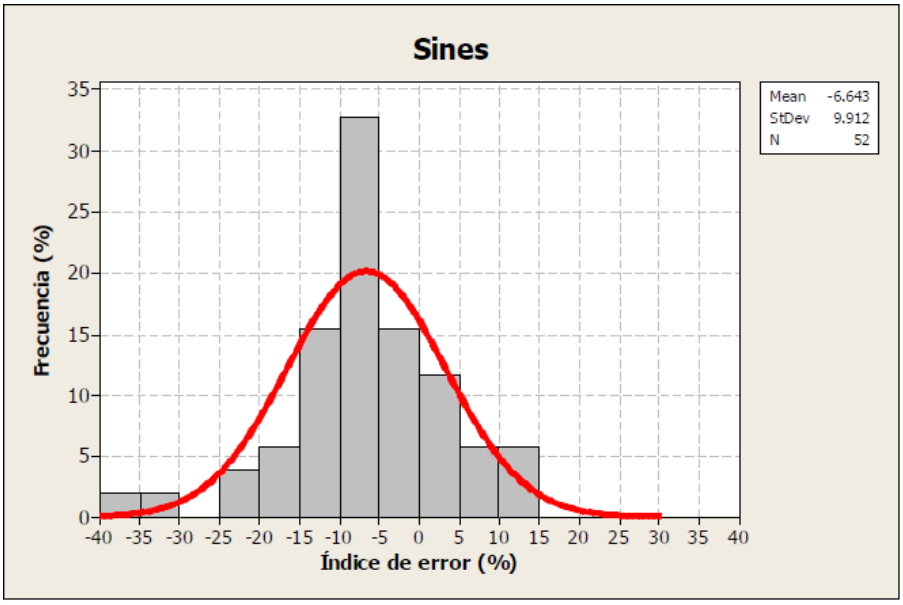

Figure 6-48. *Error distribution of Sines for phase shift effect*

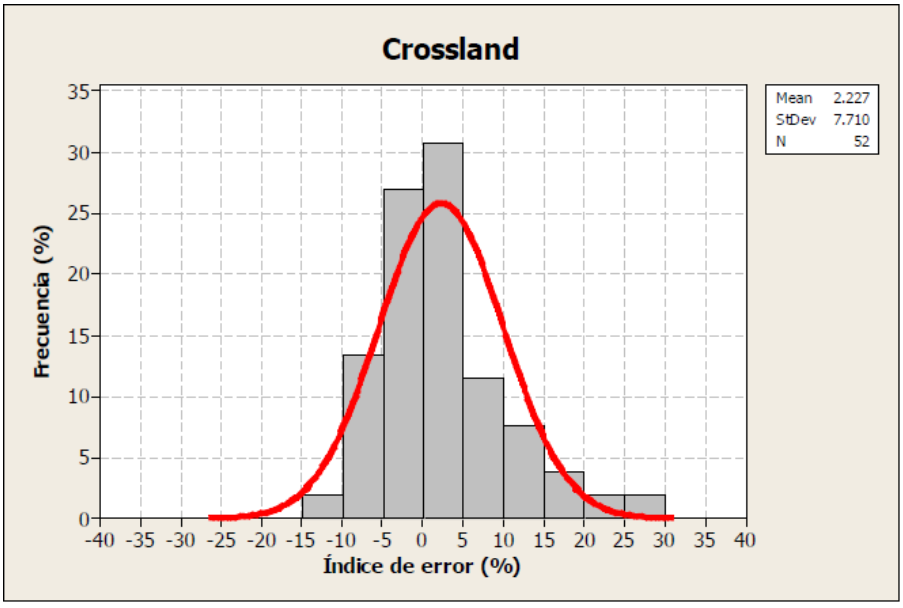

Figure 6-49. *Error distribution of Crossland for phase shift effect*

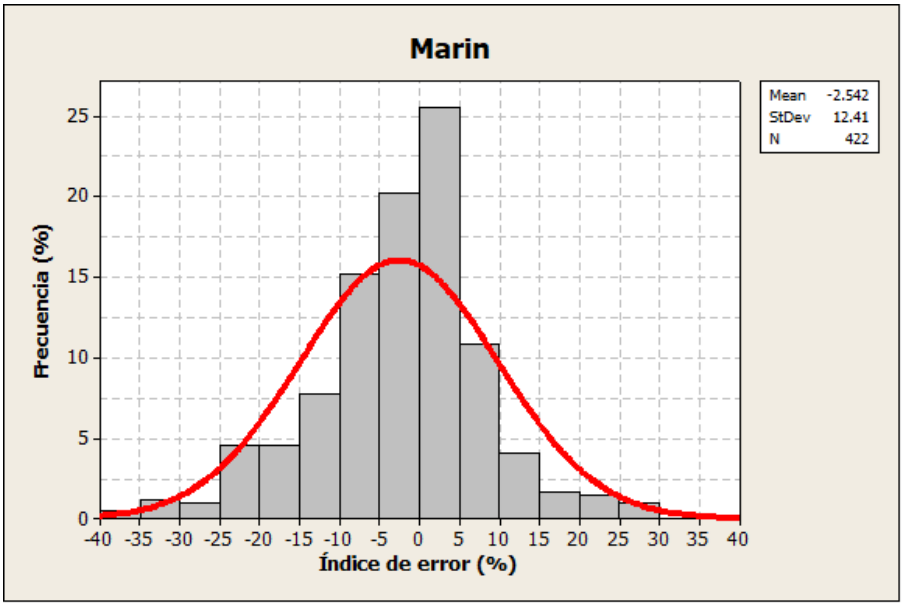

Figure 6-50. *Error distribution of Marin for phase shift effect*

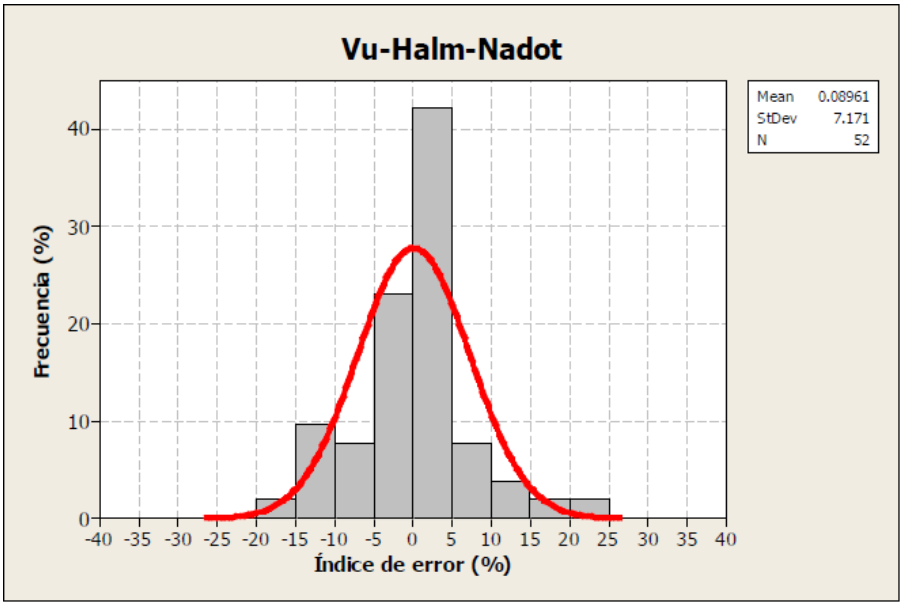

Figure 6-51. *Error distribution of Vu-Halm-Nadot for phase shift effect*

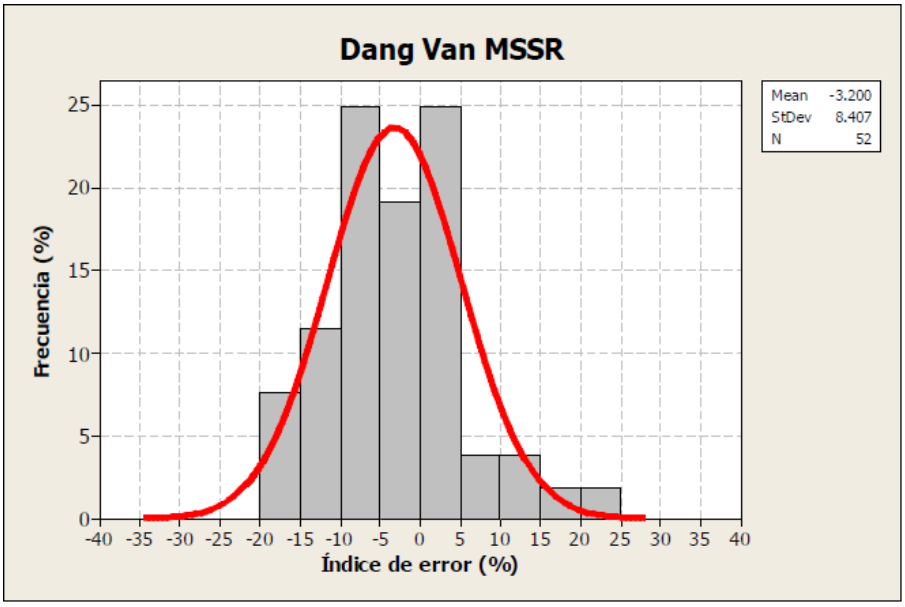

Figure 6-52. *Error distribution of Dang Van MSSR for phase shift effect*

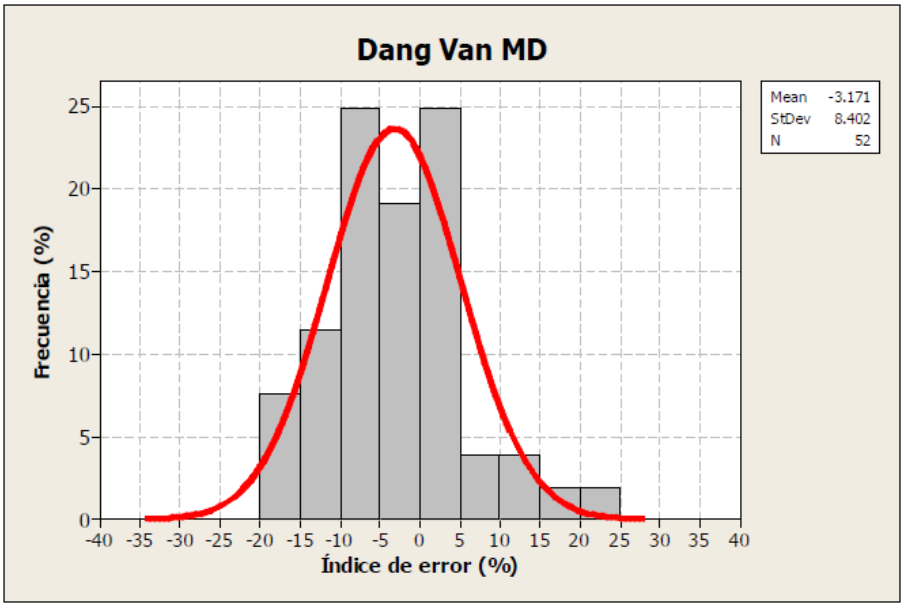

Figure 6-53. *Error distribution of Dang Van MD for phase shift effect*

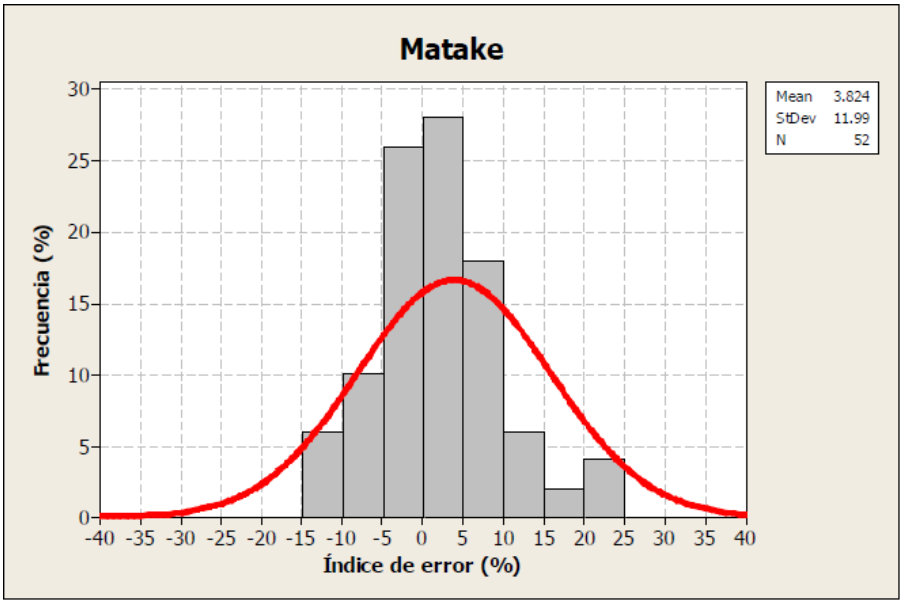

Figure 6-54. *Error distribution of Matake for phase shift effect*

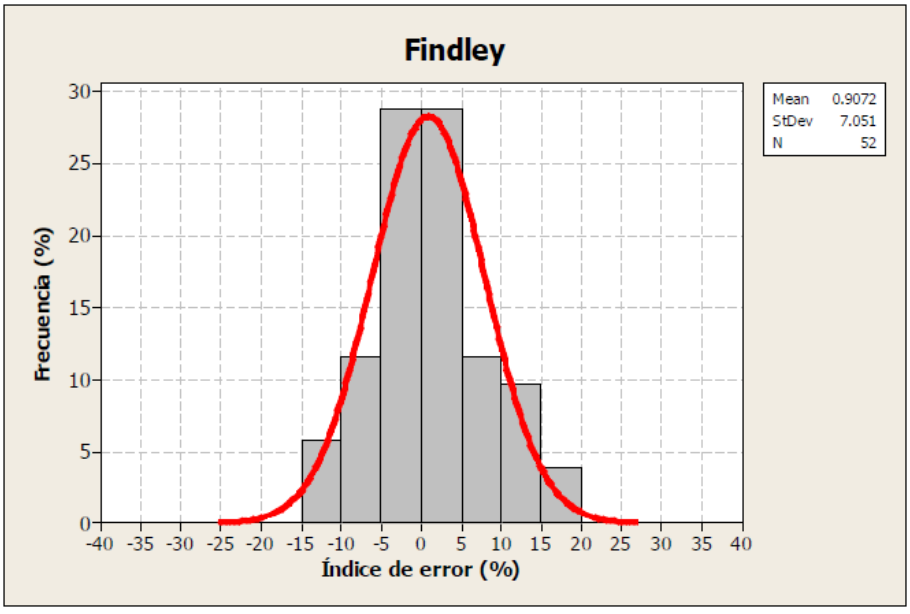

Figure 6-55. *Error distribution of Findley for phase shift effect*

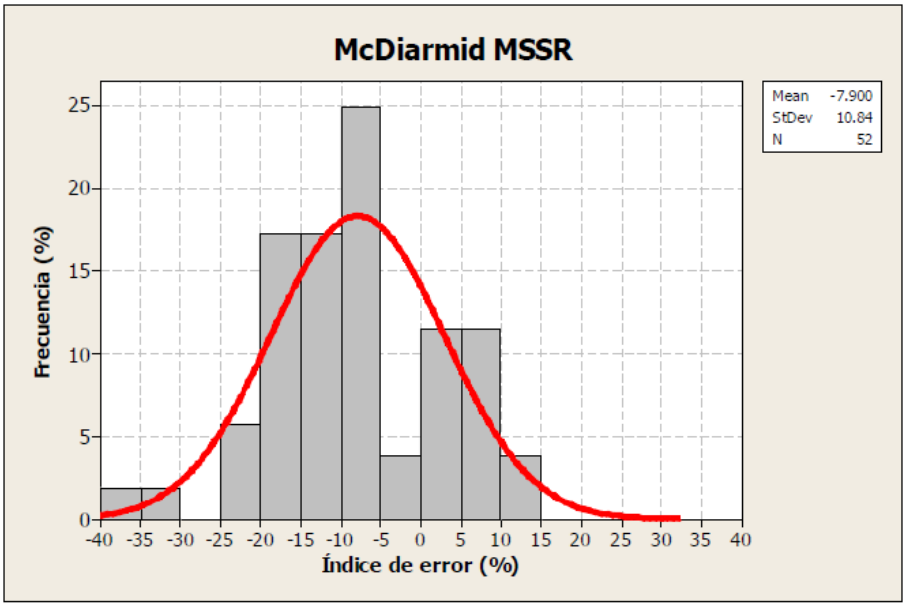

Figure 6-56. *Error distribution of McDiarmid MSSR for phase shift effect*

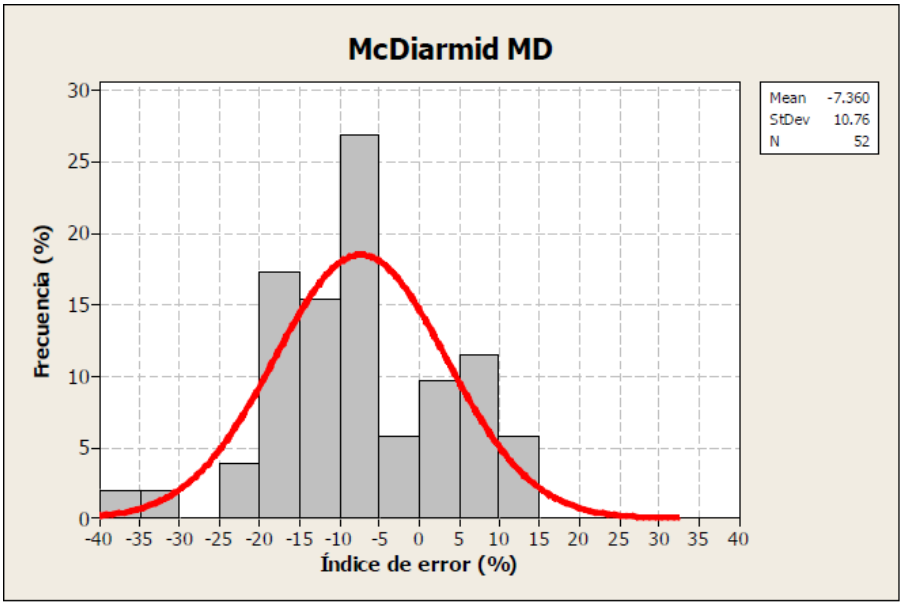

Figure 6-57. *Error distribution of McDiarmid MD for phase shift effect*

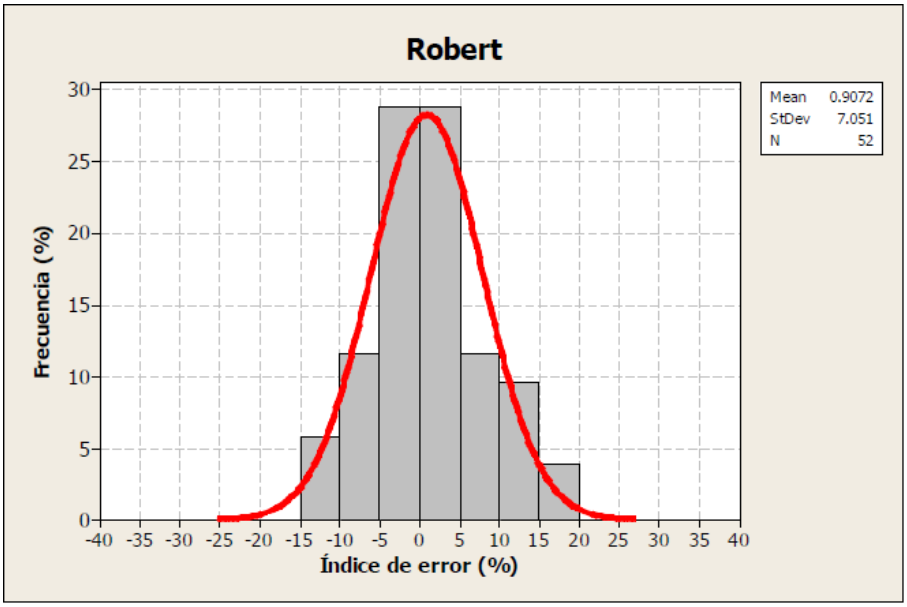

Figure 6-58. *Error distribution of Robert for phase shift effect*

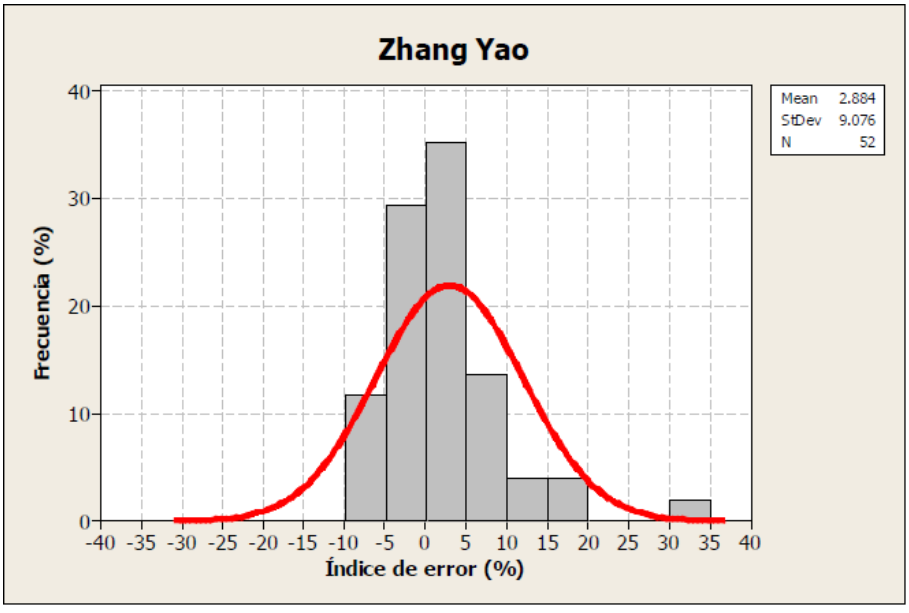

Figure 6-59. *Error distribution of Zhang-Yao for phase shift effect*

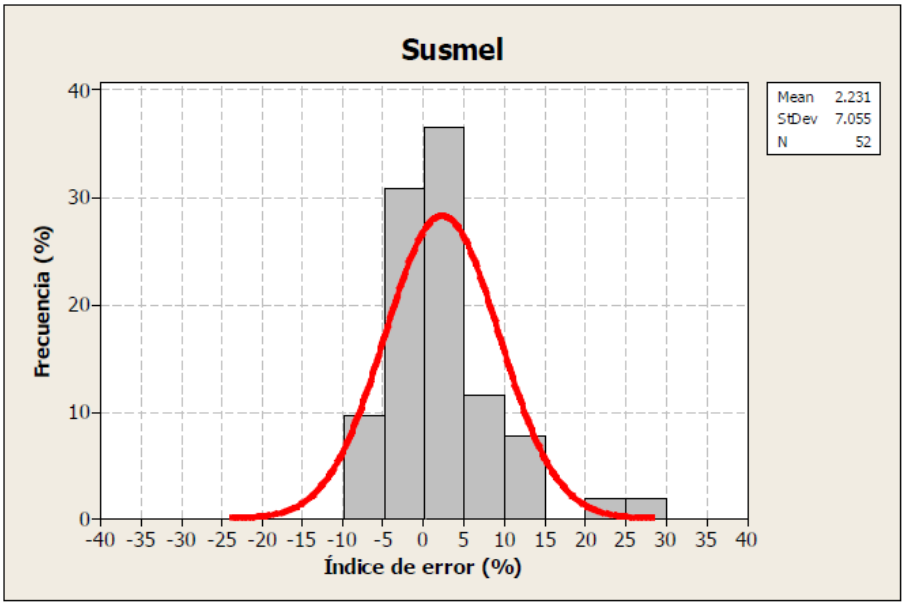

Figure 6-60. *Error distribution of Susmel for phase shift effect*

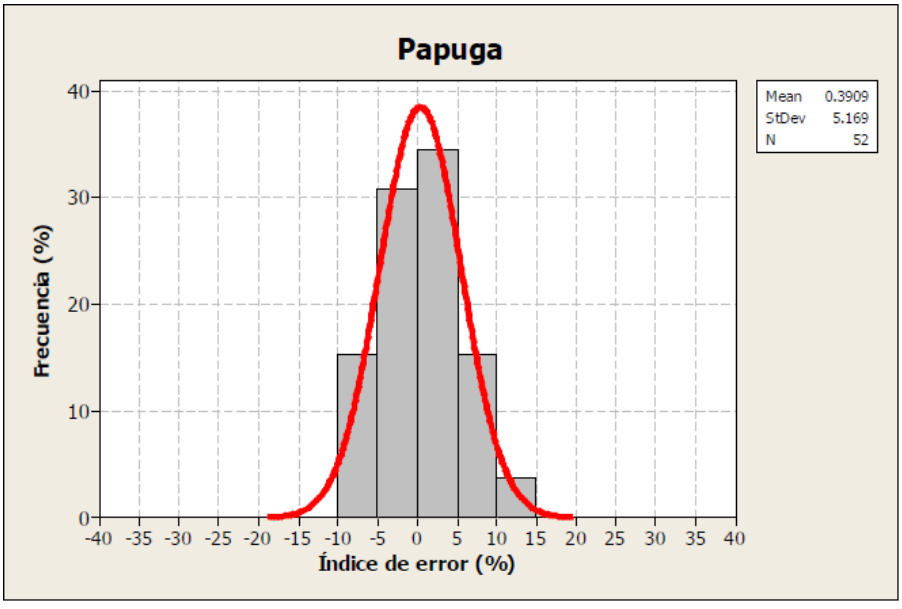

Figure 6-61. *Error distribution of Papuga for phase shift effect*

6.5. Study of the influence of mean axial stresses

In this section only those experiments will be taken into account in which there is no phase difference between axial and torsional stresses, but there are mean axial stresses. The effect of axial mean stresses has been widely discussed in literature, with different approaches according to the authors [Papuga, 2008], [Susmel, 2005], [Susmel, 2008].

In this case, 97 experimental data will be available, constituting a sufficiently large and varied sample to be able to draw conclusions from it. The results are summarized in Table 6-5.

- **Classic methods:**

The dispersion of these methods for the treatment of average axial stresses is substantially high, especially in the case of Worst Principal. The general trend is non-conservative whatever method of R transformation is used.

Comparatively speaking, the effect of mean axial stresses has a more detrimental effect than that of phase shift on the accuracy of this type of method.

- **Advanced methods of global approach:**

Unlike other individual effects, where the Sines method was a non-conservative method, in the treatment of axial mean stresses a centred distribution is obtained with one of the lowest dispersions of all the methods analysed. In this sense, the concept of the Sines method, which allows the use of a uniaxial fatigue limit with R=0 for the conversion of stresses between different stress ratios, seems undoubtedly beneficial.

Table 6-5. *Obtained results for the mean axial stress effect (97 tests)*

Criterio	Valor medio del error	Desviación estándar del error	Porcentaje de resultados en el rango [-40%,40%]	Porcentaje de resultados en el rango [-15%,15%]	Porcentaje de resultados en el rango [-5%,5%] *"Ajustados"*	Porcentaje de resultados en el rango [-5%,-40%] *"No-conservadores"*	Porcentaje de resultados en el rango [+5%,+40%] *"Conservadores"*
Worst Principal Full Range-Goodman	-12.62	47.00	66.0	44.3	19.6	11.3	35.1
Von Mises Full Range-Goodman	-4.24	36.56	75.3	44.3	16.5	23.7	35.1
Worst Principal Walker real-Goodman	-15.06	45.54	67.0	52.6	32.0	11.3	23.7
Von Mises Walker real-Goodman	-6.89	34.96	76.3	53.6	27.8	23.7	24.7
Worst Principal Walker 0.5-Goodman	-16.29	45.04	67.0	51.5	26.8	17.5	22.7
Von Mises Walker 0.5-Goodman	-8.25	34.54	76.3	54.6	27.8	28.9	19.6
Sines	2.53	8.35	100.0	83.5	48.5	16.5	35.1
Crossland	-9.47	11.68	96.9	75.3	36.1	55.7	5.2
Marin	-12.72	13.29	93.8	61.9	22.7	68.0	3.1
Vu-Halm-Nadot	-4.93	10.78	100.0	80.4	44.3	41.2	14.4
Dang Van MSSR	4.20	12.94	100.0	74.2	36.1	20.6	43.3
Dang Van MD	4.24	12.94	100.0	74.2	36.1	20.6	43.3
Matake	8.65	18.67	94.8	62.9	24.7	22.7	47.4
Findley	13.73	19.05	88.7	52.6	20.6	14.4	53.6
McDiarmid MSSR	-9.41	15.75	92.8	64.9	29.9	46.4	16.5
McDiarmid MD	-7.52	14.91	92.8	69.1	29.9	44.3	18.6
Robert	8.35	13.93	97.9	74.2	32.0	12.4	53.6
Zhang Yao	-9.42	9.93	100.0	77.3	39.2	58.8	2.1
Susmel	3.38	8.74	100.0	87.6	45.4	14.4	40.2
Papuga	-1.81	7.39	100.0	94.8	52.6	29.9	17.5

On the other hand, the other methods of global approach present a non-conservative behaviour. The Marin method, which is based on the application of the elliptical relationship to the distortion energy, obtains the results with the greatest trend towards the non-conservative zone.

Crossland's method, which uses maximum hydrostatic stress as a damage parameter, also shows markedly non-conservative results. On the other hand, the Vu-Halm-Nadot method, even without using a uniaxial fatigue limit, allows separate treatment of mean and variable hydrostatic stress. In addition, the use of the same is different depending on the strength of the material. The consequence is that the results, although slightly not conservative, are better than those of the Crossland method.

- **Critical Plane Methods:**

As in other respects, McDiarmid's methods are non-conservative and highly dispersed. Dang Van's methods achieve results that are slightly displaced towards the conservative zone. The Matake method, which uses the maximum normal stress, is more conservative than this. Findley's method increases conservatism over Matake, with a marked conservative trend. Therefore, it seems that the maximum normal stress is a parameter that tends to give more conservative results than the maximum hydrostatic stress.

The methods of Robert, Zhang-Yao, Susmel and Papuga offer a differentiated treatment of the mean and maximum normal stress. Robert's method, which uses a uniaxial fatigue limit with R=0, obtains a distribution displaced towards the

conservative zone, improving the results of Findley's method, similar to the same but without using this limit σ_0.

As for Zhang-Yao's method, the trend towards the non-conservative zone could be attributed to Goodman's use to change the stress ratio from R>-1 to R=-1.

The Papuga method obtains the best results in this section, with a percentage of results close to 95% in the range [-15%,+15%], which could be attributed to the specific treatment as a function of the fragility of the material from the effect of the mean stresses normal to the critical plane, in a similar way to the Vu-Halm-Nadot method. In this sense, [Vu, 2010] cites the great experimental correlation of the Papuga parameter, which in the case of the Vu-Halm-Nadot method is applied to the amplitude and mean value of the first invariant, while in the Papuga critical plane method it is used on the normal amplitude and mean stresses.

With respect to the Susmel method, the results offer a good experimental correlation, with a slightly conservative behaviour. The use of a test with non-zero mean stresses allows the effect of mean normal stresses to be determined. In addition, the maximum damage that can be created by normal stresses is limited depending on the characteristics of the material. As a consequence of this very specific treatment, the Susmel method obtains a good correlation with the experimental results.

The individual error distributions in the range [-40%, +40%] for the mean axial stress effect are presented in Figures 6-62 to 6-81.

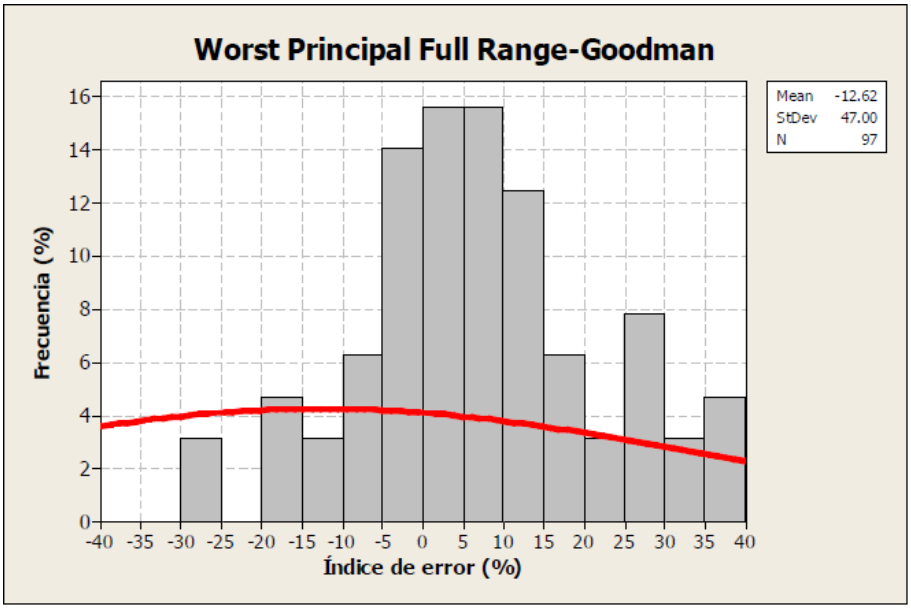

Figure 6-62. *Error distribution of Worst Principal FR-Goodman for mean axial stress*

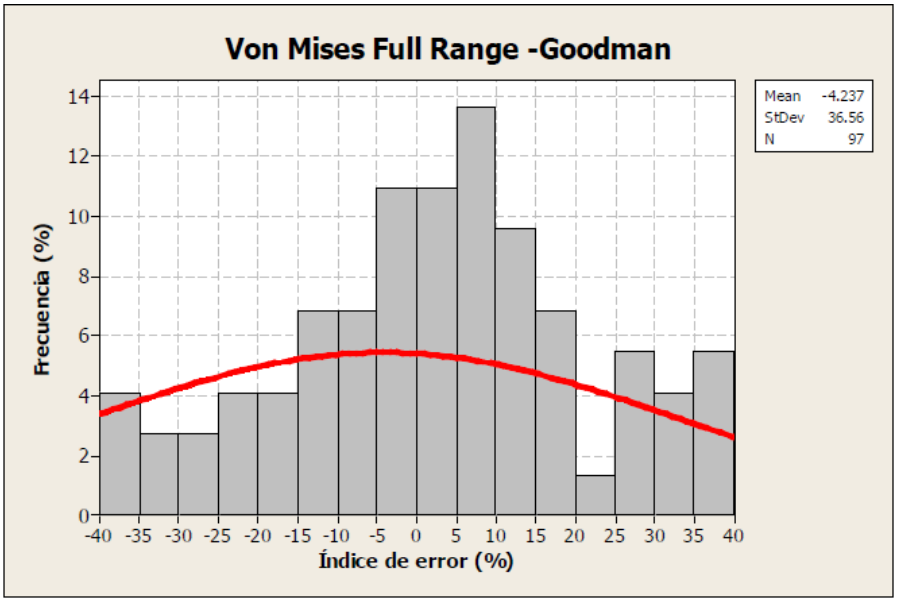

Figure 6-63. *Error distribution of von Mises FR-Goodman for mean axial stress*

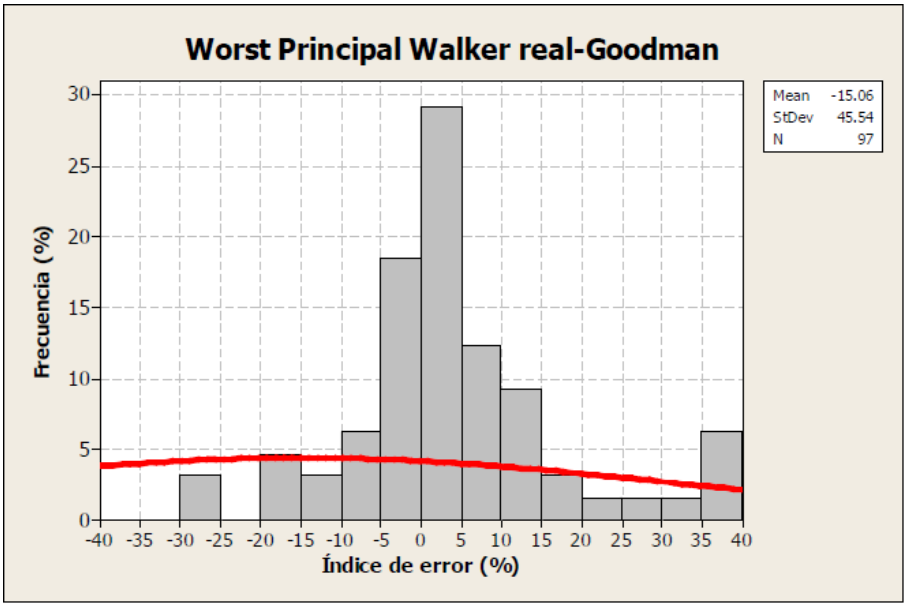

Figure 6-64. *Error distribution of Worst Pr.Walker R.-Goodman for mean axial stress*

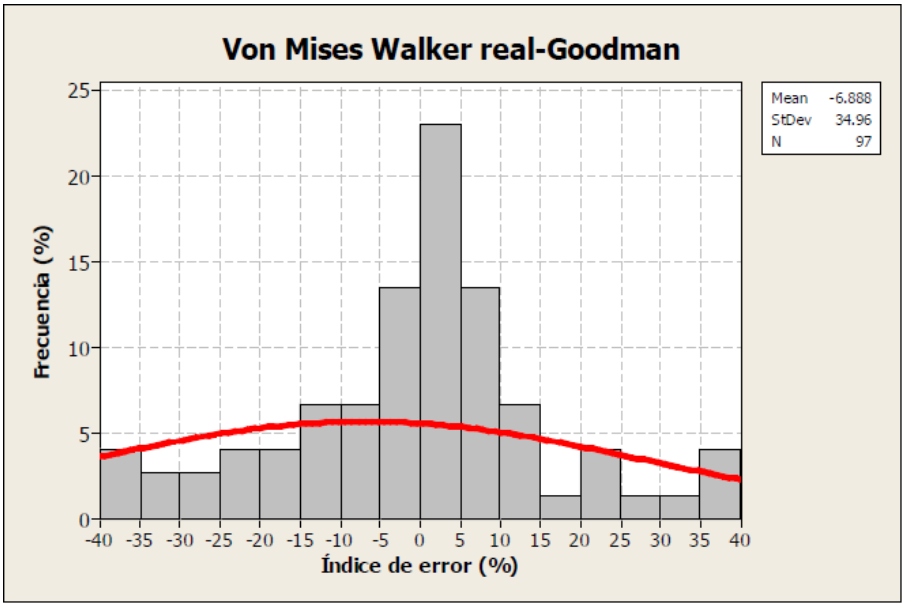

Figure 6-65. *Error distribution of von Mises Walker R.-Goodman for mean axial stress*

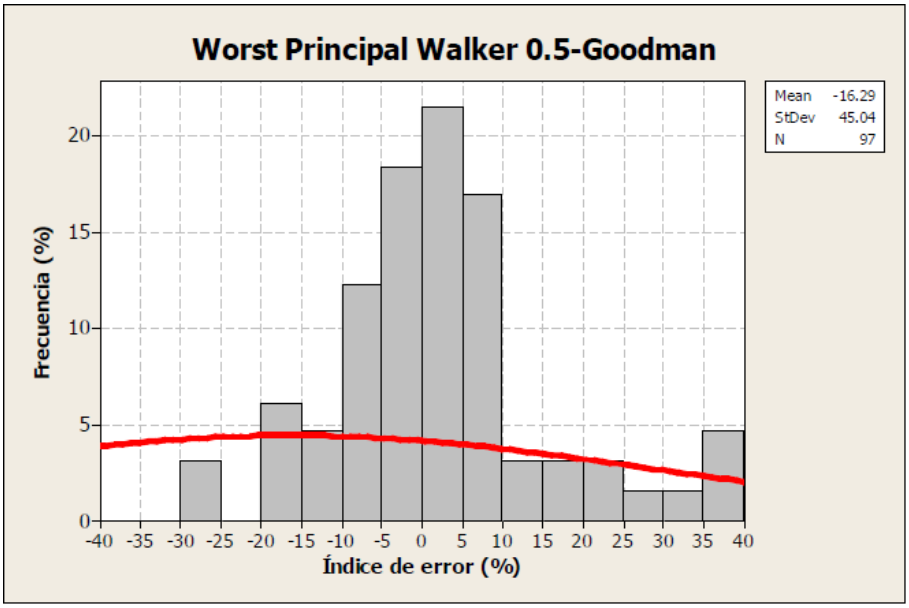

Figure 6-66. *Error distribution of Worst Pr. Walker 0.5-Goodman for mean axial stress*

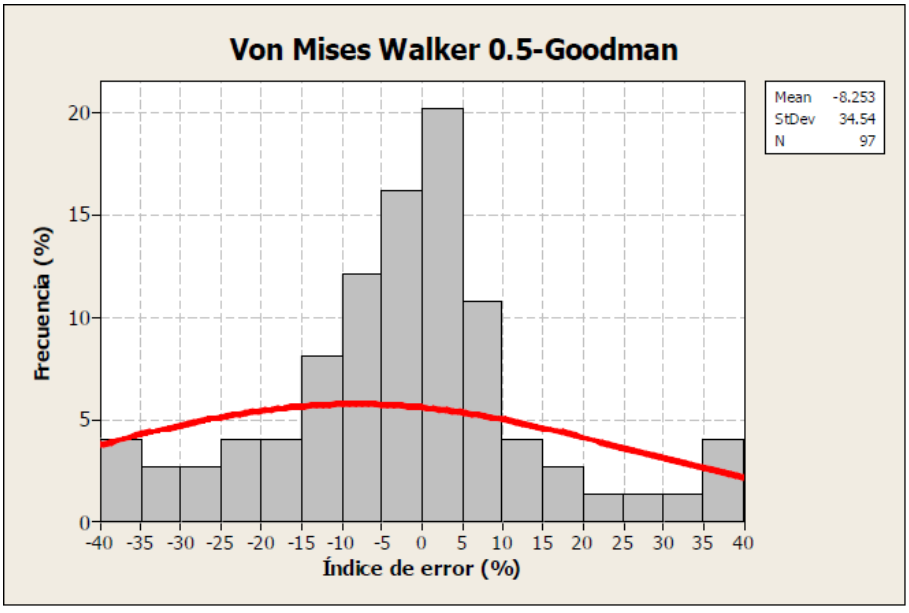

Figure 6-67. *Error distribution of von Mises Walker 0.5-Goodman for mean axial stress*

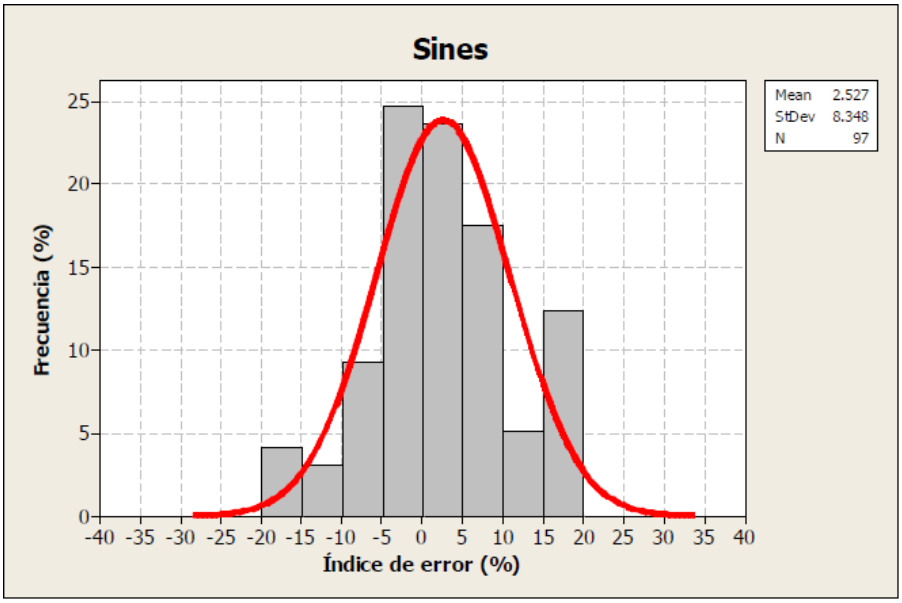

Figure 6-68. *Error distribution of Sines for mean axial stress*

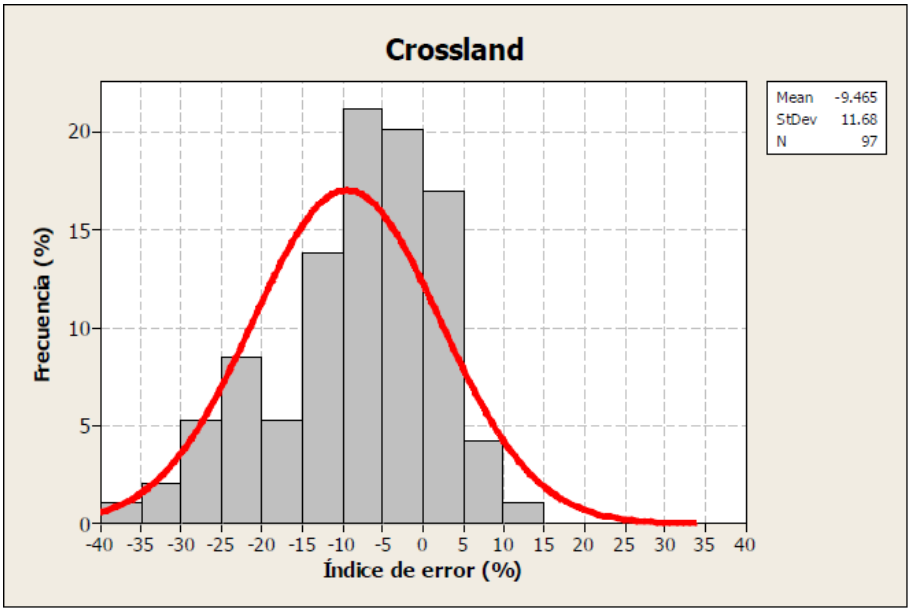

Figure 6-69. *Error distribution of Crossland for mean axial stress*

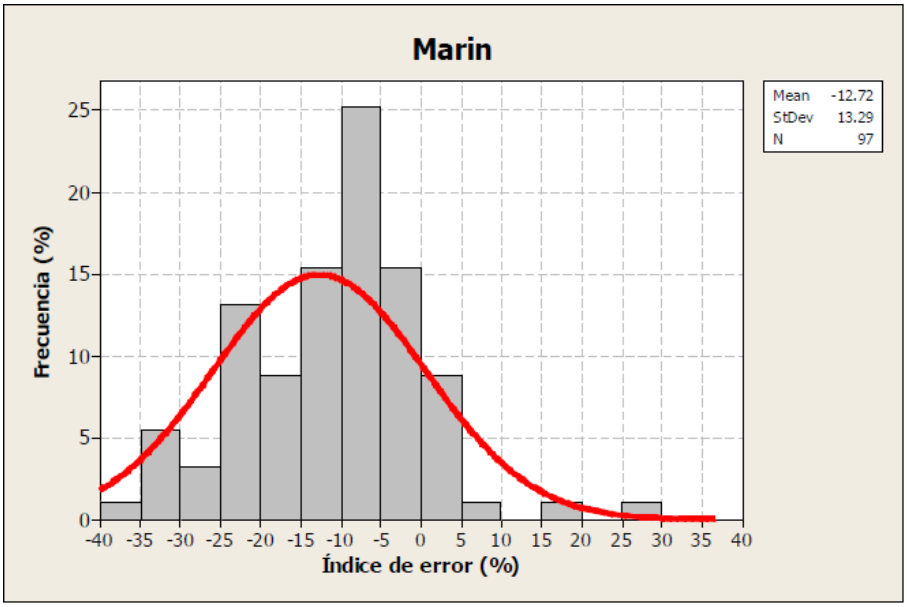

Figure 6-70. *Error distribution of Marin for mean axial stress*

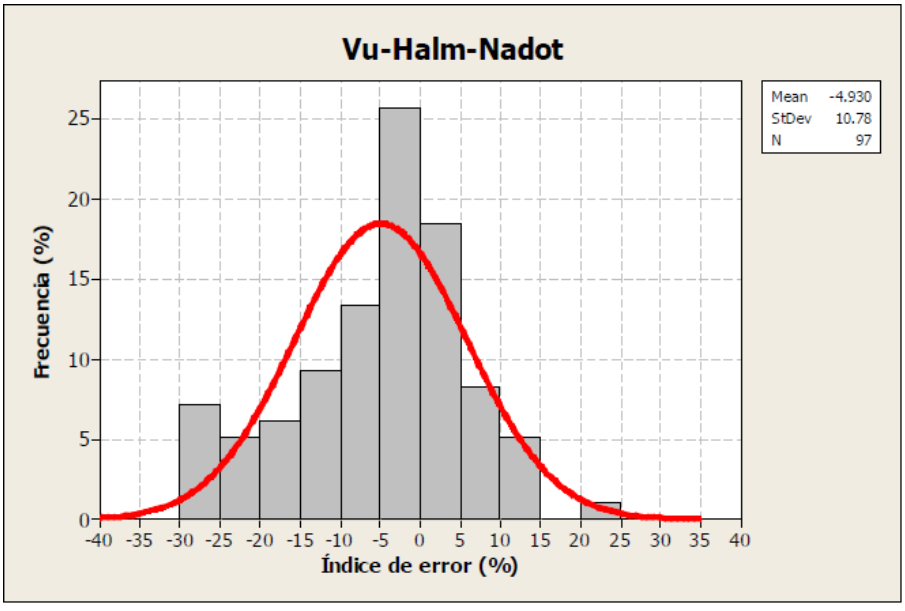

Figure 6-71. *Error distribution of Vu-Halm-Nadot for mean axial stress*

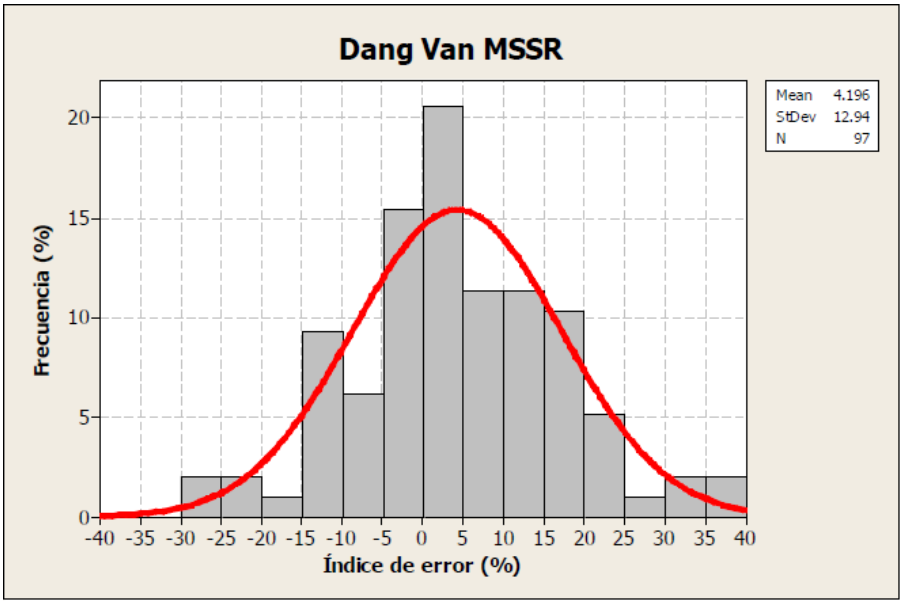

Figure 6-72. *Error distribution of Dang Van MSSR for mean axial stress*

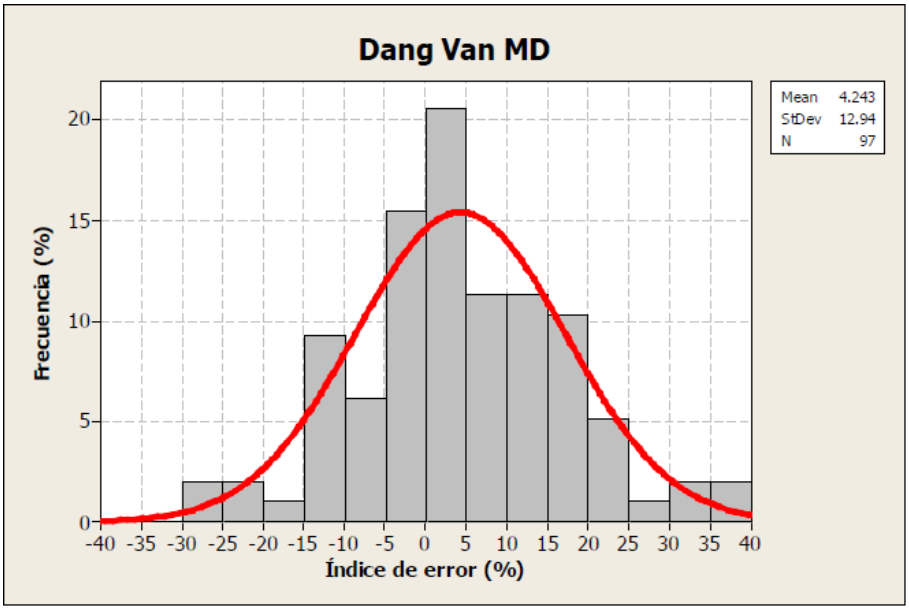

Figure 6-73. *Error distribution of Dang Van MD for mean axial stress*

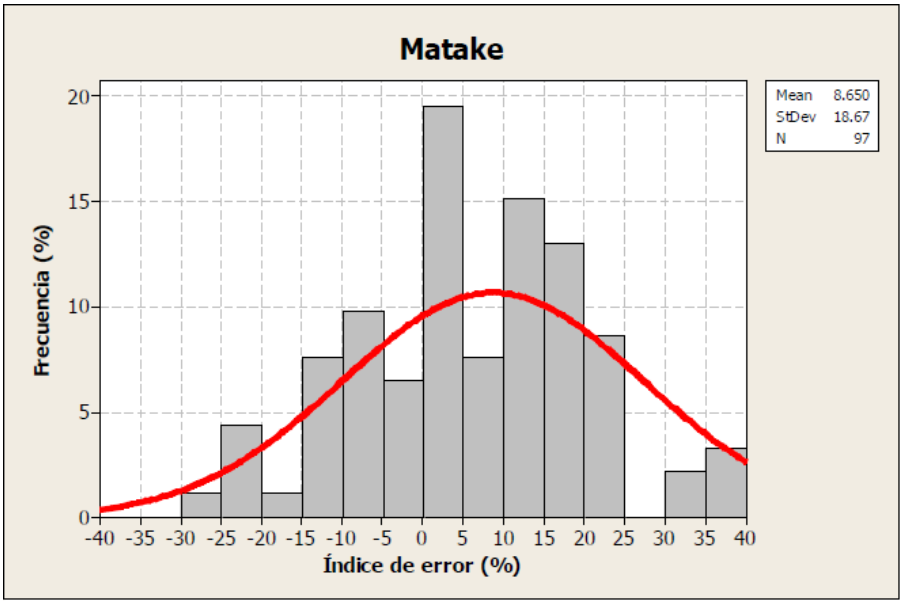

Figure 6-74. *Error distribution of Matake for mean axial stress*

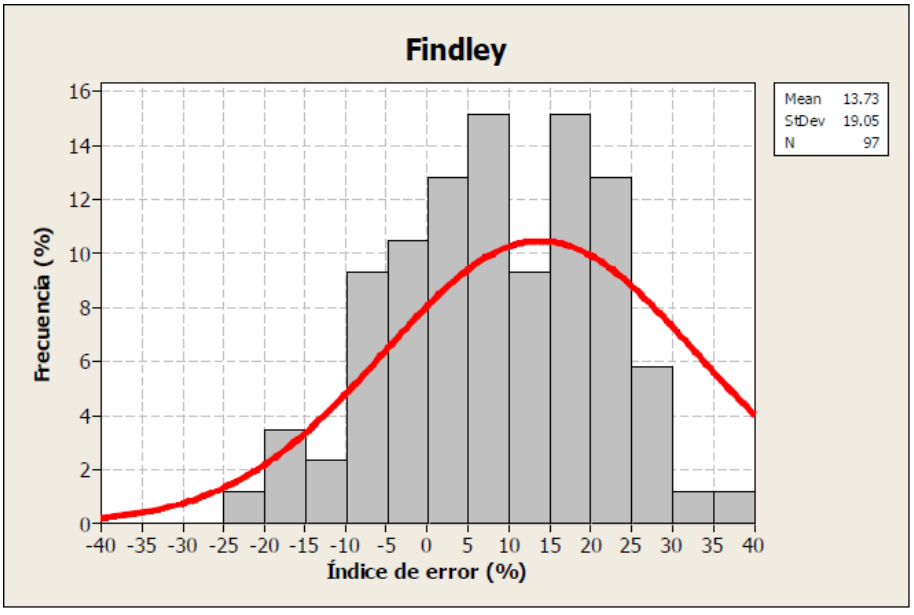

Figure 6-75. *Error distribution of Findley for mean axial stress*

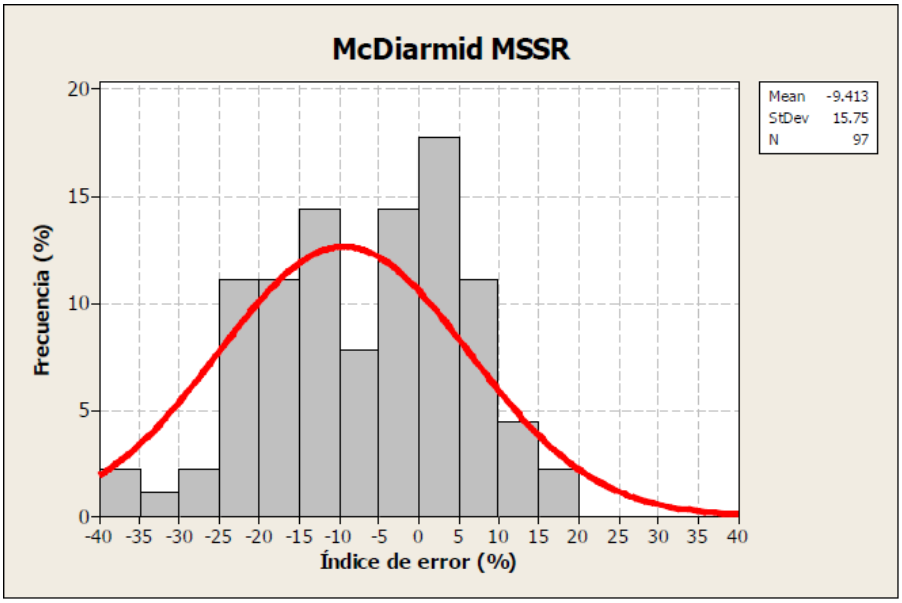

Figure 6-76. *Error distribution of McDiarmid MSSR for mean axial stress*

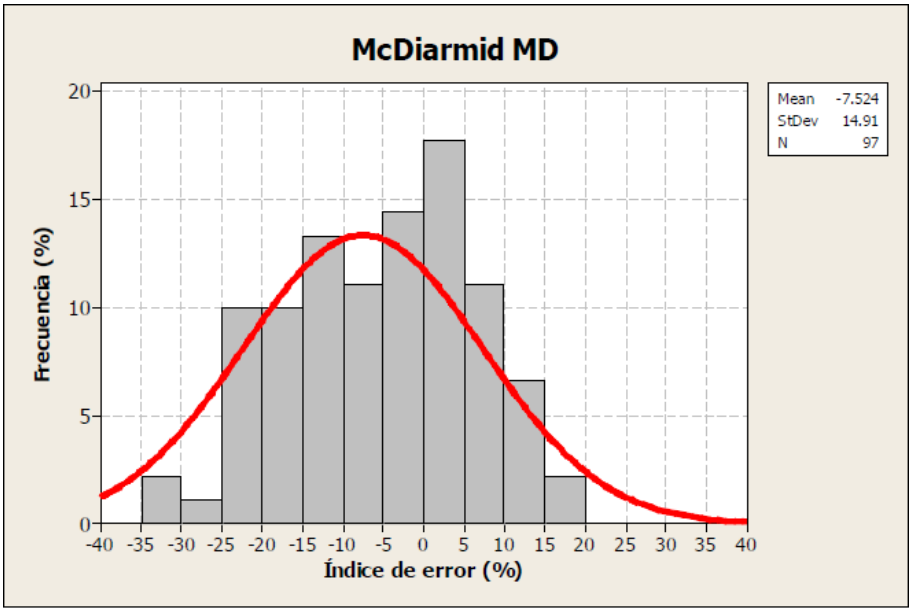

Figure 6-77. *Error distribution of McDiarmid MD for mean axial stress*

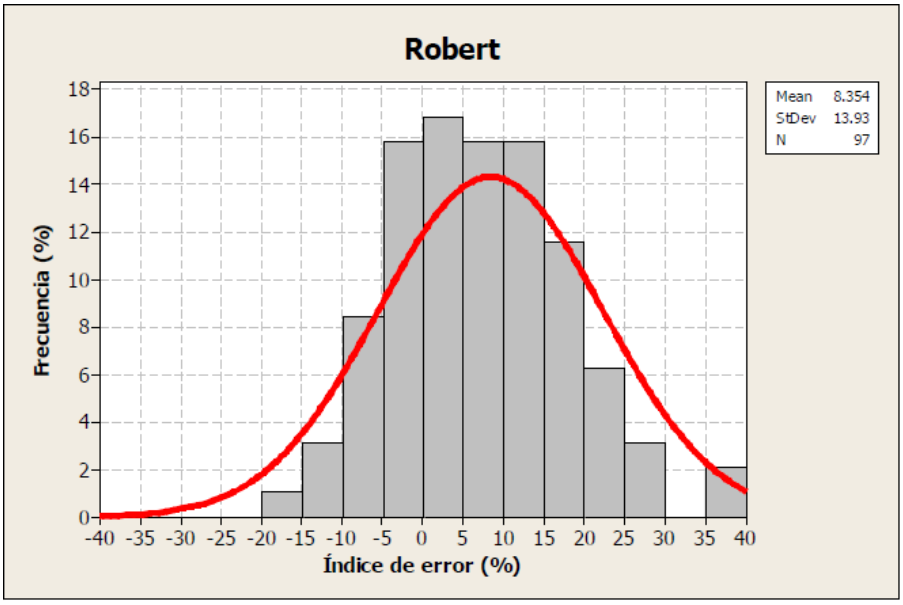

Figure 6-78. *Error distribution of Robert for mean axial stress*

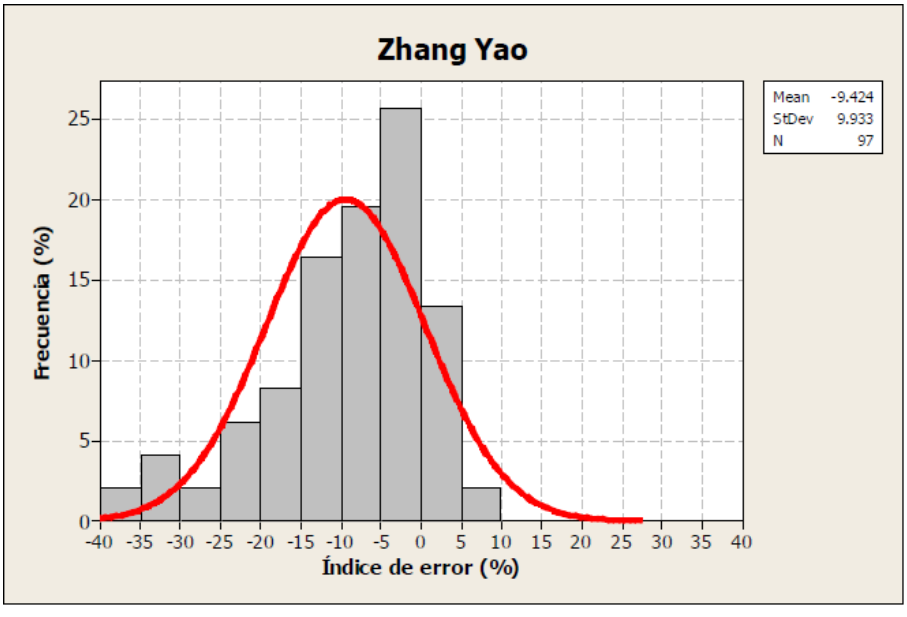

Figure 6-79. *Error distribution of Zhang-Yao for mean axial stress*

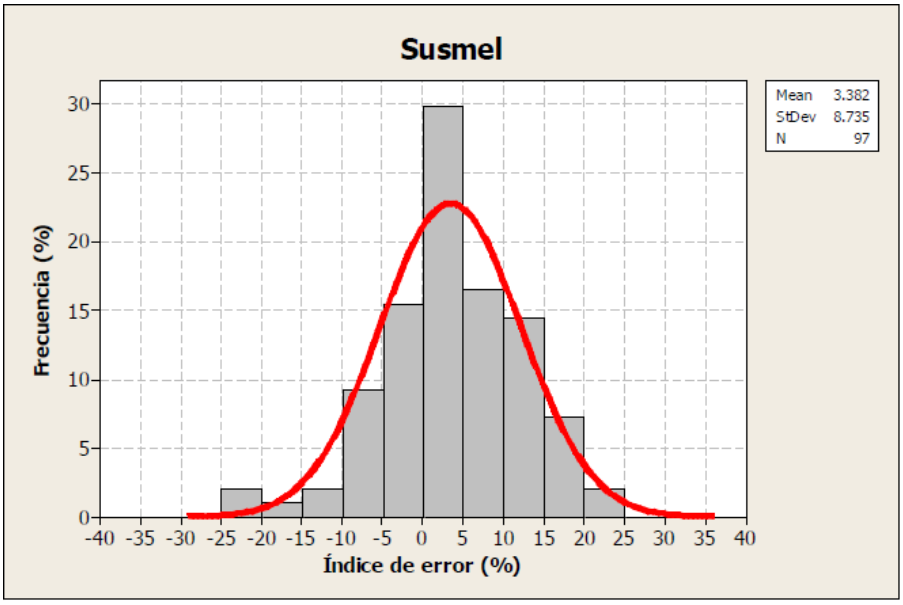

Figure 6-80. *Error distribution of Susmel for mean axial stress*

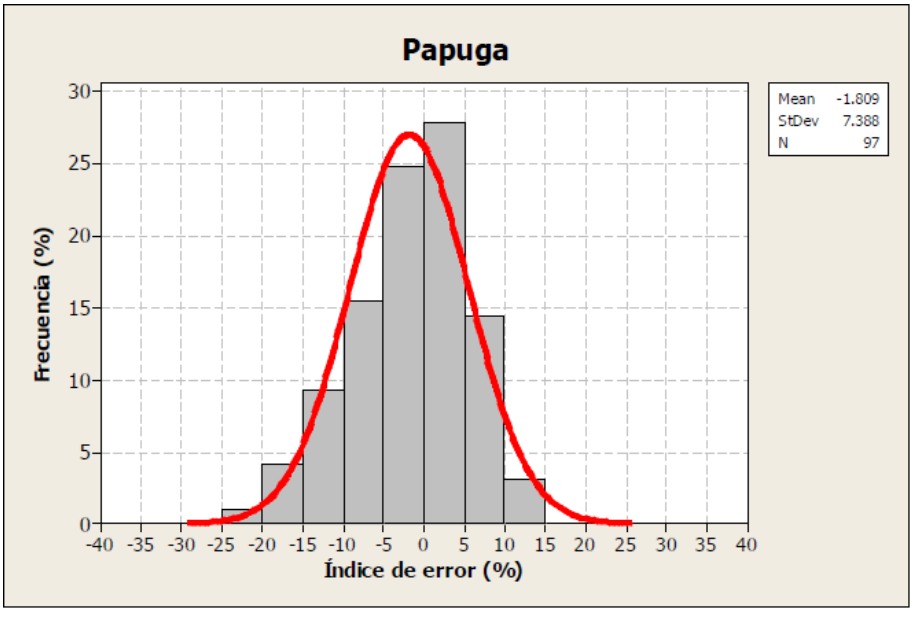

Figure 6-81. *Error distribution of Papuga for mean axial stress*

6.6. Study of the influence of the mean torsional stresses

In this section only those experiments will be taken into account in which there is no phase difference between axial and torsional stresses, but there are static torsional stresses. In this case, 42 experimental data will be available, comparable to one of the classic papers in this sense, the one published by Davoli et al. [Davoli, 2003], who use 24 tests from the literature. The results for this effect are summarized in Table 6-6.

The influence of mean torsional stresses has been a controversial issue in multi-axial fatigue research. On the one hand, researchers such as Sines, Crossland, Papadopoulos [1997] and Davoli [2003] maintain that influence does not exist. Others, such as McDiarmid, argue that influence exists but is minimal, so it can be despised [McDiarmid, 1991], [McDiarmid, 1994].

On the other hand, authors such as Robert [Robert, 1992] or Papuga [Papuga, 2011A] point out that this effect is not negligible. However, this dependence on mean torsional stress was one of Papadopoulos' reasons for not analysing Robert's method in [Papadopoulos, 1997]. This paragraph will therefore seek to shed light on a historically controversial issue.

- **Classic methods:**

The dispersion of error in these methods is proportionally greater than the other effects, especially in the case of Von Mises-based methods. In addition, in the case of Von Mises the distribution is markedly displaced towards the conservative area.

Table 6-6. *Obtained results for the mean torsional stress effect (42 tests)*

Criterio	Valor medio del error	Desviación estándar del error	Porcentaje de resultados en el rango [-40%,40%]	Porcentaje de resultados en el rango [-15%,15%]	Porcentaje de resultados en el rango [-5%,5%] *"Ajustados"*	Porcentaje de resultados en el rango [-5%,-40%] *"No-conservadores"*	Porcentaje de resultados en el rango [+5%,+40%] *"Conservadores"*
Worst Principal Full Range-Goodman	11.83	47.80	69.0	14.3	2.4	33.3	33.3
Von Mises Full Range-Goodman	65.79	82.63	50.0	16.7	2.4	7.1	40.5
Worst Principal Walker real-Goodman	-0.95	34.96	81.0	33.3	11.9	38.1	31.0
Von Mises Walker real-Goodman	50.49	76.75	66.7	28.6	4.8	7.1	54.8
Worst Principal Walker 0.5-Goodman	-10.75	27.49	85.7	38.1	14.3	57.1	14.3
Von Mises Walker 0.5-Goodman	39.15	76.56	71.4	40.5	16.7	14.3	40.5
Sines	-21.03	11.93	90.5	35.7	7.1	83.3	0.0
Crossland	-12.54	10.56	95.2	71.4	21.4	73.8	0.0
Marin	-1.62	8.40	100.0	90.5	47.6	38.1	14.3
Vu-Halm-Nadot	-11.77	10.29	95.2	73.8	23.8	71.4	0.0
Dang Van MSSR	-12.23	10.72	95.2	73.8	21.4	73.8	0.0
Dang Van MD	-12.19	10.72	95.2	73.8	21.4	73.8	0.0
Matake	8.30	26.11	83.3	50.0	14.3	31.0	38.1
Findley	13.69	18.90	85.7	64.3	35.7	7.1	42.9
McDiarmid MSSR	-12.74	11.23	95.2	69.0	26.2	69.0	0.0
McDiarmid MD	-10.70	10.09	100.0	71.4	28.6	69.0	2.4
Robert	1.45	9.17	100.0	85.7	47.6	21.4	31.0
Zhang Yao	-4.84	13.92	95.2	83.3	42.9	35.7	16.7
Susmel	-3.20	13.32	97.6	81.0	38.1	33.3	26.2
Papuga	-1.40	8.02	100.0	92.9	47.6	31.0	21.4

- **Advanced methods of global approach:**

The best performing method in this respect is the Marin method, which is dependent on the mean shear stress through the mean distortion energy that appears explicitly in the Marin method. However, the Sines method, independent of the mean shear stress, presents a markedly non-conservative distribution. The Crossland and Vu-Halm-Nadot methods, equally independent of the mean shear stress, also present a non-conservative distribution, although more centred than the Sines method.

- **Critical Plane Methods:**

The methods that best correlate with the experimental data are those of Robert and Papuga, which are precisely dependent on the mean shear stress. This effect is picked up through the normal mean stress to the plane of maximum damage, which may not be the maximum shear. MSSR methods present more scatter than maximum damage methods. Even Susmel's method, with a high correlation in other individual effects such as mean normal stresses, here presents a slightly non-conservative trend and a relatively high scatter compared to Papuga or Robert.

Consequently, and taking into account the experimental results shown, methods dependent on the mean torsional stress offer a better experimental correlation than those that are not influenced by it, so it could be deduced that there is an influence of the same in certain materials.

The individual error distribution for mean torsion stresses in the range [-40%, +40%] are presented in Figures 6-82 to 6-101.

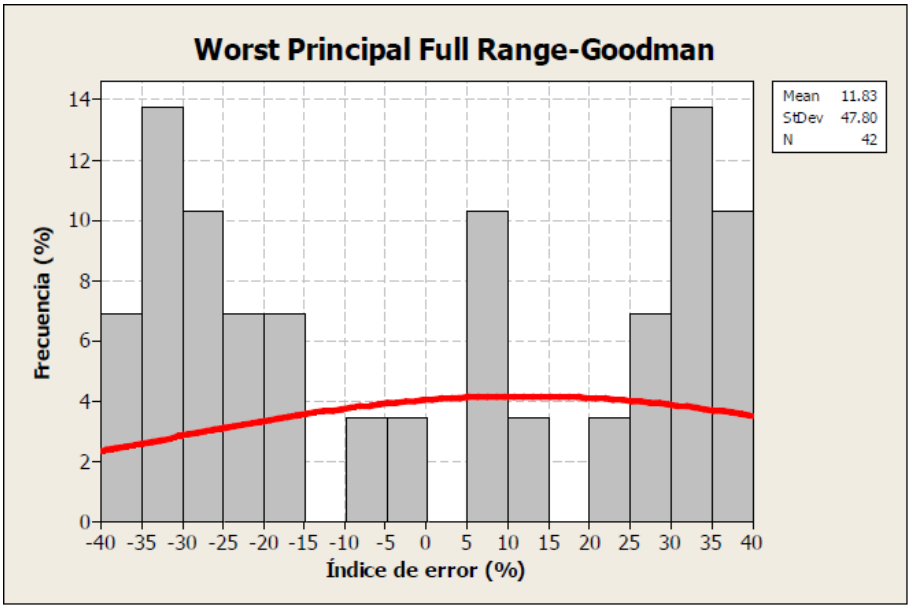

Figure 6-82. *Error distribution of Worst Principal FR-Goodman for mean shear stress*

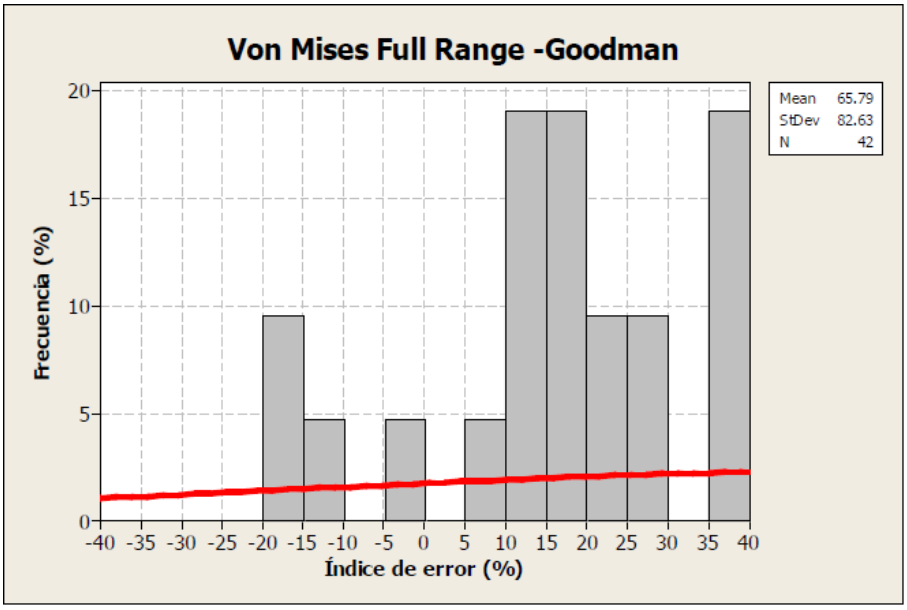

Figure 6-83. *Error distribution of von Mises FR-Goodman for mean shear stress*

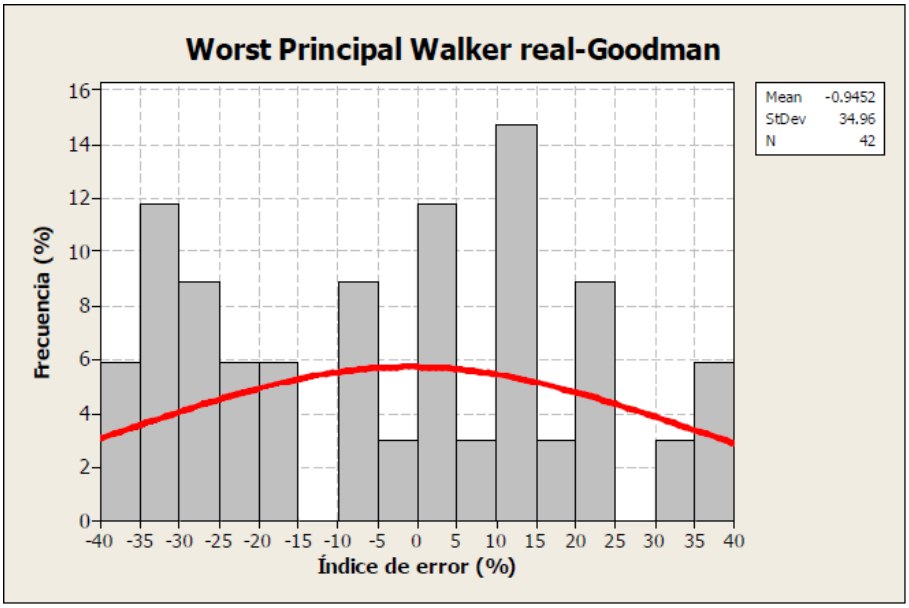

Figure 6-84. *Error distribution of Worst Pr. Walker R.-Goodman for mean shear stress*

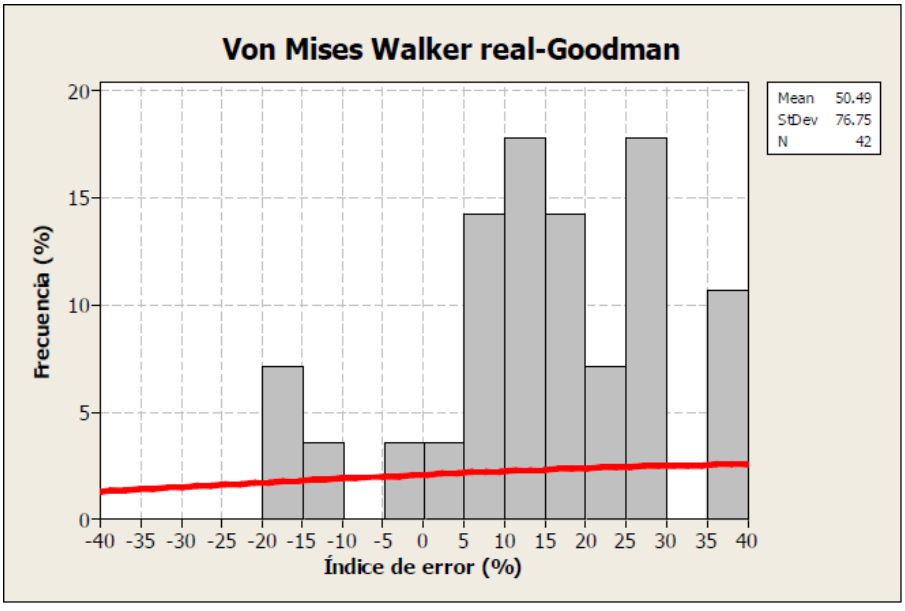

Figure 6-85. *Error distribution of von Mises Walker R.-Goodman for mean shear stress*

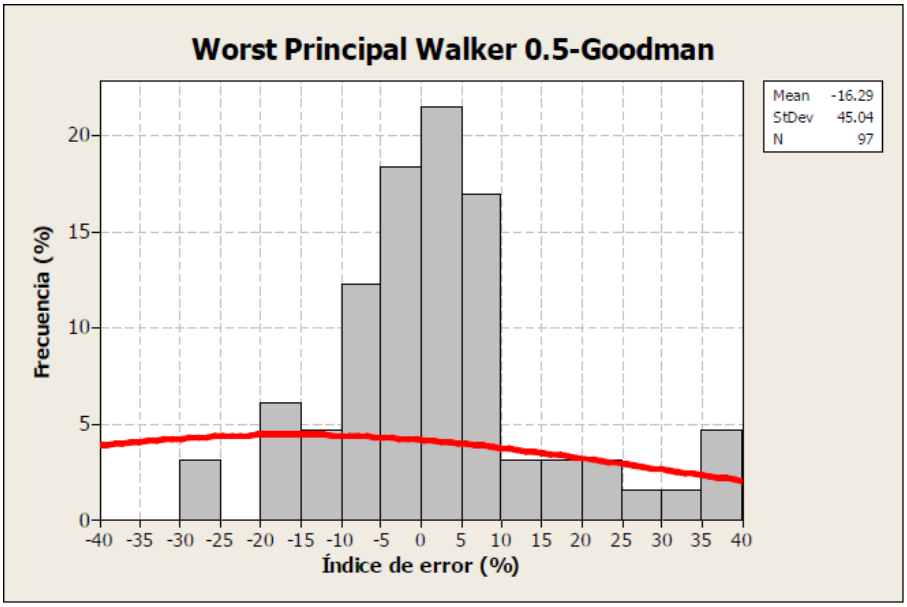

Figure 6-86. *Error distribution of Worst Pr. Walker 0.5-Goodman for mean shear stress*

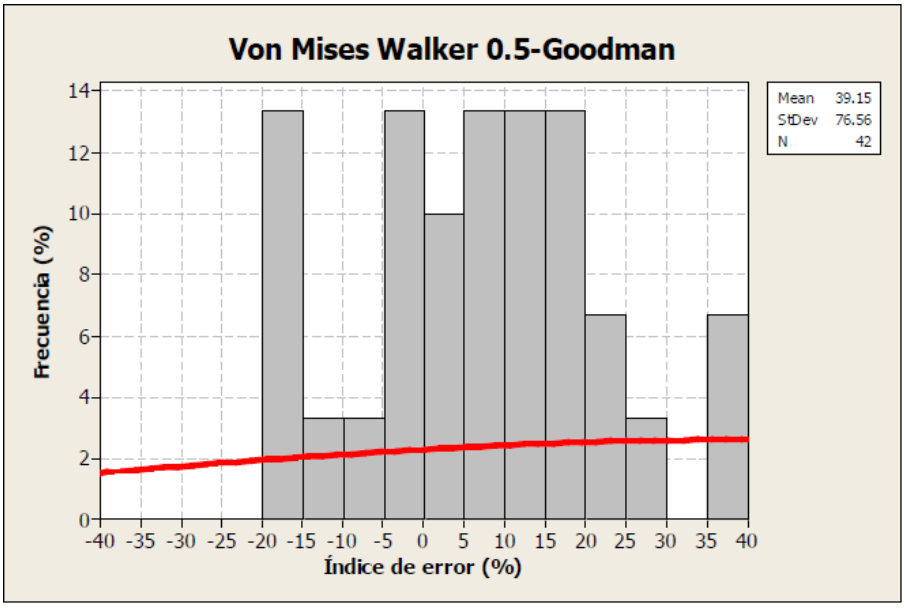

Figure 6-87. *Error distribution of von Mises Walker 0.5-Goodman for mean shear stress*

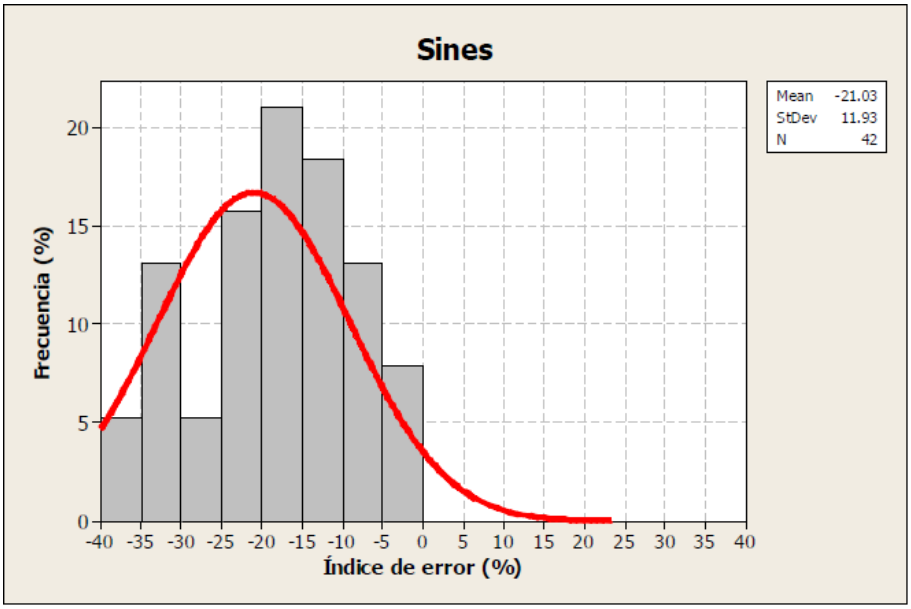

Figure 6-88. *Error distribution of Sines for mean shear stress*

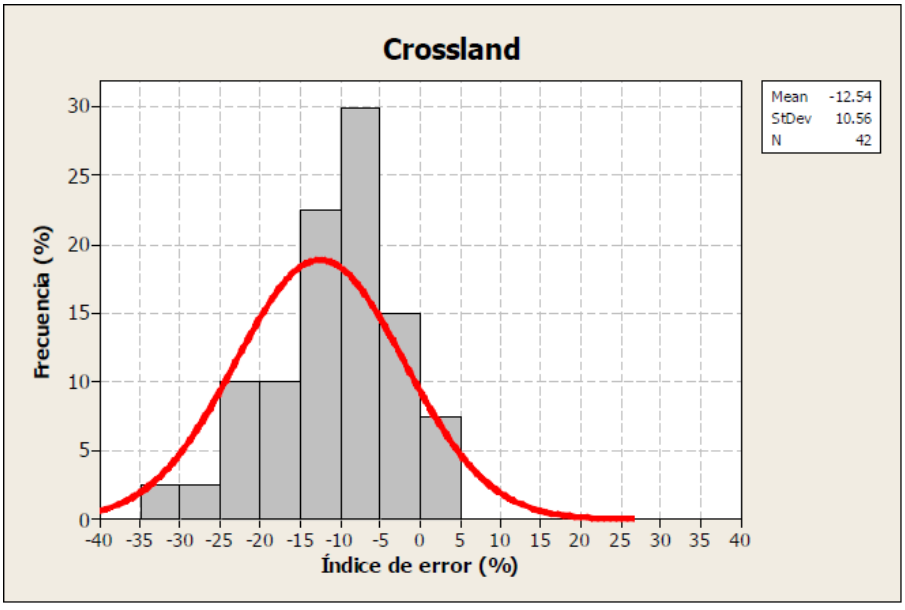

Figure 6-89. *Error distribution of Crossland for mean shear stress*

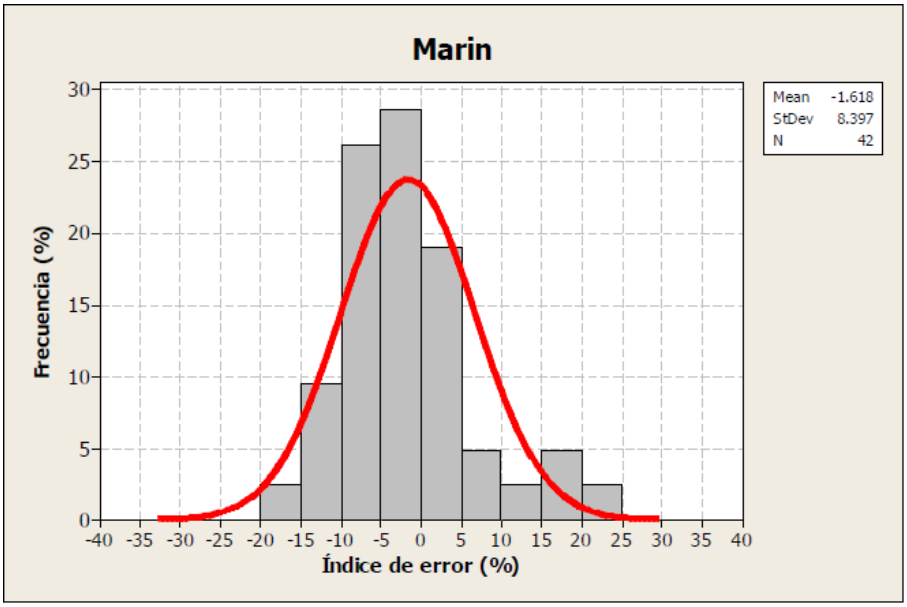

Figure 6-90. *Error distribution of Marin for mean shear stress*

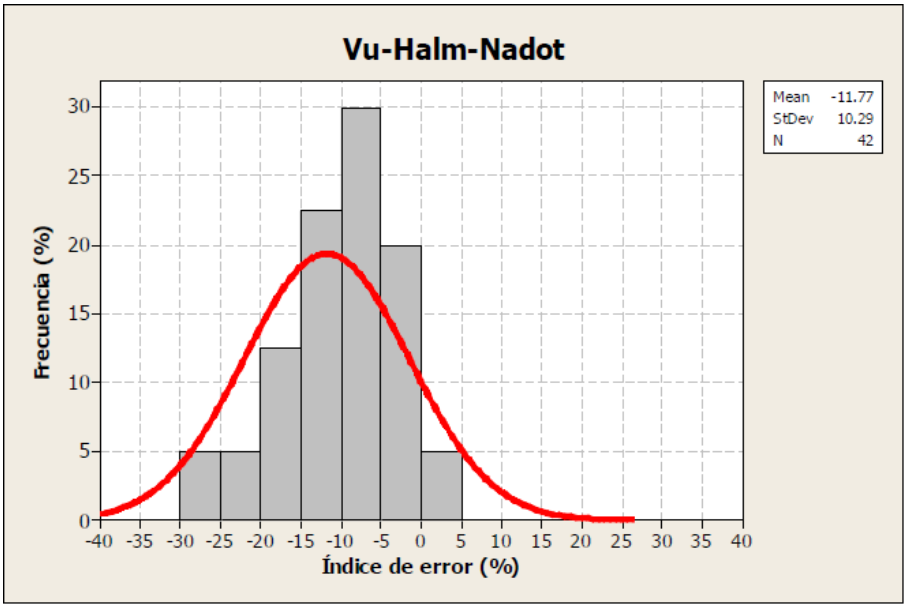

Figure 6-91. *Error distribution of Vu-Halm-Nadot for mean shear stress*

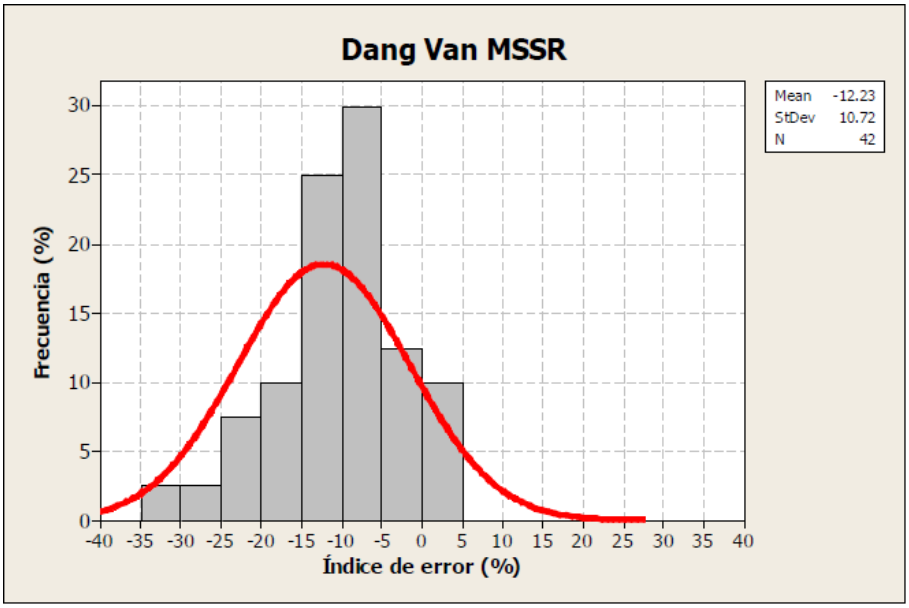

Figure 6-92. *Error distribution of Dang Van MSSR for mean shear stress*

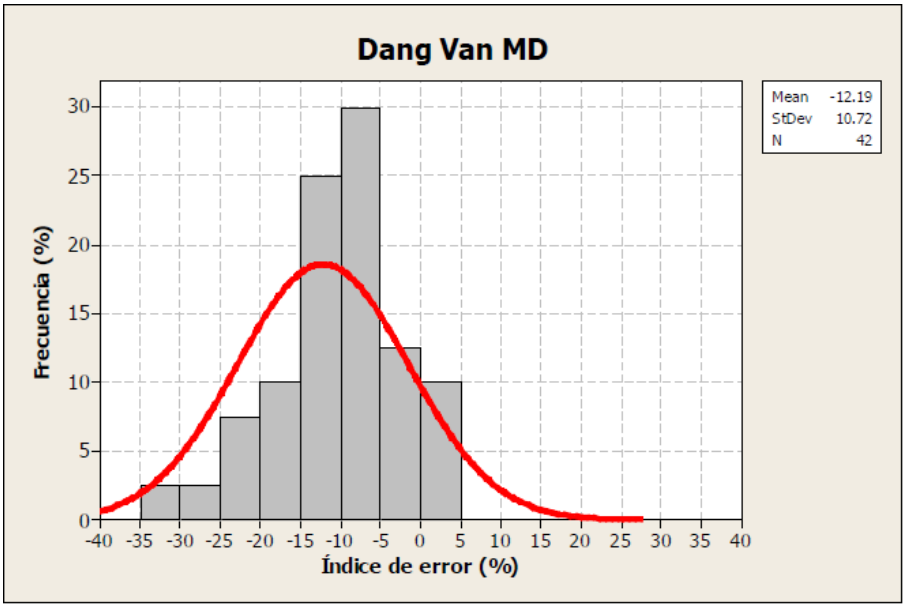

Figure 6-93. *Error distribution of Dang Van MD for mean shear stress*

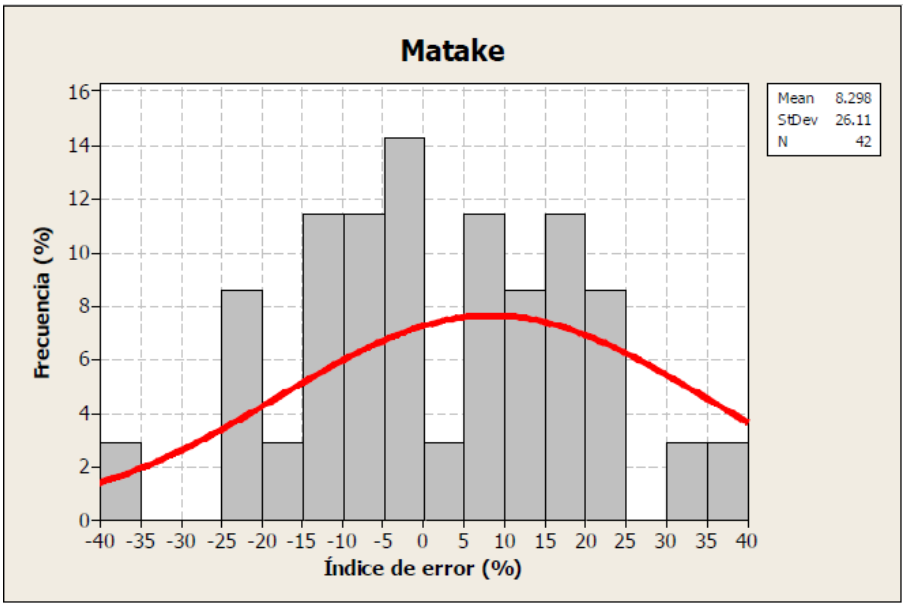

Figure 6-94. *Error distribution of Matake for mean shear stress*

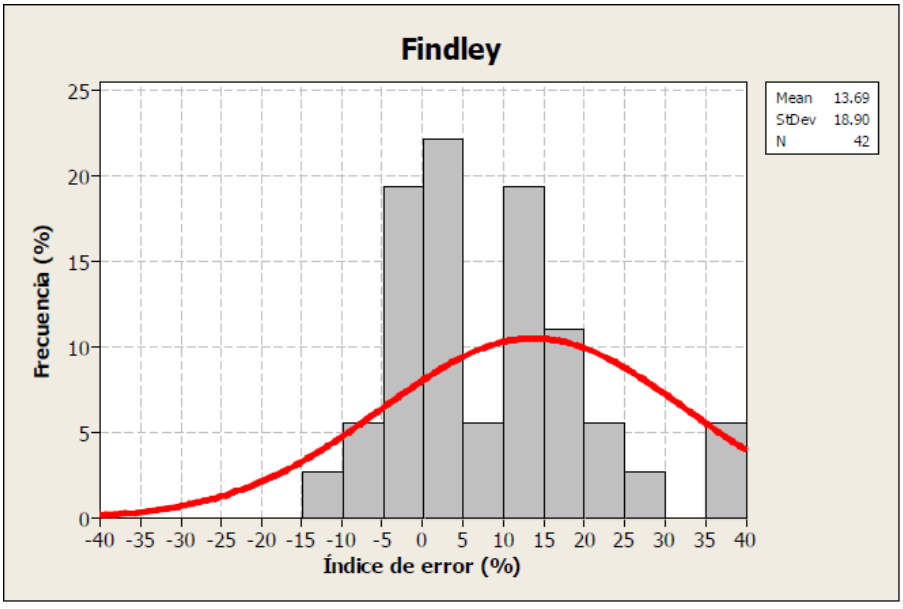

Figure 6-95. *Error distribution of Findley for mean shear stress*

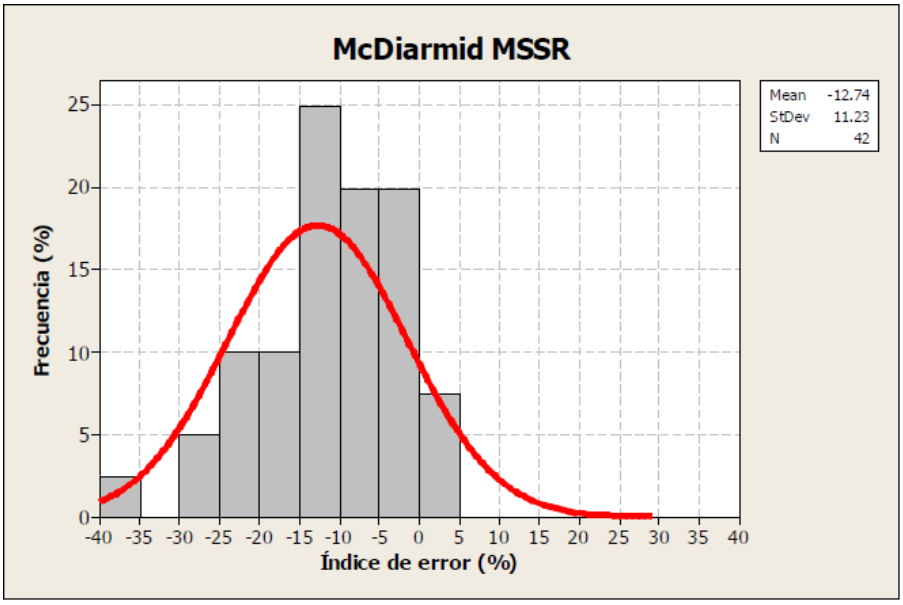

Figure 6-96. *Error distribution of McDiarmid MSSR for mean shear stress*

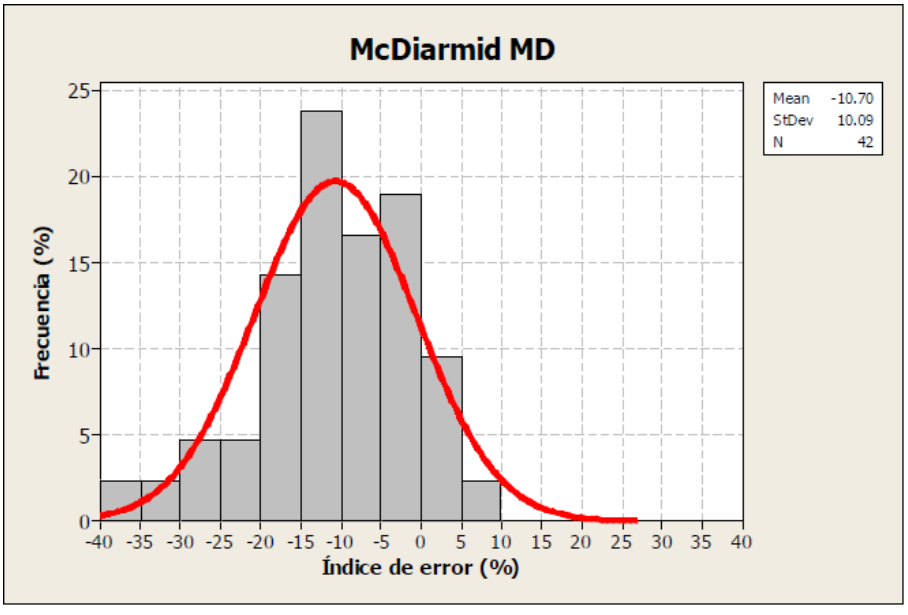

Figure 6-97. *Error distribution of McDiarmid MD for mean shear stress*

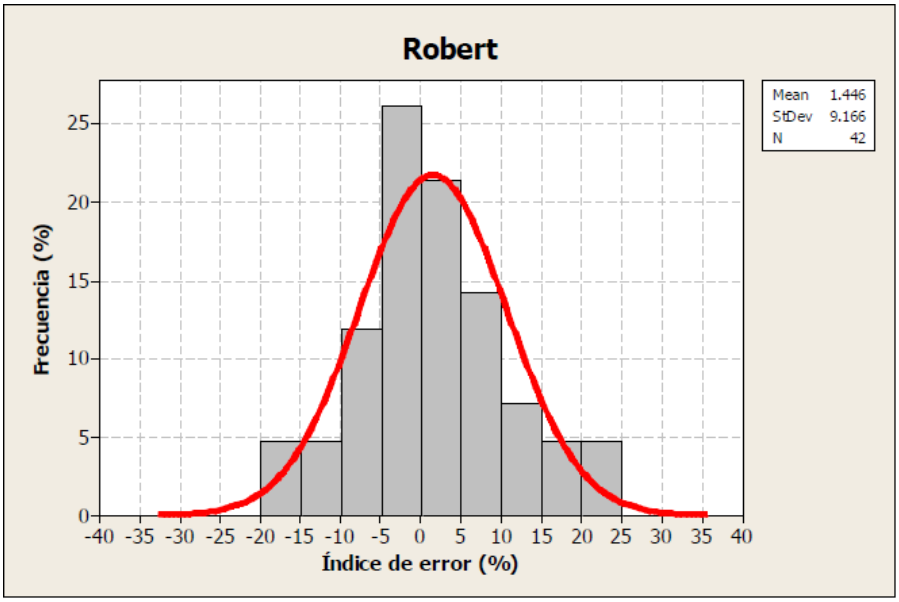

Figure 6-98. *Error distribution of Robert for mean shear stress*

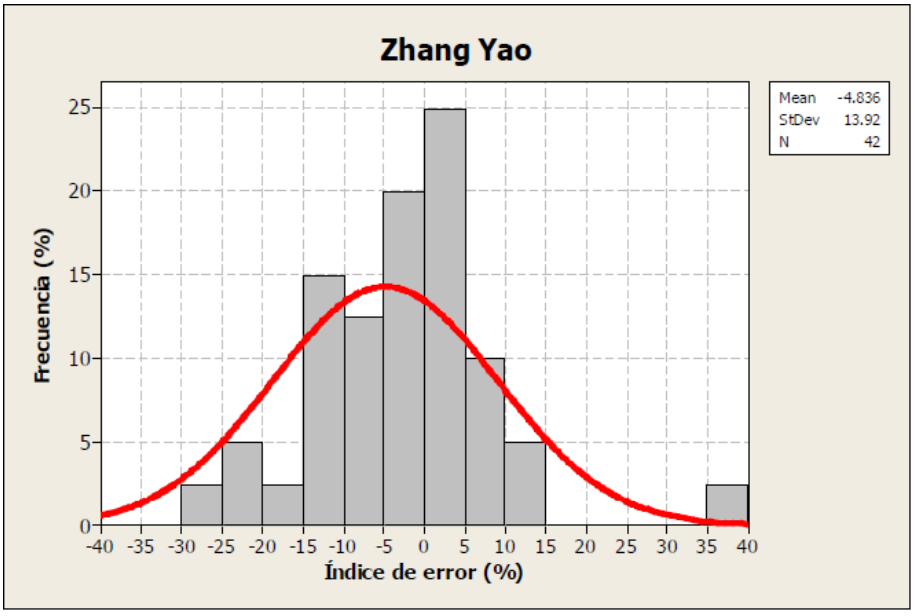

Figure 6-99. *Error distribution of Zhang-Yao for mean shear stress*

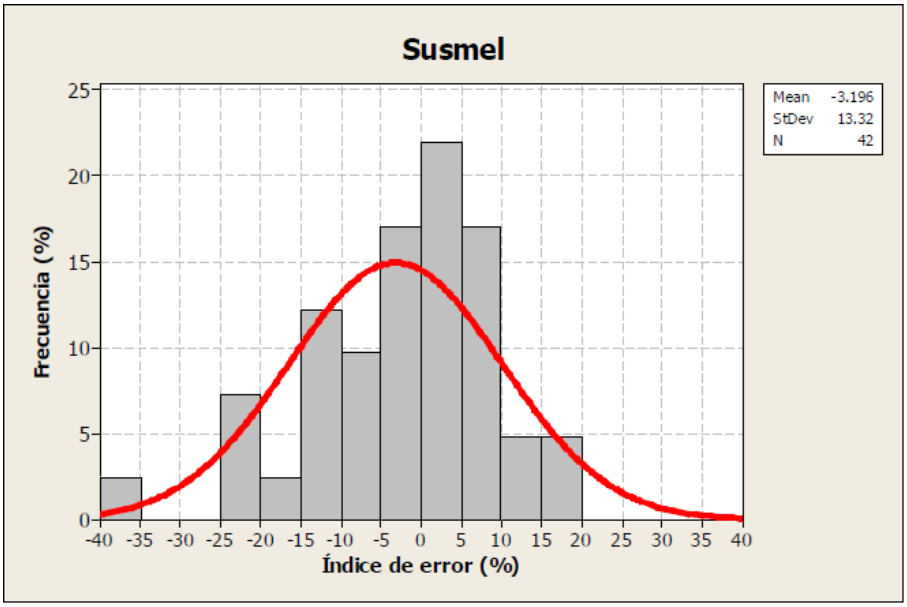

Figure 6-100. *Error distribution of Susmel for mean shear stress*

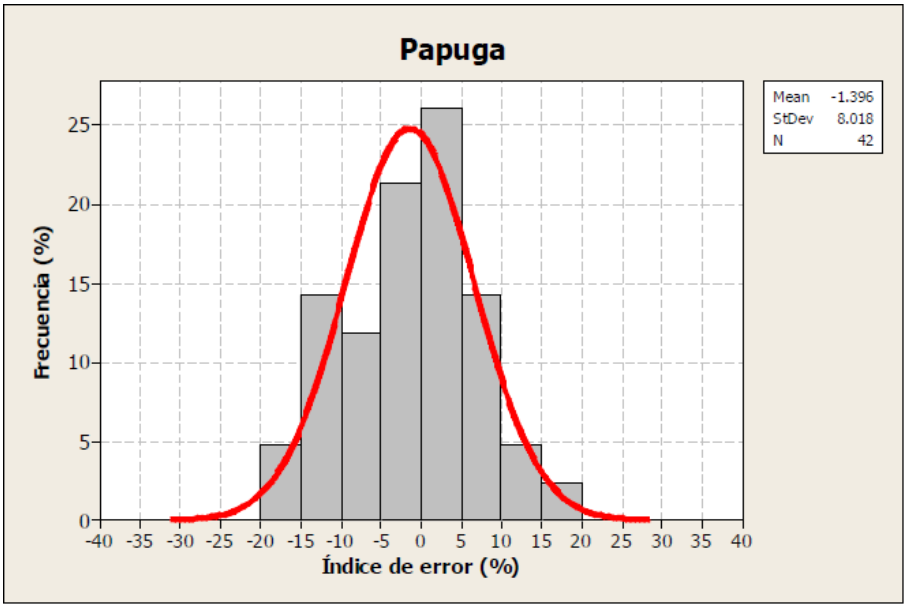

Figure 6-101. *Error distribution of Papuga for mean shear stress*

6.7. Discussion

In the present chapter, a large experimental database has been made available, with a great variety of materials in their mode of behaviour, covering fragile, semi-ductile, extra-ductile materials. In addition, there is a great variety of load states, which have allowed the detailed study of the different effects on multi-axial fatigue, allowing general conclusions to be drawn about the suitability of damage parameters according to the types of loads.

In this document, after an exhaustive analysis of the calculation methods for the database of 422 experiments, it can be concluded that there are some individual effects which take a great role in the fatigue behaviour. Moreover, some of the most known and multiaxial fatigue methods, such as the Crossland criterion, need to be improved in certain areas.

6.7.1. Relative importance of the individual effects

The analysed individual effects in fatigue have been the multiaxiality, the phase shift effect and the mean axial and torsional stress effects. It should be noted that an inspection of Tables 6-3 and 6-4 leads to the conclusion that the multiaxiality and phase shift effect do not provoke great differences in the errors distributions, with the exception of the classic methods, which are extensions of uniaxial methods.

However, the mean axial and torsional stresses produce great differences in the error distributions between the different multiaxial fatigue methods.

6.7.2. Influence of mean axial stresses

According to Table 6-5, the accumulated deviation of the methods show that the mean axial stress effect is the 1st feature to take into account for the development of multiaxial fatigue method, with high differences in the mean value of the error and the standard deviation.

The Sines method, which uses the fatigue limit for R_σ=0 performs the best among the global approach methods. Crossland and Marin methods are shifted towards the non-conservatism.

For the critical plane methods, the Susmel and Papuga criteria present an excellent agreement thanks to the limitation of the fatigue damage which can be produced in brittle materials.

6.7.3. Influence of mean torsional stresses

According to the summarized results of Table 6-6, the influence of the mean torsional stresses is the 2nd feature in terms of importance for a multiaxial fatigue method. According to the review of Chapter 4, the mean torsional stress takes a role even for ductile metals, so that the methods correctly modelling this effect should be carefully examined.

For the global approach methods, the Marin criterion offers an outstanding experimental agreement with this group of tests. It must be noted that the Marin method is dependent on mean shear stresses through the mean value of the second invariant of the stress deviator tensor $J_{2,m}$, which is related to the mean

elastic distortion energy. The Crossland method, which is not dependent on mean shear stresses, is shifted towards the non-conservatism.

The Robert and Papuga methods have also an excellent agreement for this effect, which is modelled through the mean normal stress to a plane that is not the one with the maximum shear stress amplitude, but the one with the maximum damage, which may not coincide with it. Some critical plane methods dependent on mean shear stresses do not offer as accurate results, (i.e. Findley), so that the importance lies in the way of modelling and not the dependence by itself.

6.7.4. Quantities and parameters used for the formulation of the methods

Within the comparison, the solution of some critical planes using three quantities to model the fatigue damage exhibit good experimental agreement in the effects of phase shifting and in the mean axial and torsional stresses: such is the case of the criteria of Robert and Papuga.

A careful examination of the global approach methods (based on stress invariants) allows to infer that there exist opportunities for new developments, as the quantities used to model have not been adequately combined in order to obtain improved results for different load cases (i.e. mean stress effects). An enhancement could be performed by using the stored distortion energy, which is only used by the Marin method, offering a competitive advantage of the other methods for mean shear stresses.

Finally, it must be noted that the use of 2 different axial tests to adjust the method improves the axial fatigue results, as it was the case of Sines, Susmel and Papuga methods. The Sines criterion, which uses the mean hydrostatic stress and a uniaxial fatigue limit in R=0 among other parameters, obtains a good behaviour with regard to the effect of the mean normal stresses, but presents a non-conservative effect with regard to other effects such as mean torsional stresses or phase shift.

The Papuga and Vu-Halm-Nadot methods use a damage parameter in case of axial mean stresses that is different depending on the fragility of the material, benefiting to a great extent the correlation with experimental results.

Chapter 7:

EXPERIMENTAL CAMPAIGN

CHAPTER 7. EXPERIMENTAL CAMPAIGN

7.1. Material

7.1.1. Introduction: selection of the material

The selection of the material is a fundamental point in this project. The main requirements are:

- High sensitivity to mean axial and shear stresses: this aspect is fundamental, since in fatigue the effects of mean stresses are the most important compared to other effects. A very low effect of mean stresses would not justify a test campaign.
- Elasticity to mean stresses: This greatly facilitates fatigue tests by maintaining elastic behaviour for values of no higher than zero mean stresses.
- Low number of plastic-elastic transition cycles (N_t): This value is indicative of the number of cycles in which a material becomes preferably elastic. A low number greatly eases the HCF testing.
- Low number of cycles in the fatigue limit: It allows to finish the tests before, reducing the cost by reducing the number of machine hours.
- Unicity of the microstructure: It allows a much simpler analysis of the micrographies and a less dispersion is to be expected since there is no mechanical interaction between the different microstructures.

The NIMS database [Nishijima, 1993], which contains a multitude of fatigue tests on the 15 most used Japanese structural steels, will be used to determine the most suitable steel for carrying out the tests. Quenched and tempered steels are those corresponding to numbers Nims 2 to Nims 12, and have a σ_{UTS} between 700 and 1050 MPa. These steels are shown in Table 7-1, along with their ASTM (USA) or ISO equivalents. Table 7-2 shows the mechanical characteristics obtained from the static tests.

Table 7-1. *Table of equivalences between standards of Japanese NIMS steels*

nº	Nombre ensayo	JIS	SAE/ASTM	ISO
1	NIMS 1	S25C	1025	C 25
2	NIMS 2	S35C	1035	C 35
3	NIMS 3	S45C	1045	C45
4	NIMS 4	S55C	1055	C55
5	NIMS 5	SMn438	1541	36Mn6
6	NIMS 6	SMn443	-	42Mn6
7	NIMS 7	SCr440	5140	41Cr4
8	NIMS 8	SCM435	4137	34CrMo4
9	NIMS 9	SCM440	4140	42CrMo4
10	NIMS 10	SNC631	-	-
11	NIMS 11	SNCM439	4340	34CrNiMo6
12	NIMS 12	SNCM447	-	.
13	NIMS 13	SUS403	403	.
14	NIMS 14	SUS430	430	X 6 Cr17
15	NIMS 15	SUS304	304	X 5 CrNi 18 10

Table 7-2. *Mechanical characteristics of Japanese steels studied by NIMS*

			DATOS ESTÁTICOS				
nº	Nombre ensayo	Material	E (Gpa)	RA (%)	σ_{yp} (Yield)	σ_{ut} (UTS)	σ_{ur} (fracture)
1	NIMS 1	S25C	212	63.5	363	489	980
2	NIMS 2	S35C	212	70.2	525	697	1443
3	NIMS 3	S45C	212	65.5	630	789	1505
4	NIMS 4	S55C	211	60.9	709	850	1517
5	NIMS 5	SMn438	212	66.3	656	798	1541
6	NIMS 6	SMn443	212	63.2	743	861	1575
7	NIMS 7	SCr440	213	63.1	854	956	1662
8	NIMS 8	SCM435	212	65.5	897	982	1741
9	NIMS 9	SCM440	212	62.3	936	1047	1775
10	NIMS 10	SNC631	208	67.2	813	924	1704
11	NIMS 11	SNCM439	209	63.4	926	1003	1750
12	NIMS 12	SNCM447	209	62.6	920	1013	1767
13	NIMS 13	SUS 403	218	70.8	583	727	1449
14	NIMS 14	SUS 430	232	75.7	306	494	1208
15	NIMS 15	SUS 304	199	80.8	257	614	1937

7.1.2. Sensitivity to mean stresses

With respect to the criterion of sensitivity to static stresses, Table 7-3 shows the sensitivities M_σ (axial) and M_τ (torsion), the steels being ordered by ranking.

Table 7-3. *Sensitivity to static mean stresses*

			Límite de fatiga				Mean stress sensitivity indices	
nº	Nombre ensayo	Material	σ_{-1}	τ_{-1}	σ_0	$\tau_{0\ estimado}$	M_σ	M_τ
1	NIMS 14	SUS 430	300	218	444	372	0.350	0.175
2	NIMS 11	SNCM439	560	366	851	632	0.317	0.159
3	NIMS 13	SUS 403	413	274	634	476	0.305	0.152
4	NIMS 3	S45C	409	287	627	498	0.303	0.152
5	NIMS 2	S35C	337	248	524	434	0.287	0.144
6	NIMS 12	SNCM447	555	367	870	645	0.276	0.138
7	NIMS 9	SCM440	568	374	895	659	0.269	0.134
8	NIMS 6	SMn443	446	313	705	553	0.265	0.133
9	NIMS 10	SNC631	515	330	815	583	0.265	0.133
10	NIMS 4	S55C	452	310	716	548	0.263	0.132
11	NIMS 7	SCr440	507	343	811	610	0.249	0.124
12	NIMS 5	SMn438	418	299	671	533	0.244	0.122
13	NIMS 8	SCM435	510	356	823	636	0.239	0.120
14	NIMS 1	S25C	214	145	363	266	0.178	0.089
15	NIMS 15	SUS 304	229	157	406	295	0.130	0.065

The value of the parameter τ_0 has been estimated using Zenner's empirical formula.

7.1.3. Elastic behaviour against mean stresses

As for the elasticity to static mean stresses, the criterion shown in Figure 7-1 will be used:

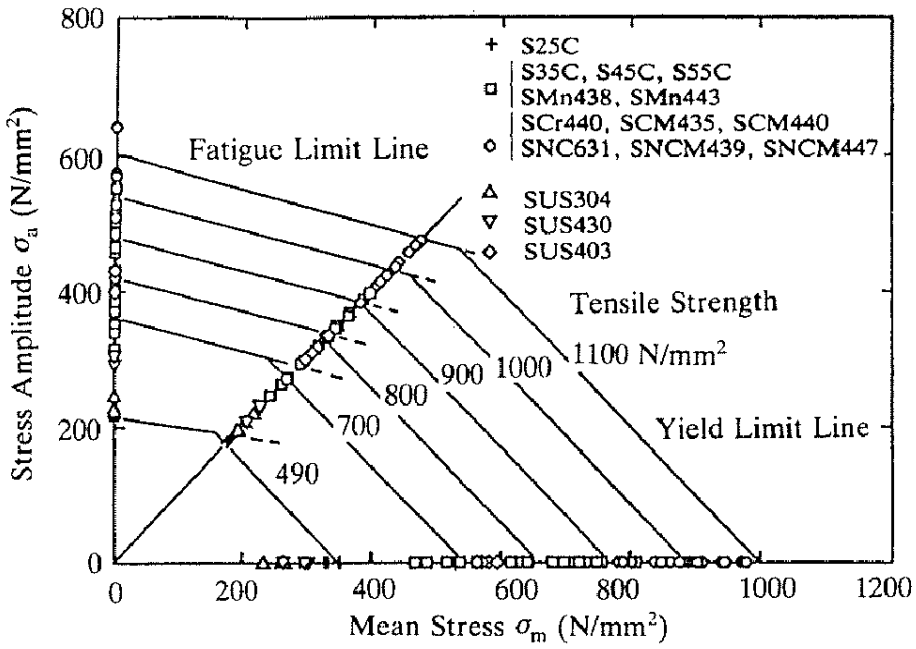

Figure 7-1. *Haigh diagram with the criterion to determine the maximum elastic stress ratio R [Nishijima, 1993]*

As shown in figure 7-1, the intersection between two lines are calculated:

- The Serensen line, which joins the fatigue limits at R=-1 and R=0 in axial stresses (or the equivalent in torsion, Chodorowski).

- The maximum line stress = yield stress. For torsion it will be considered von Mises.

The higher the R at the intersection, the higher the elastic range. Table 7-4 shows the results sorted by ranking according to this second criterion.

Table 7-4. *Maximum elastic R (Stress ratio)*

			Axial: Serensen & Yield			Torsion: Chodorowski & Yield		
nº	Nombre ensayo	Material	σ_m	σ_a	R_{axial}	τ_m	τ_a	$R_{torsion}$
1	NIMS 11	SNCM439	536	390	0.157	200	334	-0.250
2	NIMS 8	SCM435	509	388	0.135	184	334	-0.290
3	NIMS 12	SNCM447	504	416	0.096	190	341	-0.283
4	NIMS 6	SMn443	404	339	0.088	134	295	-0.377
5	NIMS 7	SCr440	462	392	0.083	171	322	-0.305
6	NIMS 9	SCM440	504	432	0.076	192	348	-0.289
7	NIMS 3	S45C	318	312	0.009	90	273	-0.503
8	NIMS 2	S35C	264	261	0.005	64	239	-0.575
9	NIMS 1	S25C	182	181	0.002	71	139	-0.324
10	NIMS 10	SNC631	405	408	-0.003	161	309	-0.315
11	NIMS 4	S55C	348	361	-0.017	114	295	-0.441
12	NIMS 5	SMn438	315	341	-0.039	91	288	-0.520
13	NIMS 13	SUS 403	244	339	-0.163	73	263	-0.563
14	NIMS 15	SUS 304	32	225	-0.752	-9	157	-1.121
15	NIMS 14	SUS 430	10	296	-0.937	-50	227	-1.571

7.1.4. Elasticity for low number of cycles

For the third criterion, that corresponding to the elasticity from a lower number of cycles, the graphical definition of Nt is necessary, see figure 4.2. The numerical definition can be made through the following equation (7.1):

$$N_t = \left(\frac{\varepsilon'_f \cdot E}{\sigma'_f} \right)^{\frac{1}{(b-c)}} \tag{7.1}$$

Constant values are not represented in the NIMS document, but can be estimated using Manson's modified universal slope method.

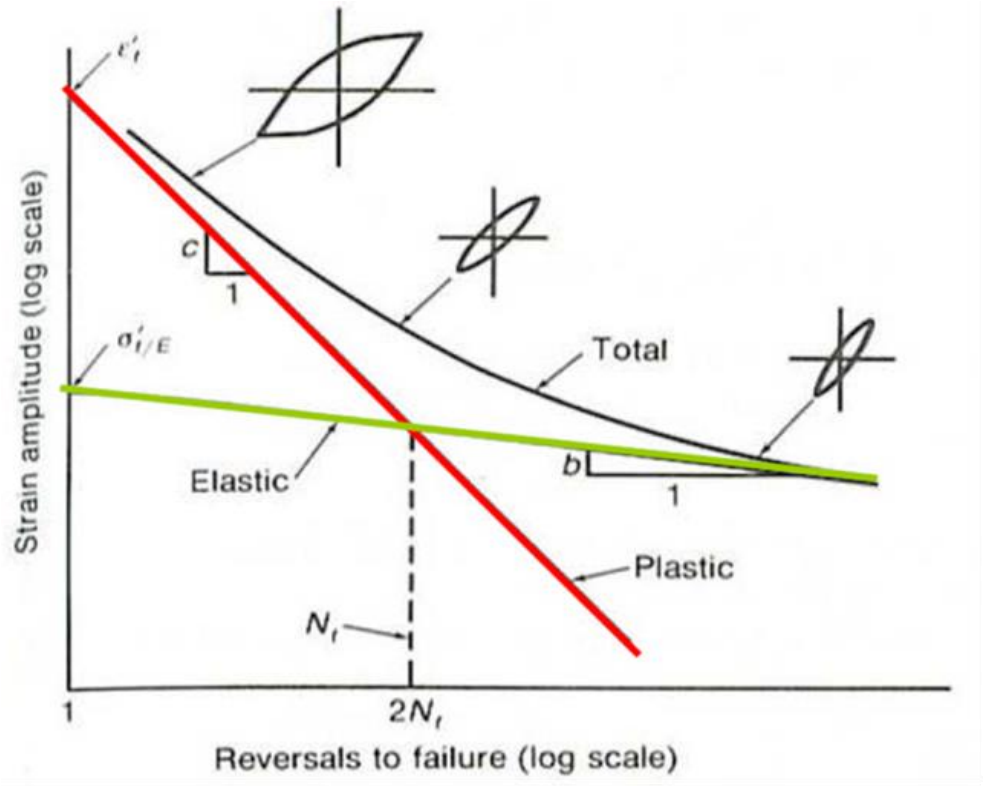

Figure 7-2. *Graphical definition of the number of transition cycles Nt*

Once the value of Nt has been found for each steel, they are shown in order in the corresponding ranking in Table 7-5:

Table 7-5. *Ranking according to the number of transition cycles Nt*

			Pendientes universales modificado		
nº	Nombre ensayo	Material	σ'_f	ε'_f	N_t
1	NIMS 9	SCM440	1592	0.33	3042
2	NIMS 12	SNCM447	1545	0.33	3236
3	NIMS 11	SNCM439	1533	0.33	3350
4	NIMS 8	SCM435	1509	0.34	3782
5	NIMS 7	SCr440	1477	0.34	4023
6	NIMS 10	SNC631	1430	0.35	4304
7	NIMS 6	SMn443	1352	0.36	5385
8	NIMS 4	S55C	1338	0.36	5457
9	NIMS 5	SMn438	1270	0.38	6908
10	NIMS 3	S45C	1258	0.38	7092
11	NIMS 13	SUS 403	1181	0.42	10301
12	NIMS 2	S35C	1135	0.42	10660
13	NIMS 15	SUS 304	1010	0.45	14081
14	NIMS 1	S25C	845	0.49	27986
15	NIMS 14	SUS 430	865	0.54	39571

7.1.5. Low number of cycles for the fatigue limit

The fourth criterion refers to the number of cycles in which the fatigue limit is found with a classical bilinear modeling. The smaller the number of cycles, the earlier the end of the test can be given, and therefore less number of machine hours will be invested. The mean value shall be determined for the different tests performed by NIMS. It should be noted that the test with the highest number of cycles for the fatigue limit is the axial with R=0, see table 7-6.

Table 7-6. *Ranking according to the number of cycles in the fatigue limit*

nº	Nombre ensayo	Material	$N_{endurance}$ R.B. R=-1	$N_{endurance}$ Axial R=-1	$N_{endurance}$ Axial R=0	$N_{endurance}$ Torsion R=-1	Promedio $N_{endurance}$
1	NIMS 15	SUS 304	2.6E+05	1.5E+05	7.3E+05	4.5E+05	4.0E+05
2	NIMS 9	SCM440	6.3E+05	9.3E+05	1.9E+06	7.5E+05	1.0E+06
3	NIMS 7	SCr440	9.8E+05	6.0E+05	2.0E+06	7.2E+05	1.1E+06
4	NIMS 2	S35C	1.2E+06	5.2E+05	1.4E+06	1.3E+06	1.1E+06
5	NIMS 6	SMn443	9.9E+05	4.7E+05	1.6E+06	1.6E+06	1.2E+06
6	NIMS 11	SNCM439	7.2E+05	8.7E+05	2.0E+06	1.2E+06	1.2E+06
7	NIMS 3	S45C	1.1E+06	4.1E+05	2.6E+06	1.3E+06	1.3E+06
8	NIMS 12	SNCM447	7.2E+05	1.3E+06	2.2E+06	1.1E+06	1.3E+06
9	NIMS 5	SMn438	1.2E+06	1.8E+06	2.1E+06	6.2E+05	1.4E+06
10	NIMS 8	SCM435	7.5E+05	1.3E+06	2.7E+06	9.4E+05	1.4E+06
11	NIMS 4	S55C	8.6E+05	6.1E+05	3.9E+06	7.8E+05	1.5E+06
12	NIMS 10	SNC631	1.2E+06	1.8E+06	2.9E+06	6.3E+05	1.6E+06
13	NIMS 13	SUS 403	1.7E+06	1.3E+06	5.5E+06	8.9E+05	2.4E+06
14	NIMS 1	S25C	3.9E+06	8.4E+05	6.2E+06	4.9E+06	4.0E+06
15	NIMS 14	SUS 430	5.3E+06	3.3E+06	8.2E+06	2.8E+06	4.9E+06

7.1.6. Homogeneity of the microstructure

With a single microstructure, the theoretical analysis is easier, since biphasic steels (e.g. ferritic-perlitic), if they have a large amount of hard phase, the effect at mean stresses is severely detrimental: e.g. S25C Normalized steel (also normalized 1045, where the effect should be greater).

In martensitics, in theory there is only one phase, but the martensite content depends on the heat treatment and the alloying elements. A drop in hardness inside the specimen would indicate a certain percentage of retained austenite.

The ideal critical diameter is the maximum diameter for which we would obtain a percentage of 50% martensite. The higher the DI, the higher the percentage of martensite. Table 7-7 shows the critical diameters for hardened steels:

Table 7-7. *Values of ideal critical diameters [Nishijima, 1993]*

Steel	Typical composition	D_I (mm)
S25C	0.25C	4
S35C	0.35C	5
S45C	0.45C	5
S55C	0.55C	6
SMn438	0.38C-1.5Mn	35
SMn443	0.43C-1.5Mn	37
SCr440	0.40C-1Cr	72
SCM435	0.35C-1Cr-0.2Mo	98
SCM440	0.40C-1Cr-0.2Mo	110
SNC631	0.31C-2.7Ni-0.8Cr	78
SNCM439	0.39C-1.8Ni-0.8Cr-0.2Mo	150
SNCM447	0.47C-1.8Ni-0.8Cr-0.2Mo	165

This effect is shown in Figure 7-3, showing the most important hardness reduction for steels with an ideal critical low diameter:

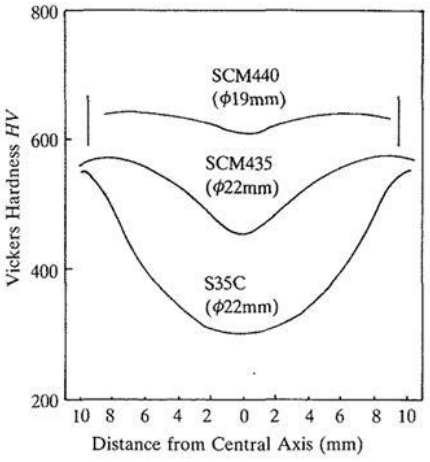

Figure 7-3. *Typical Vickers hardness after hardening as a function of depth [Nishijima, 1993]*

With respect to stainless steels, known as SUS in the Japanese standard, we find a variety of microstructures:

- SUS 403: duplex with martensite and ferrite.
- SUS 430: highly ferritic, not having undergone martensitic tempering.
- SUS 304: almost completely austenitic, approximately 94% austenite, 6% ferrite

To determine the phases in the stainless steels, we use the Schaffler diagram, see Figure 7-4:

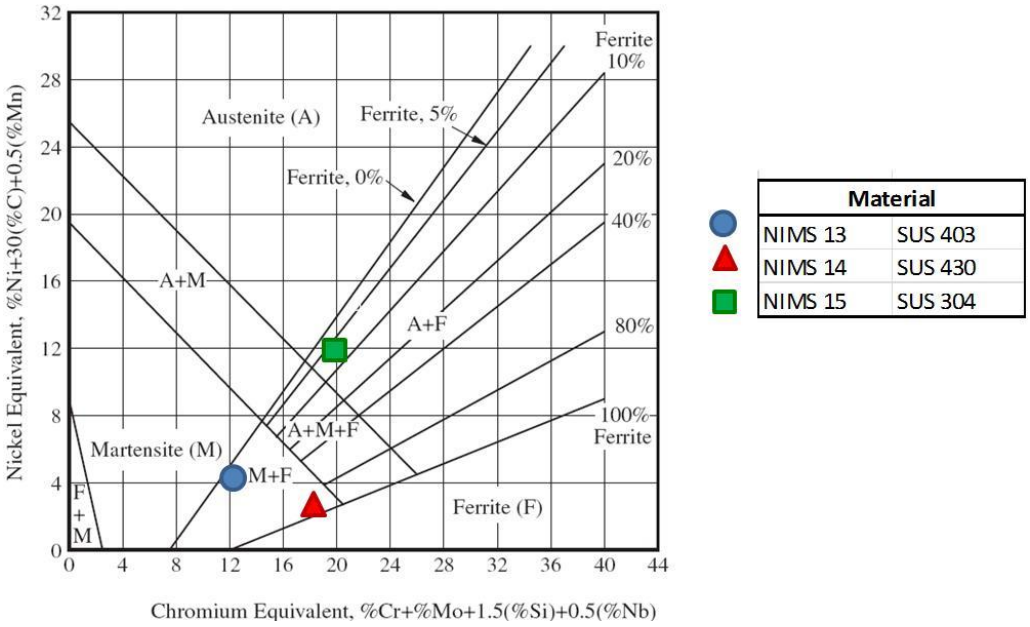

Figure 7-4. *Schaffler diagram for NIMS stainless steels*

7.1.7. Selection of the material

After having analysed the five previous criteria, and without giving priority to one over the other, Table 7-8 shows the ranking of NIMS steels in order of susceptibility, taking into account and arithmetically the respective rankings in each of the five individual criteria:

Table 7-8. *Rankings in each of the five criteria and average index*

			Ranking en cada uno de los 5 criterios					
nº	Nombre ensayo	Material	Criterio 1 $> M_\sigma$ & M_τ	Criterio 2: >Elasticidad σ_m	Criterio 3: $< N_t$	Criterio 4: $< N_{endurance}$	Criterio 5: Unicidad estr.	Indice promedio
1	NIMS 11	SNCM439	2	1	3	6	4	3.2
2	NIMS 9	SCM440	7	6	1	2	5	4.2
3	NIMS 12	SNCM447	6	3	2	8	3	4.4
4	NIMS 7	SCr440	11	5	5	3	8	6.4
5	NIMS 6	SMn443	8	4	7	5	9	6.6
6	NIMS 8	SCM435	13	2	4	10	6	7.0
7	NIMS 3	S45C	4	7	10	7	12	8.0
8	NIMS 2	S35C	5	8	12	4	13	8.4
9	NIMS 15	SUS 304	15	14	13	1	1	8.8
10	NIMS 10	SNC631	9	10	6	12	7	8.8
11	NIMS 14	SUS 430	1	15	15	15	1	9.4
12	NIMS 4	S55C	10	11	8	11	11	10.2
13	NIMS 5	SMn438	12	12	9	9	10	10.4
14	NIMS 13	SUS 403	3	13	11	13	14	10.8
15	NIMS 1	S25C	14	9	14	14	14	13.0

In particular, SNCM439 seems to be the most suitable steel for carrying out the test campaign, being a steel with high sensitivity to mean stresses, a good range of elastic behaviour, a number of cycles at the fatigue limit not too high, and with a good uniqueness of its microstructure. The European equivalent of this Japanese steel according to the German steel guide Stahlschlüssel is 34CrNiMo6 steel, which will be used for the test campaign.

7.2. Selected material: DIN 34CrNiMo6 steel

7.2.1. Chemical properties and microstructure

The material that was used in this fatigue campaign was high-strength 34CrNiMo6 steel that was provided by Thyssen–Krupp in 30-mm cross-section diameter forged bars. The heat treatment consisted of normalization at 900°C, followed by quenching in oil and tempering at 570°C. The resulting microstructure was ductile-tempered martensite. The certified chemical composition is presented in Table 7-9.

Table 7-9. *Chemical composition of 34CrNiMo6 steel (at.%)*

C	*Si*	*Mn*	*P*	*S*	*Cr*	*Mo*	*Ni*	*Fe*
0.345	0.275	0.710	0.0075	0.003	1.565	0.237	1.565	Balance

This steel shows a homogenous microstructure that is comprised of fine tempered martensite, with a banded orientation of the inclusions in the longitudinal section that are not visible in the transverse section (Figures 7-5a and 7-5b). As it was observed in other previous investigations related to the 34CrNiMo6 steel, porosity and many inclusions of manganese sulphide and alumina with different sizes were found [Branco 2012], [Branco, 2016], being round-shaped and small, with maximum defect size equal to $\sqrt{area} \approx 5$ μm.

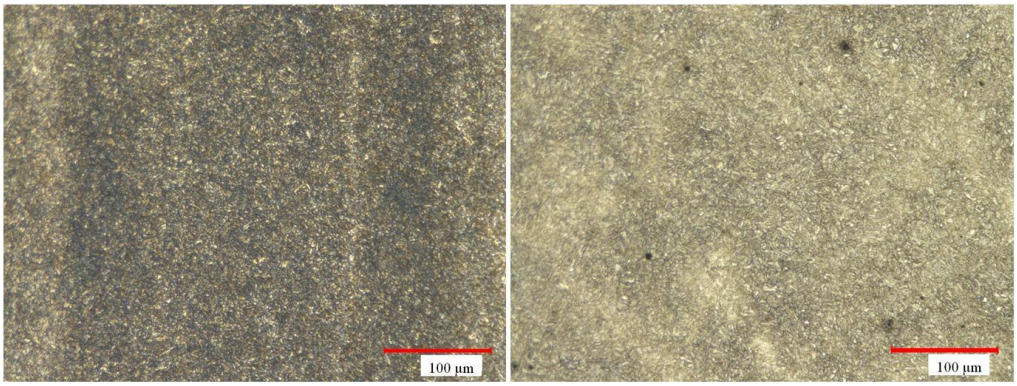

Figure 7-5. *Microstructure of 34CrNiMo6 steel* ***a.*** *Longitudinal section* ***b.*** *Transverse section*

7.2.2. Monotonic mechanical properties

Static tests showed that this 34CrNiMo6 steel with quenching and tempering exceeds 1200 MPa of ultimate tensile strength σ_{UTS}, which places it among the high strength steels, but maintaining excellent ductile properties.

Table 7-10. *Individual monotonic tests*

No.	$\sigma_{yp\ 0.2}$	σ_{UTS}	A (5d) (%)	Z (%)
1	1100	1203	11.6	58
2	1071	1215	12.1	63
3	1085	1218	12.5	60
4	1074	1208	11.8	60
5	1105	1209	12.6	58
6	1068	1200	12.5	62
Media	1083.83	1208.83	12.18	60.17

Six tests were performed and the properties of yield strength σ_{YP}, ultimate strength σ_{UTS}, elongation at break *A (5d)* and reduction of area Z were obtained, as shown in Table 7-10, where the monotonic mechanical properties and their mean values for this steel are given.

7.3. Design and calculation of a multiaxial fatigue campaign

This section will show the design and calculation of a multi-axial fatigue test campaign. The first premise will be to look for all possible effects, although giving absolute priority to cyclic torsion tests with average static torsion.

With the support of the statistical program MINITAB, a Design of Experiments (DOE), can be generated. This tool allows to generate campaigns automatically and combining different effects so that subsequently the response can be post-processed and mathematically modelled.

In this way, the campaign proposal shown in Table 7-11 was generated, where the green data are inputs and the blue data are outputs. The original campaign has up to 17 different tests. However, due to limitations regarding the available time of machine use, only pure torsion and uniaxial tests were performed within this Thesis, but the remaining group of tests can be performed in later campaigns.

It must be noted that the final axial and torsional fatigue tests were not conducted with exactly the same levels of mean stress. In the case of the pure torsional fatigue, it was decided to extend the campaign to search for a mathematical relationship for the amplitude and mean value of the shear

stresses, so that torsional fatigue tests with high values of the static torsional load were performed.

Table 7-11. *Design of a multiaxial fatigue campaign with various combinations of stress. Legend: Green colour means a fixed value; Blue indicates a test result*

Test No.	Description	$\sigma_{xx\,a}$	$\sigma_{xx\,m}$	$\tau_{xy\,a}$	$\tau_{xy\,m}$	δ_{xy}	Parameter obtained
1	Axial R = -1	σ_{-1}	0	0	0	---	σ_{-1}
2	Axial R = 0	$\sigma_{a\,0}$	$\sigma_{m\,0}$	0	0	---	σ_0
3	Axial σ_m=-500 MPa	$\sigma_{a\,m\text{-}500}$	-500	0	0	---	
4	Axial σ_m= 500 MPa	$\sigma_{a\,m500}$	500	0	0	---	
5	Axial R = -2	$\sigma_{a\,-2}$	$\sigma_{m\,-2}$	0	0	---	
6	Torsion R = -1	0	0	τ_{-1}	0	---	τ_{-1}
7	Torsion R = 0	0	0	$\tau_{a\,0}$	$\tau_{m\,0}$	---	τ_0
8	Torsion τ_m= 150 MPa	0	0	$\tau_{a\,m150}$	150	---	
9	Torsion τ_m= 250 MPa	0	0	$\tau_{a\,m250}$	250	---	
10	Interaction $\sigma_{xx\,m}$ (+) & $\tau_{xy\,a}$	0	500	X_{10}	0	---	
11	Interaction $\sigma_{xx\,m}$ (-) & $\tau_{xy\,a}$	0	-500	X_{11}	0	---	
12	Interaction $\sigma_{xx\,a}$ & $\tau_{xy\,m}$	X_{12}	0	0	250	---	
13	Interaction $\sigma_{xx\,a}$ & $\tau_{xy\,m}$	X_{13}	0	0	500	---	
Extra 1	Interaction $\sigma_{xx\,a}$ & $\tau_{xy\,a}$ (δ_{xy} = 0º)	X_{extra1}	0	$\tau_{a\,m250}$	0	0	
Extra 2	Interaction $\sigma_{xx\,a}$ & $\tau_{xy\,a}$ (δ_{xy} = 90º)	X_{extra2}	0	$\tau_{a\,m250}$	0	90	
Extra 3	Interaction $\sigma_{xx\,a}$ & $\tau_{xy\,a}$ & $\tau_{xy\,m}$ (δ_{xy} = 0º)	X_{extra1}	0	X_{extra3}	250	0	
Extra 4	Interaction $\sigma_{xx\,a}$ & $\tau_{xy\,a}$ & $\tau_{xy\,m}$ (δ_{xy} = 90º)	X_{extra2}	0	X_{extra4}	250	90	

Before the start of the torsional fatigue campaign, all the procedure was documented in order to follow the JSME method based on the ISO standard [ISO, 2012]. Therefore, all the stress values had to be calculated in order to take advantage of the available time using the torsional fatigue machine in Bordeaux. The calculations of the stress levels were performed for all the 17 load cases of Table 7-11 with the Robert critical plane and the empirical correlations presented in Chapter 2.

In Table 7-12, the experimental procedure for the pure torsional fatigue tests is presented. The executing order indicates that the higher stress levels should be performed first. Once the slope and standard deviation of the S-N curve are calculated with 4 levels of stress (8 specimens) by means of the ISO standard [ISO, 2012], the staircase can be performed.

Table 7-12. *Experimental procedure for the S-N curves and fatigue limits of pure torsional fatigue*

Pure Torsional Fatigue Tests			**Curve 6** $\tau_m = 0$ **MPa**	**Curve 8** $\tau_m = 150$ **MPa**	**Curve 9** $\tau_m = 250$ **MPa**
Executing order	**No. of specimens**	**No. of cycles (-20%,+20%)**	τ_a **(MPa)**	τ_a **(MPa)**	τ_a **(MPa)**
1^{st}	2	$4x10^4$	510	490	480
2^{nd}	2	10^5	480	460	450
3^{rd}	2	$3x10^5$	450	430	420
4^{th}	2	$7x10^5$	420	400	390
5^{th}	1^{st} RunOut	$> 2x10^6$	390	370	360
6^{th}	5	Staircase $2x10^6$	Staircase $2x10^6$	Staircase $2x10^6$	Staircase $2x10^6$

The same experimental procedure has been designed for the other load cases, taking into account the appropriate step between different levels, which has been calculated with the aid of the correlations for S-N curves presented in Chapter 2 and the Robert method, which has been applied iteratively for the load cases of Tables 7-13 and 7-14.

Table 7-13. *Experimental procedure for the S-N curves and fatigue limits of mean axial + reversed torsional fatigue tests*

Mean axial + Reversed Torsional Fatigue Tests			**Curve 10** σ_m **= +500 MPa Tension**	**Curve 11** σ_m **= -500 MPa Compression**
Executing order	**No. of specimens**	**No. of cycles (-20%,+20%)**	τ_a **(MPa)**	τ_a **(MPa)**
1st	2	$4x10^4$	380	470
2nd	2	10^5	350	440
3rd	2	$3x10^5$	320	410
4th	2	$7x10^5$	290	380
5th	1st RunOut	$> 2x10^6$	260	350
6th	5	Staircase $2x10^6$	Staircase $2x10^6$	Staircase $2x10^6$

Table 7-14. *Experimental procedure for the S-N curves and fatigue limits of mean torsion + reversed axial fatigue tests*

Mean Torsion + Reversed Axial Fatigue Tests			**Curve 12** τ_m **= 250 MPa**	**Curve 13** τ_m **= 500 MPa**
Executing order	**Number of specimens**	**No. of cycles (-20%,+20%)**	τ_a **(MPa)**	τ_a **(MPa)**
1st	2	$4x10^4$	640	530
2nd	2	10^5	610	500
3rd	2	$3x10^5$	580	470
4th	2	$7x10^5$	550	440
5th	1st RunOut	$> 2x10^6$	520	410
6th	5	Staircase $2x10^6$	Staircase $2x10^6$	Staircase $2x10^6$

7.4. Axial fatigue tests

7.4.1. Specimens

Fatigue tests were performed on standard hourglass specimens whose dimensions are given in Figure 7-5. As it was pointed out by other authors [Davoli, 2003], hourglass geometry promotes the concentration of failures in a very limited area of the specimen, so that the scatter is reduced.

The specimens were designed and manufactured following the recommendations of ASTM E-466 [ASTM, 2015]. A final average roughness R_a = 0.03 µm was measured.

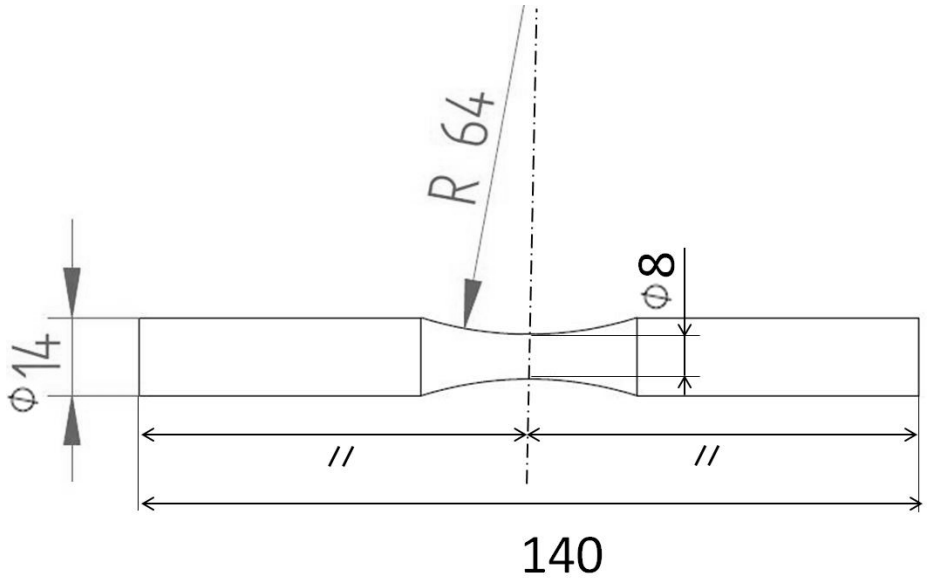

Figure 7-6. *"Hourglass" specimen used in axial fatigue tests. Dimensions in millimetres [Pallarés, 2018A]*

7.4.2. Testing machinery of axial fatigue campaign

Fatigue tests were performed in the laboratories of the Department of Mechanical Engineering of the UPV/EHU (Spain), on a servo-hydraulic axial fatigue machine Instron 8805 MTB (Figure 7-6), with a maximum available axial force of 100 kN. The tests were performed at a frequency of 20 Hz. The run-out was fixed at $2 \cdot 10^6$ cycles. The failure criterion was defined as a 10% loss in rigidity of the specimen.

Figure 7-7. *Instron 8805 MTB axial fatigue machine located at the E.T.S. de Ingenieros de Bilbao [Avilés, 2018]*

7.4.3. Experimental results on axial fatigue

An axial fatigue campaign with four different stress ratios $R_\sigma=\sigma_{min}/\sigma_{max}$ has been performed, namely R = -2, -1, -0.5 and 0.05, with a total number of 75 specimens considering all the tests. Tests were stopped at a maximum fatigue life of $2x10^6$ cycles, taking into account the recommendations for the number of cycles of the fatigue limit for this type of steel [Sonsino, 2017].

The full S-N curves (P=50%) were adjusted with the well-known Basquin formulation in the form $N=\alpha\cdot\sigma^\beta$ (α and β values in Table 7-15) commonly used in modern fatigue investigations with quenched and tempered steels as in [Li, 2017]. In Figure 7-7 the S-N curves for the different stress ratios are presented, showing a measurable effect of the mean stresses for all the range of fatigue lives: $2x10^4 < N < 2x10^6$ cycles. The ASTM E 739 standard [ASTM, 2004] has been used to obtain the Basquin parameters. The standard deviation of the fatigue curves is within the range 10-15 MPa for all the stress ratios. Thus, the staircase method according to ISO 12107:2012 [ISO, 2012] with a step of 10 MPa has been adopted for obtaining the fatigue limits.

As it can be observed in Figure 7-8, the S-N curve for R = 0.05 has a small slope, which is due to the fact that the fatigue limit has a stress amplitude of 472 MPa and a mean stress of 522 MPa. Therefore, the maximum stress is equal to 990 MPa, while σ_{YP} is 1,084 MPa. Thus, there is only a margin of about 90 MPa for the inclined part of the S-N curve.

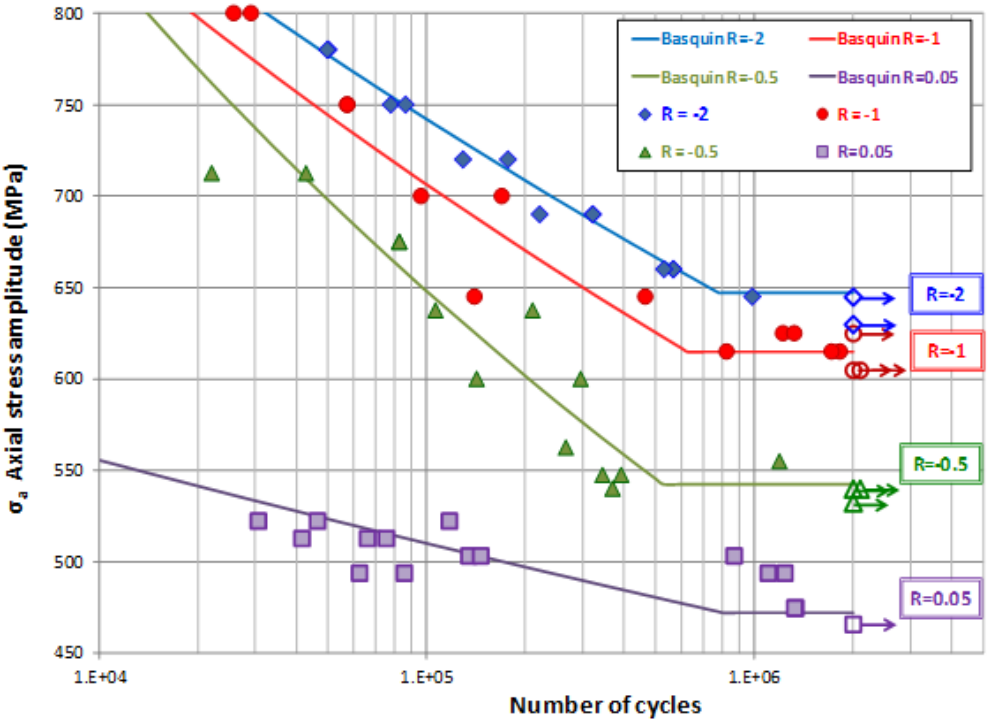

Figure 7-8. *Experimental S-N fatigue curves of DIN 34CrNiMo6 steel for different stress ratios (R) [Pallarés, 2018A]*

Table 7-15. *Obtained fatigue strengths at $2x10^6$ cycles for the different stress ratios together with the α and β Basquin parameters of the inclined part of the S-N curves*

σ_m (MPa)	σ_a (MPa)	R (stress ratio)	α	β
-216	647	-2	1.14×10^{48}	-15.000
0	615	-1	4.61×10^{42}	-13.220
181	542	-0.5	1.79×10^{31}	-9.338
522	472	0.05	6.37×10^{77}	-26.889

The results for $2x10^6$ cycles are plotted in a Haigh diagram, see Figure 7-9. A 2nd order polynomial line was used to fit the experimental results, showing a good agreement with them. The results show that the effect of the mean axial stress takes a great role in the fatigue strength. As it was shown in Figure 7-9 for other ductile materials, the results of the 34CrNiMo6 show a concave downward shape function in the Haigh diagram.

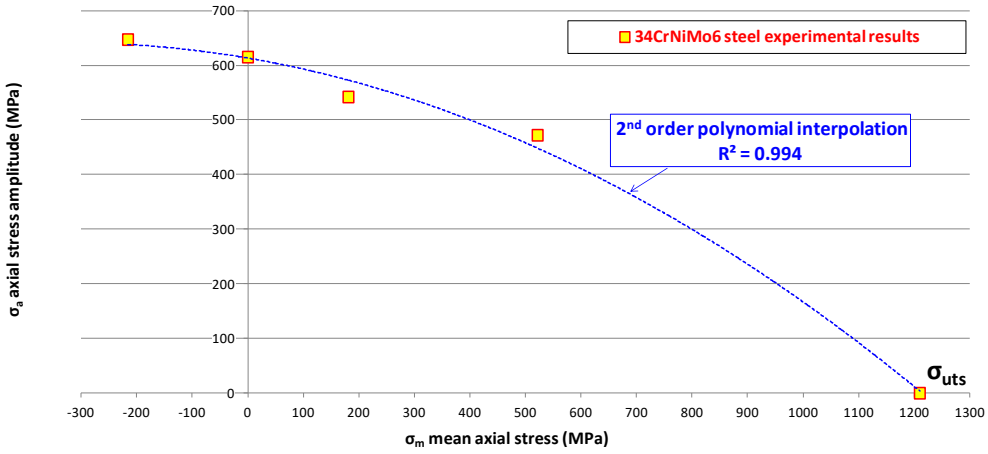

Figure 7-9. *Haigh diagram with the experimental results at $2x10^6$ cycles and a 2nd order polynomial interpolation showing a concave downward shape.*

7.4.4. Fractographic analysis

Fractographic analysis is not essential for the quantitative purposes of this work, but it enables to observe the planes of failure and the nature of the fatigue failure. Several previous works have dealt with this particular steel, such as the works of Branco et al. in [Branco, 2012], [Branco, 2016].

As usually observed in the HCF region, crack initiation occurred at the very late stage of the fatigue life: a macroscopic crack was not observed until very few cycles before the final fracture. For number of cycles exceeding one million, initiation was produced in general at the surface for the stress ratios R = -2, R = -1, R = -0.5, and R = 0.05 (Figure 7-10).

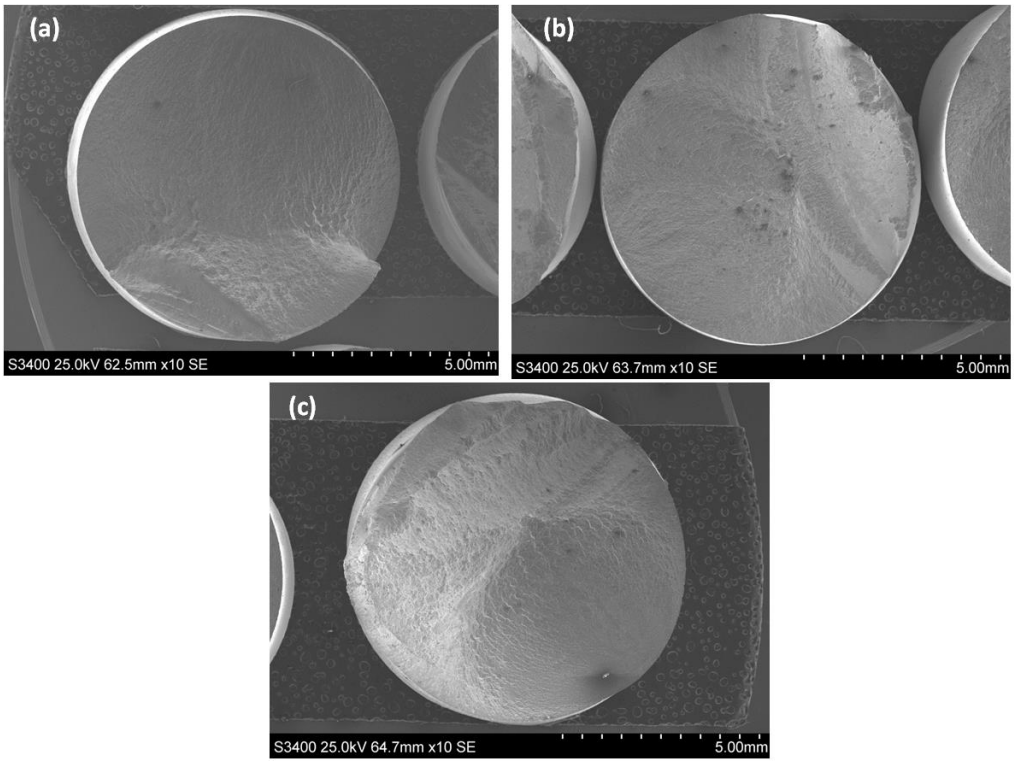

Figure 7-10. *Specimen microscopic cross-section fractures, showing initiation in the surface for the following cases:* ***(a)*** *R=-2; σ_a= 440 MPa; σ_m= 0 MPa; Ncycles=986,700;* ***(b)*** *R=-1; σ_a= 430 MPa; σ_m= 0 MPa; Ncycles=1,722,153;* ***(c)*** *R=-0.5; σ_a= 430 MPa; σ_m= 0 MPa; Ncycles=1,193,924 [Pallarés, 2018A]*

However, Figure 7-11 shows a deep subsurface initiation in an inclusion, which failed about 10^6 cycles in a R = 0.05 axial test. This failure mode is prone to appear with an increase in the stress ratio in the axial loading, as reported in [Gaur, 2016]. Moreover, a crack initiation beneath the surface is unlikely in rotating-bending tests due to the gradient of the stress field, characteristic of the bending load. Other authors have reported dissimilar behaviours between axial and rotating bending loading [Sakai, 2016], remarking that the high cycle failure for rotating bending loading takes place in the surface, and that the internal defects can only create damage for very high cycle fatigue loadings.

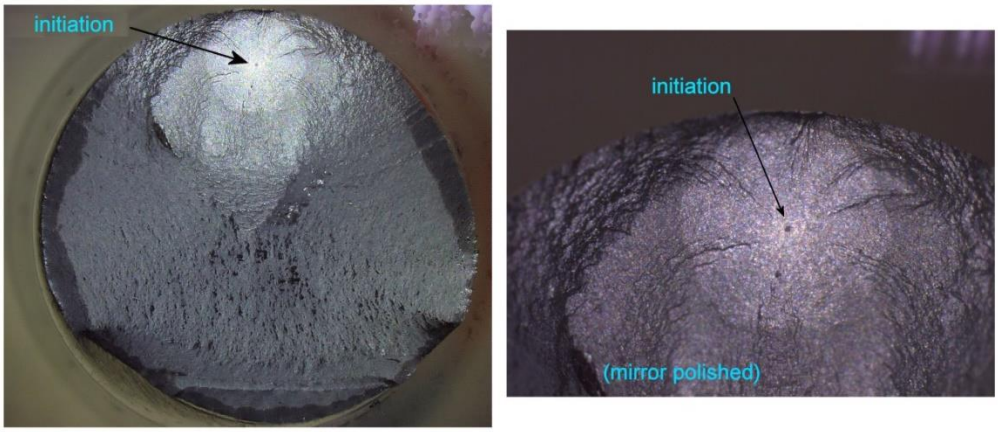

Figure 7-11. *Fatigue fracture cross-section of a test specimen after 1,101,291 cycles with a maximum stress σ_{max}=1,040 MPa in a R=0.05 axial test [Pallarés, 2018A]*

The propagation took place in planes approximately corresponding to the maximum shear stress amplitude plane, corresponding to an inclination of 45° to the axis of the specimen (Figure 7-12).

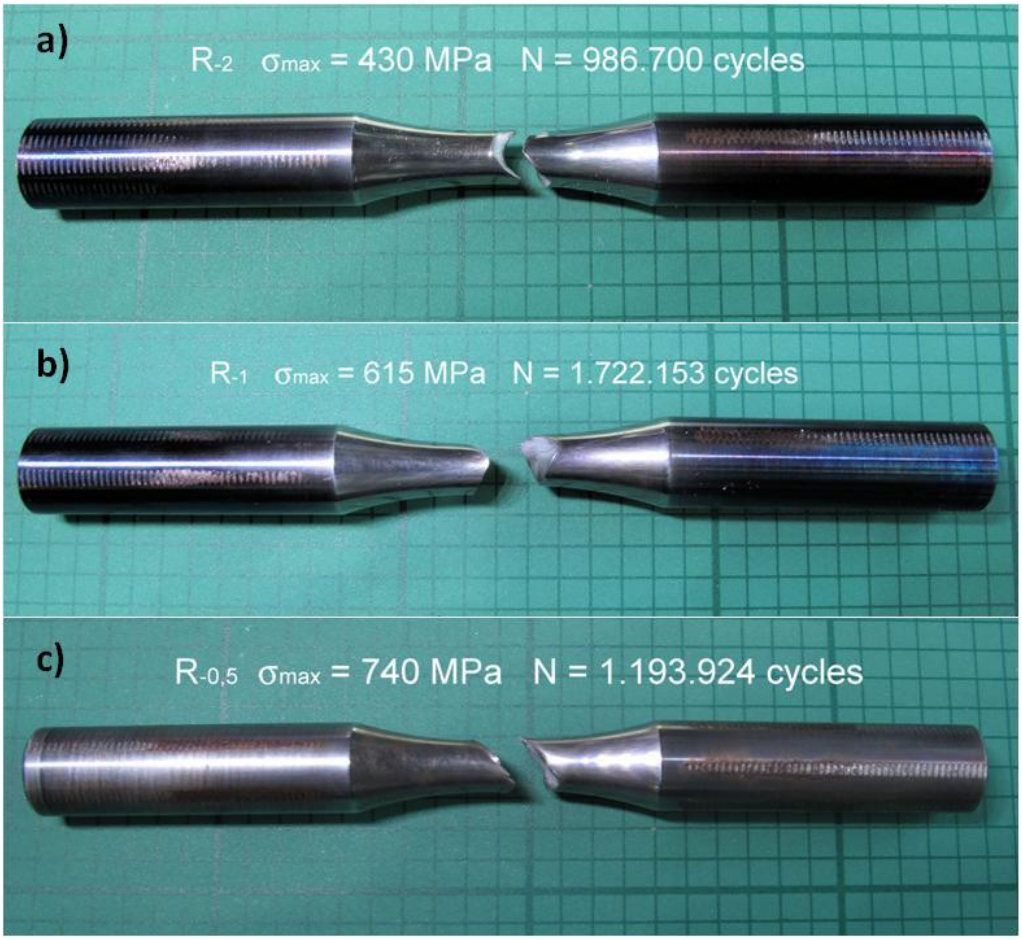

Figure 7-12. *Fatigue Specimen macroscopic fractures at:* ***(a)*** *R=-2;* σ_a*=440 MPa;* σ_m*=0 MPa; Ncycles=986,700;* ***(b)*** *R=-1;* σ_a*=430 MPa;* σ_m*=0 MPa; Ncycles=1,722,153;* ***(c)*** *R=-0.5;* σ_a*=430 MPa;* σ_m*=0 MPa; Ncycles=1,193,924 [Pallarés, 2018A]*

7.5. Torsional fatigue tests

7.5.1. Specimens

Fatigue tests were performed on standard hourglass specimens whose dimensions are given in Figure 7-13. Hourglass-shaped specimens were chosen because this geometry allows for the concentration of failures in a limited specimen area and reduces the scatter. Similar specimens have been used in previous campaigns in quenched and tempered steels, as in [Davoli, 2003]. The value of the stress concentration factor in torsion k_{tt} is lower in this case than in the cited campaign, and a value of $k_{tt} = 1.03$ has been obtained according to the Peterson formulas for stress concentration [Peterson, 1974].

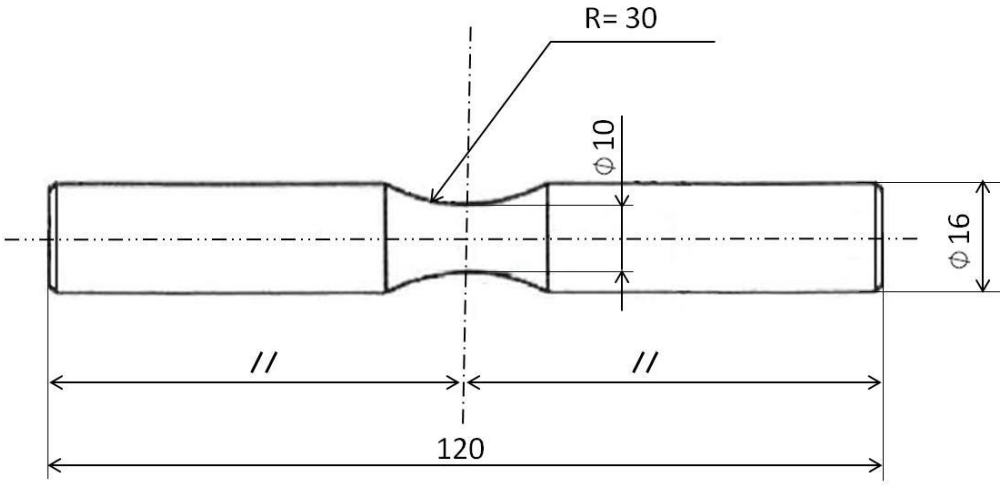

Figure 7-13. *"Hourglass" specimen used in torsional fatigue tests. Dimensions in millimetres [Pallarés, 2018B]*

The specimens were manufactured according to the recommendations of ASTM E-466 [ASTM, 2015]. After the machining processes, the following residual stresses were measured at the surface of the machined specimens: −340 MPa in the tangential direction and −280 MPa in the longitudinal direction. The machined specimens were subjected to a stress-relieve heat treatment at 190°C for 24 h to reduce residual stresses that were induced by machining, following the procedure of Nascimento et al. [Nascimento, 2001] to avoid Tempered Martensite Embrittlement (TME). This stress relieving process allowed to reduce the residual stresses of the machined specimens to -250 MPa in the tangential direction and -220 MPa in the longitudinal direction. These stresses disappear within 10 µm in depth direction. The final process was a conventional polishing with progressively finer emery papers from P800 to P4000, to obtain a mirror finish. The residual stresses of the polished specimens were measured at the surface, taking a value of -30 MPa in the longitudinal and tangential directions. A final average roughness R_a = 0.03 µm was measured.

7.5.2. Testing machinery of the torsional fatigue campaign

Fatigue tests were performed in the laboratories of the ENSAM at the Bordeaux campus (France), on a servo-hydraulic bending-torsion fatigue machine with multiple actuators, a maximum available torque of 150 N·m and at 50 Hz. This testing machine, named as *"LISE"* and shown in Figure 7-14, was used previously in other multiaxial fatigue campaigns, such as the one performed by Froustey [Froustey, 1989].

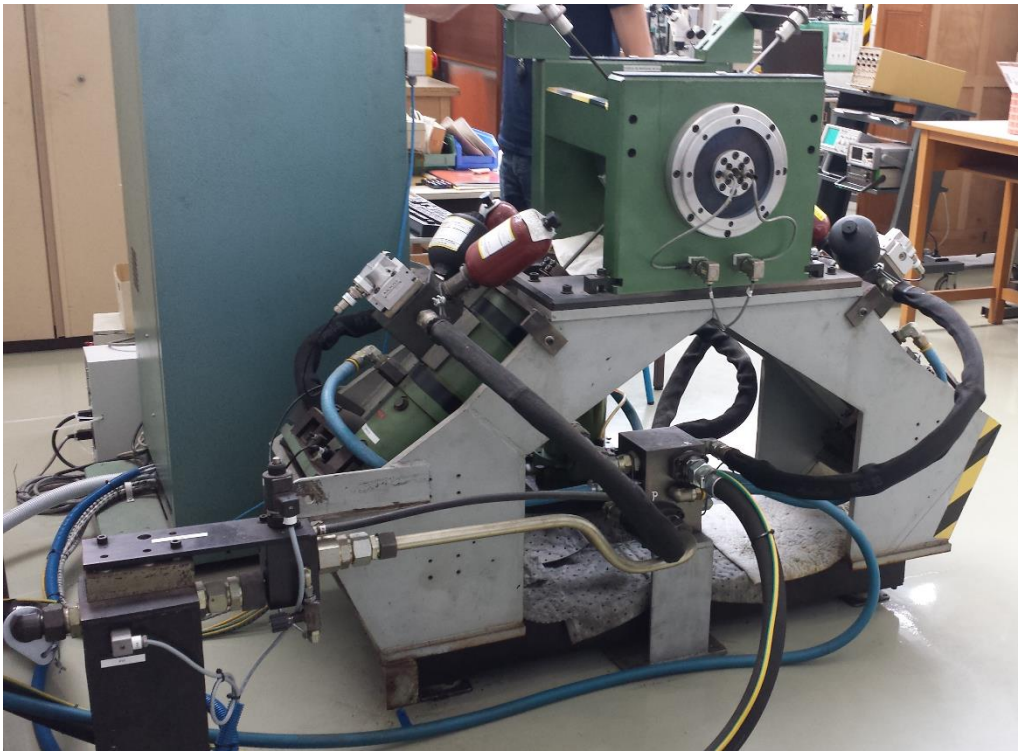

Figure 7-14. *"LISE" machine used in the torsional fatigue campaign*

The bending moment was controlled during the tests and was set to 0.0 N·m to ensure that the loading case was pure torsion. The run-out was fixed at 2×10^6 cycles, according to the recommendations for this type of steel [Sonsino, 2007]. The failure criterion was defined as a 10% loss in specimen rigidity, as was conducted in other similar campaigns of torsional fatigue with mean shear stresses [Davoli, 2003]. This enabled the test to be interrupted with cracks of an approximately 0.5-mm depth on 10-mm-diameter specimens.

7.5.3. Experimental results

A fatigue campaign of torsional fatigue with five levels of mean shear stresses has been performed, namely τ_m = 0, 150, 250, 350 and 500 MPa, with a total number of 83 specimens considering all the tests. Tests were stopped at a maximum fatigue life of 2×10^6 cycles, based on the recommendations for the number of cycles of the fatigue limit for this type of steel [Sonsino, 2007] and a previous campaign of a similar material [Findley, 1989]. The inclined part of the S–N curves and the subsequent staircases were determined following the ISO standard method [ISO, 2012]. This procedure enables to optimise the number of specimens, so that the first run-out for the inclined part of the S-N curve can be used to start the staircase process. For the superimposed static shear stress of τ_m = 500 MPa, the slope of the S–N curve was nearly horizontal, so testing was limited to the staircase. In Figure 7-15, torsional the S–N curves are presented, and show a measurable effect of the mean shear stresses for the entire fatigue-life range: $5 \times 10^4 < N < 2 \times 10^6$ cycles.

Based on the recommendations of previous campaigns [Findley, 1953], the staircase for the fully reversed torsional fatigue limit τ_{-1} was performed with a higher number of specimens, as such data are usually used to adjust the multiaxial fatigue methods, and therefore they are convenient to reduce the uncertainty. The obtained values of the torsional fatigue strengths at 2×10^6 cycles are shown in Table 7-16.

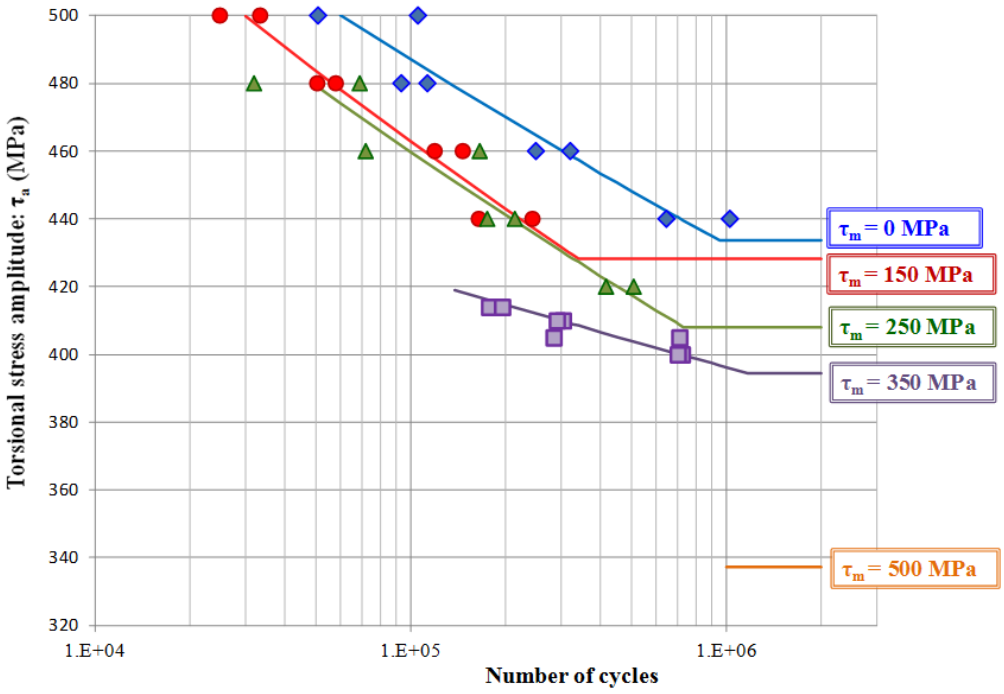

Figure 7-15. *Torsional S-N curves with different leves of mean shear stress [Pallarés, 2018B]*

Table 7-16. *Obtained torsional fatigue strengths at 2×10^6 cycles*

τ_m (MPa)	τ_a (MPa)	Standard Deviation (MPa)	No. Specimens (staircase)
0	432.5	7	15
150	428.6	5	7
250	409.1	7	7
350	394.3	3	7
500	337.1	5	7

The results for 2×10^6 cycles are plotted in a Haigh torsional diagram, Figure 7-16, and are interpolated through a polynomial line. The results show that the effect of the mean shear stresses is negligible as long as the maximum shear strength τ_{max} is below the torsional yield strength τ_{yp}. The results show a convex upward function in the Haigh torsional diagram.

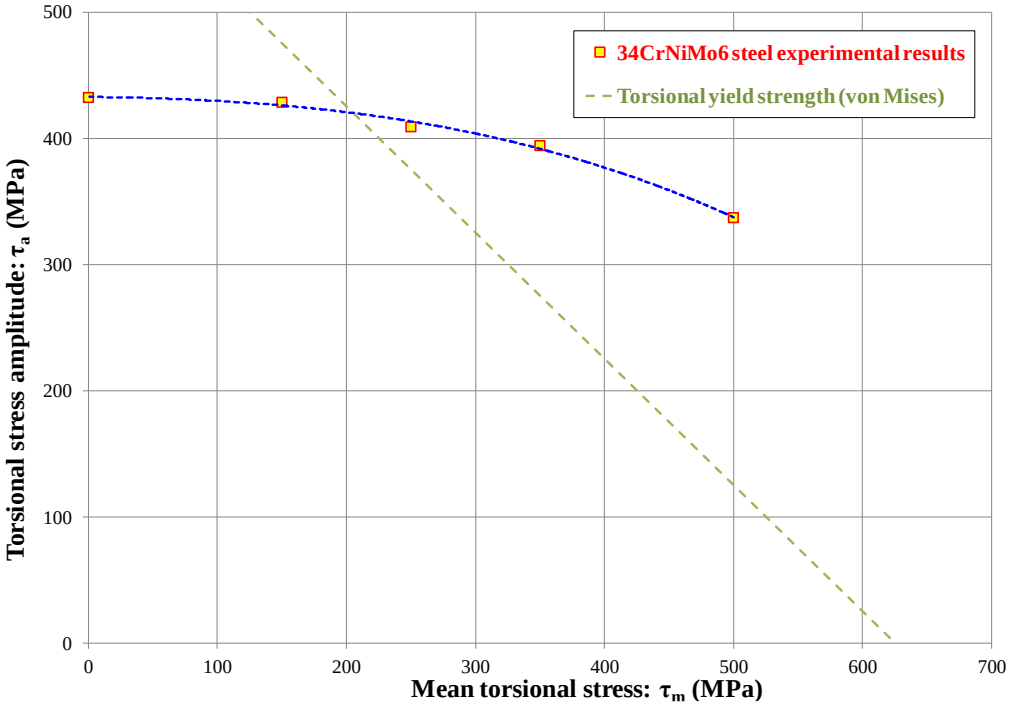

Figure 7-16. *Torsional Haigh diagram with the experimental results at 2×10^6 cycles [Pallarés, 2018B]*

7.5.4. Fractographic analysis

Fractographic analysis is not essential for the quantitative purposes of this work, but it allows for an observation of the planes of failure and the nature of the fatigue failure. As usually observed in the high cycle fatigue region [Davoli, 2003], crack initiation occurs at the very late stage of the fatigue life: a macroscopic crack was not observed until very few cycles before the final fracture. The number of initiated cracks increased with the level of cyclic torsional stresses. For instance, three or more initiated cracks existed for shear stress amplitudes that are equal to or higher than 480 MPa, irrespective of the mean shear stress that is applied.

Crack nucleation occurred in planes near the maximum shear stress planes for mean shear stresses up to 350 MPa, with maximum angular deviations of 15° (Figure 7-17). The cracks can be propagated in the maximum normal or maximum shear stress planes, irrespective of the mean shear stress that was applied. The phenomenon of crack branching was also observed.

However, a different pattern occurred for the 500-MPa mean-shear-stress loading case: in some specimens, the observed macroscopic crack was placed near the maximum principal stress plane (Figure 7-18). This observation can be explained through the aid of the mean shear stress in Mode I; stage-II crack growth has already been observed by other investigators [Wang, 1991], and is caused by an increase in maximum plastic zone size.

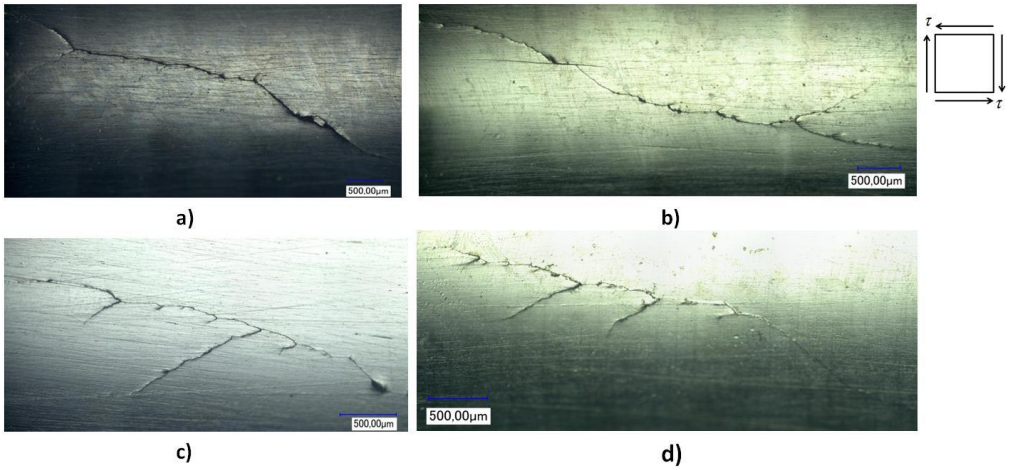

Figure 7-17. *Surface crack patterns in the failed specimens:* ***a)*** τ_a *= 440 MPa;* τ_m *= 0 MPa; Ncycles = 1,026,120* ***b)*** τ_a *= 430 MPa;* τ_m *= 150 MPa; Ncycles = 812,704* ***c)*** τ_a *= 440 MPa;* τ_m *= 250 MPa; Ncycles = 174,792* ***d)*** τ_a *= 405 MPa;* τ_m *= 350 MPa; Ncycles = 709,944 [Pallarés, 2018B]*

Figure 7-18. *Surface crack patterns in the failed specimen: τ_a = 340 MPa; τ_m = 500 MPa; Ncycles = 944,988 [Pallarés, 2018B*]

7.6. Mean axial and torsional stress sensitivities for the experimental campaign on DIN 34CrNiMo6 steel

As it was already mentioned in Chapter 4, the mean axial and torsional stress effects has been a subject of discussion in the multiaxial fatigue field. The Sines-Papadopoulos hypothesis states that the mean shear stress effect does not take place for a number of cycles exceeding 10^6.

In any case, most of the researchers agree that the mean axial stress effect is higher in torsion. In order to define the severity of the produced damage, the mean stress sensitivity index M was proposed by [Zenner, 2000] as the average slope of the Haigh diagram.

The sensitivity to the mean torsional stresses M_τ, defined as the slope of the Haigh diagram in torsion, can be calculated for the case of mean torsion of 350 MPa through equation (7-1).

$$M_\tau = \frac{\tau_{a(R=-1)} - \tau_{a(\tau_m=350)}}{350} \tag{7-1}$$

Similarly, the sensitivity to axial mean stresses M_σ can be calculated as the slope of the axial Haigh diagram, in this case using the data R=-1 and R=0.05 in equation (7-2):

$$M_\sigma = \frac{\sigma_{a(R=-1)} - \sigma_{a(R=0.05)}}{\sigma_{m(R=0.05)}} \tag{7-2}$$

Using equations (8-1) and (8-2) a representation of sensitivities to mean axial and shear stresses as a function of the number of cycles can be made, showing the values of M_σ and M_τ for the range 50,000 < Ncycles < 1,000,000 in Figure 7-19. As it can be seen, the sensitivity to axial mean stresses is notably higher than for shear mean stresses. In addition, both sensitivities decrease with the number of cycles [Pallarés, 2019].

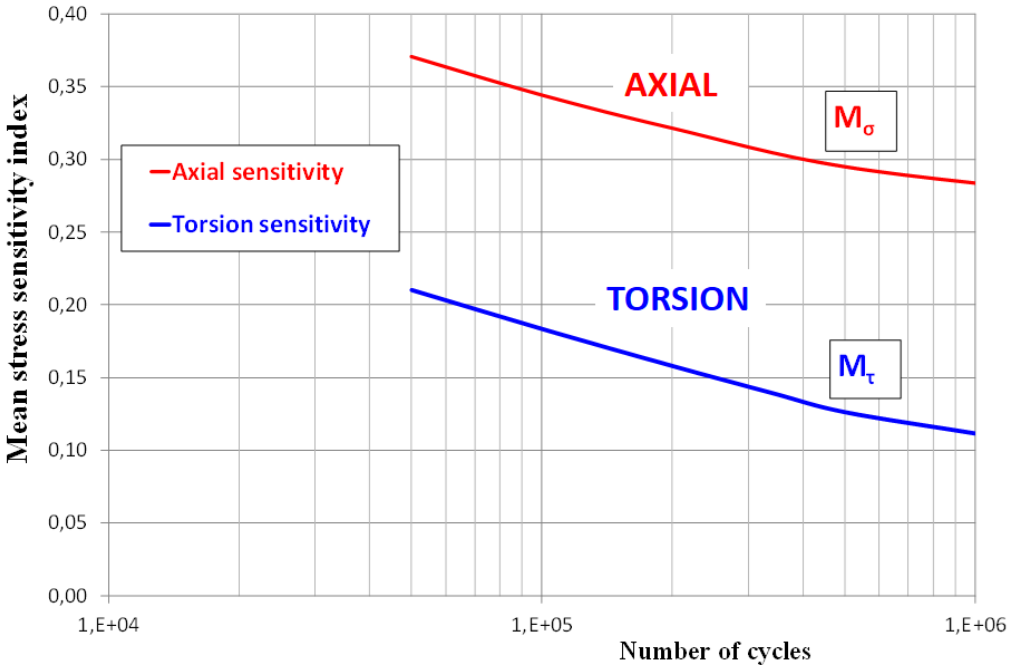

Figure 7-19. *Axial and mean shear stress sensitivity indices for the range 50,000 < Ncycles < 1,000,000 [Pallarés, 2019]*

7.7. Experimental agreement of multiaxial fatigue methods

7.7.1. Correlation of multiaxial fatigue methods with torsional fatigue tests

The experimental torsional fatigue results are represented in Figure 7-20 in a Haigh torsional diagram with different predictions from several multiaxial fatigue methods, namely the Marin stress invariants method, the Froustey energetic criterion and the Findley critical plane model, which offer analytic solutions for this load case.

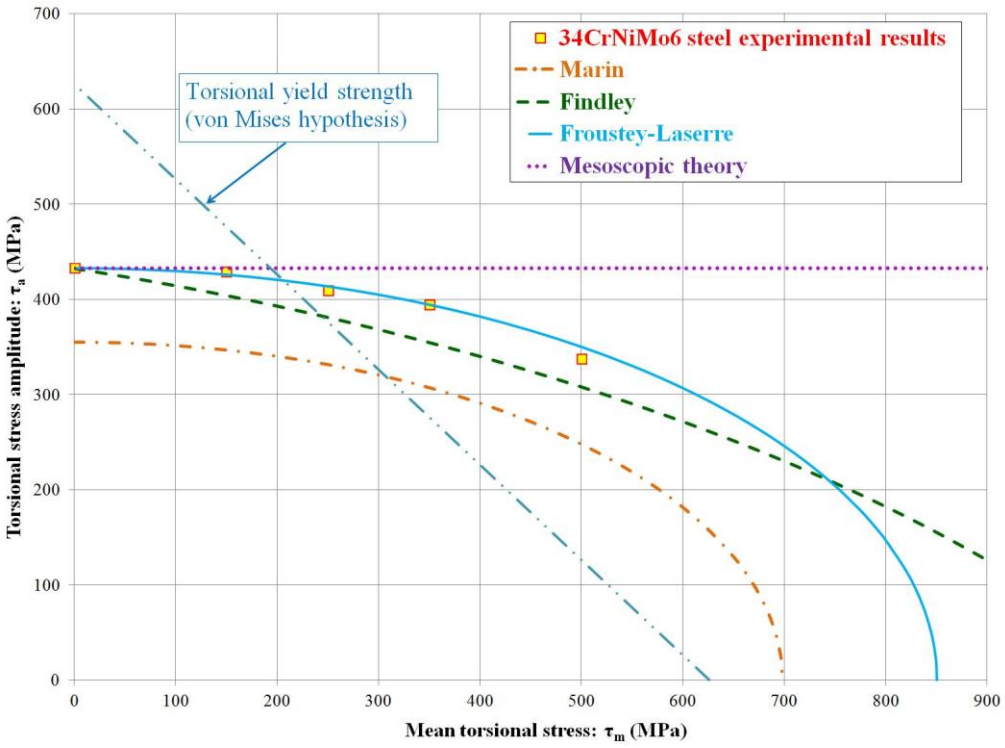

Figure 7-20. *Torsional Haigh diagram with predictions from various theories and experimental results at 2 x 10^6 cycles [Pallarés, 2018B]*

Table 7-17. *Relative errors of the multiaxial fatigue methods for torsional fatigue at 2×10^6 cycles [Pallarés, 2018B]*

Error in τ_a (%) at 2 x 10^6 cycles. (+) Conservative / (-) Non-conservative				
τ_m (MPa)	**Marin**	**Findley**	**Froustey**	**No effect hypothesis**
150	19.1	5.7	0.7	–0.9
250	19.0	6.9	-1.0	–5.7
350	22.1	10.0	0.0	–9.7
500	26.5	8.6	-3.8	–28.2

In Table 7-17, the relative errors (%) of the different theories are presented for N = 2 x 10^6 cycles. As observed, the Froustey–Lasserre method yields the best agreement with the experimental results from the selected methods. Marin's method shows a conservative behaviour because the von Mises relationship is not verified. Findley's method overestimates slightly the detrimental effect of the mean shear stresses for three out of four tests, which show good agreement with the experimental results and an error below 5% [Pallarés, 2018B].

The methods that not dependent on the mean shear stress effect, such as the Crossland method and the methodologies based on the mesoscopic approach, namely, the Dang Van critical plane, or the Papadopoulos integral method, agree for the only testing result below the torsional yield strength. For this case, the response is similar to the energetic method of Froustey–Lasserre, as claimed in [Morel, 2001]. However, the error increases for high mean torsional stresses.

7.7.2. Correlation of multiaxial fatigue methods with axial fatigue tests

In this section the correlation of the experimental results with different physical principles based theoretical models is analysed. Amongst these fatigue methods, the Crossland method, based on stress invariants, the Findley critical plane method, and the energetic approach based methods of Marin and Froustey will be considered. These methods take into account the effect of mean stresses, and can be easily expressed through analytic formulations for the axial case.

In Figure 7-20 the four different theoretical predictions by Findley, Marin, Froustey and Crossland are represented in a Haigh diagram together with the experimental results. As observed, none of the methods is able to successfully represent the fatigue behaviour with superimposed static stresses.

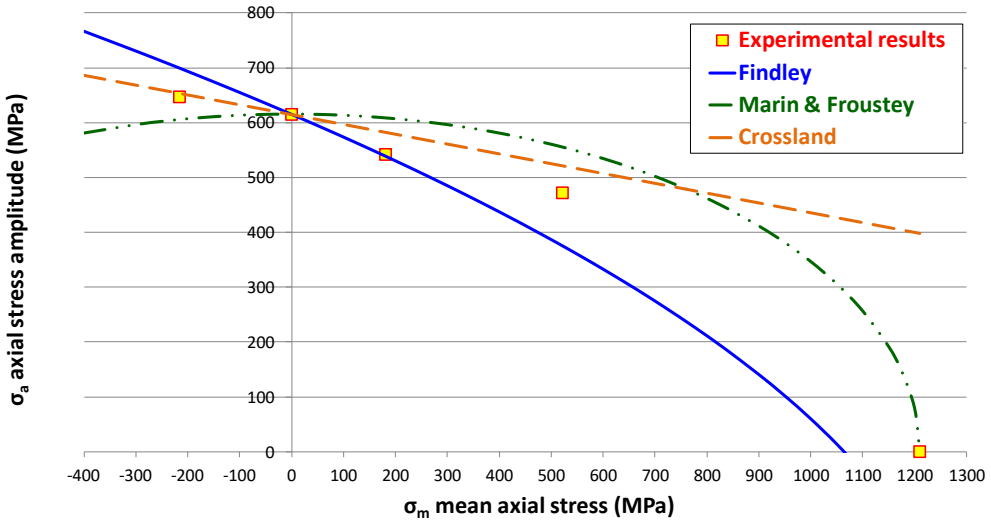

Figure 7-21. *Axial Haigh diagram with predictions from various theories and experimental results at 2 x 10^6 cycles [Pallarés, 2018A]*

Table 7-18. *Relative errors of the multiaxial fatigue methods for axial fatigue at 2×10^6 cycles [Pallarés, 2018A]*

Error in σ_a (%) at 2 x 10^6 cycles. (+) Conservative / (-) Non-conservative				
R_σ ($\sigma_{min}/\sigma_{max}$)	**σ_m (MPa)**	**Crossland**	**Marin, Froustey**	**Findley**
-2	-216	-1.0	6.5	-8.1
-0.5	181	-7.5	-12.2	0.6
0.05	522	-10.5	-17.6	20.5

In Table 7-18, the relative errors (%) of the different theories are presented for N=2x10^6 cycles. Marin's and Froustey's methods are non-conservative with mean tension loads, whereas they show a conservative behaviour in the mean compression loads region. It should be noted that the multiaxial fatigue methods predicted errors exceed the range [-10%, 10%].

The Crossland's method, which is the most accurate amongst these methods, shows a non-conservative behaviour for all the analysed cases. The Findley critical plane method is non-conservative for compression mean loads, and highly conservative for the R=0.05 case [Pallarés, 2018A].

7.8. Discussion

7.8.1. Selection of the material and design of the experimental campaign

The selection of the material was performed by using the most extensive database of steels [Nishijima, 1993] and taking into account 7 different criteria in order to ease the procedures of the experimental tests. The selected material is the SNCM439, which corresponds to the European DIN 34CrNiMo6 steel.

The design of the experimental campaign was performed with the aid of the Minitab software, which is able to deal with Design of Experiments. Before any fatigue test was performed, the test procedure and the stress levels were calculated with the Robert multiaxial fatigue method in order to take full advantage of the available time to perform the tests.

The full multiaxial fatigue campaign could not be performed due to limitations of time, so that the experimental work was focused on the mean axial and torsional effects.

7.8.2. Axial and torsional fatigue experimental campaigns

The torsional fatigue campaign was successfully performed in the laboratories of the ENSAM Bordeaux in the LISE machine. It was decided to further investigate the shape of the Haigh torsional diagram so that a mathematical expression could be inferred. This way, the S-N curves and torsional fatigue limits were determined for 5 different levels of mean torsional stresses, and an elliptical shape was fitted to the results. It was concluded that the mean shear stress effect takes place in high cycle fatigue, contrary to the postulates of the

Sines-Papadopoulos hypothesis. However, it must be noted that the effect is weak for maximum stresses below the torsional yield stress.

The axial fatigue campaign was performed in Bilbao at the laboratories of the Mechanical Engineering Department of the UPV/EHU. The S-N curves and axial fatigue limits were determined for 4 different levels of stress ratio, including mean axial tensile and compressive stresses. A concave downward shape was obtained, with a slight increase in the fatigue strength for moderate compressive mean stresses, resulting in a non-symmetrical Haigh axial diagram.

A comparison of the mean axial and torsional sensitivities was performed, showing that the effect is higher for axial fatigue and for a lower number of cycles.

7.8.3. Experimental agreement with multiaxial fatigue methods

The experimental results in axial and torsional fatigue were compared to the Crossland, Marin, Froustey and Findley methods, due to the fact that those methods can be expressed through analytic formulations for these load cases.

For the torsional fatigue case, the energetic method of Froustey is able to correctly fit the experimental results, with a maximum error of 3.8%. None of the other methods follow the trend of the experimental results.

For the axial fatigue case, none of the methods are adjusted to the shape of the Haigh diagram. The Crossland and Findley methods predict an increasing fatigue strength with the growth of the compressive mean stresses, whereas Marin and Froustey methods predict a symmetric Haigh diagram.

Chapter 8:

DEVELOPMENT OF TWO MULTIAXIAL FATIGUE METHODS

CHAPTER 8. DEVELOPMENT OF TWO MULTIAXIAL FATIGUE METHODS

8.1. Introduction

The works performed in the present Thesis started with the M.Sc. Thesis in Mechanical Engineering, presented in September 2012. From that date, to June 2016, all the data and the planification were focused towards the development of a multiaxial fatigue critical plane method. There were several reasons behind that reasoning, namely the excelent performance of the Papuga critical plane method, and the fact that improving the Findley's method with a non-linear formulation for the effect of the mean stresses was probably one of the easiest possible solutions to describe the multiaxial fatigue problem.

However, for June 2016 the provisional experimental results in pure torsion fatigue for the 34CrNiMo6 steel were leading to an elliptical shape in the Haigh diagram. Moreover, while attending the International Conference of Multiaxial Fatigue in Seville in 2016, I had several interesting discussions with Dr. Jan Papuga from the Czech Republic. He warned me about the extreme difficulty of the process of the adjustment of the parameters for the critical plane methods. He himself had experienced several negative experiences with the management of the algebraic problem, obtaining several solutions which were complex for some ranges of the parameters.

By September 2016, the experimental results for pure torsional fatigue loading case were completed, and the elliptic shape in the Haigh torsional diagram was

the most probable hypothesis: a near zero slope for zero mean stresses, an excellent agreement for all the tested torsional fatigue cases, and even the estimated static torsional strength according to Smith was in excellent agreement with the elliptic shape. That elliptic shape had been predicted in 1956 by Marin [Marin 1956], taking into account a balance of energy of distortion.

Therefore, the difficulties in the terms of the algebraic problem for the critical plane, and the fact the experimental results in torsion were not in optimal agreement led to the research in another direction: the energetic criteria. The starting point was the Marin method, presented in the 1st International Conference on Fatigue of Metals in 1956 together with Findley's and Crossland's methods.

Taking into account the discussion and a large database of experimental results, a local multiaxial fatigue criterion was devised, combining the concepts of Marin and Crossland so that both formulations were summarized in one theory which takes into account a balance of distortion energy and Gough's theory of fatigue damage based on the maximum damage by using the maximum hydrostatic stress along the cycle. This method was developed during summer and autumn 2017, when the axial tests had not been still fully completed.

After the development of the local multiaxial fatigue criterion, the focus was to develop an energetic criterion fully based on physical considerations, so that the method would be further developed in the future. This method was devised during early 2018, taking into account the extensive revision performed in Chapter 3 of the present Thesis. The proposed method can be interpreted as a balance of distortion and hydrostatic (change of volume) elastic energies.

8.2. Modelling of torsional fatigue with mean torsional stresses

An ellipse in the Haigh torsional diagram that fits the results of 34CrNiMo steel can be expressed through equation (8-1), which is a modification of the Marin criterion. In equation (8-1), *"a"* and *"b"* are constants whose values are the longitudes of the vertical and horizontal axis, respectively, of the ellipse that is drawn in the Haigh torsional diagram τ_m–τ_a.

$$\left(\frac{\sqrt{J_{2,a}}}{a}\right)^2+\left(\frac{\sqrt{J_{2,m}}}{b}\right)^2=1 \qquad (8\text{-}1)$$

Equation (8-1) meets the condition for isotropic materials, that is, the polarity of the mean shear stress has no influence, which results in a symmetrical Haigh torsional diagram. This equation can be explained in terms of a balance of energy of distortion: The elastic energy of distortion W_D is proportional to the second invariant of the stress deviator tensor J_2. Therefore, equation (8-1) equalizes the energy that is stored for the static torsional loading to the fatigue torsional loading, where *"a"* and *"b"* are constants of the material. The constants *"a"* and *"b"* of equation (8-1) represent respectively the alternating and static von Mises stress at which the material fails [Marin, 1956]. The values of the constants "a" and "b" can be determined by means of two different torsional fatigue tests, namely the fully reversed and repeated torsional fatigue limits, τ_{-1} and τ_0.

However, equation (8-1) is not suitable for a general multiaxial fatigue loading, as it is not sensitive to the hydrostatic stresses, and predicts a similar influence

of the mean shear and mean axial stress effects, which is not in agreement with the experimental results for ductile materials in the literature.

The formulation of Marin's method is the simplest way to model the axial fatigue problem with mean loads with an energetic approach. However, its application to the axial fatigue loading with mean axial stresses gives a symmetrical Haigh diagram σ_m-σ_a, giving a conservative prediction for the compressive mean stresses. Equation (8-1) can be interpreted as a balance of distortion energy. The elastic energy of distortion W_D is proportional to the second invariant of the stress deviator tensor J_2. Therefore, Equation (8-2) equalizes the distortion energy of amplitude to the static distortion energy, where "a" and "b" are constants of the material:

The elliptical shape represented by Equation (8-1) is suitable for extra ductile materials in which the compressive mean stresses are as damaging as the tensile mean stresses, as it was shown in the results collected in Chapter 4. However, it is widely accepted in the literature that the Haigh diagrams are generally non-symmetrical, even for ductile materials. Moreover, equation (8-1) is not sensitive to the sign and magnitude of the hydrostatic stresses, which has been clearly demonstrated in experimental campaigns as remarked in [Morrison, 1956] and [Papadopoulos, 1997] among others.

8.3. *"Global approach"* multiaxial fatigue method

The Froustey method offers excellent agreement for the 34CrNiMo6 steel used in the present Thesis in the torsional fatigue loading cases with mean shear stresses. However, its application to axial fatigue loading with mean axial stresses yields a symmetrical Haigh diagram σ_m–σ_a. It is accepted in the literature that the Haigh diagrams are non-symmetrical, with a slightly increasing trend for the mean compressive stresses due to the effect of the hydrostatic stresses. The application of equation (8-1) to the uniaxial case results in a symmetrical Haigh diagram σ_m–σ_a, which contradicts the experimental results for most ductile steels as remarked in [Pallarés, 2018A] and [Lüpfert, 2004] among others. Moreover, Crossland demonstrated in [Crossland, 1956A] that mean compressive hydrostatic stresses produce a benefitial effect on the torsional fatigue limit, and proposed a linear function to model their effect.

According to the conclusions of the extensive review of the multiaxial fatigue methods performed by Papuga [Papuga, 2011A], which has been confirmed along the Chapter 6 of this Thesis with new methodologies, the mean stress effect is the most important factor in determining the accuracy of a multiaxial fatigue method. As mentioned in the discussion of the 1st International Conference of Fatigue [Crossland, 1956B], Crossland remarked on the need for an extension of the theory that he had proposed to include the mean-shear-stress effect. The equation (8-1) can be modified by adding the maximum hydrostatic stress $\sigma_{H,max}$, to take into account the beneficial effect of the compressive hydrostatic stresses. The extension of the Crossland method to take into account the mean shear stress effect is expressed by means of Equation (8-2):

$$\sqrt{\left(\frac{\sqrt{J_{2,a}}}{a}\right)^2+\left(\frac{\sqrt{J_{2,m}}}{b}\right)^2}+\frac{\sigma_{H,\max}}{c}=1 \qquad (8\text{-}2)$$

The proposed method in equation (8-2) is in fact an extension of the well proven Crossland multiaxial fatigue method, which in its original formulation is not able to deal with mean shear stresses. It has been added the feature to deal with mean shear stresses, highlighted by Crossland as a necessary extension to improve the method. The improvement of the multiaxial fatigue method of Crossland is motivated by the conclusions of Papuga in his extensive review [Papuga, 2011A], and confirmed in Chapter 6 of this Thesis: the first factor in developing a multiaxial fatigue method is the mean stress effect.

Equation (8-2) conserves the linear influence of the maximum hydrostatic stress on the von Mises stress amplitude, and takes into account the mean-shear-stress effect. All the qualities of the Crossland method are conversed, and a specific area of the Crossland method regarding the mean shear stress effect is improved.

Therefore, the proposed fatigue model is consistent with the increasing influence of the hydrostatic stresses with a greater mean axial stress effect, but it is preserved the low influence of the mean shear stresses for ductile materials, as demonstrated in the review of the experimental results on steels and aluminium alloys.

The determination of the parameters can be done with 3 different tests in order to determine the 3 constants *"a"*, *"b"* and *"c"*. The values of the constants "a"

and “b” can be adjusted by means of two different torsional tests, as there are no hydrostatic stresses involved in the pure torsion tests.

In order to adjust the model of torsional fatigue, equation (8-1), two fatigue tests are necessary: the fully reversed torsional fatigue limit and the repeated torsional fatigue limit. For torsional loading, there is no hydrostatic stress involved, so that the parameter *“c”* of equation (8-2) needs another test.

For a general multiaxial fatigue loading, another test is necessary to adjust the model, namely the fully reversed axial fatigue limit σ_{-1}, due to the fact that in that in axial fatigue testing, there are hydrostatic stresses involved. Therefore, the algebraic determination of the values of the constants *“a”*, *“b”* and *“c”* can be performed by the adjustment with 3 different tests: τ_{-1}, τ_0 and σ_{-1}. The derivation of the parameters of this method is presented in Annex A, and the values of the parameters are shown in equations (8-3) to (8-5):

$$a = \tau_{-1} \tag{8-3}$$

$$b = \frac{\tau_0}{2\sqrt{1-\left(\frac{\tau_0}{2\cdot\tau_{-1}}\right)}} \tag{8-4}$$

$$c = \frac{\sigma_{-1}}{3-\sqrt{3}\cdot\kappa} \tag{8-5}$$

The proposed method is applied to the 34CrNiMo6 steel, and the parameters for this material are shown in Table 8-1. The application of the method presented in equation (8-2) to the Haigh torsional diagram is represented in Figure 8-1 and

in the Haigh axial diagram in Figure 8-2, together with the experimental results in torsion and axial fatigue loading.

Table 8-1. *Parameters of the proposed method applied to 34CrNiMo6 steel*

Parameters	τ_{-1}	τ_0	σ_{-1}	***a***	***b***	***c***
Values for 34CrNiMo6 steel (MPa)	433	765	615	433	819	1145

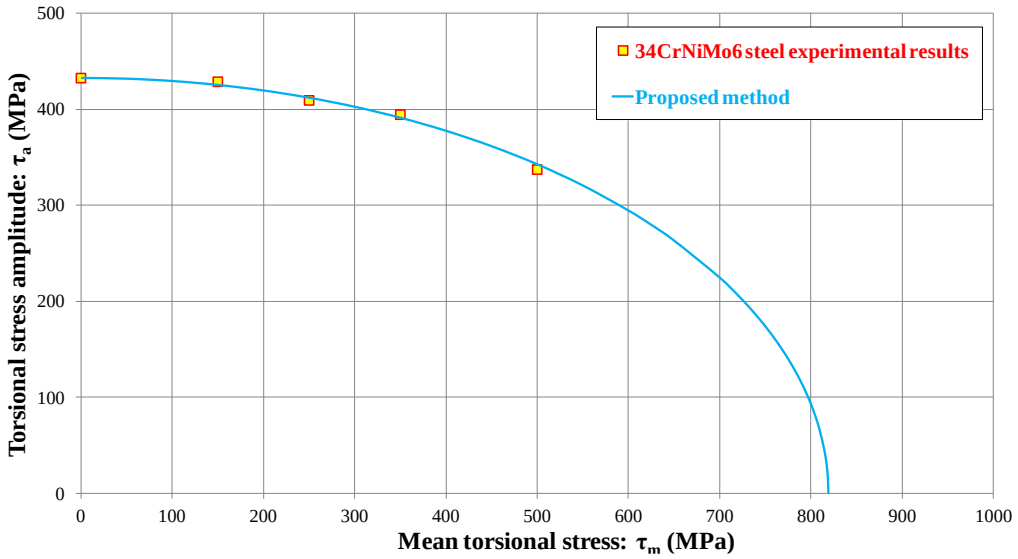

Figure 8-1. *Proposed method in a torsional Haigh diagram together with the experimental fatigue results [Pallarés, 2018B]*

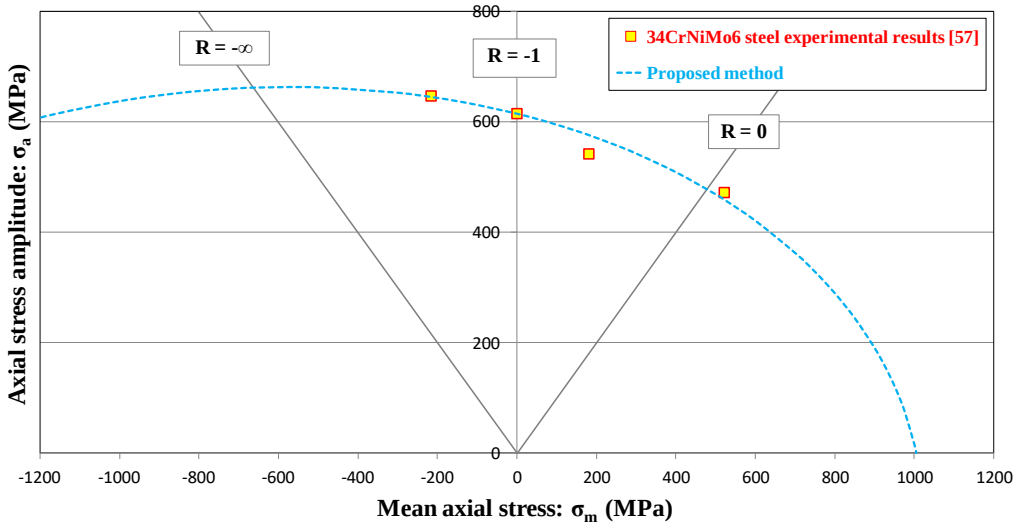

Figure 8-2. *Proposed method in an axial Haigh diagram together with the experimental fatigue results [Pallarés, 2018B]*

In Tables 8-2 and 8-3, the relative errors of the proposed method are presented for the torsional and axial fatigue loading cases respectively.

Table 8-2. *Relative errors in τ_a (%) of the proposed physical theory for N = $2x10^6$ cycles. Positive values mean conservative results predicted by the theory, negative values non-conservative results.*

τ_m (MPa)	Proposed model (equation (8-2))
150	0.8
250	−0.6
350	0.8
500	-1.6

Table 8-3. *Relative errors in σ_a (%) of the proposed physical theory for N = 2 x 10^6 cycles. Positive values mean conservative results predicted by the theory, negative values non-conservative results.*

σ_m (MPa)	Proposed model (equation (8-2))
−216	0.2
181	−6.3
522	2.8

The proposed method predicts an asymmetric shape in the Haigh diagram (Figure 8-2), with an increase in fatigue strength for low to mean values of mean axial compressive stresses, and a decrease of the fatigue strength for tensile mean loads, giving support to the modelling based on the detrimental effect of the maximum hydrostatic stresses proposed by Crossland.

Moreover, by adding the maximum hydrostatic stress term in the proposed multiaxial damage function, the mean stress effect is increased in axial compared with the torsion case, which explains why the effect of mean stress is higher in the axial and bending directions than for torsion of ductile materials. This result has been documented in the review of the experimental results.

Although the proposed function (8-2) has been developed and verified experimentally for the 34CrNiMo6 steel, it could be used for other isotropic ductile materials. Its application should be limited to isotropic materials in the range that is defined by other authors for Crossland-based methods

[Papadopoulos, 1997], $1.25 < \kappa < \sqrt{3}$, which includes mild steels and low-alloy steels [Nishijima, 1993] and aluminium alloys. A large database of materials with the values of the κ ratio can also be found in [Papuga, 2011].

The upper limit of the proposed method arises because, in the von Mises relationship ($\kappa = \sqrt{3}$), the method becomes the Marin function, which was devised for materials where there was no effect of hydrostatic stresses.

The new developed expression is an extension of the Crossland method, and therefore it should be applied to the same type of materials, the so called "hard metals". The definition of "hard metals", was performed by Papadopoulos et al. in [Papadopoulos, 1997]. It basically states that the category of hard metals is the one in which the fatigue ratio κ (defined as $\kappa = \sigma_{-1}/\tau_{-1}$) is contained within the range $(1.25, \sqrt{3})$. One problem that can arise is that not all the materials have been tested in fully reversed axial and torsion, so that this ratio is not always available, such as for the globular graphite cast iron. However, some of the most used metals in engineering pertain to that category, such as the mild steels, the low alloy steels, and the aluminium alloys, which take a value of κ ranging from (1.3 to 1.73).

The ones that are not part of the category of hard metals are the grey cast irons, the compacted (vermicular) graphite cast irons, cast aluminium such as AS7G06 cast aluminium [Mu, 2014], which take a value of κ bellow 1.25. The value of the ratio κ is not only dependent on the ductility of the matrix, but also on the size and shape of the pores and inclusions. For instance, some ductile cast aluminium alloys have a value of κ bellow 1.25.

Sines in [Sines, 1959] states that, for very low fatigue ratios (approximately $\kappa < 1.25$), which correspond to materials with large defects, such as cast irons and cast aluminium alloys [Mu, 2014], [Koutiri, 2013] the nature of the fatigue failure changes, and the failure can be described through a maximum normal stress criterion. As shown in the review of the experimental results on cast irons, the effect of the mean shear stresses is strong for materials with large defects, and the proposed function will underestimate the mean-shear-stress effect for this type of materials.

Finally, from a computational cost point of view, it can be said that this method, which pertains to the class of the stress invariants methods, is one order of magnitude less demanding than the critical plane methods in terms of computational cost, and two orders of magnitude when compared to the integral methods [Papuga, 2005].

Finally, among the limitations, it must be noted that there exists no analytic expression for the simple case of axial fatigue loading. Moreover, it is not fully based on physical considerations, as the effect of the hydrostatic stresses is modelled through an empirical observation by means of a linear influence of the maximum hydrostatic stress.

8.4. Energetic multiaxial fatigue criterion

The motivation for the development of this method is the need of a fatigue model fully based on physical considerations, in order to be extended in the future to different conditions and materials. This criterion has therefore been created as a method describing the fatigue process from a physical point of view, and it is inherently multiaxial, as the quantities which describe the method, namely the stress invariants, are able to deal with the multiaxial fatigue problem.

In order to develop this method, the main feature of a multiaxial fatigue method has been studied: the mean stress effect, both in axial and torsional fatigue. In Figure 8-3, a sketch is shown comparing the complexity of both problems, and relating the different quantities (stress invariants) involved.

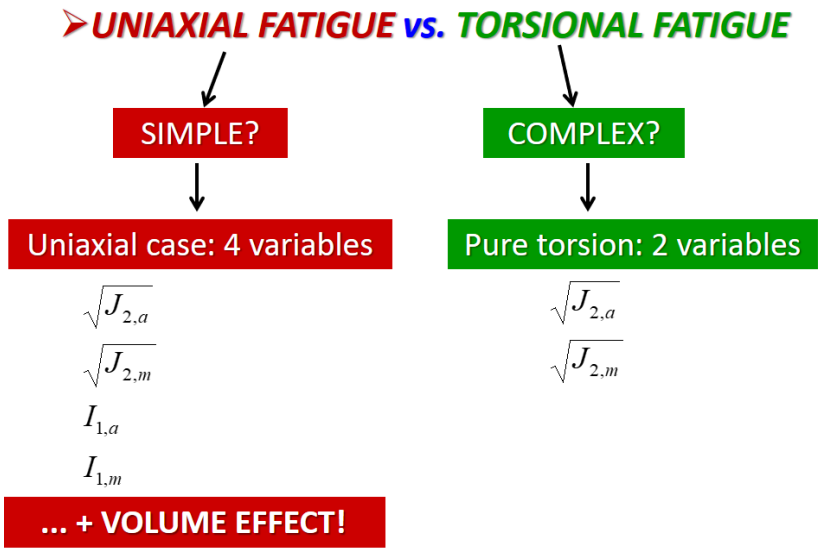

Figure 8-3. *Sketch of the uniaxial and torsional variables in terms of stress invariants [Pallarés, 2019]*

As it can be observed, the uniaxial fatigue problem must be described by 4 variables, whereas the torsional fatigue problem can be modelled with only 2 variables. In the engineering field it is highly extended the belief that the uniaxial problem is the simplest one in fatigue, leading to ad-hoc solutions which extend uniaxial formulations to the multiaxial field. However, the energetic method proposed herein is based on physical considerations, and can be applied to different load states, including uniaxial and multiaxial fatigue.

The basis of the development of the method was to progressively construct the mathematical relationships involving the quantities (stress invariants). The 1st step was obviously to solve the pure torsion case by performing enough tests to be fitted by a mathematical expression. It was found that the elliptical relationship in terms of $\sqrt{J_{2,a}}$ and $\sqrt{J_{2,m}}$ presented in equation (8-1) is able to fit the data with an excellent experimental agreement with an average value of the absolute error less than 1%. However, as it was already mentioned, equation (8-1) is unable to deal with the axial fatigue problem, as it does not take into account the hydrostatic stresses.

The uniaxial fatigue problem involves the 4 different quantities (Figure 8-3), namely $\sqrt{J_{2,a}}$ and $\sqrt{J_{2,m}}$ which are proportional to the distortion energy W_D; and $I_{1,a}$ and $I_{1,m}$ which are proportional to the stored elastic energy of volume change W_H. For ductile metals, it is considered that the influence of the hydrostatic stress amplitude is negligible as it does not provoke the movement of dislocations, so that its contribution can take place only through the mean [Sines, 1959] or the maximum value [Crossland, 1956A] of the hydrostatic

stress. The influence of $I_{1,a}$ will therefore be considered as negligible in the developed formulation.

In order to take into account the influence of the hydrostatic stresses as a source of mean stress effect, and to obtain a non-symmetrical shape of the Haigh diagram for ductile to extra-ductile metals, a new formulation is proposed by modifying the Marin equation, by including the mean value of the first invariant of the stress tensor $I_{1,m}$, resulting in Equation (8-6):

$$\left(\frac{\sqrt{J_{2,a}}}{a}\right)^2+\left(\frac{\sqrt{J_{2,m}}}{b}\right)^2+\left(\frac{I_{1,m}+\Lambda}{c}\right)^2=1 \qquad (8\text{-}6)$$

Equation (8-6) is presented using the Dymensional Analysis techniques described in [Bridgman, 1922], so that the constants used in the denominators present a physical meaning, and have units of stress. The third term of the Equation (8-6) represents the stored mean hydrostatic energy, which is proportional to the squared value of the first invariant of the stress tensor $I_{1,m}$, and related to the energy required to change the volume. The parameter Λ, which can take a value equal or higher than zero, allows a symmetry breaking of the Haigh diagram, as it was predicted by the mesoscopic theory defined in [Papadopoulos, 1997], which states that the hydrostatic stresses create a non-symmetrical Haigh diagram. Moreover, the constant Λ is linked with the hydrostatic stresses in the volume defects, which according to the Gurson theory would increase the static strength in compression compared to that in tension [Gurson, 1977], as the Equation (8-6) predicts when the parameter Λ takes a value higher than 0.

The parameter *"c"* of Equation (8-6) is a material constant which represents the static hydrostatic load at which the material fails, and according to Bridgman's extensive work [Bridgman, 1952], this constant should be higher than the constant "b", as ductile materials are more susceptible to fail from shear stresses than from hydrostatic stresses.

The determination of the parameters can be done with 4 different tests in order to determine the 4 constants *"a"*, *"b"*, *"c"* and "Λ". Following the procedure by Zenner and Liu in [Zenner, 2000], the four different selected test are the fully reversed axial and torsional fatigue limits σ_{-1} and τ_{-1}, the repeated axial and torsional fatigue limits σ_0 and τ_0. The algebraic determination of the values of the constants *"a"* and *"b"* can be performed with the same procedure as the extended Crossland method, using equations (8-3) and (8-4). The values of the parameters *"c"* and "Λ" is presented in Equations (8-7) and (8-8):

$$c = \frac{\sigma_0}{2 \cdot \left(\sqrt{1 - \left(\frac{\sigma_0}{2\sqrt{3}} \right)^2 \cdot \left(\frac{1}{a^2} + \frac{1}{b^2} \right)} - \sqrt{1 - \left(\frac{\sigma_{-1}}{\sqrt{3}\tau_{-1}} \right)^2} \right)} \tag{8-7}$$

$$\Lambda = c \cdot \sqrt{1 - \left(\frac{\sigma_{-1}}{\sqrt{3}\tau_{-1}} \right)^2} \tag{8-8}$$

In case that some of the torsional fatigue tests were not available, one can use several correlations. The value of the fully reversed torsional fatigue limit τ_{-1} can be estimated for steels using the mean value of the NRIM extensive campaign on structural steels [Nishijima, 1993], Equation (8-9) for normalized steels and Equation (8-10) for quenched and tempered steels:

$$\tau_{-1} \approx 0.30 \cdot \sigma_{uts} \tag{8-9}$$

$$\tau_{-1} \approx 0.36 \cdot \sigma_{uts} \tag{8-10}$$

The approximate Equations (8-9) and (8-10) have a good agreement with experimental results of torsional fatigue on steels, leading to errors lower than 1%.

The repeated torsional fatigue limit τ_0 can be estimated for any ductile material through the well-known by the classic formula defined in [Zenner, 2000] by means of Equation (8-11):

$$\tau_0 \approx \frac{4 \cdot \tau_{-1}}{2 \cdot \frac{\sigma_{-1}}{\sigma_0} + 1} \tag{8-11}$$

The proposed physical method is applied to the 34CrNiMo6 steel, and the experimental and parameters for this material are shown in Table 8-4. The parameter σ_0, which is near to the experimental test $\sigma_{0.05}$ = 994 MPa, has been obtained by means of linear interpolation within the Haigh diagram. The values of torsional fatigue strengths τ_{-1} and τ_0 have been obtained by means of staircase tests following ISO 12107:2012 [ISO, 2012].

Table 8-4. *Parameters of the proposed method applied to 34CrNiMo6 steel*

Material parameters	**σ_{-1}**	**τ_{-1}**	**σ_0**	**τ_0**	**a**	**b**	**c**	**Λ**
34CrNiMo6 steel	615	433	961	765	433	819	4092	2337

As it can be observed in Table 8-4, the energetic method presents the same parameters “a” and “b” as the Crossland extension method, being those parameters the ones which the define the behavior in torsional fatigue. Therefore, the agreement with the experimental results of the developed energetic method presents the same behavior in pure torsion when compared to the *“global approach”* method. Thus, the results presented in Figure 8-1 and Table 8-2 apply directly to the ones of the fully energetic formulation, and a good agreement with experimental results of 34CrNiMo6 steel in torsional fatigue are achieved.

According to Brigdman’s theory for static stresses [Bridgman, 1952], the constant *"c"* should be significantly higher than the constant *"b"*, as steels and other ductile materials can withstand much better hydrostatic stresses than shear stresses. In Table 8-4, the parameter *“c”* (hydrostatic strength) takes a value 5 times higher than the parameter *“b” (static shear strength)*, showing a good agreement with Bridgman's theory for static stresses.

The application of this method for the axial fatigue case with mean stress can be expressed in terms of σ_a and σ_m through the analytic expression (8-12):

$$\sigma_a = \sqrt{3} \cdot a \cdot \sqrt{1 - \left(\frac{\sigma_m}{\sqrt{3} \cdot b} \right)^2 - \left(\frac{\sigma_m + \Delta}{c} \right)^2} \qquad (8\text{-}12)$$

Therefore, the application of the energetic method to the axial fatigue problem of 34CrNiMo6 leads to a concave downward shape (Figure 8-4). Moreover, the use of the parameter Λ allows a rupture of the symmetry, so that the axial fatigue strength slightly increases for moderate compression loads. In Table 8-5, the

relative errors (%) of the different theories are presented for N=2 x 10^6 cycles. the errors of the proposed physical method are within the range [-10%,10%].

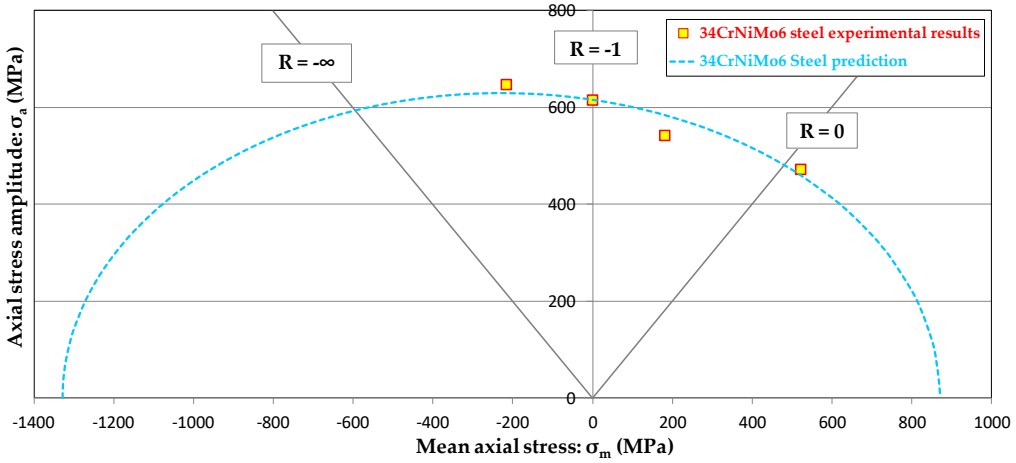

Figure 8-4. *Axial Haigh diagram with the experimental results for 34CrNiMo6 steel and the predictions from the proposed energetic method, Equation (8-6).*

Table 8-5. *Relative errors (%) of the proposed physical theory for N=2x10^6 cycles. Positive values mean conservative results predicted by the theory, negative values non-conservative results.*

R (σ_{min}/ σ_{max})	σ_m (MPa)	Proposed theory (Equation 8-6)
-2	-216	2.6
-0.5	181	-7.5
0.05	522	2.6

In order to verify the applicability of the proposed energetic method to other steels, the criterion is compared to experimental fatigue data on other steels. The material fatigue tests and the obtained parameters for the energetic method are shown in Table 8-5. Due to the fact that the repeated torsion fatigue limit τ_0 is rarely available, the well-known Zenner formula, Equation (8-13), has been applied to all the steels of Table 8-5.

Table 8-6. *Parameters of the proposed method applied to several structural steels extracted from the literature. The values of τ_0 were obtained by means of the Zenner formula, Equation (8-11)*

Material	σ_{-1}	τ_{-1}	σ_0	τ_0	a	b	c	Λ
En25 steel [O'Connor, 1956]	483	301	770	534	301	578	2163	813
30NiCrMo8 steel [Klubberg, 2001]	414	311	644	543	311	560	3528	2251
25CrMo4 steel [Grün, 1991]	361	228	600	414	228	493	2113	857
0.1C steel [Ukrainetz, 1960]	197	114	343	213	114	293	709	94

In these materials the hydrostatic strength is higher than the distorsion strength, as the constant "c" is significantly higher than the constant "b" for all the analysed steels, following the trend of a good agreement with Bridgman's theory. The ratio between the parameters *c* and *b* ranges from 2.4 for the very low carbon steel of [Ukrainetz, 1960] to 6.3 for the 30NiCrMo8 steel of [Klubberg, 2001].

The predictions from the energetic method and experimental results are shown together in a Haigh diagram in Figure 8-5. As it can be observed, the method is able to be adapted to each of the experimental data sets with a concave downward shape, and predicts the slight increase of the fatigue strength for moderate mean compressive loads.

The values of the parameter Λ represent the strength differential effect appearing between tensile and compressive static loads. For instance, for the the 0.1% carbon steel the Λ parameter takes of low value of 96 MPa, resulting in a nearly symmetrical diagram. The other steels, with higher valuers of the Δ parameter, present a non-symmetrical Haigh diagram with slight increases in the fatigue strength for moderate value of compressive mean loads.

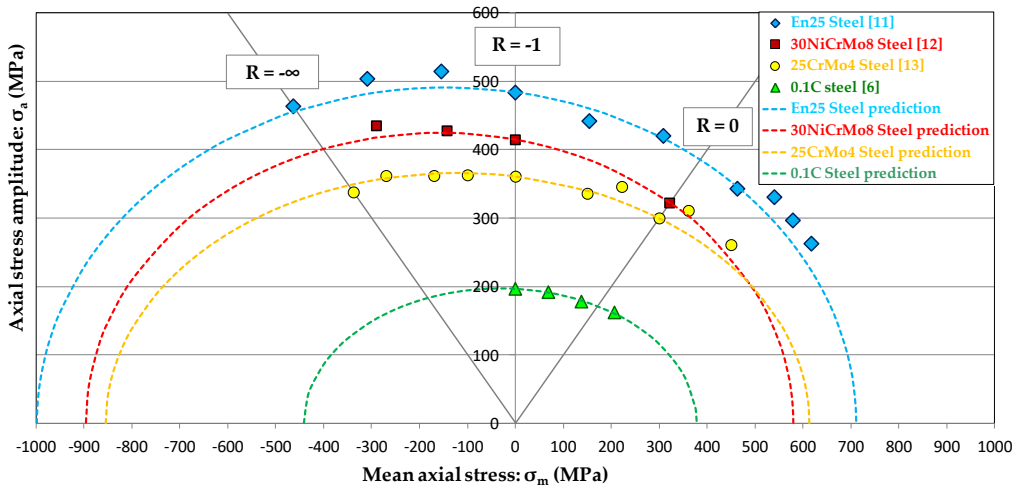

Figure 8-5. *Haigh diagram with the experimental results for several structural steels and their predictions from the proposed method, Equation (8-6).*

Therefore, the developed energetic method is able to deal with mean stresses in fatigue of ductile materials, a feature which is considered the most important for a multiaxial fatigue method. The derivation of the parameters can be done through the Annex B with 4 different fatigue limits; or by adjusting the 4 parameters with the least squares method to fit 4 different axial fatigue tests with mean stresses. Therefore, the multiaxial fatigue properties of a given ductile material could be predicted with uniaxial fatigue tests due to the inherently multiaxial quantities (stress invariants) used in its formulation.

This method, which is based on physical assumptions, could be further developed for other scenarios, such as the limited life zone, as some of the quantities and stored energies can be scaled with the number of cycles.

Chapter 9:

CONCLUSIONS AND FURTHER WORKS

CHAPTER 9. CONCLUSIONS AND FURTHER WORKS

9.1. Conclusions

In this Thesis, two different multiaxial fatigue models have been developed, reflecting the fatigue behavior of a quenched and tempered 34CrNiMo6 steel and similar ductile engineering materials such as structural and mild steels, and alluminium alloys among others. These original multiaxial criteria improve the experimental agreement in ductile materials over the existing methods due to their improved formulation to deal the mean stress effect on ductile materials, which has been demonstrated in this Thesis as the most important feature of a multiaxial fatigue method.

Due to the importance of the mean axial stress effect, regarded as the most critical variable in multiaxial fatigue, a research on its influence in the fatigue strength has been undergone.

- A review of the experimental results of the literature on uniaxial fatigue has been performed, including results from ductile and fragile materials, and have been plotted in Haigh diagrams. Brittle materials exhibit a convex downwards shape, whereas ductile materials present a concave downwards line in the axial Haigh diagram.

- A uniaxial fatigue campaign has been designed and conducted on 34CrNiMo6 steel specimens, including one set of S-N curves with

compressive mean stresses. The fatigue limits were obtained with the staircase method. The results are presented in Figure 7-7 and Table 7-9.

- The axial mean stress effect involves the elastic strain energy of change of volume (W_H) and the distortion strain energy (W_D). The latter had been already used by Marin with mixed results for ductile materials due to the symmetry presented by this theory in the Haigh diagram. An extra parameter based on the hydrostatic stresses must be taken into account in order to properly represent the moderate increase of fatigue strength in the compressive zone for a number of ductile materials.

- In the multiaxial fatigue model based on the extension of the Crossland method, the break of the symmetry in the axial Haigh diagram has been achieved by the maximum hydrostatic stress in the same way as the Crossland method.

- In the fully energetic multiaxial fatigue model, the axial mean stress effect is modelled through the contributions of the accumulated elastic strain energies of distortion (W_D) and change of volume (W_H) provoked by the mean hydrostatic stresses.

- The developed multiaxial fatigue methods have been validated against the experimental results on the axial fatigue campaign on 34CrNiMo6 steel. Moreover, the energetic fatigue method has been validated with experimental results on other similar ductile steels collected from the literature.

The mean shear stress effect has been considered as a controversial issue in the fatigue field. It is considered as the second most important feature of a multiaxial fatigue method, as remarked by [Papuga, 2011A] and confirmed within the present Thesis. Therefore, its influence on the torsional fatigue has been studied, so that the effect has been incorporated into the developed methodologies.

- An historical review has been performed, considering the experimental results and conclusions inferred by several researchers. The differences in the conclusions of these authors are based on the purposes of the different studies, as some as intended as basic design rules for engineering [Smith, 1942], whereas other works are focus on the physical process of fatigue damage [Findley, 1959].

- A large datasets of experimental results on torsional fatigue from the last 70 years have been collected, including results from ferritic materials and alluminium alloys, and have been compared altogether in various ways in Haigh torsional diagrams. The mean shear stress effect takes place for the majority of ductile metals, even for maximum stresses not exceeding the shear yield strength. Brittle materials are much more sensitive than ductile materials to the mean shear stress effect.

- For ductile metals, the mean shear stress effect is weaker than the mean axial stress effect. It was also confirmed experimentally for the 34CrNiMo6 steel analysed. For this type of materials, the Haigh torsional diagram presents a concave downward shape with a slope taking a value near zero for the intersection with the ordinates axis.

- A torsional fatigue campaign has been designed and performed for a 34CrNiMo6 high strength steel, including 5 different levels of static torsion and comprising 83 specimens. The S-N curves and the torsional fatigue limit values were obtained with the ISO standard based on the JSME method.

- The torsional fatigue results of 34CrNiMo6 are presented in a Haigh torsional diagram, showing an elliptic shape. The mean shear stress effect involves the distortion strain energy (W_D), and can be modelled through the theory of [Froustey, 1992], which is based on the balance of energies presented by [Marin, 1956].

- In the both of the multiaxial fatigue developed models, the mean shear stress effect is modelled by means of a balance of distortion energy, equation (8-1). The parameters *"a"* and *"b"* of this equation can be obtained by using the torsional fatigue limits τ_{-1} and τ_0.

- The elliptical criterion selected for the modelling of the mean shear stress is able to correctly represent the horizontal slope in the intersection with the ordinates axis in the Haigh torsional diagram for ductile steels, as shown in Chapter 4.

The multiaxial fatigue methods have been studied and compared with experimental results of an extensive database by using the latest formulations as demanded by [Susmel, 2011], and taking into account the calculations of the shear stress amplitude with the Minimum Circumscribed Ellipse (MCE). The analysis and discussion of these methods have decisively contributed to the

formulation of the developed multiaxial fatigue methods presented in this Thesis.

- A database has been created gathering the results presented in [Papuga, 2011A] and [Zhang, 2010], correcting some minor errors and storing the data in Excel format in order to manage the experimental results and the calculations related to multiaxial fatigue methods.

- The most known multiaxial fatigue methods have been programmed in Matlab, including uniaxial fatigue methods extended to the multiaxial fatigue; and the some of the latest methods as the empirical criterion by [Vu, 2010] and the latest versions of the critical planes by [Zhang, 2010] and [Susmel, 2011] among others.

- The calculation of the amplitude of shear stress has been performed by the use of the Minimum Circumscribed Ellipse (MCE), offering an improvement in the agreement for out-of-phase loads.

- The analysis of the experimental agreement of the multiaxial fatigue methods have been performed in a global way, and also by analysing 4 individual categories, namely multiaxiality, phase-shift effect, mean axial stresses, and mean torsional stresses.

- The mean axial and torsional stress effects are the most important features in a multiaxial fatigue method. A good agreement with those effects leads to a general good agreement with all the database. It must

be noted that the multiaxiality by itself and the phase-shift-effect are not critical for the multiaxial fatigue methods.

- The methods using three or more quantities to describe the fatigue damage offer improved agreement with experimental results. Usually, the most available experimental data to adjust the tests are the fully reversed torsional and axial fatigue limits τ_{-1} and σ_{-1}; and the repeated axial fatigue limit σ_0. The repeated torsional fatigue limit can be obtained experimentally or with the Zenner formula.

- The mathematical formulations of the most known methods have been obtained and applied to the experimental results of DIN 34CrNiMo6. The method by Froustey is able to correctly represent the shape of the Haigh torsional diagram. However, none of the methods is able to correctly represent the concave downward shape of the Haigh axial diagram, with a slight increase of fatigue strength for moderate compressive loads.

- The energetic formulation of Froustey for the torsional fatigue problem has been conserved to develop the presented multiaxial fatigue methods. In order to solve the uniaxial fatigue problem, two different alternatives have been proposed, a global approach criterion and an energetic multiaxial fatigue method.

- The proposed global approach criterion can be regarded as an improvement of the Crossland and Marin methods, showing a low

sensitivity for mean shear stresses, and increasing the effect for mean axial loads thanks to the use of the maximum hydrostatic stress.

- The developed energetic multiaxial fatigue method conserves the formulation of distortion energies of [Froustey, 1992] for the torsional fatigue case. Moreover, this method takes into account the stored hydrostatic elastic energy, so that the mean axial stress effect is higher than the mean shear stress effect. In order to correctly model the non-symmetrical shape of the axial Haigh diagram, a parameter of the rupture of the symmetry Λ has been introduced. The physical meaning of this parameter is related to the Gurson theory, so that the predicted static strength in compression is higher than the tensile static strength for materials with defects.

9.2. Further works

The works presented in this Thesis have opened several subjects of interest in the field of fatigue, so that some tasks are being performed at present or planned for a near future.

The multiaxial fatigue test campaign originally designed was extremely large and some of the tests have been partially completed, as the combination of mean torsional stresses with rotating bending fatigue, obtaining the whole S-N curves in a similar way to the case of pure torsional fatigue. The designed experiments will test the formulation of the multiaxial fatigue methods due to the high mean shear stresses applied.

In the same way, the remaining tests of the designed multiaxial fatigue campaign could be performed. A combination of static axial loads (preferably compressive) combined with torsional fatigue could be highly demanding for a great number of multiaxial methodologies. Another load case of great interest would be the out-of-phase loading of torsional and rotating bending fatigue combined with high values of static torsion, as mentioned in [Papuga, 2011A].

With respect to the analysed fatigue database with 422 experiments, there are some limitations, namely the lack of mean compressive loads, and the use of some data of very fragile materials, with failures in internal inclusions which are not representative of ductile materials. The database is currently being updated with new experimental results on fatigue, and including mean compressive stresses which were neglected in [Papuga, 2011A]. Subsequently,

the developed methods will be applied to the enhanced database of ductile metals.

Regarding the presented methods, those can be further developed in order to be applied to the limited life zone, namely between 10^3 to 10^6 cycles, in the same way as the methods by Cristofori [Cristofori 2008] and Mamiya [Mamiya, 2011] among others (see Figure 9-1).

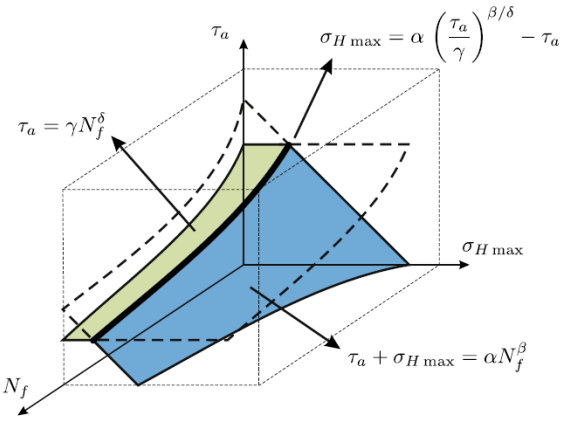

Figure 9-1. *Multiaxial fatigue method in the medium fatigue life range [Mamiya, 2011]*

The energetic multiaxial method can be furtherly developed to take into account the volume effect by formulating the Λ parameter by means of the damaged volume, enabling the method to distinguish between axial, rotating bending and plane bending fatigue cases as it is the case in [Palin-Luc, 1998]

Finally, the energetic fatigue method, as it is defined with physical quantities involving stored elastic energies, can be furtherly developed to the LCF range by adding the plastic energies to the formulation, and scaling the works with the number of cycles.

BIBLIOGRAPHY

[Altenbach, 1994] Altenbach, U., Zolochevsky, A.A. "Eine energetische Variante der Theorie des Kriechens und der Langzeitfestigkeit für isotrope Werkstoffe mit komplizierten Eigenschaften". ZAMM, 74(3):189-199, (1994).

[Araujo, 2011] Araújo et al. "On the characterization of the critical plane with a simple and fast alternative measure of the shear stress amplitude in multiaxial fatigue" Int. J. Fatigue 33 (2011) 1092-1100

[ASTM, 2004] ASTM E739-91, Standard Practice for Statistical Analysis of Linear or Linearized Stress-Life (S-N) and Strain-Life (e-N) Fatigue Data. ASTM International, West Conshohocken, PA, (2004).

[ASTM, 2015] ASTM E466-15, Standard Practice for Conducting Force Controlled Constant Amplitude Axial Fatigue Tests of Metallic Materials. ASTM International, West Conshohocken, PA, (2015).

[Avilés, 2005] Avilés, R. *"Análisis de fatiga en máquinas"* Ed. Paraninfo. Madrid, 2005

[Avilés, 2013] Avilés, R., Albizuri, J., Rodríguez, A. & López de Lacalle, L.N., 2013. Influence of low-plasticity ball burnishing on the high-cycle fatigue strength of medium carbon AISI 1045 steel. International Journal of Fatigue, Volumen 55, pp. 230-244.

[Avilés, 2015] Avilés, R. *"Métodos de cálculo de fatiga para ingeniería. Metales."* Ed. Paraninfo. Madrid, 2015

[Avilés, 2018] Alexander Avilés Ajuria. *"Modelos de predicción del comportamiento a fatiga de componentes sometidos a tratamientos mecánicos"*. Tesis doctoral, UPV-EHU, 2018.

[Avilés, 2019] Alexander Avilés, Rafael Avilés, Joseba Albizuri, Luis Pallarés Santasmartas, Adrián Rodríguez. Effect of shot-peening and low-plasticity burnishing on the high-cycle fatigue strength of DIN 34CrNiMo6 alloy steel. Volume 119, February 2019, Pages 338-354

[Baier, 1970] Baier, F.: Time and fatigue strength with superimposed static and oscillating tensile compression and torsion loading. [PhD thesis]. Stuttgart, University of Stuttgart (1970).

[Bauschinger, 1886] Bauschinger, J.: Nethn. A.D. Mechn. Techn. Laboratory, München, Vol. 13. (1886).

[Beiss, 2008] Beiss, P.; Klubberg, F.; Schäfer, H.J.; Krug, P.; Weiß, H. Fatigue Behaviour of High Performance Spray-Compacted Aluminium Alloys, Proc. 11. Int. Congr. Aluminium Alloys, Aachen, Vol. 2, 1583-1588, Wiley-VCH, 2008.

[Beretta, 2003] Beretta, S. "Application of multiaxial fatigue criteria to materials containing defects". Fatigue and Fracture of Engineering Materials and Structures, Vol. 26 (2003), pp. 551-559

[Bhongbhibhat, 1986] Bhongbhibhat, T.: Strength behaviour of steels under multi-axial phase-shifted vibration loading with different vibration modes and frequencies. [PhD thesis]. Stuttgart, University of Stuttgart (1986).

[Bomas, 2009] Bomas, H.; Bacher-Hoechst, M.; Kienzler, R.; Kunow, S.; Loewisch, G.; Muehleder, F.; Schroeder, R. Crack initiation and endurance limit of a hard steel under multiaxial cyclic loads. Fatigue Fract Engng Mater Struct 2009 33, 126–139. doi: 10.1111/j.1460-2695.2009.01423.x

[Bonnand, 2011] V. Bonnand et al. "Investigation of multiaxial fatigue in the context of turboengine applications" Int. J. Fatigue 33 (2011) 1006-1016

[Branco, 2012] Branco, R.; Costa, J.D.; Antunes, F.V. Low-cycle fatigue behaviour of 34CrNiMo6 high strength steel. Theoretical and Applied Fracture

Mechanics 2012, Volume 58, Issue 1, April 2012, Pages 28-34. https://doi.org/10.1016/j.tafmec.2012.02.004

[Branco, 2016] Branco, R.; Costa, J.D.M.; Antunes, F.V.; Perdigão, S. Monotonic and Cyclic Behavior of Din 34CrNiMo6 Tempered Alloy Steel. Metals 6 (2016), 98

[Brand, 1992] A. Brand, J.F. Flavenot, R. Gregoire, C. Tournier. *"Données technologiques sur la fatigue"*. CEntre Technique des Industries Mécaniques (CETIM), 1992. ISBN 2-85400-200-4, 3ème edition.

[Bridgman, 1922] Bridgman, P.W., "Dimensional Analysis". Yale University Press, (1922).

[Bridgman, 1952] Bridgman, P.W. Studies in large plastic flow and fracture with special emphasis on the effects of hydrostatic pressure, 1st ed.; Publisher: McGraw-Hill Book Company, Country, 1952; pp. 38–86, ISBN0674731336

[Brune, 1991] Brune M. Preparation of a stress standard for rolling mill drives and experimental verification of the service life estimation methods, Diss. TU Clausthal 1991.

[Castillo, 2009] E. Castillo, A. Fernández-Cantelli: "A Unified Statistical Methodology for Modeling Fatigue Damage", Springer Science + Business Media B.V. (2009). ISBN 978-1-4020-9181-0

[Chan, 2010] K.S. Chan "Roles of microstructure in fatigue crack initiation" Int. J. Fatigue 32 (2010) 1428-1447

[Chodorowski, 1956] Chodorowski W.T., Fatigue strength in shear of an alloy steel, with particular reference to the effect of mean stress and directional properties. In: Proc. Int. Conf. Fatigue of Metals (1956). London: I. Mech. Eng.; pp. 122–131.

[Cristofori, 2008] A. Cristofori, L. Susmel, R. Tovo. “A stress invariant based criterion to estimate fatigue damage under multiaxial loading”. International Journal of Fatigue 30 (2008) 1646–1658

[Crossland, 1956A] Crossland B., Effect of large hydrostatic pressure on the torsional fatigue strength of an alloy steel. In: Proceedings of international conference on fatigue of metals. London: Institution of Mechanical Engineers (1956); pp. 138–149.

[Crossland, 1956B] Crossland B.,"Authors' replies", In: Proceedings of international conference on fatigue of metals. London: Institution of Mechanical Engineers (1956); pp. 896–897.

[Dang Van, 1973] Dang Van K., “Sur la résistance à la fatigue des métaux.” Thèse de Doctorat ès Sci, Sci Techniq l´Armement (1973);47:647.

[Davoli, 2003] Davoli, P.; Bernasconi, A.; Filippini, M.; Foletti, S.; Papadopoulos, I.V.; Independence of the torsional fatigue limit upon a mean shear stress. Int. J. Fatigue (2003), 25, pp. 471-480. https://doi.org/10.1016/S0142-1123(02)00174-3.

[Delahay, 2003] Delahay, T. “Estimation of the fatigue strength distribution in high-cycle multiaxial fatigue taking into account the stress–strain gradient effect”. International Journal of Fatigue 28 (2006) 474–484

[Dietmann, 1973] Dietmann, H.; Festigkeitsberechnung bei Mehrachsiger Schwingbeansoruchung. Z. Konstruktion (1973) 25, pp. 181–189.

[Dowling, 2009A] Dowling, N. E. (2009). “Mean stress effects in strain-life fatigue” Fatigue Fract. Eng. Mater. Struct. 32, 1004-1019.

[Dowling, 2009B] Dowling, N.E.; Calhoun, C.A.; Arcari, A. Mean stress effects in stress-life fatigue and the Walker equation. Fatigue Fract Engng Mater Struct (2009) 32, 163–179. doi: 10.1111/j.1460-2695.2008.01322.x

[Dubar, 1992] Dubar L. Fatigue multiaxiale des aciers. Passage de l'endurance à l'endurance limitée. Prise en compte des accidents géometriques. PhD thesis. ENSAM, Talence; 1992.

[El Magd, 1977] El Magd E, Mielke S. Dauerfestigkeit bei überlagerter zweiachsiger statischer Beanspruchung. Konstruktion 1977;29:253–7.

[Filippini, 2010] M. Filippini et al. "Assessment of multiaxial fatigue life prediction methodologies for Inconel 718" Procedia Engineering 2 (2010) 2347-2356

[Findley, 1953] Findley W.N., "Combined-stress fatigue strength of 76S-T61 Aluminum alloy with superimposed mean stresses and corrections for yielding." NACA-TN-2924. NACA, Washington. (1953).

[Findley, 1956] Findley W.N. et al., "Theory for combined bending and torsion fatigue with data for SAE 4340 steel". In: Proceedings of international conference on fatigue of metals. London: Institution of Mechanical Engineers (1956); p. 150–157.

[Findley, 1959] Findley W.N., "A theory for the effect of mean stress on fatigue of metals under combined torsion and axial load or bending". J Eng. Ind., Trans ASME (1959); 81(4): pp 301–306.

[Findley, 1989] Findley W.N., Effects of extremes of hardness and mean stress on fatigue of AISI 4340 steel in bending and Torsion. Journal of Engineering Materials and Technology (1989), Vol. 111, pp 119-122.

[Forrest, 1962] Forrest, P. G., (1962), Fatigue of Metals, Pergamon Press Inc., London.

[Freudenthal, 1946] Freudenthal, A.M. "The Statistical Aspect of Fatigue of Materials", Proceedings of the Royal Society (London), Series A, Vol. 187 (1946) p. 416

[Freudenthal, 1974] Freudenthal, A.M. “New aspects of fatigue and fracture mechanics. Eng. Fract. Mechanics”, 1974, Vol. 6, pp. 775-793

[Froustey, 1989] Froustey C., Lasserre S., "Multiaxial fatigue endurance of 30NCD16 steel". Int J Fatigue 11 No 3 (1989), pp. 169-175

[Froustey, 1992] Froustey, C., Lasserre, S., Dubar, L. "Multiaxial and block fatigue tests validation of a criterion for metallic materials". MAT-TEC 92, Grenoble (1992).

[Gaur, 2016] Gaur, V.; Doquet, V.; Persent, E.; Mareau, C.; Roguet, E.; Kittel, J. Surface versus internal fatigue crack initiation in steel: Influence of mean stress. International Journal of Fatigue (2016), 82, pp. 437–448. http://dx.doi.org/10.1016/j.ijfatigue.2015.08.028

[Gerber, 1874] Gerber, H. Bestimmung der zulassigen Spannungen in Eisenkonstructionen. Z. Bayerischen Architeckten Ingenieur-Vereins, 1874, 6, pp. 101–110.

[Gómez, 2011] C. Gómez, M. Canales, S. Calvo, R. Rivera, J.R. Valdés, J.L. Núñez: “High and low cycle fatigue life estimation of welding steel under constant amplitude loading: Analysis of different multiaxial damage models and in-phase and out-of-phase loading effects”. International Journal of Fatigue 33 (2011) 578–587

[Gonçalves, 2004] Gonçalves et al. Multiaxial fatigue: a stress based criterion for hard metals International Journal of Fatigue 27 (2005) 177–187

[Goodman, 1899] Goodman, J. Mechanics Applied to Engineering, Longmans Green, London, 1899.

[Gough, 1924] Gough, H. J. The Fatigue of Metals, Scott, Greenwood & Son, London, 1924.

[Gough, 1935] Gough HJ, Pollard HV. The strength of metals under combined alternating stresses. Proc Inst Mech Eng 1935;131:1–103.

[Gough, 1937] Gough J, Pollard HV. Properties of some materials for cast crankshafts, with special reference to combined stresses. Proc Inst Automotive Eng 1937;31:821–96 [London].

[Gough, 1950] Gough HJ. Engineering steels under combined cyclic and static stresses. J Appl Mech 1950:113–25.

[Gough, 1951] Gough H.J., Pollard H.V., Clenshaw W.J. "Some experiments on the resistance of metals to fatigue under combined stresses". Aeronautical Research Council reports and memoranda, London: His Majesty's Stationery Office; (1951).

[Grover, 1951] Grover, H. J., Bishop, S. M., and Jackson, L. R., 'Axial Load Fatigue Tests of Unnotched Sheet Specimens of 24S-T3 and 75S-T6 Aluminum Alloys and SAE 4130 Steels. National Advisory Committee for Aeronautics, Technical Note, 1951.

[Grubisic, 1979A] Grubisic, V. et Neugebauer, J., Guβeisen mit Kugelgraphit unter mehrachsiger Schwingbeanspruchung. Gieβereiforschung 31 (1979) Nr. 4, 123-128.

[Grubisic, 1979B] Grubisic, V. et Neugebauer, J., Festigkeitsverhalten von Sphäroguβ bei kombinierter statischer und dynamischer mehrachsiger Beanspruchung. Fraunhofer-Institut f. Betriebsfestigkeit Darmstadt, LFB-Ber.-Nr. FB-149 (1979).

[Grün, 1991] Grün P.; Troost, A.; Akin, O.; Klubberg, F.; Langzeitund Dauerschwingfestigkeit des Vergütungsstahls 25CrMo4 bei mehrachsiger Beanspruchung durch dreischwingende Lastspannungen. Mat.wiss. u. Werkstofftech. 1991 , 22 (3), pp. 73-80.

[Gunn, 1955] Gunn, K. "The Effect of Yielding on the Fatigue Properties of Test Pieces Containing Stress Concentrations". The Aeronautical Quarterly, vol. 6 (1955), p.277

[Gurson, 1977] Gurson, A. Continuum theory of ductile rupture by void nucleation and growth: part I yield criteria and flow rules for porous ductile media. J Engng Mater Technol 1977, 99, pp. 2–15

[Haibach, 2003] Haibach, E., FKM-Guideline: Analytical strength assessment of components in mechanical engineering (5th Rev ed.), English version. Germany, Frankfurt/Main: Forschungskuratorium Maschinenebau (2003).

[Haigh, 1922] Haigh, B. P. Elastic and Fatigue Fracture in Metals. Metal Industries (London) 1922, Vol. 21, p. 466.

[Heidenreich, 1976] Heidenreich R, Zenner H. Festigkeitshypothese – Berechnung der Dauerfestigkeit für beliebige Beanspruchungskombinationen. Forschungshefte FKM, Heft 55. FKM, Frankfurt am Main – Niederrad; 1976.

[Heidenreich, 1979] Heidenreich R, Zenner H. Schubspannungsintensitätshypothese – Erweiterung und experimentelle Abschätzung einer neuen Festigkeitshypothese für schwingende Beanspruchung. Forschungshefte FKM, Heft 77. FKM, Frankfurt am Main – Niederrad; 1979.

[Heidenreich, 1983] Heidenreich R. Schubspannungsintensitätshypothese – Dauerschwingfestigkeit bei mehrachsiger Beanspruchung. Forschungshefte FKM, Heft 105. FKM, Frankfurt am Main – Niederrad; 1983.

[Heidenreich, 1984] Heidenreich, Richter, Zenner: Schubspannungsintensitätshypothese —weitere experimentelle und theoretische Untersuchungen. Konstruktion (1984); 36(3): pp. 99–104.

[ISO, 2012] ISO 12107:2012, Metallic materials- Fatigue testing- Statistical planning and analysis of data. International Organization for Standardization, Switzerland, (2012).

[Issler, 1973] Issler L. Strength behaviour of metallic materials under multi-axial phase-shifted vibration stress (In German). PhD Thesis. University of Stuttgart, (1973).

[Jasper, 1923] T.M. Jasper, Philosophical Magazine, Series. 6, vol. 46, pp. 609-627, Oct. 1923.

[JSMS, 1996] JSMS Databook: Databook on fatigue strength of metallic materials. The Society of Materials Science, Japan. Amsterdam: Elsevier, (1996). Vol. 2, p. 1066–67 and Vol. 3, p. 305.

[Kakuno, 1979] Kakuno, H. and Kawada, Y. Fatigue Engng Mater. Struct. (1979), 2, 229

[Klubberg, 2001] Klubberg, F.; Schäfer, H.J.; Hempen, M.; Beiss, P.: Mittelspannungsempfindlichkeit metallischer Werkstoffe bei schwingender Beanspruchung. In: Roell Amsler Symposium 2001 "World of Dynamic Testing", Bd. 01/4, S. 111-134, 2. Aufl. 2001, Verlag Mainz, Aachen, ISBN 3-89653-983-3

[Klubberg, 2009] Klubberg, P.; Beiss, P.; Broeckmann, C. Schwingfestigkeit von Gusseisen mit Lamellengraphit. Gießtechnik im Motorenbau 2009 pp.107-118

[Klubberg, 2011] Klubberg, F.; Klopfer, I.; Broeckmann, C.; Berchtold, R.; Beiss. P. Fatigue testing of materials and components under mean load conditions. In: Anales de Mecánica de la Fractura 28, Vol. 1, 2011.

[Koutiri, 2013] Koutiri I., Bellett D., Morel F., Pessard E. A probabilistic model for the high cycle fatigue behaviour of cast aluminium alloys subject to complex loads. International Journal of Fatigue 47 (2013) 137–147

[Lee, 2012] Lee Y.L. et al., Stress-Based Uniaxial Fatigue Analysis, In: Metal Fatigue Analysis Handbook, Elsevier (2012), pp. 115-160.

[Lempp, 1977] Lempp W. Strength behaviour of steels under multiaxial fatigue stress due to normal stresses with superimposed in-phase and phase-shifted shear stresses.PhD Thesis. University of Stuttgart, 1977 [in German].

[Li, 2009] B. Li, L.Reis, M. de Freitas ”Comparative study of multiaxial fatigue damage models for ductile structural steels and brittle materials” International Journal of Fatigue 31 (2009) 1895–1906

[Li, 2017] Li, C.; Li, S:; Duan, F.; Wang, Y.; Zhang, Y.; He, D.; Li, Z.; Wang, W. Statistical Analysis and Fatigue Life Estimations for Quenched and Tempered Steel at Different Tempering Temperatures. Metals 2017, 7, 312; doi:10.3390/met7080312

[Liu, 1993] Liu J., Zenner H., "Berechnung der Dauerschwingfestigkeit bei mehrachsiger Beanspruchung". Mat.-wiss. u. Werkstofftech (1993); 24-7, pp 240-249 [in German].

[Lüpfert, 2001] H.-P. Lüpfert, H.-J. Spies, Influence of compressive prestressing on the fatigue strength of metallic materials under single- and multi-axial loading. Mat.-wiss. and materialtech. 32 (2001), pp. 837-844.

[Lüpfert, 2004] Lüpfert, H.P.; Spies, H.J.; Fatigue strength of heat-treated steel under static multiaxial compression stress. Advanced Engineering Materials, vol. 6, n. 7, (2004) pp. 544–550.

[Mamiya, 2009] E.N. Mamiya et al. “Prismatic hull: A new measure of shear stress amplitude in multiaxial high cycle fatigue” Int. J. Fatigue 31 (2009) 1144-1153

[Mamiya, 2011] E.N. Mamiya, F.C. Castro, R.D. Algarte, J.A. Araújo “Multiaxial fatigue life estimation based on a piecewise ruled S–N surface” International Journal of Fatigue 33 (2011) 529–540

[Marin, 1952] Marin, J., Theories of failure for ultimate strength, In: Engineering Materials: Their mechanical properties and applications. Prentice-Hall, New York, (1952), pp. 140-147.

[Marin, 1956] Marin, J., Interpretation of fatigue strengths for combined stresses, In: Proceedings of international conference on fatigue of metals. London: Institution of Mechanical Engineers (1956); pp. 184–195.

[Marquis, 2000] Marquis G, Socie D. Long-life torsion fatigue with normal mean stresses. Fatigue Fract Eng Mater Struct 2000;23(4):293–300.

[Marquis, 2001] Marquis, G., Solin J., Long-Life Fatigue Design of GRP 500 Nodular Cast Iron Components, VTT research notes 2043 (2001), Espoo.

[Matake, 1977] Matake T. "An explanation on fatigue limit under combined stress." Bull JSME 1977;20:257–63.

[Matsubara, 2013] Go Matsubara, Kenji Nishio. "Multiaxial high-cycle fatigue criterion considering crack initiation and non-propagation". International Journal of Fatigue 47 (2013) 222–231

[Mayer, 2015] Mayer H. et al., Cyclic torsion very high cycle fatigue of VDSiCr spring steel at different load ratios. International Journal of Fatigue 70 (2015) 322-327.

[Mayer, 2016] Mayer, H. et al., Mean stress sensitivity and crack initiation mechanisms of spring steel for torsional and axial VHCF loading. International Journal of Fatigue 93 (2016) pp. 309-317.

[McAdam, 1924] McAdam, D.J. The endurance range of steel. Proc. Amer. Soc. Test. Mater. 24, Pt II, 574—600. (1924).

[McDiarmid, 1985] D. L. McDiarmid. "The effects of mean stress and stress concentration on fatigue". Fatigue & Fracture of Engineering Materials & Structures. 1985. 8 (1) p 1-12

[McDiarmid, 1991] McDiarmid DL. “A general criterion for high cycle multiaxial fatigue failure.” Fatigue Fract Eng Mater Struct 1991;14:429–53.

[McDiarmid, 1994] McDiarmid DL. “A shear stress based critical-plane criterion of multiaxial fatigue failure for design and life prediction.” Fatigue Fract Eng Mater Struct 1994;17:1475–84.

[Meggiolaro, 2011A] M.A. Meggiolaro, J.T.P. de Castro “An improved multiaxial rainflow algorithm for non-proportional stress or strain histories- Part I: Enclosing surface methods” Int. J. Fatigue (2011)

[Meggiolaro, 2011B] M.A. Meggiolaro, J.T.P. de Castro “An improved multiaxial rainflow algorithm for non-proportional stress or strain histories- Part II: The Modified Wang-Brown method” Int. J. Fatigue (2011)

[Mielke, 1980] Mielke S. Festigkeitsverhalten metallischer Werkstoffe unter zweiachsiger schwingender Beanspruchung mit verschiedenen Spannungszeitverlaufen. PhD thesis. RWTH Aachen, Aachen; 1980.

[Moore, 1921] Moore H.F. , Kommers J.B., An investigation of the fatigue of metals. A report of the investigation. University of Illinois Engineering Experiment Station, Bulletin series No. 124 (1921)

[Moore, 1923] Moore H.F. , Jasper T.M., An investigation of the fatigue of metals. Series of 1922. A report of the investigation. University of Illinois Engineering Experiment Station, Bulletin series No. 136 (1923)

[Moore, 1924] Moore H.F. , Jasper T.M., An investigation of the fatigue of metals. Series of 1923. A report of the investigation. University of Illinois Engineering Experiment Station, Bulletin series No. 142 (1924)

[Moore, 1925] Moore, H.F., Jasper T.M., An investigation of the fatigue of metals. Series of 1925. A report of the investigation. University of Illinois Engineering Experiment Station, Bulletin series No. 152 (1925).

[Morel, 2001] Morel, F. et al., Comparative study and link between mesoscopic and energetic approaches in high cycle multiaxial fatigue. International Journal of Fatigue 23 (2001) pp. 317-327.

[Morel, 2002] Morel F, Palin-Luc T. A non-local theory applied to high cycle multiaxial fatigue. Fatigue Fract Eng Mater Struct 2002;25:649–65.

[Morrison, 1956] Morrison, J.L.M., Session 2: Stress Distribution, In: Proceedings of international conference on fatigue of metals. London: Institution of Mechanical Engineers, 1956, pp. 741–742.

[Morrow, 1968] Morrow, J.; Fatigue properties of metals, section 3.2. In: Fatigue Design Handbook. Pub. No. AE-4. SAE, Warrendale, 1968.

[Mu, 2014] Mu P., Nadot Y., Serrano-Munoz I., Chabod A.; Influence of complex defect on cast AS7G06-T6 under multiaxial fatigue loading. Engineering Fracture Mechanics 123 (2014) 148–162

[Murakami, 2002] Yukitaka Murakami "Metal Fatigue: Effects of Small Defects and Nonmetallic Inclusions". Publisher: Elsevier Science (2002). ISBN: 0-08-044064-9

[Nadai, 1931] Nadai, A. "Plasticity", p.126 (Mc. Graw-Hill Publishing Co., New York and London), 1926.

[Nascimento, 2001] Nascimento M.P., Souza R.C., Pigatin W.L., Voorwald H.J.C. Effects of surface treatments on the fatigue strength of AISI 4340 aeronautical steel. International Journal of Fatigue 23 (2001) 607–618.

[Nicholas, 2002] T. Nicholas and D.C. Maxwell, Fatigue and Fracture Mechanics: 3 3rd Volume, ASTM STP 1417, W.G. Reuter and R.S. Piascik, Eds., ASTM, West Conshohocken, PA, pp. 476-492, 2002.

[Nicholas, 2003] Nicholas, T.: "Recent Advances in High Cycle Fatigue". International Conference on the Mechanical Behavior of Materials [9th], ICM-9, Held in Geneva, Switzerland on 25-29 May 2003

[Nishihara, 1945] Nishihara T, Kawamoto M. The strength of metals under combined alternating bending and torsion with phase difference. Mem College Eng, Kyoto Imperial University (1945); Vol. 11: pp. 85–112.

[Nishijima, 1993] Nishijima, S. Basic Properties of JIS Steels for Machine Structural Use; NRIM Special Report (Technical Report) No. 93-02; National Research Institute for Metals: Tokyo, Japan, 1993.

[Nolte, 1973] Nolte F. Dauerfestigkeitsuntersuchungen an Stahlwellen bei umlaufender Beige- und überlagerter statischer Verdrehbeanspruchung. PhD thesis. TU Berlin, Berlin; 1973.

[O'Connor, 1956] O'Connor, H.C.; Morrison, J.L.M., The Effect of Mean Stress on the Push-Pull Fatigue Properties of an Alloy Steel. In: 'Proc. Int. Conf. on Fatigue of Metals', Institution of Mechanical Engineers, London, 1956, pp. 102-109.

[Oguma, 2004] Oguma, Harada and Sakai: Strength Level Dependence of Long-Life Fatigue Behavior for Bearing Steel in Rotating Bending. Proc. 3rd Int. Conf. VHCF (2004), p. 617-624.

[Orowan, 1939] Orowan, E. "Theory of the Fatigue of Metals". Proceedings of the Royal Society (London), Series A, Vol. 171, p. 79 (1939).

[Palin-Luc, 1998] Thierry Palin-Luc, Serge Lasserre. *"An energy based criterion for high cycle multiaxial fatigue".* European Journal of Mechanics - A/Solids Volume 17, Issue 2, March–April 1998, Pages 237-251

[Pallarés, 2018A] Pallarés-Santasmartas, L.; Albizuri, J.; Avilés, A.; Avilés, R. "Mean Stress Effect on the Axial Fatigue Strength of DIN 34CrNiMo6 Quenched and Tempered Steel." Metals 2018, 8, 213.

[Pallarés, 2018B] Pallarés-Santasmartas, L.; Albizuri, J.; Avilés, A.; Saintier, N.; Merzeau, J. "Influence of mean shear stress on the torsional fatigue behaviour of 34CrNiMo6 steel." International Journal of Fatigue, 2018(113), pp 54-68.

[Pallarés, 2019] Pallarés Santasmartas, Luis & Albizuri, Joseba & Leguinagoicoa, Nelson & Saintier, Nicolas & Merzeau, Jonathan. (2019). The effect of mean axial and torsional stresses on the fatigue strength of 34CrNiMo6 high strength steel. MATEC Web of Conferences. 300. 16004. 10.1051/matecconf/201930016004.

[Papadopoulos, 1994] Papadopoulos I.V., "A new criterion of fatigue strength for out-of-phase bending and torsion of hard metals". International Journal of Fatigue, Vol.16, Issue 6, August (1994), pp. 377-384.

[Papadopoulos, 1997] Papadopoulos I.V.; Davoli P., Gorla C., Filippini, M.; Bernasconi, A. A comparative study of multiaxial high-cycle fatigue for metals. International Journal of Fatigue 1997, 19, pp. 219-235. https://doi.org/10.1016/S0142-1123(96)00064-3

[Papuga, 2005] Jan Papuga "Mapping of fatigue damages – program shell of FE calculation" [PhD thesis]. Prague: Czech Technical University in Prague; 2005

[Papuga, 2008] Papuga J., Ruzicka M., Two new multiaxial criteria for high cycle fatigue computation. Int. J. Fatigue 30 (2008) pp. 58-66

[Papuga, 2009] Papuga J. Improvements of two criteria for multiaxial fatigue limit evaluation.Bull Appl Mech 2009;5:80–6.

[Papuga, 2011A] Papuga J., A survey on evaluating the fatigue limit under multiaxial loading. Int. J. Fatigue 33 (2011) pp.153-165

[Papuga, 2011B] Jan Papuga "Answer to Comments on "A survey on evaluating the fatigue limit under multiaxial loading" [Int. J. Fatigue 33 (2011) 153-165]" Int. J. Fatigue 33 (2011) 1396-1402

[Paysan, 1970] Paysan B. Untersuchungen des Einflusses einiger Kerbformen auf die Tragfähigkeit von Wellen bei umlaufender Biegung und überlagerter statischer Torsion. PhD thesis. TU Berlin, Berlin; 1970.

[Peterson, 1952] Peterson R.E. Brittle fracture and fatigue in machinery, MIT Symp., (1952) p. 74—10.

[Peterson, 1974] Peterson R.E. Stress concentration factors. John Wiley & Sons, New York, Chichester, Brisbane, Toronto, Singapore, 1974.

[Pyttel, 2011] B. Pyttel, D. Schwerdt, C. Berger "Very high cycle fatigue – Is there a fatigue limit?" International Journal of Fatigue 33 (2011) 49–58

[Rausch, 2011] Rausch, T.: "On the fatigue strength behaviour of cast iron materials under uniaxial and multi-axial loading using the example of EN-GJV-450" (In German). PhD. Thesis, Aachen University, (2011).

[Robert, 1992] Robert, J.-L., Contribution à l'étude de la fatigue multiaxiale sous sollicitations périodiques ou aléatoires, Thèse de Doctorat, Institut National des Sciences Appliquées de Lyon, Lyon, (1992).

[Rotvel, 1970] Rotvel F. Biaxial fatigue tests with zero mean stresses using tubular specimens. Int J Mech Sci 1970;12:597–613.

[Sakai, 2016] Sakai, T.; Nakagawa A.; Oguma N.; Nakamura, Y.; Ueno, A.; Kikuchi S.; Sakaida, A. A review on fatigue fracture modes of structural metallic materials in very high cycle regime. International Journal of Fatigue 2016, 93, pp. 339–351. https://doi.org/10.1016/j.ijfatigue.2016.05.029.

[Sauer, 1948] Sauer, J.A., A study of fatigue phenomena under combined stress. Proceedings of the seventh international congress for applied mechanics pp. 150-164 (1948)

[Schütz, 1996] Walter Schütz, A History of Fatigue, Eng. Fract. Mechanics, Vol. 54, pp 263-300, 1996

[Simbürger, 1975] Simbürger A. Festigkeitsverhalten zäher Werkstoffe bei einer mehrachsigen phaseverschobenen Schwingbeanspruchungmit körperfesten und veränderlichen Hauptspannungsrichtungen. TH Darmstadt, Darmstadt; 1975.

[Sines, 1959] Sines G., In: Behavior of Metals under Complex Static and Alternating Stresses, in: Metal Fatigue, Editors: George Sines and J.L. Waisman. McGraw-Hill Book company, (1959).

[Smith, 1939] Smith, J.O., The effect of range of stress on the torsional fatigue strength of steel. University of Illinois Engineering Experiment Station, Bulletin series No. 316 (1939)

[Smith, 1942] Smith, J.O., The effect of range of stress on the fatigue strength of metals. University of Illinois Engineering Experiment Station, Bulletin series No. 334 (1942)

[Smith, 1970] Smith, K. N., Watson, P. and Topper, T. H. (1970) A stress-strain function for the fatigue of metals. J. Mater. ASTM 5, 767–778

[Sochava, 1977] Sochava, A.I. Approximating the diagram of limiting amplitudes taking into consideration the area of mean compressive stresses. Strength Mater 1977, 9: 1169. https://doi.org/10.1007/BF01528902

[Soderberg, 1930] Soderberg, C. R. "Factors of safety and working stresses", Transactions of the ASME, Applied Mechanics Division, Vol. 52 (1930), p. 13

[Sonsino, 2007] Sonsino, C.M., Course of SN-curves especially in the high-cycle fatigue regime with regard to component design and safety, International Journal of Fatigue 29 (2007) pp. 2246-2258.

[Stulen, 1954] Stulen, F.B.; Cummings, H.N., *"A Failure Criterion for Multi-Axial Fatigue Stresses"*, Proc., ASTM, Vol. 54, 1954, p.822

[Stüssi, 1955] Stüssi, F. "Die Theorie der Dauerfestigkcit und die Vcrsuche von August Wohler", Mitt. TKVSB—No. 13 (1955).

[Susmel, 2002] Susmel L, Lazzarin P. "Estimating fatigue damage under variable amplitude multiaxial fatigue loading" Fatigue Fract Engng Mater Struct 2002;25:63–78.

[Susmel, 2003] L. Susmel "A Bi-parametric modified Wöhler curve for high cycle multiaxial fatigue assessment." Fatigue Fract Engng Mater Struct 34, 2003: 1053–1077.

[Susmel, 2005] Susmel et al. "The mean stress effect on the high-cycle fatigue strength from a multiaxial fatigue point of view" Int. J. Fatigue 27 (2005) 928-943

[Susmel, 2007] Susmel L. The theory of critical distances: a review of its applications in fatigue. Engineering Fracture Mechanics 75 (2008) 1706–1724

[Susmel, 2008] Susmel L, Tovo R. "Multiaxial fatigue limits and material sensitivity to non-zero mean stresses normal to the critical planes" Fatigue Fract Engng Mater Struct 31, 2008: 295-309.

[Susmel, 2010] L. Susmel "A simple and efficient numerical algorithm to determine the orientation of the critical plane in multiaxial fatigue problems" Int. J. Fatigue 32 (2010) 1875-1883

[Susmel, 2011] Susmel L. "Comments on "A survey on evaluating the fatigue limit under multiaxial loading by Jan Papuga" [Int. J. Fatigue 33 (2011) 153-165]" Int. J. Fatigue 33 (2011) 1392-1395

[Susmel, 2012] L. Susmel, D. Taylor "A critical distance/plane method to estimate finite life of notched components under variable amplitude uniaxial/multiaxial loading" Int. J. Fatigue 38 (2012) 7-24

[Tovo, 2014] Tovo, R. et al., Experimental investigation of the multiaxial fatigue strength of ductile cast iron. Theoretical and Applied Fracture Mechanics 73 (2014) p. 60-67.

[Trapp, 1953] Trapp, W. J.; Schwartz, R. T. Elevated Temperature Fatigue Properties of SAE 4340 Steel. Proceedings of American Society for Testing Materials 1953, Vol. 53, pp. 825–838.

[Troost, 1987] Troost A, Akin O, Klubberg F. Dauerfestigkeitsverhalten metallischer Werkstoffe bei zweiachsiger Beanspruchung durch drei phasenverschoben schwingende Lastspannungen. Konstruktion 1987;39:479–88.

[Ukrainetz, 1960] Ukrainetz, P.R., The effect of the mean stress on the endurance limit. M.Sc. Thesis, The University of Columbia (1960).

[Velleman, 1980] P.F. Velleman "Definition and Comparison of Robust Nonlinear Data Smoothing Algorithms, "Journal of the American Statistical Association, Volume 75, Number 371, pp.609-615. (1980).

[Vu, 2010] Vu, Halm, Nadot “Multiaxial fatigue criterion for complex loading based on stress invariants” Int. J. Fatigue 32 (2010) 1004-1014

[Walker, 1970] Walker, K. (1970) The effect of stress ratio during crack propagation and fatigue for 2024-T3 and 7075-T6 aluminum. Effects of Environment and Complex Load History on Fatigue Life. ASTM STP 462, Am. Soc. for Testing and Materials, Philadelphia, PA, pp. 1–14.

[Wang, 1991] Wang C.H., Miller K.J., The effect of mean shear stress on torsional fatigue behaviour. Fatigue and Fracture of Engineering Materials and Structures, Vol. 14 (1991), No.2/3, pp.293-307.

[Wang, 2004] Wang, Yao “Evaluation and comparison of several multiaxial fatigue criteria” Int. J. Fatigue 26 (2004) 17-25

[Weber, 1999] Bastien Weber "Multiaxial fatigue of industrial structures under any load" PhD Thesis. INSA Lyon, Lyon; 1999

[Weibull, 1961] Weibull, W. Fatigue Testing and Analysis of Results. Chapter VIII: Presentation of Results p.153. Pergamon Press Oxford, London, Paris, 1961.

[Wöhler, 1870] A. Wöhler, On strength tests with iron and steel, Zeitschrift für Bauwesen, XX, 73-106 (1870).

[Yokobori, 1963] Yokobori T. Unified engineering theory of metal fatigue. Technological Reports of Tohoku University, Sendai, Japan, 1963;27(2):53–73.

[Zenner, 2000] Zenner, H.; Simbürger, A.; Liu, J. On the fatigue limit of ductile metals under complex multiaxial loading. International Journal of Fatigue 2000, 22, pp. 137–145. https://doi.org/10.1016/S0142-1123(99)00107-3.

[Zhang, 2010] Zhang et al. “An improved multiaxial high-cycle fatigue criterion based on critical plane approach” Fatigue Fract Engng Mater Struct 34 (2010), 337–344

ANNEX A: PARAMETERS OF GLOBAL APPROACH METHOD

The derivation of the parameters takes into account previous works as those of [Papadopoulos, 1997] and [Papuga, 2008] to derive the parameters. It must be noted that the derivation of the parameters could have been done in other ways, for instance selecting different tests or by doing a best fit to a number of cases. The presented derivation follows the procedure of [Pallarés, 2018B].

Three different tests will be necessary to adjust the parameters, namely the fully reversed axial and torsional fatigue limits σ_{-1} and τ_{-1}, and the repeated torsional fatigue limit τ_0.

Fully Reversed Torsion Fatigue Test

The fully reversed torsion is suitable for the determination of the parameter *"a"* of equation (8-2), as the mean value of the second invariant of the deviator tensor $J_{2,m}$ is equal to zero. Moreover, in pure torsion tests, there are no hydrostatic stresses involved. The application of the fully reversed torsional fatigue limit τ_{-1} to Equation (8-2) yields the following Equation (A-1):

$$\sqrt{\left(\frac{\tau_{-1}}{a}\right)^2} = 1 \qquad \text{(A-1)}$$

Therefore, the parameter *"a"* takes the value of the fully reversed torsional fatigue limit τ_{-1}, as shown in equation (A-2):

$$a = \tau_{-1} \qquad \text{(A-2)}$$

Repeated Torsion Fatigue Test

The repeated torsional fatigue limit τ_0 is suitable for the determination of the parameter *"b"*, as the there is no hydrostatic energy involved in this test and the parameter *"a"* has previously been determined. The application of this test to equation (8-2) yields equation (A-3):

$$\sqrt{\left(\frac{\tau_0}{2\cdot\tau_{-1}}\right)^2+\left(\frac{\tau_0}{2\cdot b}\right)^2}=1 \qquad \text{(A-3)}$$

Therefore, the parameter "b" can be expressed through Equation (A-4):

$$b=\frac{\tau_0}{2\sqrt{1-\left(\frac{\tau_0}{2\cdot\tau_{-1}}\right)}} \qquad \text{(A-4)}$$

Fully reversed axial fatigue test

In the pure torsional fatigue tests, the hydrostatic stress is equal to zero. Therefore, an additional test with a non-zero maximum hydrostatic $\sigma_{H,max}$ is needed to derive the parameter "c". The fully reversed axial fatigue test satisfies this condition, and it is usually applied in the derivation of the parameters, as the value of $J_{2,m}$ is equal to zero.

The maximum hydrostatic stress takes a value of $\sigma_{-1}/3$. The quantity $\sqrt{J_{2,a}}$ takes a value of $\sigma_{-1}/\sqrt{3}$. The application of this test to equation (8-2) yields equation (A-5):

$$\sqrt{\left(\frac{\sigma_{-1}}{\sqrt{3}\cdot\tau_{-1}}\right)^2}+\frac{\sigma_{-1}}{3\cdot c}=1 \qquad \text{(A-5)}$$

The parameter *"c"* can be expressed by means of equation (A-6):

$$c=\frac{\sigma_{-1}}{3-\sqrt{3}\cdot\kappa} \qquad \text{(A-6)}$$

ANNEX B: PARAMETERS OF ENERGETIC METHOD

The derivation of the parameters *"a"* and *"b"* of the energetic method, defined by the equation (8-6) can be performed through the procedure described in Annex A, so that the values of those parameters can be calculated by means of equations (A-2) and (A-4).

In order to determine the parameters "c" and "Λ", two extra tests with hydrostatic stresses will be used, namely the fully reversed axial fatigue test and the repeated axial fatigue test. The derivation described herein follows the procedure of [Pallarés, 2018A].

Fully reversed axial fatigue test

This test is usually applied in the derivation of the parameters as the mean values of I_1 and J_2 are zero. The quantity $\sqrt{J_{2,a}}$ takes a value of $\sigma_{-1}/\sqrt{3}$. The constant Λ takes a non-zero value as this is a test without gradient and all the volume is loaded. The application of this test to Equation (8-6) yields Equation (B-1):

$$\left(\frac{\sigma_{-1}}{\sqrt{3}\cdot\tau_{-1}}\right)^2+\left(\frac{\Lambda}{c}\right)^2=1 \qquad \text{(B-1)}$$

As there are two unknown quantities, namely "Λ" and "c", an extra equation is needed, and the repeated axial fatigue test will be used, as it is usually available or it can be calculated with the equations of Chapter 2.

Repeated axial fatigue test

All the quantities take a non-zero value for the repeated axial fatigue limit σ_0. The application of this test to Equation (8-6) yields Equation (B-2):

$$\left(\frac{\sigma_0}{2\cdot\sqrt{3}\cdot\tau_{-1}}\right)^2+\left(\frac{\sigma_0}{2\cdot\sqrt{3}\cdot b}\right)^2+\left(\frac{\frac{\sigma_0}{2}+\Lambda}{c}\right)^2=1 \qquad \text{(B-2)}$$

The two unknown quantities *"Λ"* and *"c"* can be obtained by equalizing (B-1) and (B-2). After lengthy algebraic calculations, both parameters can be obtained, Equations (B-3) and (B-4):

$$c=\frac{\sigma_0}{2\cdot\left(\sqrt{1-\left(\frac{\sigma_0}{2\sqrt{3}}\right)^2\cdot\left(\frac{1}{a^2}+\frac{1}{b^2}\right)}-\sqrt{1-\left(\frac{\sigma_{-1}}{\sqrt{3}\tau_{-1}}\right)^2}\right)} \qquad \text{(B-3)}$$

$$\Lambda=c\cdot\sqrt{1-\left(\frac{\sigma_{-1}}{\sqrt{3}\tau_{-1}}\right)^2} \qquad \text{(B-4)}$$